Molecular machinery and cell biology of sleep control



Raffaele Sarnataro

University of Oxford

Department of Physiology, Anatomy and Genetics

Jesus College

A thesis submitted for the degree of

Doctor of Philosophy

in Neuroscience

Trinity Term 2022

Table of Contents

Table of Contents 3

Abstract 6

Abbreviations, list of figures and tables 7

1. Introduction 11

1.1 Sleep *11*

1.2 Sleep in Drosophila *14*

1.3 Dorsal fan-shaped body-projecting neurons *18*

1.4 Aims of this thesis *20*

2 Materials and Methods 21

2.1 Reagents *21*

2.1.1 Antibodies 21

2.1.2 Chemicals 21

2.1.3 Fly Strains 22

2.2 Drosophila culture *27*

2.3 Sleep measurements *27*

2.3.1 Open-Loop optogenetics 27

2.3.2 Thermogenetics 28

2.3.3 Sleep deprivation 28

2.4 Single-cell transcriptomics *29*

2.4.1 Brain dissociation and cell collection for single-cell RNA-sequencing 29

2.4.2 scRNA-seq data processing, alignment and analysis 29

2.4.3 Differential gene expression analysis and gene ontology 30

2.5 In vivo two-photon imaging *31*

2.6 Brain dissections, staining and confocal imaging *32*

2.6.1 Mitochondria morphometric analysis 33

2.6.2 Synaptic tagging measurements 33

2.7 Molecular cloning *34*

2.8 Connectomics *36*

2.9 Softwares and Algorithms *36*

2.10 Statistics and reproducibility *37*

2.11 Technical acknowledgments *38*

3 The transcriptome of dFB neurons 39

3.1 Introduction *39*

3.2 Results *41*

3.2.1 Experimental design of scRNA-seq and quality control validation 41

3.2.2 Identification of dFB neurons within scRNA-seq dataset 46

3.3 Discussion *50*

4 The neurotransmitter identity of dFB neurons 53

4.1 Introduction *53*

4.2 Results *56*

4.2.1 VGlut repression and loss-of-function in dFB neurons abolishes sleep-control properties 56

4.2.2 Genetic intersectional studies reveal dFB neurons are glutamatergic and sleep-controlling 60

4.2.3 In vivo two-photon imaging of glutamate release in the dFB 67

4.3 Discussion *69*

5 Sleep history-regulated transcriptome of dFB neurons reveals presynaptic plasticity and bidirectional control of mitochondrial dynamics and sleep 73

5.1 Introduction *73*

5.2 Results *75*

5.2.1 Sleep history-regulated transcriptome of dFB neurons 75

5.2.2 Sleep deprivation induces structural synaptic plasticity 79

5.2.3 Bidirectional control of sleep and mitochondrial dynamics 81

5.3 Discussion *94*

5.3.1 Sleep pressure and dFB plasticity 94

5.3.2 Mitochondria shaping (sleep) behaviour 97

6 Heterogeneity of octopamine receptors within dFB neurons 104

6.1 Introduction *104*

6.2 Results *107*

6.2.1 Transcriptional heterogeneity within dFB neurons 107

6.2.2 Tools to target and manipulate octopamine receptors heterogeneity 109

6.2.3 Octopaminergic inputs to dFB neurons 113

6.3 Discussion *115*

7 Conclusions 118

7.1 Methodological considerations and limitations *119*

7.2 Future work *122*

7.3 Concluding remarks *124*

8 Acknowledgments 125

9 Appendices 127

9.1 Criteria and markers used to label cell clusters *127*

9.2 Transcriptomic reads alignment and annotation script *128*

9.3 Genes differentially expressed in dFB neurons, compared to the rest of fly brain *130*

9.4 Two-photon imaging analysis script of response to arousing stimulus *131*

9.5 Two photon imaging analysis script of response to optogenetic stimuli *134*

9.6 Anterograde trans-synaptic tracing of dFB neurons *137*

9.7 Genes differentially expressed in dFB neurons, upon sleep deprivation *138*

9.8 Heatmaps of Gene Ontology for differentially expressed genes in dFB neurons *141*

9.9 Gene ontology on DEGs in dFB neurons (PANTHER full tables) *142*

9.9.1 Genes upregulated upon sleep deprivation, “biological process” 142

9.9.2 Genes upregulated upon sleep deprivation, “cellular component” 144

9.9.3 Genes upregulated upon sleep deprivation, “reactome” 146

9.9.4 Genes downregulated upon sleep deprivation, “biological process” 147

9.9.5 Genes downregulated upon sleep deprivation, “cellular component” 150

9.9.6 Genes downregulated upon sleep deprivation, “reactome” 151

9.10 Genes differentially expressed between two dFB neurons sub-clusters *152*

10 Bibliography 153

Abstract

Sleep is vital and universal, yet its essential biological functions remain elusive.

The sleep homeostat tracks an internal process that generates sleep pressure during waking, which is then periodically discharged by initiating sleep. Understanding the molecular nature of sleep pressure and its regulation by the homeostat will help to elucidate the physiological variables linked to the essential function of sleep.

In *Drosophila*, rising sleep pressure increases the activity of sleep-control neurons projecting to the dorsal fan-shaped body (dFB). Sleep need is encoded in the intrinsic excitability of these neurons, which fluctuates because two potassium conductances, voltage-gated Shaker and the leak channel Sandman, are modulated antagonistically. Signalling cascades transducing sleep pressure into sleep must thus converge on the regulation of currents flowing through these two ion channels.

To obtain a comprehensive view of the molecular machinery operating within dFB neurons, I have characterised transcriptomes of single cells isolated from dissociated brains of rested and sleep-deprived flies.

These studies revealed a mechanism of bidirectional control of mitochondrial dynamics and sleep in dFB neurons. Sleep loss selectively upregulates genes encoding mitochondrial proteins and alters mitochondrial dynamics in these neurons. Conversely, manipulating mitochondrial fission and fusion in dFB neurons affects sleep in opposing ways. Since mitochondrial dynamics reflect and influence ATP synthesis and ROS production, they suggest a causal link to cellular oxidative stress, which is recorded by Shaker's redox-sensitive β-subunit and converted to heightened neuronal excitability driving sleep.

At the synaptic level, sleep deprivation decreases the strength of dFB neuron output synapses, which release the (in the *Drosophila* CNS inhibitory) transmitter glutamate. The neurons are heterogeneous in the expression of an octopamine receptor, whose cognate monoamine calibrates sleep.

These studies, based on the first single-cell transcriptome of an animal's sleep-control neurons in different conditions of sleep pressure, advance our understanding of how sleep-control is implemented in the brain.

Abbreviations, list of figures and tables

AD	Activation domain
ANOVA	Analysis of variance
AOX	Alternative oxidase
AstA	Allatostatin A
BDSC	Bloomington Drosophila Stock Center
ChAT	Choline acetyltransferase
CNS	Central nervous system
CRISPR	Clustered Regularly Interspaced Short Palindromic Repeats
CS	Canton-S
DA	Dopamine
DBD	DNA-binding domain
DEG	Differentially expressed gene
(d)FB	(Dorsal) fan-shaped body
dFB neurons	Dorsal fan-shaped body-projecting neurons
DNA	Deoxyribonucleic acid
ER	Endoplasmic reticulum
FACS	Fluorescence-activated cell sorting
GABA	γ-aminobutyric acid
Gad1	Glutamic acid decarboxylase 1
Gal	Galanin
(E)GFP	(Enhanced) Green fluorescent protein
KC	Kenyon cell
KD	Knockdown
K_{ir}	Inwardly rectifying potassium channel
KO	Knockout
MERC	Mitochondria-endoplasmic reticulum contact (site)
mRNA	Messenger ribonucleic acid
mtDNA	Mitochondrial deoxyribonucleic acid
nDNA	Nuclear deoxyribonucleic acid
NE	Norepinephrine
NGS	Normal goat serum
NREM	Non-rapid eye movement (sleep)
NT	Neurotransmitter
OA	Octopamine

OXPHOS	Oxidative phosphorylation
PA	Phosphatidic acid
PBS	Phosphate buffered saline
POA	Preoptic area
PTM	Post-translational modification
REM	Rapid eye movement (sleep)
RNAi	Ribonucleic acid interference
ROI	Region of interest
ROS	Reactive oxygen species
rRNA	Ribosomal ribonucleic acid
(sc)RNA-seq	(Single-cell) RNA-sequencing
SEM	Standard error of the mean
sgRNA	Single guide RNA
SHY	Synaptic homeostasis hypothesis
SIP	Superior intermediate protocerebrum
SLP	Superior lateral protocerebrum
SMP	Superior medial protocerebrum
STaR	Synaptic Tagging with Recombination
TNT	Tetanus toxin
tRNA	Transfer ribonucleic acid
UAS	Upstream Activation Sequence
UMAP	Uniform Manifold Approximation and Projection
UMI	Unique molecular identifier
VAChT	Vesicular acetylcholine transporter
VDRC	Vienna Drosophila Resource Centre
VGlut	Vesicular glutamate transporter
VLPO	Ventrolateral preoptic nucleus
VTA	Ventral tegmental area
ZT	Zeitgeber time

Figure 1.1 | Anatomical schematics of circuits and cell types controlling sleep and wakefulness in the *Drosophila* brain.

Figure 3.1 | Schematics of the single-cell RNA-sequencing experimental procedure.

Figure 3.2 | Quality control on single-cell transcriptomics of fly brain.

Figure 3.3 | Cell types are identifiable among the cell clusters.

Figure 3.4 | dFB neurons distinctly cluster as glutamatergic neurons.

Figure 3.5 | Identified dFB neurons recapitulate their known genetic features.

Figure 4.1 | Schematics of major circuits and cell types downstream of dFB neurons.

Figure 4.2 | *VGlut-driven* transcriptional repression abolishes gene expression in *R23E10-GAL4-labelled* dFB neurons.

Figure 4.3 | *VGlut-driven* transcriptional repression abolishes the sleep-induction phenotype of dFB neurons.

Figure 4.4 | Knockdown of *VGlut* in *R23E10-GAL4* neurons decreases sleep.

Figure 4.5 | Expression patterns of *VAChT-AD* and *Gad1-AD* combined with *R23E10-DBD.*

Figure 4.6 | Expression pattern of the *VGlut-AD; R23E10-DBD* line.

Figure 4.7 | Anatomical expression pattern overlap between VGlut-AD; R23E10-DBD and R23E10-LexA lines.

Figure 4.8 | Chronical inhibition of the glutamatergic subset of *R23E10-GAL4-labelled* dFB neurons decreases sleep.

Figure 4.9 | Abolishing synaptic transmission from the glutamatergic subset of *R23E10-GAL4-labelled* dFB neurons decreases sleep.

Figure 4.10 | Light activation of *R23E10-GAL4-labelled* neurons raises sleep.

Figure 4.11 | Light activation of *VGlut-AD; R23E10-DBD-labelled* neurons raises sleep.

Figure 4.12 | Arousing stimulation of flies elicits glutamate release *in vivo* in the fan-shaped body.

Figure 4.13 | Optogenetic stimulation of dFB neurons elicits glutamate release *in vivo* in the fan-shaped body.

Figure 5.1 | Sleep history modulates transcriptome of dFB neurons for mitochondrial metabolism and synaptic genes.

Figure 5.2 | Genes differentially expressed depending on sleep history, in Kenyon cells and projection neurons.

Figure 5.3 | Sleep deprivation affects synaptic plasticity in sleep-dedicated circuits.

Figure 5.4 | Mitochondrial dynamics in dFB neurons is modulated by sleep pressure.

Figure 5.5 | Overexpression of the mitochondrial fission-promoting Dynamin-related protein 1 (*Drp1*) in dFB neurons reduces sleep.

Figure 5.6 | Overexpression of the mitochondrial fusion-promoting Dynamin-like GTPase Opa1 in dFB neurons increases sleep.

Figure 5.7 | Overexpression of the mitochondrial fusion-promoting Dynamin-family GTPase Marf in dFB neurons does not affect sleep.

Figure 5.8 | Knockdown of mitochondrial fusion-promoting core genes in dFB neurons reduces sleep.

Figure 5.9 | Knockdown of the mitochondrial fusion-promoting dynamin-related GTPase *Opa1* in dFB neurons impairs sleep homeostasis.

Figure 5.10 | Knockdown of MERCs-forming gene *Miga* decreases sleep.

Figure 5.11 | Visualisation of MERCs in dFB neurons.

Figure 5.12 | Knockdown of mitochondrial phospholipases reduces sleep.

Figure 5.13 | Working model of the relationship between mitochondrial dynamics, bioenergetics, ROS, and sleep pressure.

Figure 6.1 | Transcriptional heterogeneity for octopamine receptors within dFB neurons subpopulations.

Figure 6.2 | Expression patterns of OA receptors-derived AD lines, combined with *R23E10-DBD.*

Figure 6.3 | Knockdown of *Octβ1R* and *Octβ3R* receptors with double, but not with single, RNAis decreases sleep.

Figure 6.4 | Cell-specific CRISPR knockout of octopamine receptors does not affect total sleep.

Figure 6.5 | VPM3 neurons are synaptically connected to *R23E10-GAL4-labelled* dFB neurons and affect sleep.

Figure 9.1 | Anterograde trans-synaptic mapping of dFB neurons.

Figure 9.2 | Gene ontology of differentially expressed genes upon sleep deprivation in dFB neurons.

Table 9.1 | Genes differentially expressed in dFB neurons compared to the rest of the brain.

Table 9.2 | Genes differentially expressed in dFB neurons upon sleep deprivation.

Table 9.3 | Genes differentially expressed between the two dFB neurons sub-clusters reported in Figure 6.1.

1. Introduction

1.1 Sleep

"Come l'araba fenice:

Che vi sia, ciascun lo dice;

Dove sia, nessun lo sa." *

Sleep is vital and universal, yet its essential biological functions remain elusive.

An unknown but crucial benefit must be provided, in order to balance the enormous risks to which an animal is exposed every time it disconnects from the external world during sleep, when it is unable to eat, mate, or escape predators, and thus diminishing apparently its Darwinian fitness.

Sleep pressure builds up as a function of elapsed waking time and decreases with sleep. The need to submit to this process is felt by any animal species endowed with a nervous system, from the *Cassiopea* jellyfish[1] to whales[2], though executed in diverse ways, depending on the ecological niche[2].

Since ancient times, understanding how night (or the mythological goddess Nyx) and sleep (her fatherless son Hypnos) interact has puzzled humanity.

A commonly used modern theoretical framework that captures essential features of sleep is the "two-process model"[3], which postulates that two main processes govern sleep and waking: the circadian clock and the sleep homeostat[3]. Oscillations of the circadian clock[4] (or process C) synchronise physiological processes, including wakefulness and sleep, with the Earth's rotation; they explain how organisms have adapted their habits to their habitats but fall short of elucidating the basic functions that underlie sleep.

The other process, sleep homeostasis (or process S), in contrast, responds to an internal process that generates sleep pressure, and once a set threshold is reached, enforces the periodic discharge of this pressure by initiating sleep.

Understanding the molecular nature of sleep pressure and its regulation by the homeostat is a burning quest of neuroscience as it would demystify physiological variables linked to the essential function of sleep[5].

* *"Like the phoenix: that it exists, they all say; where it may be, no one knows.",*
Wolfgang Amadeus Mozart and Lorenzo da Ponte (1790), Così fan tutte.

The two-process model remains the conceptual framework into which current findings on sleep[6,7] are placed, from the integration of cortical firing rates[8] to the -omics interactions of clock and sleep[9].

While the two-process model conceptualises sleep control, several hypotheses have been developed on the nature of the main or primary function of sleep.

One of the most widely appreciated theories on this topic is the "synaptic homeostasis hypothesis" (SHY), first postulated by Giulio Tononi and Chiara Cirelli[10] and based on theoretical considerations and experimental evidence in numerous studies[11–16]. According to SHY, sleep is the price to pay for synaptic plasticity[13]: as we are awake, synapses are overall strengthened by experience and interaction with the world; such potentiation would eventually increase cellular metabolic needs, decrease signal-to-noise ratios, and saturate learning. To prevent this, a period of disconnection from the external world, when the overall synaptic strengths can be scaled down and renormalized, while leaving relative synaptic strengths unaltered, is required: this period of disconnection is sleep.

An alternative group of theories, called "restorative theories", proposes that sleep repairs and replenishes necessary cellular components of the brain, to a condition present at the beginning of the previous period of waking[17]. While the details of each specific restorative hypothesis vary, some considered neuronal components that may be depleted during wakefulness, and others have proposed that some harmful compounds may be produced while awake, and need to be cleared with sleep. In fact, pioneering sleep deprivation studies showed "degenerative" changes in the nervous system[18].
Interestingly, the involvement of synapses and restoration of nerve cells, in fact, had been pinpointed already in the mid XX century, when Giuseppe Moruzzi proposed that neurons and synapses that are active during conscious experience undergo plastic synaptic and chemical changes that need to be restored with sleep[19].

In addition, since this need is likely to be felt by widespread circuits and neurons in the brain, Moruzzi postulated the necessity of centralised control, which would prevent spending "most of our life in a *dormiveglia*". Indeed, brain regions controlling sleep and wakefulness have been

identified, since pioneering work from Von Economo[20] and Moruzzi[21], in mammalian midbrain, posterior hypothalamus, and brainstem. In fact, modern neuroscience has identified in those regions, circuits and nuclei controlling sleep and wakefulness, whose mutual inhibition helps regulate sleep state switching[22,23]. A key brain region for sleep-control is the hypothalamic ventrolateral preoptic nucleus (VLPO), which is active during (NREM) sleep, and releases a cocktail of inhibitory neurotransmitters, mainly GABA and galanin, which inhibit ascending wake-promoting neurons[23,24]. VLPO itself is mutually inhibited by wake-active nuclei: this relationship of the arousal- and sleep-inducing projections generates the conditions for a "flip-flop" switch, leading to rapid and complete transitions between sleep and wake[23].

Not only is sleep centrally controlled by subcortical structures, but it is locally executed in the cortex[25,26], in a use-dependent fashion[27], and its need is encoded via intraneuronal chloride levels[28].

An alternative, but not mutually exclusive, hypothesis to the "flip-flop" circuit switch is the "somnogen" theory, which proposes the existence of sleep-inducing factors that are released as a function of time spent awake, and that induce sleep homeostatically[29]. While much attention has been given to adenosine as a potential somnogen[30], conflicting results have been reported[23].

However, whether the accumulation of sleep pressure is due to a recurrent mutual inhibitory circuitry, to the accumulation of a sleep-inducing substance, or to a combination of both, any homeostatic system needs 1) a sensor that tracks the state variable, 2) an integrator that accumulates the evidence as homeostatic pressure 3) an effector that responds to the pressure by executing actions that directly manipulate the state variable[31].

The search for the nature of these components is still ongoing.

1.2 Sleep in *Drosophila*

The invertebrate model fruit fly *Drosophila melanogaster* has been used for more than a century to interrogate life. Its exceptional genetic makeup, combined with an easy breeding that allows high statistical power, led to seminal discoveries in genetics and developmental biology.

With the advent of the molecular biology era and a novel vast arsenal of genetic tools available, *Drosophila* research has spearheaded the understanding of the cellular and molecular bases of behaviours. In addition, the recent releases of the fly brain's connectome[32,33] and the single-cell transcriptome of the full CNS[34–36] and body[37] have provided unprecedented level of detail to the neurobiological investigation.

Seminal findings in the field of circadian biology, for example, are an indisputable achievement of fly research[4], and their implications have been directly translated to other species, including humans[38].

Using flies for examining the other component of two-process model, instead, dates to more recent work[39,40].

Flies display all the key features of sleep: behaviourally they recapitulate reversible periodic quiescence[39,40], increased arousal thresholds[39,40], specific sleep posture[39,40], homeostatic control[39,40], impairment in learning and memory upon sleep loss[41]. At the molecular level, sleep is controlled by the same or analogous neurotransmitters[42] and stimulants[39,40] that regulate vertebrate sleep; fly brains respond to sleep loss by mobilising genetic pathways comparable to those found in rodents[39,43], and with similar consequences on synapses[14].

In more recent years, dynamic electrical signatures of sleep and wake states have been discovered in the fly brain[44–46] and in dedicated circuits[47], hinting towards a possibility of an electrical activity-based definition of sleep, rather than a purely behavioural account.

In fact, the current definition of sleep in flies relies solely on locomotor activity. The "golden rule" that has been used in most fly sleep studies since their foundation is that inactivity periods of 5 minutes or more can be scored as sleep[39,40,48]. Despite the apparently unsophisticated definition, this rule has provided solid results across locomotor activity tracking methods[49] and recent work has shown that a qualitative state transition in rest behaviour occurred around the time scale of 5 minutes[50].

Interestingly, while sleep disruption induced learning deficits, increasing sleep in flies by genetic or pharmacological interventions could reverse memory deficits in classical memory mutants[51] and in fly models of Alzheimer's disease[52].

The search for the neural substrates of sleep control in flies has led to the discovery of several brain regions modulating sleep. A primary one is the dorsal fan-shaped body, that I will describe in the next paragraph, as it is the main focus of this thesis (**Figure 1.1a**).

Downstream to dFB neurons, a population of wake-active neurons, called Helicon cells, receives visual inputs and conveys them to the ellipsoid body's R5, R3m and R3d neurons[53,54] (**Figure 1.1b**). The activity of these cells is gated by the release of the neuropeptide allatostatin A onto them from dFB neuron synapses, suggesting these neurons as crucial nodes for sensory gating[53,55,56].

Another sleep-control hub is the central complex's ellipsoid body, which is composed of several concentric subclasses of ring neurons; one of them, R5 neurons, were described as integrators of sleep pressure (**Figure 1.1b**). Sleep need is encoded in R5 enhanced activity, excitability and synaptic potentiation upon sleep loss[57]; in fact, sleep deprivation increases NMDAR in these neurons, which is necessary for driving the plastic synaptic changes[57]. Rhythmic oscillatory activity of these neurons has been observed, with peaks at 1 Hz, and the frequency range of 0.5-1.5 Hz ("delta power") increases until the onset of consolidated sleep or with sleep pressure[47]. NMDAR coincidence detection is also necessary for the correct synchronisation pattern and frequency distribution of these oscillations[47].
R5 neurons also sense paracrine signalling generated by astrocytes as a function of their Ca^{2+} oscillations[58], similarly to the astrocytic mechanisms of sleep[59] and circadian control[60] in mammals (**Figure 1.1b**).
Ring neurons' activity is conveyed to dFB neurons, along yet unexplored connections, in a recurrent activity network[53,56,57]; in fact, ring neurons receive inputs from helicon cells, which are post-synaptic to dFB neurons[53].
Within the ellipsoid body, two other cell subclasses lie downstream of helicon cells: the sleep-inducing R3m and wake-inducing R3d neurons (potentially inhibited by R3m neurons)[54] .

The dFB-helicon cell-R5 circuit generates intra-network coherent oscillations, that tune sleep and the visual arousal threshold[53,56].

Dopaminergic neurons in flies promote wakefulness[61–63], and are distributed in many clusters; however, the most studied ones are the PPL1 and PPM3 clusters, which project to the dFB[33,64–66] (Figure 1.1b). While a mutual interaction between dFB neurons and DANs has been anatomically described[33], reminiscent of a flip-flop model of mutual inhibition of sleep and wake-inducting circuits, no functional study has demonstrated it.

While mutations in the serotonin synthetic enzymes or in serotonin receptors reduced sleep, a circuit in the ellipsoid body that received serotonergic inputs only modulates sleep architecture[67]; however, when serotonin receptors were removed from dFB neurons, sleep and its homeostasis were impaired[68].

Octopaminergic neurons, akin to the serotonergic nuclei of the locus coeruleus, are wake-inducing in flies[69,70], and their activation impairs tracking of sleep need[63] (Figure 1.1b).

In addition to the mentioned brain regions, several other areas, previously known for their role in other behaviours, are involved in sleep (Figure 1.1b).

The well-studied fly circadian neurons give rise to sleep-wake patterns that feed into the purely sleep-control circuits[71].

The fly centres for associative memory, the mushroom bodies, also include sleep-control microcircuits[72]: sleep-inducing Kenyon cells (KCs) activate cholinergic Mushroom Body output neurons (MBONs)[73], and wake-promoting KCs[73] and dopaminergic neurons[74] (DANs) activate glutamatergic MBONs; the activity of the microcircuitry is enhanced upon sleep deprivation[73] and their synapses are plastically remodelled[75] (Figure 1.1b).

Furthermore, a neurosecretory region of the fly brain, *pars intercerebralis*, not only mediates wake-promoting octopamine inputs[70], but also secretes sleep-inducing SIFamide neuropeptides[76] (Figure 1.1b).

Finally, one of the latest central complex regions found to be sleep-controlling is the protocerebral bridge which includes sleep- and wake-promoting neurons, and receives dopaminergic inputs[77] (Figure 1.1b).

Interestingly, the peripheral nervous system seems involved in regulating sleep[78,79], too.

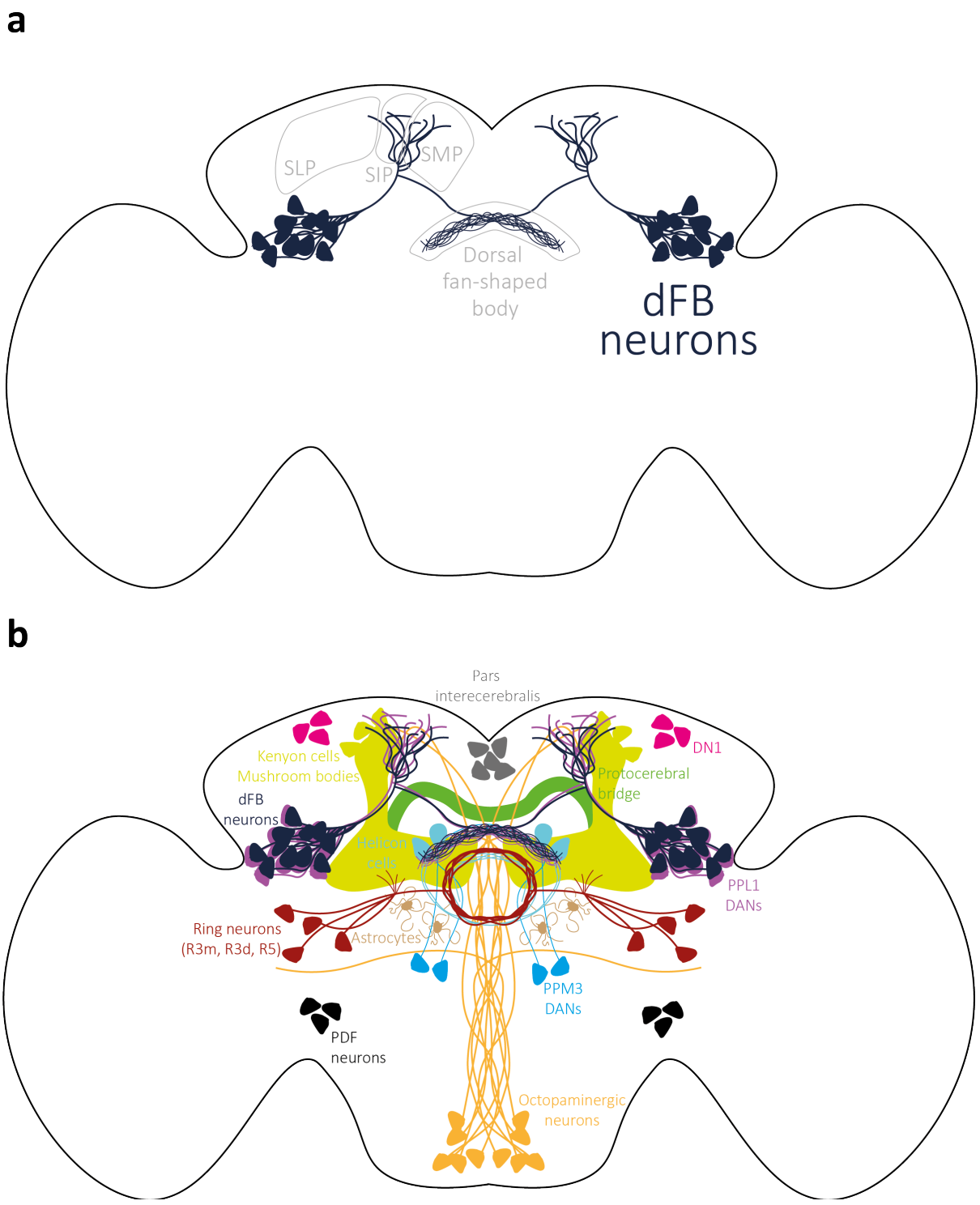

Figure 1.1 | Anatomical schematics of circuits and cell types controlling sleep and wakefulness in the *Drosophila* brain.
a, Anatomical schematics of dorsal fan-shaped body-projecting (dFB) neurons: somata, arborisations (mostly dendrites) in the superior medial, intermediate and lateral protocerebrum, and processes (mostly axons) in the dorsal fan-shaped body region.
b, Anatomical schematics of circuits and cell types controlling sleep and wakefulness. In particular: dFB neurons (Oxford blue), PPL1 DANs (purple), Kenyon cells and mushroom bodies (olive green), protocerebral bridge (emerald), pars intercerebralis (grey), circadian clock neurons including DN1 (fuchsia) and PDF neurons (black), helicon cells (turquoise), ring neurons (red), astrocytes (khaki), PPM3 DANs (azure), octopaminergic neurons (orange).

1.3 Dorsal fan-shaped body-projecting neurons

A brain region key to sleep control is the dorsal fan-shaped body (dFB).
A cluster of two dozen neurons innervating this area shows all the necessary features for being described as sleep-controlling: they are sufficient[80] and also necessary[79] to induce sleep, upon chronic and acute activation or inactivation (cf. **Chapter 4**), and physiologically their electrical activity is modulated by sleep pressure[66,81]. Artificial activation of these neurons decreases behavioural responsiveness[82], and consolidates sleep and memory[80].
dFB neurons possess dendrites mostly located in the superior medial, intermediate and lateral protocerebrum (SMP, SIP, SLP) areas, and axons mainly in the dFB[53], however pre- and post-synaptic sites can be localised in both regions[33,53] (**Figure 1.1a**).

Two potassium channels dominate dFB neurons' electrical activity: the voltage-gated Shaker, and the leak channel Sandman.
Specifically, binding of dopamine to Dop1R2 membrane receptors of dFB neurons rapidly induces the fusion of intracellular vesicles containing a voltage-independent two-pore domain potassium leak (K_2P) channel termed Sandman with the cell membrane, which hyperpolarises the neurons[66]. The dFB neurons can be arrested in a similar non-spiking state by mutating the Rho-GTPase-activating protein crossveinless-c (*cv-c*): homozygous carriers suffer severely reduced, fractured sleep, and loss of sleep rebound, caused by a large potassium shunt, presumably the result of Sandman's defective endocytosis[66,81].
Shaker's redox-sensitive β-subunit Hyperkinetic instead contributes to temporal integration of time spent awake via sensing oxidative by-products of mitochondrial metabolism. As sleep pressure builds up, reactive oxygen species and their by-products are produced, and Hyperkinetic, which is an aldo-keto reductase, is converted to its $NADP^+$-bound form; this slows the A-type current inactivation, and produces heightened neuronal excitability, driving sleep[83].

These neurons receive diverse inputs: a group of circadian pacemaker neurons activates dFB neurons via excitatory synaptic connections[84]; dopaminergic neurons project to the dFB and are recurrently synaptically connected to those cells[33,64,66,84], and induce wake. About a third

of dFB neurons receive octopaminergic inputs[33], and serotonin receptors in a single pair of these cells are necessary for sustaining sleep and its homeostasis[68] (Figure 1.1a).
In addition to monoamines, dFB neurons respond to several neuropeptidergic inputs: the antimicrobial peptide nemuri[85], which prolongs sleep, accumulates in this region; hugin^{+} neurons, downstream of clock cells, project to dFB neurons[86]; cells releasing the feeding- and wakefulness-promoting neuropeptide F project to the fan-shaped body[87].

dFB is therefore a crucial hub for integrating states (arousal, immune condition, feeding status, circadian inputs, etc…), and translating them into sleep outputs[88].

In terms of outputs, to impose sleep on the organism, dFB neurons release the inhibitory neuropeptide allatostatin A, which inhibits helicon cells[53]. Also, dFB neurons inhibit arousal-promoting octopaminergic (likely VPM3 neurons)[33,84] and are synaptically connect to intra-FB columnar neurons hΔK, hΔF, and PFG cells[33] (Figure 1.1a).

These neurons show voltage[56] and calcium[89] oscillations in the 0.5-1.5 Hz range, which increase during the night[56] and with higher sleep pressure[89], and can be entrained by R5 neurons[56]. dFB oscillations can also be recorded as LFP oscillations in the 6-15 Hz band, which propagate through the brain[45]. This oscillatory activity is probably orchestrated by mutual synaptic contacts among dFB cells[33] and via electrical coupling mediated by gap junctions[82].

dFB neurons share numerous parallels with cells in the mammalian hypothalamic ventrolateral preoptic (VLPO) nucleus: dFB neurons' activity increases as sleep need accrues[66,81,83,90,91], they mediate sensitivity to general anaesthetics[92], are inhibitory and inhibit arousal centres[22,23,53], and release AstA, whose cognate receptor homolog is the receptor for the sleep homeostasis-controlling mammalian neuropeptide galanin, expressed in the preoptic area[24,93–96].

In conclusion, dFB neurons, similarly to VLPO hypothalamic neurons, modulate sleep via a combination of cell-autonomous and network mechanisms.

1.4 Aims of this thesis

Questions regarding sleep and its homeostasis can be then reduced to the study of the regulation of the electrical activity of dFB neurons.

While the ion channels involved are known, less is understood about the underlying molecular machinery.

To uncover the signalling pathways involved in sleep control, I aimed at obtaining the transcriptome of sleep-control dFB neurons (Chapter 3), which will unveil, in an unbiased and hypotheses-generating fashion, cellular and molecular features.

The data generated by my transcriptomics analysis will shed light on three broad topics.

- Novel cell markers (Chapter 4)
- Sleep history-dependent changes (Chapter 5)
- Functional heterogeneity (Chapter 6)

Interesting leads in each of these directions will then be pursued in targeted studies.

2 Materials and Methods

2.1 Reagents

2.1.1 Antibodies

Reagent	Source	Identifier
Mouse nc82 anti-brp	DSHB	RRID: AB_2314866
Chicken anti-GFP	Abcam	RRID: AB_10561923
Mouse anti-V5	Thermo Fisher Scientific	RRID: AB_2556564
Goat anti-Chicken Alexa 488	Thermo Fisher Scientific	RRID: AB_2534096
Goat anti-Mouse Alexa 546	Thermo Fisher Scientific	RRID: AB_2534089
Goat anti-Mouse Alexa 633	Thermo Fisher Scientific	RRID: AB_2535719

2.1.2 Chemicals

Reagent	Source	Identifier
Paraformaldehyde 20% solution, EM Grade	Electron Microscopy Sciences	15713-S
All-*trans* retinal	Molekula	52326571
Dimethyl sulfoxide (DMSO)	Sigma-Aldrich	D2650
DPBS (calcium and magnesium free)	Thermo Fisher Scientific	14190169
Papain	Sigma	P4762
Collagenase	Sigma	C2674
d(-)-2-amino-5-phosphonovaleric acid (AP5)	Sigma	A8054
6,7-dinitroquinoxaline-2,3-dione (DNQX)	Sigma	D0540
Tetrodotoxin (TTX)	Abcam	ab120054
20 µm CellTrics strainer	Sysmex	04-0042-2315
Schneider's *Drosophila* Medium (+ L-Glutamine)	Thermo Fisher Scientific	21720024
Protein LoBind Tube	Eppendorf	30108116
Normal goat serum (NGS)	Sigma	G9023
Phosphate buffered saline tablets	Oxoid	BR0014G
Vectashield antifade mounting medium	Vector Laboratories	H-1000
TritonX-100	Sigma	T8787
Sodium chloride	Sigma-Aldrich	S7653
Potassium chloride	Sigma-Aldrich	P9333
TES	Sigma	T5691
D-(+)-Trehalose dihydrate	Sigma	T9531
D-(+)-Glucose	Sigma	G7528
Sucrose	Sigma	S0389
Sodium bicarbonate	Sigma-Aldrich	S6297
Sodium phosphate monobasic	Sigma-Aldrich	S8282

Calcium chloride solution	Sigma	21115
Magnesium chloride solution	Fluka	63020
pCFD6 plasmid	Addgene	73915
BbsI-HF®	NEB	R3539
CutSmart buffer	NEB	B7204
Nuclease-free water	Invitrogen	7732-18-5
REDTaq® ReadyMix™ PCR Reaction Mix	Sigma-Aldrich	R2523
Phusion® High-Fidelity PCR Master Mix with HF Buffer	NEB	M0531
NucleoSpin Gel and PCR Clean up Columns for gel extraction and PCR clean up	Macherey-Nagel	740609
NucleoSpin Tissue, Mini kit for DNA from cells and tissue	Macherey-Nagel	740952.50
One Shot™ TOP10 Chemically Competent E. coli	Thermo Fisher Scientific	C404006
Gibson Assembly® Cloning Kit	NEB	E5510
Agar	Fisher BioReagents	BP2641-500
LB Broth (Lennox), Tablet microbial growth medium	Sigma-Aldrich	L7275-500TAB
Ethidium bromide solution	Sigma-Aldrich	E1510
TAE Buffer, Tris-Acetate-EDTA, 50X Solution, Electrophoresis, Fisher BioReagents™	Thermo Fisher Scientific	BP13324
FastGene Molecular Biology Grade Agarose	FastGene®	A4-0746
Fisher Bioreagents 5 GR Carbenicillin Disodium Salt	Fisher Bioreagents	12737149
100bp DNA Ladder Plus	NBS	NBS-LP100
DNA primers	Sigma	N/A

2.1.3 Fly Strains

Genotype *(abbreviation)*	Source	Identifier
Canton-S *(CS* or *+)*	Miesenböck lab (University of Oxford)	N/A
w[1118]; P{y[+t7.7] w[+mC]=GMR23E10-GAL4}attP2 *(R23E10-GAL4)*	BDSC	RRID:BDSC_49032
w[1118]; P{y[+t7.7] w[+mC]=GMR23E10-lexA}attP40 *(R23E10-LexA)*	BDSC	RRID:BDSC_52693
w[1118]; P{y[+t7.7] w[+mC]=R23E10-GAL4.DBD}attP2/TM3, Sb[1] *(R23E10-DBD)*	BDSC	RRID:BDSC_69269
20XUAS-6XGFP @VK00018 *(UAS-6xEGFP)*	Stowers lab (Montana State University)	[97]
y[1] w[*]; Mi{Trojan-p65AD.2}Gad1[MI09277-Tp65AD.2]/TM6B, Tb[1] *(Gad1-AD)*	BDSC	RRID:BDSC_60322
w[*]; Mi{Trojan-p65AD.2}VGlut[MI04979-Tp65AD.2]/CyO *(VGlut-AD)*	BDSC	RRID:BDSC_82986

w[1118]; P{y[+t7.7] w[+mC]=R59E04-p65.AD}attP40 *(VAChT-AD)*	BDSC	RRID:BDSC_71191
w[*]; P{w[+mC]=UAS-Hsap\KCNJ2.EGFP}1 *(UAS-K_{ir}2.1)*	BDSC	RRID:BDSC_6596
20XUAS-IVS-CsChrimson::tdTomato @VK00005 *(UAS-CsChrimson::tdTomato)*	Jayaraman lab (Janelia Research Campus)	RRID:Addgene_111545[98] (origin plasmid)
w[*]; P{y[+t7.7] w[+mC]=UAS-TrpA1(B).K}attP16 *(UAS-TrpA)*	BDSC	RRID:BDSC_26263
Mi{Trojan-3XGAL80.2}VGlut[MI04979-T3XG80.2] *(VGlut-3xGAL80)*	BDSC	RRID:BDSC_60316
w[*]; P{y[+t7.7] w[+mC]=VGlut-GAL80.V}attP40/CyO; TM6B, Tb[1]/TM3, Sb[1] *(VGlut-GAL80)*	BDSC	RRID:BDSC_58448
w[1118]; P{w[+mC]=UAS-myr-mRFP}2/TM6B, Tb[1] *(UAS-myr::RFP)*	BDSC	RRID:BDSC_7119
w[*]; P{y[+t7.7] w[+mC]=10XUAS-IVS-myr::tdTomato}attP40 *(UAS-tdTomato)*	BDSC	RRID:BDSC_32222
P{UAS-CD4-tdTom}7M1 *(UAS-CD4:tdTomato)*	BDSC	RRID:BDSC_35841
w[*]; P{w[+mC]=lexAop-rCD2-GFP}2 *(LexAop-GFP)*	BDSC	RRID:BDSC_66687
w[1118]; P{y[+t7.7] w[+mC]=20XUAS-iGluSnFR.A184V}attP2 *(UAS-iGluSnFR(A184V))*	BDSC	RRID:BDSC_59611
y[1] v[1]; P{y[+t7.7] v[+t1.8]=TRiP.JF02689}attP2 *($VGlut^{RNAi\ \#27538}$)*	BDSC	RRID:BDSC_27538
y[1] sc[*] v[1] sev[21]; P{y[+t7.7] v[+t1.8]=TRiP.HMS02175}attP40 *($VGlut^{RNAi\ \#40927}$)*	BDSC	RRID:BDSC_40927
P{KK107498}VIE-260B *($VGlut^{RNAi\ 104324KK}$)*	VDRC	104324
w[1118]; P{GD834}v2574/TM3 *($VGlut^{RNAi\ 2574GD}$)*	VDRC	2574
w[*]; P{w[+mC]=UAS-TeTxLC.tnt}G2 *($UAS\text{-}TNT_{Active}$)*	BDSC	RRID:BDSC_28838
w[*]; P{w[+mC]=UAS-TeTxLC.(-)V}A2 *($UAS\text{-}TNT_{Inactive}$)*	BDSC	RRID:BDSC_28840
w[1118]; P{y[+t7.7] w[+mC]=20XUAS-IVS-GCaMP6f}attP40 *(UAS-GCamp6f)*	BDSC	RRID:BDSC_42747
LexAOP-CD8::GFP; UAS-flp, PBac{y[+mDint2]w[+mc] = brp(FRT.Stop)V5-2A-LexA-VP16} (*LexAop-GFP; UAS-STaR*)	Zipursky and Donlea labs (UCLA)	[99]
w[1118]; P{y[+t7.7] w[+mC]=GMR69F08-GAL4}attP2	BDSC	RRID:BDSC_39499

w[*]; P{w[+mW.hs]=GawB}OK107 ey[OK107]/In(4)ci[D], ci[D] pan[ciD] sv[spa-pol] (*OK107-GAL4*)	BDSC	RRID:BDSC_854
w[1118]; P{w[+mC]=UAS-mito-HA-GFP.AP}2/CyO (*UAS-mito-HA-GFP*)	BDSC	RRID:BDSC_8442
y[1] w[1118]; P{w[+mW.hs]=GawB}GH146	BDSC	RRID:BDSC_30026
UAS-AOX.F24 (*UAS-AOX*)	Jacobs lab (Tampere University)	[100]
UAS-Drp1	Feany lab (Harvard Medical School)	[101]
w[*]; P{w[+mC]=UAS-Drp1.D}3 *(UAS-Drp1.D)*	BDSC	RRID:BDSC_51647
UAS-Drp1-HA	Chung lab (Seoul National University)	[102]
UAS-Opa1-FLAG	Chung lab (Seoul National University)	[102]
UAS-Marf-FLAG	Chung lab (Seoul National University)	[102]
y[1] w[*]; P{w[+mC]=UAS-Marf.HA.S}3/T(2;3)TSTL, CyO: TM6B, Tb[1] *(UAS-Marf-HA)*	BDSC	RRID:BDSC_67157
w1118; P{GD11094}v40478 (*UAS-Marf$^{RNAi\ 40478GD}$*)	VDRC	40478
P{KK105681}VIE-260B (*UAS-Marf$^{RNAi\ 105261KK}$*)	VDRC	105261
y[1] sc[*] v[1] sev[21]; P{y[+t7.7]v[+t1.8]=TRiP.HMC03883}attP40 (*UAS-Marf$^{RNAi\ \#55189}$*)	BDSC	RRID:BDSC_55189
UAS-smMarf (II)	Guo lab (UCLA)	[103]
UAS-smMarf (III)	Guo lab (UCLA)	[103]
w[*]; Bl[1]/CyO; P{w[+mC]=UAS-Opa1.miRNA.CDS}3 (*UAS-Opa1$^{miRNA.CDS}$*)	BDSC	RRID:BDSC_67159
P{KK105706}VIE-260B (*UAS-Opa1$^{RNAi\ 106290KK}$*)	VDRC	106290
P{VSH330266}attP40 (*UAS-Opa1$^{shRNA\ 330266SH}$*)	VDRC	330266
y[1] sc[*] v[1] sev[21]; P{y[+t7.7] v[+t1.8]=TRiP.HMS00349}attP2 (*UAS-Opa1$^{RNAi\ \#32358}$*)	BDSC	RRID:BDSC_32358
UAS-smOpa1 (X)	Guo lab	[103]

	(UCLA)	
UAS-smOpa1 (II)	Guo lab (UCLA)	[103]
UAS-smOpa1 (III)	Guo lab (UCLA)	[103]
w1118; P{GD3283}v5492 (*UAS-Miga*$^{RNAi\ 5492GD}$)	VDRC	5492
P{KK102948}VIE-260B (*UAS-Miga*$^{RNAi\ 110737KK}$)	VDRC	110737
y[1] sc[*] v[1] sev[21]; P{y[+t7.7] v[+t1.8]=TRiP.GL00111}attP2 (*UAS-zuc*$^{RNAi\ \#35227}$)	BDSC	RRID:BDSC_35227
w1118; P{GD7487}v38626 (*UAS-Pld*$^{RNAi\ 38626GD}$)	VDRC	38626
P{KK102153}VIE-260B (*UAS-Octβ1R*$^{RNAi\ 110537KK}$)	VDRC	110537
w[1118] P{GD701}v47895 (*UAS-Octβ1R*$^{RNAi\ 47895GD}$)	VDRC	47895
w1118; P{GD701}v47896 (*UAS-Octβ1R*$^{RNAi\ 47896GD}$)	VDRC	47896
P{KK107078}VIE-260B (*UAS-Octβ3R*$^{RNAi\ 101189KK}$)	VDRC	101189
w1118; P{GD3923}v9068 (*UAS-Octβ3R*$^{RNAi\ 9068GD}$)	VDRC	9068
P{KK111871}VIE-260B (*UAS-Octβ3R*$^{RNAi\ 102515KK}$)	VDRC	102515
P{KK111828}VIE-260B (*UAS-Octβ3R*$^{RNAi\ 106519KK}$)	VDRC	106519
P{KK111456}VIE-260B (*UAS-Oamb*$^{RNAi\ 106511KK}$)	VDRC	106511
w1118; P{GD696}v2861 (*UAS-Oamb*$^{RNAi\ 2861GD}$)	VDRC	2861
P{KK112557}VIE-260B (*UAS-Octβ2R*$^{RNAi\ 104050KK}$)	VDRC	104050
P{KK109808}VIE-260B (*UAS-Octβ2R*$^{RNAi\ 104524KK}$)	VDRC	104524
P{KK113910}VIE-260B (*UAS-Octβ2R*$^{RNAi\ 106912KK}$)	VDRC	106912
w1118; P{GD13188}v26876 (*UAS-Oct-TyrR*$^{RNAi\ 26876GD}$)	VDRC	26876
w1118; P{GD13188}v26877 (*UAS-Oct-TyrR*$^{RNAi\ 26877GD}$)	VDRC	26877

w[1118]; P{y[+t7.7] w[+mC]=R19G08-p65.AD}attP40 (*Octβ1R-AD*$^{\#70104}$)	BDSC	RRID:BDSC_70104
w[1118]; P{y[+t7.7] w[+mC]=VT045793-p65.AD}attP40 (*Octβ1R-AD*$^{\#71441}$)	BDSC	RRID:BDSC_71441
w[1118]; P{y[+t7.7] w[+mC]=VT040542-p65.AD}attP40 (*Octβ3R-AD*$^{\#72058}$)	BDSC	RRID:BDSC_72058
w[1118]; P{y[+t7.7] w[+mC]=VT040541-p65.AD}attP40/CyO (*Octβ3R-AD*$^{\#71436}$)	BDSC	RRID:BDSC_71436
w[1118]; P{y[+t7.7] w[+mC]=R49C04-p65.AD}attP40 (*Oamb-AD*$^{\#71075}$)	BDSC	RRID:BDSC_71075
w[1118]; P{y[+t7.7] w[+mC]=VT040576-p65.AD}attP40 (*Octβ2R-AD*$^{\#71552}$)	BDSC	RRID:BDSC_71532
w[1118]; P{y[+t7.7] w[+mC]=VT034615-p65.AD}attP40 (*Oct-TyrR-AD*$^{\#71334}$)	BDSC	RRID:BDSC_71334
w[1118]; P{y[+t7.7] w[+mC]=R68B06-p65.AD}attP40; MKRS/TM6B, Tb[1] (*Oct-TyrR-AD*$^{\#70787}$)	BDSC	RRID:BDSC_70787
w[1118]; PBac{w[+mC]=IT.GAL4}CG6145[0665-G4] (*0665-GAL4*)	BDSC	RRID:BDSC_63739
w[1118]; PBac{w[+mC]=IT.GAL4}CG13627[0891-G4] (*0891-GAL4*)	BDSC	RRID:BDSC_63876
w[1118]; P{y[+t7.7] w[+mC]=R24E06-p65.AD}attP40; P{y[+t7.7] w[+mC]=R95A10-GAL4.DBD}attP2 (*MB021B*)	BDSC	RRID:BDSC_68297
w[1118]; P{y[+t7.7] w[+mC]=R24E06-p65.AD}attP40; P{y[+t7.7] w[+mC]=Tdc2-GAL4.DBD}attP2 (*MB022B*)	BDSC	RRID:BDSC_68298
UAS-4xOctβ1R^{sgRNA} (II) @attP40	This work	N/A
UAS-4xOctβ1R^{sgRNA} (III) @attP2	This work	N/A
UAS-4xOctβ3R^{sgRNA} (II) @attP40	This work	N/A
UAS-4xOctβ3R^{sgRNA} (III) @attP2	This work	N/A
P{ry[+t7.2]=hsFLP}12, y[1] w[*]; P{y[+t7.7] w[+mC]=UAS-u^{L}Cas9}attP40 (*UAS-u^{L}Cas9*)	Port lab, CRISPR fly design (German Cancer Research Center)	[104]
y[1] w[*]; P{w[+mC]=tubP-GAL4}LL7/TM3, Sb[1] Ser[1] (*tub-GAL4*)	BDSC	RRID:BDSC_5138
CS; UAS-myrGFP; QUAS-mtdTomatoX3HA; Trans-Tango	Jepson and Gilestro labs (University College London and Imperial College London)	[105]

2.2 Drosophila culture

Fly stocks were grown on medium containing sucrose, yeast, molasses, and agar under a 12 h light:12 h dark cycle at 25 °C with 60% relative humidity, unless otherwise indicated. All studies were performed on randomly selected females aged 2–6 days post-eclosion. Genetic crosses for behavioural studies were performed with 8 virgin female and 4 male flies.

Crosses for optogenetics experiments were prepared in vials wrapped in aluminium foil to prevent activation of CsChrimson by ambient light; the resulting experimental female flies were reared in darkness and, at 1-2 days post-eclosion, transferred onto food supplemented with 2 mM all-trans retinal in DMSO, or DMSO only, 2 days prior to the experiments.

2.3 Sleep measurements

Females aged 2–4 days were individually inserted into 65-mm glass tubes containing food reservoirs, loaded into the Trikinetics Drosophila Activity Monitor system (Trikinetics Inc; Waltham MA, USA), and housed under 12 h light:12 h dark conditions with 60% relative humidity and at 25 °C, unless otherwise indicated. Flies were allowed to habituate for at least one day before sleep measurement.

Movement was detected when flies crossed the infrared light beams bisecting the glass tubes; 5-minute periods without beam breaks were scored as sleep[39,40]. Trikinetics activity records were analysed using the Sleep and Circadian Analysis MATLAB Program (S.C.A.M.P.) scripts (Vecsey lab, Skidmore College). Immobile flies (<2 beam breaks per 24 h) were excluded from the analysis.

2.3.1 Open-Loop optogenetics

Female flies were individually inserted into 65-mm glass tubes and loaded into a custom-built array of light-tight chambers, which were each equipped with a high-power LED (Multicomp OSW-4388, 630 nm)[53]. The apparatus was operated in a temperature-controlled incubator (Sanyo MIR-154) at 25 °C, in dark-dark cycle and 60% humidity. For movement tracking, the chambers were continuously illuminated from below using low power infrared (850 nm) LEDs and imaged from above with a high-resolution CMOS camera (Thorlabs DCC1545M), using an 8-mm lens (Thorlabs MVL8M23) and a long-pass filter (Thorlabs, FEL800nm) to reject photostimulation light. A virtual instrument written in LabVIEW 9 (National Instruments)

extracted real-time position data from video images by subtracting the most recently acquired image from a temporally low-pass filtered background. Non-zero pixels in the difference image indicated that a movement had occurred, with the centroid of the largest cluster of non-zero pixels taken to represent the fly's new position. To eliminate noise, intensity and size thresholds were applied to pixel clusters in the difference image, and movements < 2.5 mm were discarded. If no movement was detected, the fly was assumed to have remained at its last known location. Open-loop stimulation used trains of 10 pulses of 3 ms light (28 mW cm^{-2}) at 20 Hz, repeated every second, for 12 h. Continuously immobile flies (>29.5 min of sleep per 30-min bin for more than 3 consecutive bins until the end of the recording) were excluded from the analysis from the onset of immobility onwards.

2.3.2 Thermogenetics

Genetic crosses and flies used for thermogenetic studies were cultured and kept at 21 °C, and the temperature was raised to 29 °C for 24 h only during the activation day.

2.3.3 Sleep deprivation

Flies were mechanically sleep deprived in Trikinetics monitors placed on a spring-loaded platform (Sleep Nullifying Apparatus, or SNAP machine) which was slowly tilted by an electric motor, released, and allowed to snap back to its original position[106,107] (every 10 seconds) for 12 h during the dark phase.

For the experiment in Figure 5.9, sleep deprivation was performed mechanically via horizontal shaking using Talboys Multi-Tube Vortexer with 3.5 units of speed, delivered for 2 s randomly within 20 s bins, for 12 h during the dark phase.

After the exclusion of dead flies, quantification of sleep rebound was performed only on flies that lost at least 95% of their sleep during the sleep deprivation period, compared to the corresponding baseline time. Cumulative sleep lost/gained was internally normalised for each genotype by subtracting the mean sleep lost during the first bin to all time bins, and dividing them all by the total cumulated sleep lost reached at the last bin of the sleep deprivation period. Sleep rebound was calculated by subtracting sleep during the baseline day to the sleep during the rebound day, and normalising it as percentage to the sleep during baseline day.

2.4 Single-cell transcriptomics

2.4.1 Brain dissociation and cell collection for single-cell RNA-sequencing

Fly brains were dissected and dissociated as previously described[34]: on each experimental day, around 320 brains of sleep deprived and rested female flies were dissected, in parallel, in toxin-supplemented (50 mM d(-)-2-amino-5-phosphonovaleric acid, 20 mM 6,7-dinitroquinoxaline-2,3-dione and 0.1 mM tetrodotoxin) calcium- and magnesium-free DPBS (tDPBS) and immediately transferred into Protein LoBind microcentrifuge tubes with Schneider's medium supplemented with the same toxins (tSM), on ice. Brains were washed once with 1 ml tSM and incubated in tSM containing 1.11 mg ml^{-1} papain and 1.11 mg ml^{-1} collagenase I. Brains were washed once more with tSM and subsequently triturated with flame-rounded 200 µl pipette tips. Dissociated brain cells were resuspended in 1 ml DPBS and filtered through a 20 µm CellTrics strainer. Single cells were isolated by flow cytometry (FACS), and both the $EGFP^{+}$ fraction and the $EGFP^{-}$ flow-through were collected for sequencing. Samples were submitted immediately after sorting to the single-cell RNA-sequencing facility, deploying droplet microfluidics (10X Chromium v3 and v3.1) single-cell technology, followed by NovaSeq6000 sequencing, where samples from each replicate were multiplexed in the same round. Brains and dissociated cells were kept on ice or at ice-cold temperatures from dissection to sample submission, including during the FACS sorting procedure.

2.4.2 scRNA-seq data processing, alignment and analysis

Cell barcodes were extracted as previously described[34,108–110] and corresponding reads were aligned with STAR's default parameters, to a combination of the *Drosophila melanogaster* genome release BDGP6.22 and the reference sequence of the GAL4 and EGFP-$p10^{3'UTR}$ transgenes used in this study[97]. The Flybase v. FB2018_03 gene names were used for gene annotation.

The cumulative fraction of reads plotted as a function of the cell barcodes sorted by number of reads in descending order was visually inspected for each alignment, and only the fraction of cells with a high number of reads up to the inflection points was selected for the next steps, to discard beads with low reads, potentially ambient RNA.

All subsequent analyses were performed in R, using the Seurat package.

Three independent biological replicates, collected on different days and from independent genetic crosses, were merged, variation driven by individual batches was regressed out, and data were normalised (gene counts for each cell were divided by the total counts for that cell and multiplied by 10,000).

Standard quality filtering for fly neurons was applied[34,111]: genes detected in fewer than 3 cells and cells expressing fewer than 3 genes were filtered out, and only cells with 800 - 10,000 UMIs per cell and 200 – 5000 genes per cell were analysed. 10,000 genes were used as variable features.

Data were integrated using 50 dimensions, followed by PCA analysis. To visualise the data, Uniform Manifold Approximation and Projection (UMAP) dimensionality reduction was performed, using 50 dimensions. Clusters were identified by constructing a Shared Nearest Neighbor graph and applying the Louvain algorithm as modularity optimisation technique, with resolution 0.2. Clusters were manually annotated according to known cell markers (see Appendix 9.1 for details). For the re-clustering of neurons expressing only specific fast-acting neurotransmitters, KCs, and PNs, 150 genes were used as variable features.

2.4.3 Differential gene expression analysis and gene ontology

Differentially expressed genes were identified in Seurat via the "FindMarkers" function, using the "RNA assay" counts of the two cell groups compared, and all the genes of the full brain dataset detected in at least 1% of cells in either population, and which showed, on average, at least 0.01-fold difference (log-scale) between the two groups of cells. Differentially expressed genes were statistically tested with Wilcoxon Rank Sum test and the p-value was adjusted using Bonferroni correction based on the total number of variable genes in the dataset.

Gene ontology was performed on the identified differentially expressed genes using PANTHER v17 for the Fold enrichment, while ViSEAGO 1.4.0 and topGO 2.42.0 for the heatmaps: PANTHER Overrepresentation Test (released 2022-07-12) was run with the *Drosophila melanogaster* reference list (10.5281/zenodo.6799722, released 2022-07-01) and reactome (version 65, released 2021-10-01), and statistically analysed using Fisher's Exact test with False Discovery Rate correction. The ViSEAGO and topGO packages were used to analyse the enrichment of gene ontology terms (annotated in Ensembl) in the set of significantly

differentially expressed genes identified with Seurat vis-à-vis a reference set of all variable genes used in Seurat and only GO terms with more than 40 attached genes were considered[112]; enriched GO terms with unadjusted $p < 0.001$ were clustered hierarchically according to Wang's distance in the heatmaps.

2.5 *In vivo* two-photon imaging

Mated female flies aged 3-4 days were head-fixed to a custom mount with eicosane (Sigma), and cuticle, adipose tissue, and trachea were removed to gain optical access to the brain. The preparation was superfused with extracellular carbogenated solution (95% O_2 – 5% CO_2) containing 103 mM NaCl, 3 mM KCl, 5 mM TES, 8 mM trehalose, 10 mM glucose, 7 mM sucrose, 26 mM $NaHCO_3$, 1 mM NaH_2PO_4, 1.5 mM $CaCl_2$, 4 mM $MgCl_2$, pH 7.3.

Two-photon imaging was performed using a movable objective resonant scanning microscope (MOM, Sutter Instruments), controlled through ScanImage software (Vidrio Technologies) running on MATLAB R2015a.

iGluSnFR(A148V) and GCaMP6f fluorophores were excited by a MaiThai DeepSee two-photon laser (Spectra Physics; 80 fs pulse width; centre wavelength of 930 nm) and the laser power was modulated via a Pockels cell (302RM, Conoptics). Emitted photons were collected by a 20X 1.0 NA water immersion objective (W-Plan-Apochromat, Zeiss) and emission paths for green and red signals were separated by a dichroic mirror, followed by bandpass filters (ET525/70 (490-560 nm) #259655 for green; ET605/70 (570-640 nm) M-2P (#262191) for red), and detected by GaAsP photomultiplier tubes (H10770PA-40 SEL, Hamamatsu Photonics). Photocurrents were passed through high-speed amplifiers and custom-designed integrator circuits to maximize the signal-to-noise ratio. Images were acquired at a rate of 208.56 Hz (128X60 pixels).

Light pulses (repeated every 2 s, 40 per fly) for optogenetic stimulation were delivered by a 625 nm LED (M625L3, ThorLabs) controlled by a dimmable LED driver (ThorLabs) and focused on the head of the fly. The red-light beam was passed through a 647/57 nm bandpass filter (Brightline Semrock) to avoid contamination of the green emission path of the 2-photon microscope. The voltage steps to trigger the LED were produced via a Digidata 1440 digitizer and recorded in a separate imaging channel for post-hoc alignment. The light source delivered 11–80 mW cm^{-2} of optical power.

Regions of interest (ROIs) were selected manually using Fiji and the mean pixel intensity in the ROI was computed for each frame. All subsequent pre-processing and analyses were performed using MATLAB (R2017b). Background-subtraction was performed by element-wise subtraction of a time varying background signal (from a non-fluorescent ROI) from the raw fluorescence traces. ΔF/F curves from the resulting signals were calculated separately for each light pulse as $\Delta F_t/F_0 = (F_t - F_0)/F_0$, where F_0 is the mean fluorescence intensity of 1043 frames (5 s) for the arousal experiment and 63 (0.3 s) frames for the optogenetics experiment prior to the stimulus and F_t is the fluorescence intensity at frame t. The stimulus-aligned $\Delta F_t/F_0$ signals were averaged across trials. The signals were then averaged across flies (mean and SEM shown in Figure 4.12 and Figure 4.13 were computed over flies). For illustration purposes, traces were smoothed by a hundred-element (Figure 4.12) and twenty-element (Figure 4.13) moving average filter.

For the delivery of an arousing stimulus, an infrared beam focused onto the fly's abdomen was used. The infrared LED (Thorlabs, 808 nm) was mounted on a temperature-controlled heat sink (ThorLabs LDC210C Laser Diode controller 1A heat sink and ThorLabs TED200C temperature controller) and controlled by a ThorLabs LDC210C laser diode controller. The controller attenuated the current to this high-powered LED to below 250 mA, which resulted in a maximum power of 50 mW. The voltage signal to trigger the LED controller was generated on an Arduino board controlled by custom LabVIEW software.

2.6 Brain dissections, staining and confocal imaging

Fly brains and ventral nerve cords were dissected in phosphate buffer saline (PBS), immediately transferred to Eppendorf tubes on ice, and fixed in 4% (w/v) paraformaldehyde (PFA) diluted in 0.3% (v/v) TritonX-100 in PBS (PBST) for 20 min on a nutator, then quickly washed twice and then three times rocking for 20 min each, with PBST.

For immunostaining, brains were then incubated on a nutator in blocking solution containing 10% normal goat serum in 0.3% PBST at 4 °C overnight, with primary antibody diluted in blocking solution at 4 °C for 2-3 days (nc82 1:10, chicken anti-GFP 1:1000 or 1:500 for STAR, anti-V5 1:400), washed with PBST five times, and incubated with the secondary antibody dissolved in blocking solution, at 4 °C for two days (Alexa 546 anti-mouse 1:1000, Alexa 488 anti-goat 1:1000 or 1:500 for STAR, Alexa 633 anti-mouse 1:500). Finally, they were washed as

before, mounted in Vectashield and imaged on a Leica TCS SP5 confocal microscope using an HCX IRAPO L 25x/0.95 water immersion objective. Microscopy images were not acquired if the anatomical structures of interest were damaged during dissection or if flies had died during sleep deprivation.

2.6.1 Mitochondria morphometric analysis

Mitochondria were labelled by GFP fused to a mitochondrial protein localisation tag, expressed in the brain structures of interest. Fly brains were dissected and fixed as described, and mounted in Vectashield.

Anatomical regions of interest were imaged on a Leica TCS SP5 confocal microscope using a HCX IRAPO L 25x/0.95 water immersion objective, and fully acquired at the Nyquist limit resolution as Z-stacks[113]. Point Spread Functions were created using the "PSF Generator" plugin in Fiji[114] and used to deconvolve the images with the "Deconvolution Lab2" software[115,116] employing the Richardson-Lucy TV algorithm with regularization set to 0.0001 and maximum iterations of 2[113]. Deconvolved images were then inputs for the Mitochondria Analyzer plugin in Fiji using standard "subtract background" (radius 1.25 µm) to remove background noise; "sigma filter plus", to reduce noise and smooth object signal while preserving edges; "enhance local contrast" (slope 1.5) to enhance dim areas while minimizing noise amplification; and "gamma correction" (value 0.90). The thresholding method was "Weighted Mean", the block size 1.25 µm, while the C value was adjusted to the anatomical structure to minimise background noise[113] (value 2 for dFB neurons and 12 for projection neurons). The resulting thresholded images where then examined via Batch 3D analysis on a per-cell basis, to extract the morphological metrics. Given the extensive arborisation of PNs in the glomeruli and mitochondrial abundancy there, sub-stacks of 4.35 µm were randomly selected from the deconvolved images, for the following analysis, to make the computations practicable.

2.6.2 Synaptic tagging measurements

Single-housed females were analysed 6 days post eclosion, after 12 h of sleep deprivation or *ad libitum* sleep.

Their brains were dissected, fixed and stained as indicated, with mouse anti-V5 and chicken anti-GFP as primary antibodies, and Alexa 633 anti-mouse and Alexa 488 anti-chicken as secondary antibodies.

Images were acquired as indicated, with identical acquisition parameters across conditions, for the whole structures of interest in both green (511-537 nm) and red channels (642-681 nm), and analysed in Fiji.

Fluorescence was quantified, blind to sleep history, on summed Z-stack of both channels; manually-defined average background signal in areas close to the structure of interest was subtracted from the mean fluorescence intensity of the structures of interest, and the red-to-green ratio was calculated.

2.7 Molecular cloning

Fly lines for cell-specific CRISPR knockout were generated according to the CRISPR Fly design protocol[117,118].

Briefly, best sgRNA sequences for *Octβ1R, Octβ3R* and *Oct-TyrR* were selected using CHOPCHOP[119], ensuring the targeted sequences were on two different strands orientations, and at least 200 bp apart.

pCFD6 vector (Addgene #73915) was digested with BbsI (NEB #R3539), and used as template for creating overlapping PCR products, using DNA primers (reported below) harbouring overlapping fragments between the *pCFD6* vector and tRNA-flanked sgRNAs sequences; the PCR was performed with a high-fidelity Phusion polymerase (NEB #M0531). The amplified sequences were purified on gel, extracted using the Macherey Nagel gel extraction kit (MN #740609) and fragments were ligated to the digested *pCFD6* vector via Gibson assembly reaction (NEB #E5510), using two to three molar excess inserts/vector. Ligated products were transformed into One Shot™ TOP10 Chemically Competent *E. coli* (ThermoFisher #C404006) cells, pre-incubated in SOC medium, plated on carbenicillin-containing LB plates and incubated overnight at 37°C. The following day, single colonies were expanded in liquid cultures, in orbital shaking at 37° overnight. Minipreps from clonal cultures were obtained using the Macherey-Nagel DNA purification kit (MN #740952.50), screened via PCR and electrophoresis for verifying the correct inclusion of fragments. Subsequently, the DNA sequence of those with the correct sizes was verified by sequencing, and the selected recombinant plasmids were used

by BestGene Inc. to generate transgenic flies bearing UAS-controlled four, three and two sgRNAs, on II and III chromosomes, targeting *Octβ1R*, *Octβ3R* and *Oct-TyrR*.

Primer's name	Protocol ID	Sequence
Octβ1R		
pCFD6_CG6919_F1	gseq1F	CGGCCCGGGTTCGATTCCCGGCCGATGCATGAGGCTGACTCCTCCAGAAGTTTCAGAGCTATGCTGGAAAC
pCFD6_CG6919_R1	gseq 2R	CTGTTGCATATCGGTCGACATGCACCAGCCGGGAATCGAACC
pCFD6_CG6919_F2	gseq 2F	TGTCGACCGATATGCAACAG GTTTCAGAGCTATGCTGGAAAC
pCFD6_CG6919_R2	gseq 3R	CCTTGGATCTGGGCGCACACTGCACCAGCCGGGAATCGAACC
pCFD6_CG6919_F3	gseq 3F	GTGTGCGCCCAGATCCAAGGGTTTCAGAGCTATGCTGGAAAC
pCFD6_CG6919_R3	gseq 4R	ATTTTAACTTGCTATTTCTAGCTCTAAAACCAGGTACATCGTATCCTCGC TGCACCAGCCGGGAATCGAACC
pCFD6_CG6919_3X_F1	gseq1F	CGGCCCGGGTTCGATTCCCGGCCGATGCATGAGGCTGACTCCTCCAGAAGTTTCAGAGCTATGCTGGAAAC
pCFD6_CG6919_3X_R1	gseq 2R	CTGTTGCATATCGGTCGACATGCACCAGCCGGGAATCGAACC
pCFD6_CG6919_3X_F2	gseq 2F	TGTCGACCGATATGCAACAGGTTTCAGAGCTATGCTGGAAAC
pCFD6_CG6919_3X_R2	gseq 3R	ATTTTAACTTGCTATTTCTAGCTCTAAAACCCTTGGATCTGGGCGCACACTGCACCAGCCGGGAATCGAACC
pCFD6_CG6919_2X_F1	gseq1F	CGGCCCGGGTTCGATTCCCGGCCGATGCATGTCGACCGATATGCAACAGTTTCAGAGCTATGCTGGAAAC
pCFD6_CG6919_2X_R1	gseq 2R	ATTTTAACTTGCTATTTCTAGCTCTAAAACCCTTGGATCTGGGCGCACAC TGCACCAGCCGGGAATCGAACC
Octβ3R		
pCFD6_CG42244_F1	gseq1F	CGGCCCGGGTTCGATTCCCGGCCGATGCATGTCGAGAGGAGCTCAAACGGTTTCAGAGCTATGCTGGAAAC
pCFD6_CG42244_R1	gseq 2R	CTGATATGCAGCACAGGTGCTGCACCAGCCGGGAATCGAACC
pCFD6_CG42244_F2	gseq 2F	GCACCTGTGCTGCATATCAGGTTTCAGAGCTATGCTGGAAAC
pCFD6_CG42244_R2	gseq 3R	TGTTGACCACAAACGAGCACTGCACCAGCCGGGAATCGAACC
pCFD6_CG42244_F3	gseq 3F	GTGCTCGTTTGTGGTCAACAGTTTCAGAGCTATGCTGGAAAC
pCFD6_CG42244_R3	gseq 4R	ATTTTAACTTGCTATTTCTAGCTCTAAAACCAGAGCGATGTGATGACATA TGCACCAGCCGGGAATCGAACC
pCFD6_CG42244_3X_F1	gseq1F	CGGCCCGGGTTCGATTCCCGGCCGATGCATGTCGAGAGGAGCTCAAACGGTTTCAGAGCTATGCTGGAAAC
pCFD6_CG42244_3X_R1	gseq 2R	TGTTGACCACAAACGAGCAC TGCACCAGCCGGGAATCGAACC
pCFD6_CG42244_3X_F2	gseq 2F	GTGCTCGTTTGTGGTCAACA GTTTCAGAGCTATGCTGGAAAC
pCFD6_CG42244_3X_R2	gseq 3R	ATTTTAACTTGCTATTTCTAGCTCTAAAACCAGAGCGATGTGATGACATATGCACCAGCCGGGAATCGAACC
pCFD6_CG42244_2X_F1	gseq1F	CGGCCCGGGTTCGATTCCCGGCCGATGCATGTCGAGAGGAGCTCAAACGGTTTCAGAGCTATGCTGGAAAC
pCFD6_CG42244_2X_R1	gseq 2R	ATTTTAACTTGCTATTTCTAGCTCTAAAACCAGAGCGATGTGATGACATA TGCACCAGCCGGGAATCGAACC
Oct-TyrR		
pCFD6_CG7485_F1	gseq1F	CGGCCCGGGTTCGATTCCCGGCCGATGCAAGAATGCGAAGGAGCTGTGGGTTTCAGAGCTATGCTGGAAAC
pCFD6_CG7485_R1	gseq 2R	TGGTTCTCTCGGTCATTATC TGCACCAGCCGGGAATCGAACC
pCFD6_CG7485_F2	gseq 2F	GATAATGACCGAGAGAACCA GTTTCAGAGCTATGCTGGAAAC
pCFD6_CG7485_R2	gseq 3R	CATGGCAACAGCGATCCCCA TGCACCAGCCGGGAATCGAACC
pCFD6_CG7485_F3	gseq 3F	TGGGGATCGCTGTTGCCATG GTTTCAGAGCTATGCTGGAAAC

pCFD6_CG7485_R3	gseq 4R	ATTTTAACTTGCTATTTCTAGCTCTAAAACCAATGAACTGGTTAACCCCATGCACCAGCCGGGAATCGAACC
pCFD6_CG7485_3X_F1	gseq1F	CGGCCCGGGTTCGATTCCCGGCCGATGCAAGAATGCGAAGGAGCTGTGGGTTTCAGAGCTATGCTGGAAAC
pCFD6_CG7485_3X_R1	gseq 2R	TGGTTCTCTCGGTCATTATC TGCACCAGCCGGGAATCGAACC
pCFD6_CG7485_3X_F2	gseq 2F	GATAATGACCGAGAGAACCAGTTTCAGAGCTATGCTGGAAAC
pCFD6_CG7485_3X_R2	gseq 3R	ATTTTAACTTGCTATTTCTAGCTCTAAAACCAATGAACTGGTTAACCCCATGCACCAGCCGGGAATCGAACC
pCFD6_CG7485_2X_F1	gseq1F	CGGCCCGGGTTCGATTCCCGGCCGATGCAGATAATGACCGAGAGAACCAGTTTCAGAGCTATGCTGGAAAC
pCFD6_CG7485_2X_R1	gseq 2R	ATTTTAACTTGCTATTTCTAGCTCTAAAACCAATGAACTGGTTAACCCCATGCACCAGCCGGGAATCGAACC

2.8 Connectomics

Connectomics figures and analyses were generated with *neu*Print+ using hemibrain:v1.2.1 release, selecting the relevant neurons' IDs, and using "Find neurons" with skeleton view, "Connectivity graph", and "Synapse connectivity" queries.

2.9 Softwares and Algorithms

Name	Source	Reference
MATLAB_R2017b	Mathworks	https://www.mathworks.com
LabVIEW 9	National Instruments	https://www.ni.com
Vecsey Sleep and Circadian Analysis MATLAB Program (SCAMP) 2020_v3	Vecsey lab (Skidmore College)	https://academics.skidmore.edu/blogs/cvecsey/?page_id=57
Open-loop optogenetics coupled with videotracking software (running on LabVIEW)	Miesenböck lab (Clifford Talbot)	[53,83]
Videotracking movement analysis script	Miesenböck lab (Clifford Talbot)	[53,83]
Fiji	Open source	https://imagej.net/software/fiji/ [120]
PRISM 9.4.1	GraphPad	https://www.graphpad.com
R Studio 1.4	Open source	https://www.rstudio.com
ScanImage 5.4-0 (running on MATLAB2015a)	Vidrio Technologies	https://vidriotechnologies.com
Arousing infrared LED stimulus delivery control LabVIEW software	Miesenböck lab (Clifford Talbot)	[89]

Clampex 10.5	Molecular Devices	https://www.moleculardevices.com
Seurat 4.1	Satija lab	[121]
Two-photon imaging MATLAB analysis scripts	Miesenböck lab (Peter S. Hasenhuetl and Raffaele Sarnataro)	This work (see Appendices)
PANTHER v17	Gene Ontology Consortium	http://www.pantherdb.org[122–124]
ViSEAGO 1.4.0	Bioconductor	https://www.bioconductor.org/packages/release/bioc/html/ViSEAGO.html[125]
topGO 2.42.0	Bioconductor	https://www.bioconductor.org/packages/release/bioc/html/topGO.html[126]
PSF Generator	Biomedical Imaging Group, EPFL	http://bigwww.epfl.ch/algorithms/psfgenerator/[114]
DeconvolutionLab2	Biomedical Imaging Group, EPFL	http://bigwww.epfl.ch/deconvolution/deconvolutionlab2/[116]
Mitochondria Analyzer v2.1.0	Ahsen Chaudhry, University of British Columbia	https://github.com/AhsenChaudhry/Mitochondria-Analyzer[113]
Transcriptomic reads alignment and annotation	James Nemesh, McCarroll Lab Drop-seq core computational protocol V2.0.0	Adapted from[110] (see Appendices)
***neu*Print+**	Janelia HHMI	https://neuprint.janelia.org/[127]
CHOPCHOP v3	University of Bergen	https://chopchop.cbu.uib.no[119]

2.10 Statistics and reproducibility

Data were statistically analysed in Prism 9 (GraphPad).

Group means were compared by t-tests, two-way ANOVA, or one-way ANOVA, using repeated measures designs where indicated, followed by planned pairwise post-hoc analyses using Šidák's multiple comparisons test. All behavioural experiments were run at least three times, on different days and with batches of flies from different crosses, unless otherwise stated; data shown are pooled from all replicates. Dead flies were excluded from the analyses as detailed in the relevant paragraphs. Two-photon imaging data were analysed and plotted with custom-made MATLAB scripts (see Appendices). For the morphometric analyses, random sub-stacks of PNs were generated from a MATLAB random generator function, with reproducible seeding. Significant DEGs from scRNA-seq were identified with Wilcoxon Rank Sum test, with P-value adjusted using Bonferroni correction based on the total number of variable genes in the

dataset. Gene ontology enrichment was statistically analysed using Fisher's Exact test (with False Discovery Rate correction for PANTHER analysis).

2.11 Technical acknowledgments

I thank Michal Maj, Line Eriksen, Robert Hedley and Vasiliki Tsioligka for providing technical assistance for the cell sorting at the Flow Cytometry Facility, Sir William Dunn School of Pathology, University of Oxford; the Oxford Genomics Centre at the Wellcome Centre for Human Genetics (funded by Wellcome Trust grant reference 203141/A/16/Z) for the generation of the single-cell RNA-sequencing data; Fiona Woods for the administrative support; Ruth Brain and the CNCB lab technicians for assisting with stock maintenance and fly food preparation; BestGene Inc. Drosophila Embryo Microinjection Service for generating novel transgenic flies; Source Bioscience for the DNA sequencing services; BioRender.com for the creation of Figure 3.1b, Figure 6.4a and b, Figure 5.13; Katerina Christodoulou, Anissa Kempf, Alina Krebbers, Christof Treiber, Vincent Croset, Timothy Wong, Lea Ballenberger, Celina Hartmann for their help in large-scale dissections and dissociation of fly brains; S. L. Zipursky, J. M. Donlea, V. Jayaraman, H. Jacobs, M. B. Feany, J. Chung, M. Guo, A. J. Whitworth, F. Port, J. Jepson, G. Gilestro, the Bloomington Stock Center, and the Vienna Drosophila Resource Center for the provided flies.

3 The transcriptome of dFB neurons

3.1 Introduction

Transcription plays a central role in transducing genetic instructions into phenotypes: the finely tuned control of gene expression allows the specification of cell identities and execution of cell-specific functions. Although the correlation between the transcriptome (the set of all transcripts) and the proteome (the entirety of proteins) in a cell is often loose[128–130], significant insight has been obtained from the study of transcriptomes, which remain good proxies for phenotypes[128], from the functional inference of co-regulated genes or genes participating in the same pathway[131], to the understanding of regulatory gene networks[132]. The analysis of the transcriptome of a tissue or of a cell population therefore permits the identification of novel genetic markers[133], and, if different conditions are compared, one can distinguish genes or pathways differentially regulated across states[134].

In the last decade, technological advancements have led to the development of single-cell omics techniques, whose benchmark is the uncovering of a set of biological data per each cell of a given sample[135]. The combination with droplet-based methods[108] has allowed massively parallel sequencing approaches to be easily deployed for obtaining transcriptomes of thousands of cells at once, providing unprecedented level of detail in the understanding of cell identities of full vertebrates' CNS[34,36], of the aging brain[136], of comparative neurobiological features[137], of mammalian brain regions[138,139] and sleep-control centres[140], just to name a few interesting examples. The additional advantage of single-cell granularity is the opportunity to identify and genetically disentangle subpopulations of cells, uncovering genetic heterogeneity and infer functional correlates[34]. Therefore, single-cell RNA-sequencing provides three potential classes of insights: uncovering novel cell markers, revealing differentially expressed genes across conditions, and unveiling population heterogeneity.

I sought to obtain such insights for sleep-control centres in the fly.

Sleep affects gene expression brain-[43,141] and body[142]-wide; however, the study of sleep-dependent transcriptional changes in key sleep-control regions within the brain is limited: only recently has the transcriptome of the mammalian $VLPO^{Gal}$ sleep-control cells[22,24,93] been compared between conditions of high and low sleep pressure[96], with several classes of genes, predominantly unfolded protein response and ER stress genes, upregulated upon sleep

deprivation. This sort of study can help identifying pathways mobilised by different sleep pressure states, and could hint at the underlying mechanisms. The focus of the present study, which sought to take advantage of the numerically simpler brain of a behaviourally complex and well-studied animal[143], was a key sleep-control population of *Drosophila*: the dorsal fan-shaped body-projecting (dFB) neurons.

Although some of the key molecular players that control the electrical properties of these neurons (and, therefore, sleep) are known, the underlying molecular and cellular mechanisms are yet to be fully uncovered. Being central to sleep homeostasis, understanding which inputs are received, how the outputs are transmitted, and which subcellular pathways are engaged, would be beneficial for understanding key variables linked to sleep control.

In addition, dFB neurons appear electrically[56,81,89] and morphologically[33] heterogeneous, but neither the molecular basis nor the functional consequences of this diversity are understood. Finally, these cells have been so far identified by several sleep-promoting *GAL4* lines targeting the dFB, and yet there is no known unique set of markers that distinctively labels these cells.

Single-cell RNA-sequencing of these cells, in conditions of high and low sleep pressure, was the technique of choice for trying to answer these questions.

Far from being a purely descriptive study, this chapter illustrates the scRNA-seq procedure, its *in silico* validation and broad findings of my transcriptomic analysis. The main functional implications will be addressed in subsequent chapters.

3.2 Results

3.2.1 Experimental design of scRNA-seq and quality control validation

The goal was to obtain the single-cell transcriptome of *R23E10-GAL4*-labelled dFB neurons, in conditions of high and low sleep pressure. In a single-cell RNA-sequencing with 10X technology, usually a few thousand dissociated cells are captured and sequenced per sample. Because dFB neurons form a small population (*R23E10-GAL4* expresses in 12-13 cell pairs in the brain), the desired population must be enriched in the sample in order to maximise the number of sequenced cells of interest. In addition, while several genes expressed in dFB neurons and constituting part of their operative machinery are known, no study has identified selective genetic markers that distinctively label dFB neurons within the brain. Therefore, I genetically labelled dFB neurons with an exogenous gene, *EGFP*, which allowed me to distinguish dFB cells from a vast majority of $EGFP^-$ brain cells and use fluorescence for selectively sorting dFB cells via flow cytometry and thus enriching my experimental samples in cells of interest.

To this end, I generated flies where *R23E10-GAL4* drove the expression of hexameric EGFP. The flies were collected, loaded into sleep monitors, and divided into two groups: one group slept *ad libitum* (control group), while the other underwent 12 h of sleep deprivation overnight (**Figure 3.1a**). At the end of the night of either sleep deprivation or *ad libitum* sleep, brains of both groups of flies were dissected in parallel. This allowed me to obtain brain cells from animals at the opposite ends of the sleep pressure spectrum. After the dissections, brains were enzymatically and mechanically dissociated and FACS-sorted for EGFP; the $EGFP^+$ and $EGFP^-$ fractions then underwent single-cell RNA-sequencing with 10X Chromium technology (**Figure 3.1b**). From the reads, I obtained Digital Gene Expression matrices, which consist of the number of reads arrayed per each gene and per each cell. I merged all replicates from $EGFP^+$ (dFB enriched) and $EGFP^-$ (whole brain) samples and, for the purposes of this chapter, samples from sleep deprived and control brains, regressing out variations driven by different batches. I applied standard quality control filters for fly brain (see Materials and Methods section for details), clustered cells according to their gene expression profile similarity, and used dimensionality reduction methods to visualise the results in two dimensions. Quality control checks on the whole dataset, composed of 13,173 cells, (**Figure 3.2**) showed that cells originating from sleep deprived and control brains, and coming from different replicates, were vastly distributed throughout the clusters (**Figure 3.2 a**, **b**).

a

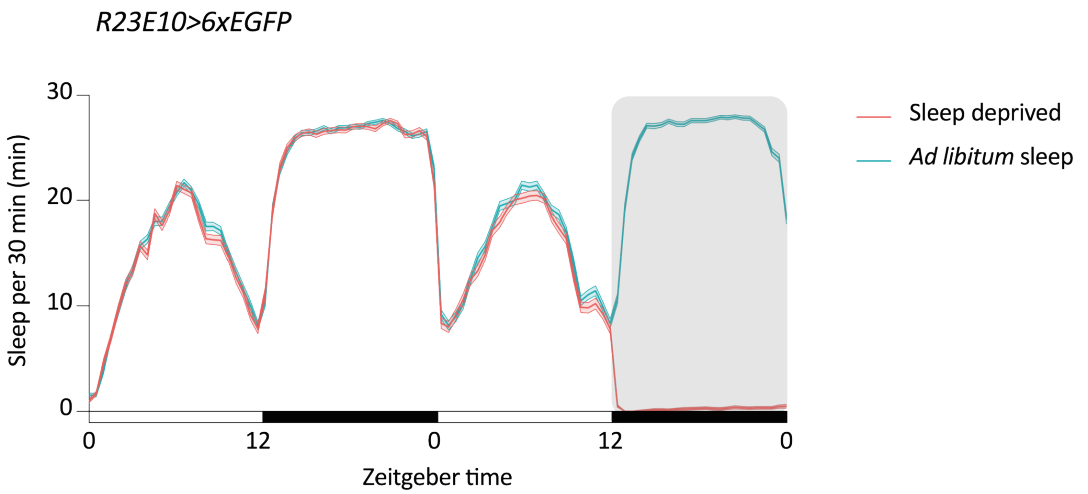

b

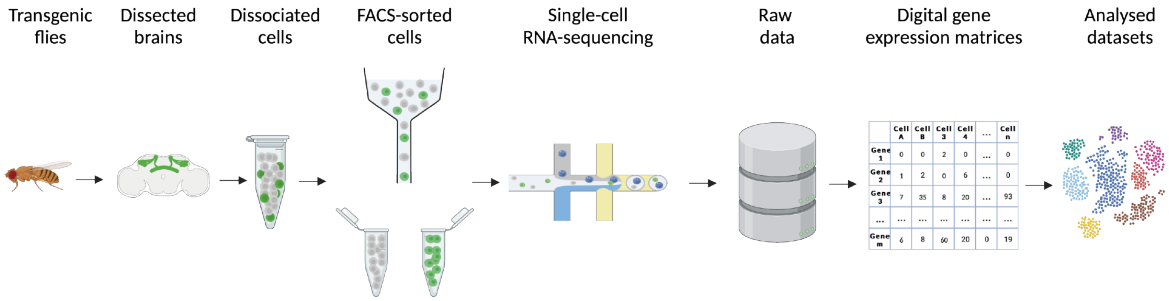

Figure 3.1 | Schematics of the single-cell RNA-sequencing experimental procedure.
a, Sleep per 30 min bins in flies expressing hexameric EGFP under the control of *R23E10-GAL4*. A group of flies was sleep deprived for 12 h (salmon, n = 432, sleep deprivation time in grey), while simultaneously the control group was allowed to rest *ad libitum* (cyan, n = 558). Means (solid lines) ± SEM (shaded areas) are plotted for the data pooled from the three biological replicates per condition performed.
b, Schematics of the experimental procedure. At ZT 0, brains of *R23E10>6xEGFP* transgenic flies (sleep deprived and not) were dissected in parallel, their brains were dissociated and FACS-sorted. Both the $EGFP^+$ and $EGFP^-$ fractions were collected and submitted for scRNA-sequencing. Sequencing raw data were extracted, assigned to specific cells, annotated, and digital gene expression matrices were created, and analysed.

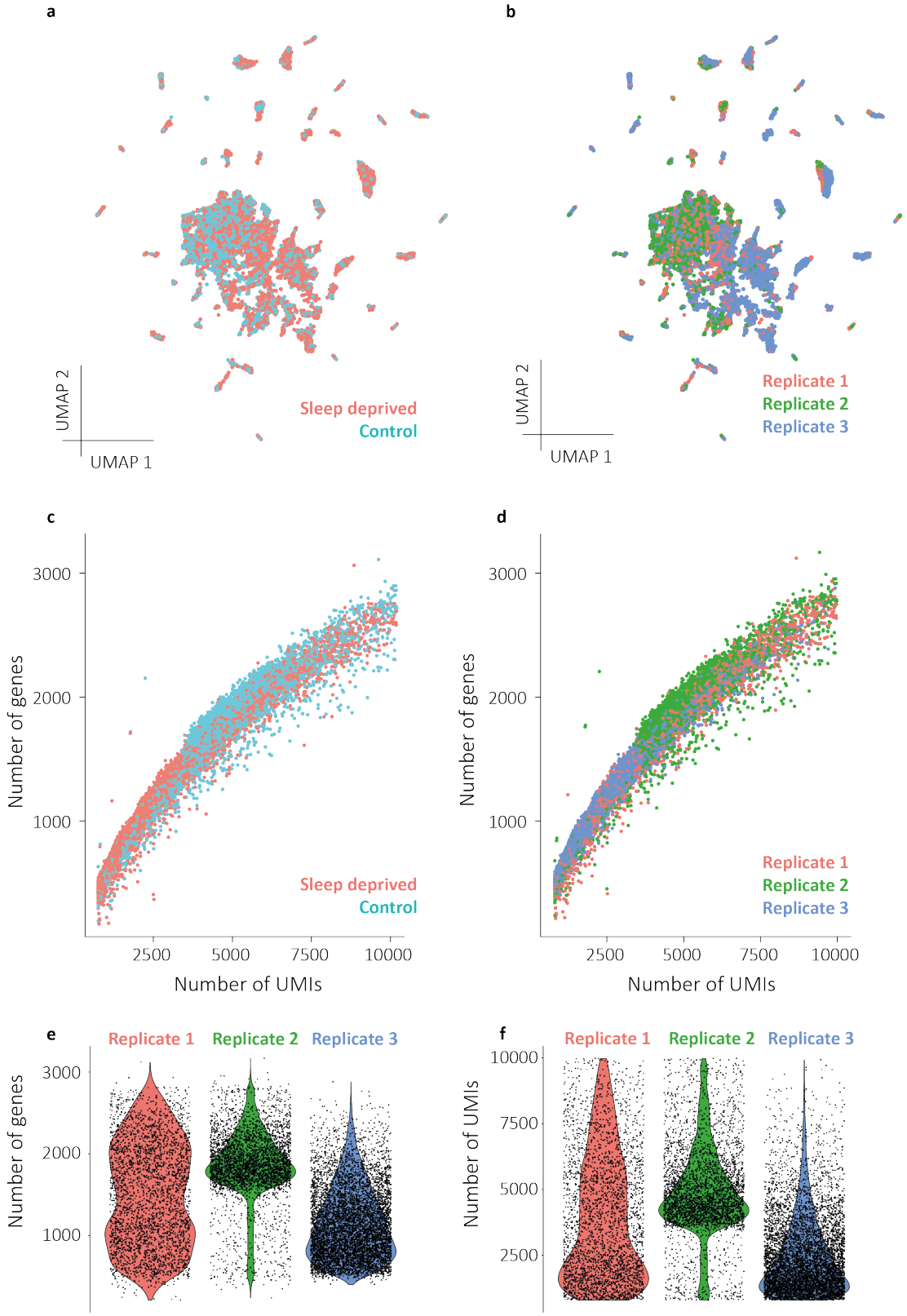

Figure 3.2 | Quality control on single-cell transcriptomics of fly brain.
Two-dimensional uniform manifold approximation and projection representation of the whole fly brain, integrated and regressed with all the datasets, grouped according to sleep history of the originating flies (**a**) and biological replicate of origin (**b**). Relationship between number of UMIs collected and number of genes detected in the whole dataset (Pearson correlation coefficient = 0.97), grouped according to sleep history of the originating flies (**c**) and biological replicate of origin (**d**).
Distribution of number of genes detected (**e**) and number of UMIs collected (**f**) per each biological replicate.
Dots represent individual cells in all plots.

Correlation analysis between the number of unique molecular identifiers (UMIs) collected and genes detected per each cell, shows high linearity (Pearson correlation coefficient = 0.97), which indicates even sampling in the dataset, through sleep states and replicates (Figure 3.2 c, d). Finally, the distribution of the number of genes in each replicate shows that, despite commonly described variations[111], my filtering boundaries captured distribution peaks of all the replicates, and equally kept distribution peaks of UMIs, filtering out low-UMI tails, usually empty droplets with residual ambient RNA[144].

The analysis of the whole brain, similarly to published datasets, revealed many clusters of identifiable cell types (Figure 3.3): for example, different subtypes of Kenyon cells, glial cells, projection neurons, and monoaminergic cells. In addition, *bona fide* dFB neurons could be identified as neurons highly expressing *EGFP* and their GAL4 line enhancer *AstA-R1* (Figure 3.3a). Details on the markers used for annotating each cluster are in Appendix 9.1. In addition to previously annotated cell clusters, my analysis identified 29 additional clusters, which I made no attempt to annotate further (Figure 3.3b). All clusters showed comparable distributions in the number of UMIs and the number of genes per cell (Figure 3.3c).

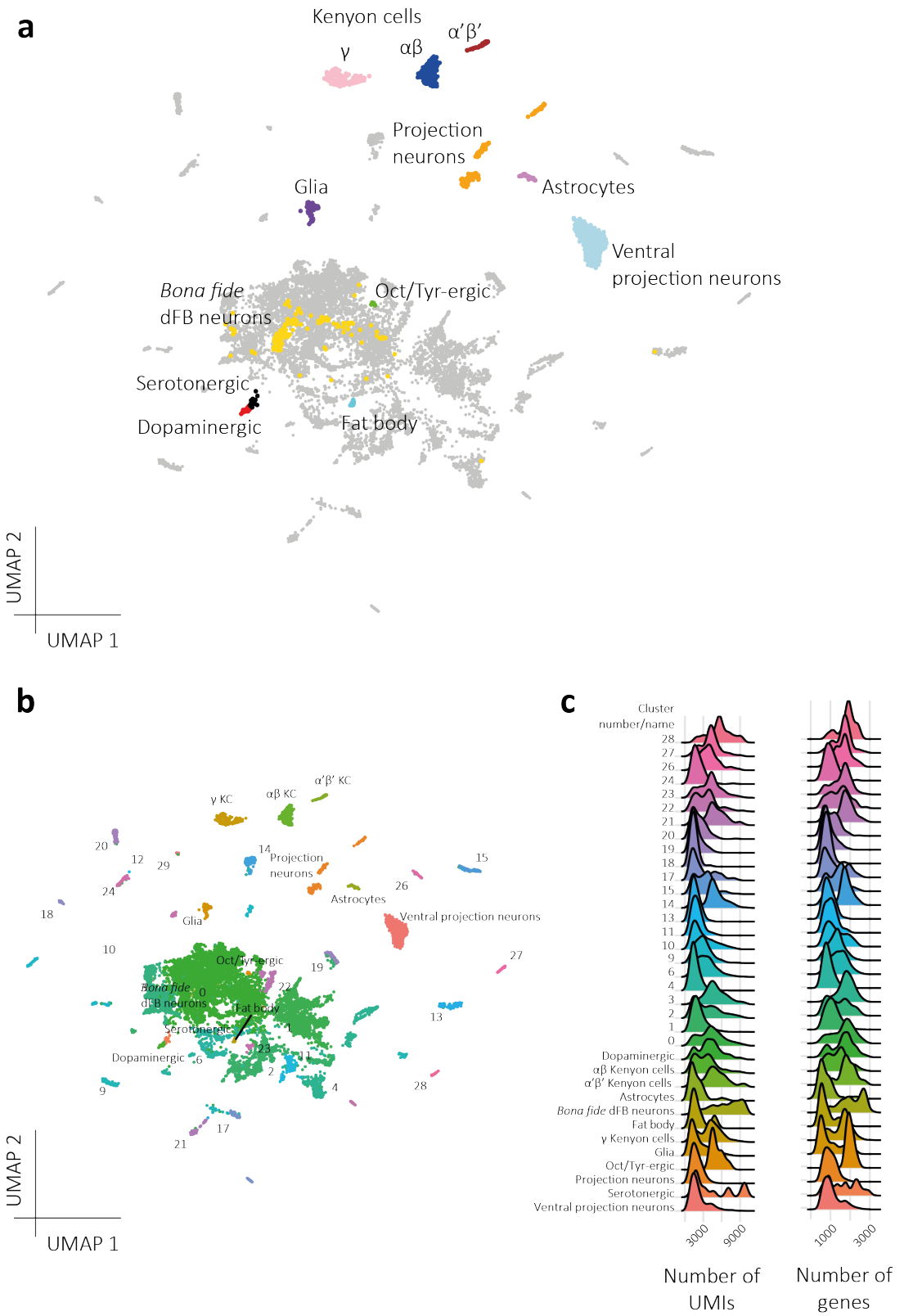

Figure 3.3 | Cell types are identifiable among the cell clusters.
a, Two-dimensional uniform manifold approximation and projection representation of the whole fly brain, integrated and regressed with all the datasets, with main cell types highlighted: γ (pink), αβ (dark blue), α'β' (brown) Kenyon cells, projection neurons (orange), ventral projection neurons (light blue), astrocytes (violet), glia (purple), octopaminergic and tyraminergic cells (green), residual fat body tissue (cyan), serotonergic cells (black), dopaminergic cells (red), and *bona fide* dFB neurons (gold). **b**, Same as in (**a**) with all the clusters detected at resolution = 0.2 labelled. **c**, Distribution of number of UMIs and genes per cell, per each identified cluster. Clusters with <2 cells are not shown.

3.2.2 Identification of dFB neurons within scRNA-seq dataset

A major feature determining the identity of neuronal types is their fast-acting neurotransmitter. In the fly CNS, the principal transmitters are glutamate, acetylcholine, and GABA, usually identified via their classical markers Vesicular glutamate transporter (*VGlut*), Vesicular acetylcholine transporter (*VAChT*), and Glutamic acid decarboxylase 1 (*Gad1*), respectively. I probed my dataset with these markers and found that they orderly pattern it, consistently with previous work[34] (**Figure 3.4a**).

The vast majority of *bona fide* dFB neurons expressed *VGlut* at levels significantly and substantially higher than those of the other two markers (**Figure 3.4b**, where the expression levels are Log-scaled). In addition, the expression of those markers was mainly mutually exclusive, with marginal co-expression levels (**Figure 3.4c, d, e**). I then divided the whole dataset into glutamatergic, cholinergic and GABAergic cells: to define such NT identities, I applied to each of them two threshold criteria to the NT markers' expression levels: a more relaxed and stringent one (details in **Appendix 9.1**). I re-clustered the resulting neurons, and mapped the *bona fide* dFB neurons onto those datasets (**Figure 3.4e**). In the case of the glutamatergic cells, for both the relaxed and stringent datasets, many *bona fide* dFB neurons distinctly mapped onto two clusters (**Figure 3.4e**, **left**); conversely for the cholinergic and GABAergic sets, fewer *bona fide* dFB neurons were included in those datasets and none mapped onto distinct clusters for either the relaxed or stringent sets (**Figure 3.4e**, **centre and right**).

Given that unsupervised re-clustering of glutamatergic neurons revealed distinct groups of cells containing the vast majority of *bona fide* dFB neurons, and given that most *bona fide* dFB neurons express VGlut at high levels, I tentatively identify these clusters of 323 cells as dFB neurons (**Figure 3.5a**). Direct experimental evidence presented in **Chapter 4** will validate this inference, along with the clear enrichment of these clusters in EGFP compared to the rest of the glutamatergic brain (**Figure 3.5b**), as well as in genes used to create GAL4 lines targeting dFB neurons: *AstA-R1* for R23E10-GAL4[66], *Eip93F* for R84C10-GAL4[79,145], *CG44153* for R72G06-GAL4[57], and *dve* for R40E08-GAL4 (a line targeting a single pair of dFB neurons identified in the Miesenböck lab, data not shown) (**Figure 3.5c**).

Finally, I verified that dFB neurons expressed known markers, such as the RhoGAP cv-c[81], the dopamine receptor Dop1R2[66], the neuropeptide allatostatin A[53], and the serotonin receptor 5-

HT2B[68] (Figure 3.5d, e). In addition, I compiled the full list of genes enriched in dFB neurons compared to the rest of the brain, in order to provide a list of markers that can be validated *in vivo* in further studies (Appendix 9.3).

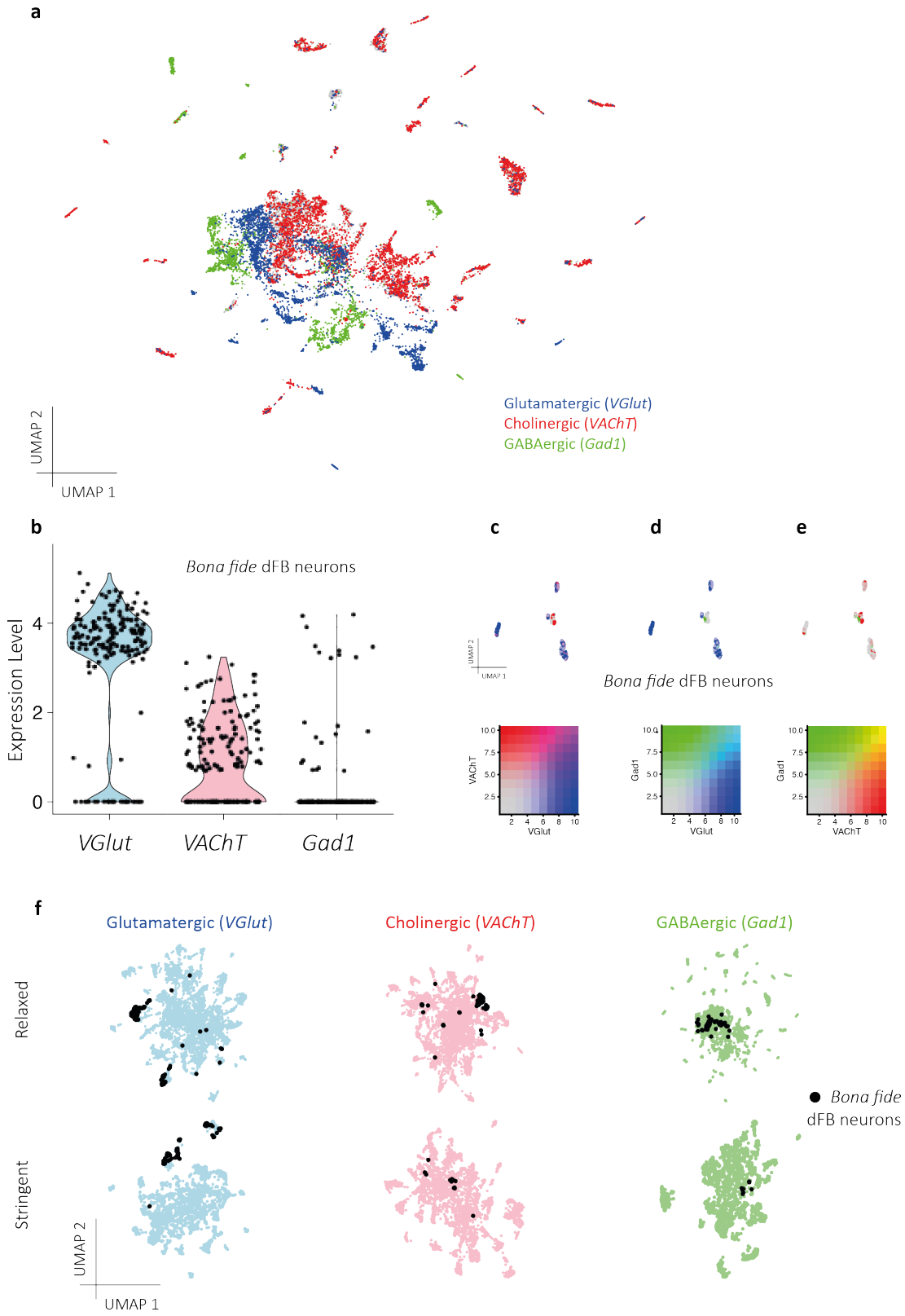

Figure 3.4 | dFB neurons distinctly cluster as glutamatergic neurons.
a, Two-dimensional uniform manifold approximation and projection representation of the whole fly brain, with highlighted distribution of cells expressing different fast-acting NTs markers (*VGlut* in blue, *VAChT* in red, *Gad1* in green). For graphical reasons, cells expressing each marker above a log normalized value of 2 are coloured. **b**, Log normalised distribution of expression levels of NT markers in *bona fide* dFB neurons. **c-e**, Co-expression analysis of NTs in re-clustered *bona fide* dFB neurons, between *VGlut* and *VAChT* (**c**), *VGlut* and *Gad1* (**d**), *VAChT* and *Gad1* (**e**); colour codes are reported in the bottom graphs. **f**, Location of *bona fide* dFB neurons (black dots), within re-clustered brain cells expressing glutamatergic, cholinergic and GABAergic markers, according to relaxed (top) and stringent (bottom) NT expression levels. In all graphs, each dot is an individual cell.

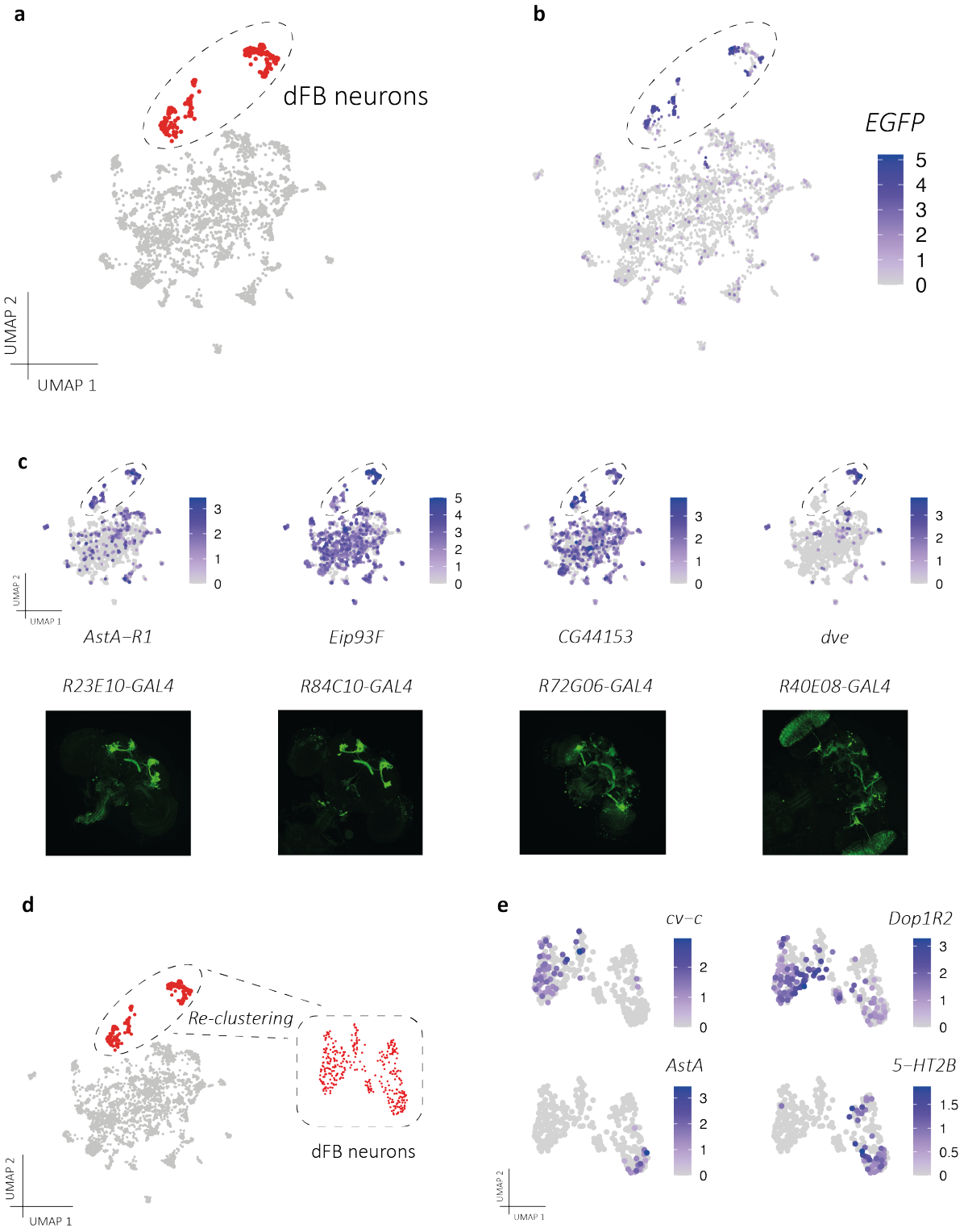

Figure 3.5 | Identified dFB neurons recapitulate their known genetic features.
a, The identified cluster of dFB neurons (red, circled in dashed line) is enriched in *EGFP* compared to the rest of the glutamatergic brain (**b**), and in genes from which enhancers defining four GAL4 lines used to target dFB neurons are derived (**c**): bottom rows depicts the images of the GAL4 lines indicated, which derive from the corresponding top genes (**c**). Images in (**c**) are z-stacks of 623.88 x 632.88 µm^2 from FlyLight project[146]. **d**, Re-clustering the dFB neurons cluster generates a novel UMAP pattern, on which it is possible to detect the expression of known markers of dFB neurons (**e**), whose log-normalised expression levels are colour-coded according to the bars on the right per each gene. In all graphs, each dot is an individual cell.

3.3 Discussion

My study has identified the transcriptome of dFB neurons, in conditions of high and low sleep pressure.

To this end, I dissected around 160 fly brains for each condition, three times. Considering that the fly brain is thought to contain around 10^5 cells and that my QC-filtered dataset recovered about 10^4 cells, this implies the recovery of 1 cell out of each 10^4 dissected. Given that I dissected brains harbouring around 27,000 dFB neurons in total, I should have recovered about 3 dFB neurons. However, I identified more than 300 dFB cells. This shows that the FACS strategy did enrich the sample by a factor of 10^2.

In addition, my filtering criteria to identify those cells were strict: not only I used tight quality filtering for the whole datasets compared to other studies, but also dFB neurons were identified as a stringently-defined distinct cluster of glutamatergic cells, vastly populated by neurons highly expressing *EGFP* and the *R23E10-GAL4*-originating gene *AstA-R1*.

I observed slight variations in the recovery quality and abundance between replicates (**Figure 3.2**), but I accounted for those via the normalisation of cell counts per each cell over the total number of UMIs per sample, to avoid amplification bias, and when I merged the datasets, I regressed out the variability driven by each dataset batch.

In addition to dFB neurons, my dataset included the rest of the brain (**Figure 3.3**), valuable information for several reasons. For example, if one were to study genes differentially expressed in dFB neurons as a function of sleep history, one can ask whether the changes are specific to those cells; conversely, the dataset is a useful resource to investigate sleep history-dependent changes in other cell populations, and its control subset could contribute to enriching general fly brain atlases and allow the research community to define novel cell markers. Indeed, the identified cell populations in my dataset have relatively similar levels of UMIs and genes recovered per cell, apart from dFB neurons, which have higher numbers, possibly because they have been sorted and sequenced separately (**Figure 3.3**). This allows a higher statistical power when comparing differentially expressed genes within dFB neurons across sleep states.

On the other hand, astrocytes and projection neurons, for example, have lower levels of UMIs and genes recovered per cell, compared to most clusters. This is potentially due to their vast

anatomical arborisations which are lost during the cell dissociation procedure that is therefore likely to damage those cell types more and hinder the detection of all transcripts contained in their processes[147]. This is a general caveat of single-cell transcriptomics, which can be limited when using other RNA-seq techniques not including cell dissociation, such as spatial single-cell transcriptomics.

Although *bona fide* dFB neurons express *VGlut* at high levels, they also express substantially lower levels of other markers. This also happens for other cell types, for example Kenyon cells, which are established to be cholinergic[148], also express low levels of other NTs markers in my dataset (data not shown). Despite *VAChT* and *Gad1* being expressed in the *bona fide* dFB neurons, the few cells expressing them are mostly relegated to a small distinct sub-cluster (**Figure 3.4d, e**) which could be spurious, or a group of non-dFB *R23E10-GAL4* neurons (see **Figure 4.5**): indeed, while some grouping of cells appears in the relaxed cholinergic and GABAergic subset, they are wiped out if the required expression levels are more stringent (**Figure 3.4e**). Such stringent criteria still reflect physiological levels, as, for example, cholinergic Kenyon cells could be distinctly identified in the stringent cholinergic subset (data not shown). Also, the findings of **Chapter 4** further support the notion that dFB neurons are glutamatergic. The re-clustering of these cells and the differential expression of some known markers (**Figure 3.5d, e**) highlights sub-clusters and suggests an underlying functional heterogeneity, which will be further explored in **Chapter 6**.

My technique of choice must acknowledge several limitations: in addition to the mechanical removal of cellular processes and the concurrent cell damage and loss of spatial resolution, scRNA-seq also produces high levels of noise, due to the intrinsic variability of the technique, which complicate the data interpretation. In addition, transcriptional changes are only a proxy for changes in protein expression levels[129,130]; other techniques such as the study of the translatome via Translating ribosome affinity purification, or single-cell proteomics could complement the findings.

In addition, the method used requires dissections of many fly brains, subsequent dissociation, sorting and final processing for scRNA-seq: this pipeline can take up to 5-6 h from the chosen time point until the cellular transcripts are barcoded. To circumvent spurious changes in the transcriptome, I kept flies and cells one ice or at 4° for the whole procedure, processed all the

samples in parallel for all the steps, and used solutions with toxins inhibiting neuronal activity. Although I cannot rule out that cellular stress-related genes may have been transcribed in certain cell populations because of the experimental procedure, when comparing different conditions processed in parallel, such effects should cancel out.

Finally, the enrichment via FACS could be improved by combining it with functional fluorescence labelling: since ROS accumulate in sleep deprived dFB neurons[83], they could be further selected by marking them with a ROS-specific dye like DCFH-DA[149]; alternatively, cells could be sorted according to their response kinetics to calcium influx or biosensor activation with combined optogenetics and flow cytometry[150].

In conclusion, scRNA-seq allowed me to reliably retrieve the transcriptome of dFB neurons at single-cell granularity, and in general permits the identification of cellular markers, transcriptional changes between states, and heterogeneity within a cell population. I pursued interesting leads from all three lines of investigation in Chapters 4, 5 and 6, respectively.

4 The neurotransmitter identity of dFB neurons

4.1 Introduction

Understanding the logic of a neural network requires comprehending the wiring diagram of its circuitry as well as the functional sign of each connection. This knowledge gap is currently being covered at an unprecedented pace, with stunning results in the invertebrate model *Drosophila*, by efforts to dissect the nervous system connectome[151,32,33] and decipher the neurochemical identity and gene expression profile of individual neurons with single-cell granularity[34,36,37,136]. Both approaches then need to be bridged and complemented by functional studies[152]. Here, I will focus on the mediators of information transmission.

In chemical synapses, the neurochemical identity of a cell, and the array of cognate receptors on its connected neuronal partners, is the key functional property. Neurons deploy two strategies of chemical transmission: slow and fast synaptic transmission[153]. Fast synaptic transmission acts within a few milliseconds via the release of fast-acting neurotransmitters (in flies, glutamate, γ-aminobutyric acid, and acetylcholine) which induce opening of ligand-gated ion channels. Slow synaptic transmission, in contrast, operates in the time range of hundreds of milliseconds to minutes and involves biogenic amines, neuropeptides, gaseous molecules, and also the same fast-acting neurotransmitters, which now trigger second messengers via G protein-coupled signal transduction cascades that often result in modulation of the efficiency of fast synaptic transmission[153]. Since neurons can make use of both transmission modes simultaneously, it is clear that determining their nature is fundamental to understand the operation of a neural population within a wider circuit context.

Circuits controlling sleep behaviour are no exception: the integration of physiological variables via diverse neurotransmitters from different brain regions enables timed tuning of sleep[154,155]. In *Drosophila*, decades of studies have uncovered the major neurotransmitters involved in sleep control, which can be summarily grouped as wake-promoting (dopamine, octopamine and histamine), sleep-promoting (GABA and serotonin, despite sometimes conflicting evidences[67]), and dual function neurotransmitters (glutamate and acetylcholine, whose functions vary depending on the circuits they are involved in), according to the consistency of the effects of genetic loss and gain-of-function, artificial neuronal activation and inhibition, and

pharmacological manipulations, broadly in the organism and brain or in selected circuits[42]. In addition, a vast number of neuropeptides has been implicated in sleep control[53,85,87,156–159], often in co-transmission with other neurotransmitters[160].

The fly's dorsal fan-shaped body projecting (dFB) neurons, a key sleep-control neuronal population, has been identified as peptidergic, since it exerts sleep-promoting properties by releasing a cocktail of neurotransmitters, including the allatostatin A peptide which signals to helicon cells[53]. However, the nature of its fast-acting neurotransmitter remains unidentified. Two reports have suggested dFB neurons are GABAergic, despite limited experimental evidences[53,84].

In this chapter, I aim to identify the major fast-acting neurotransmitter of dFB neurons, via a combination of transcriptomic, behavioural, genetic, and imaging methodologies.

Understanding the nature of the fast-acting neurotransmitter of this neural population will open up experimental opportunities for probing the circuitry output with specific neurotransmitter sensors, and will be decisive for identifying novel functional post-synaptic partners of dFB neurons, the temporal dynamics of their interactions, and the resulting modes of sleep control. In particular the fast-acting neurotransmitter could be involved in one or more of three additional circuits dFB neurons are likely to be part of (**Figure 4.1**):

- A potential "flip-flop" circuit arising from extensive reciprocal interactions between DANs and dFB neurons[33], for which mutual inhibitory connections are postulated, but dFB neuron to DAN inhibition has not been shown[33,66].
- Intrinsic dFB neuron to dFB neuron interactions, given the vast connections within dFB neuron types[33] and the moderately mixed pre- and post-synaptic arborisations in both the superior median protocerebrum and the fan-shaped body layers, where dFB cells have their processes[33,53,84,161].
- Novel downstream circuits relaying dFB outputs to inhibit arousal centres[33,53,84], or gate sleep-related changes[33,53,55].

Diverse dedicated output circuits of dFB neurons, controlled by peptidergic and fast-acting neurotransmission, in combination with distinct circuit dynamics, could account for the fine tuning of the physiological manifolds of sleep[53].

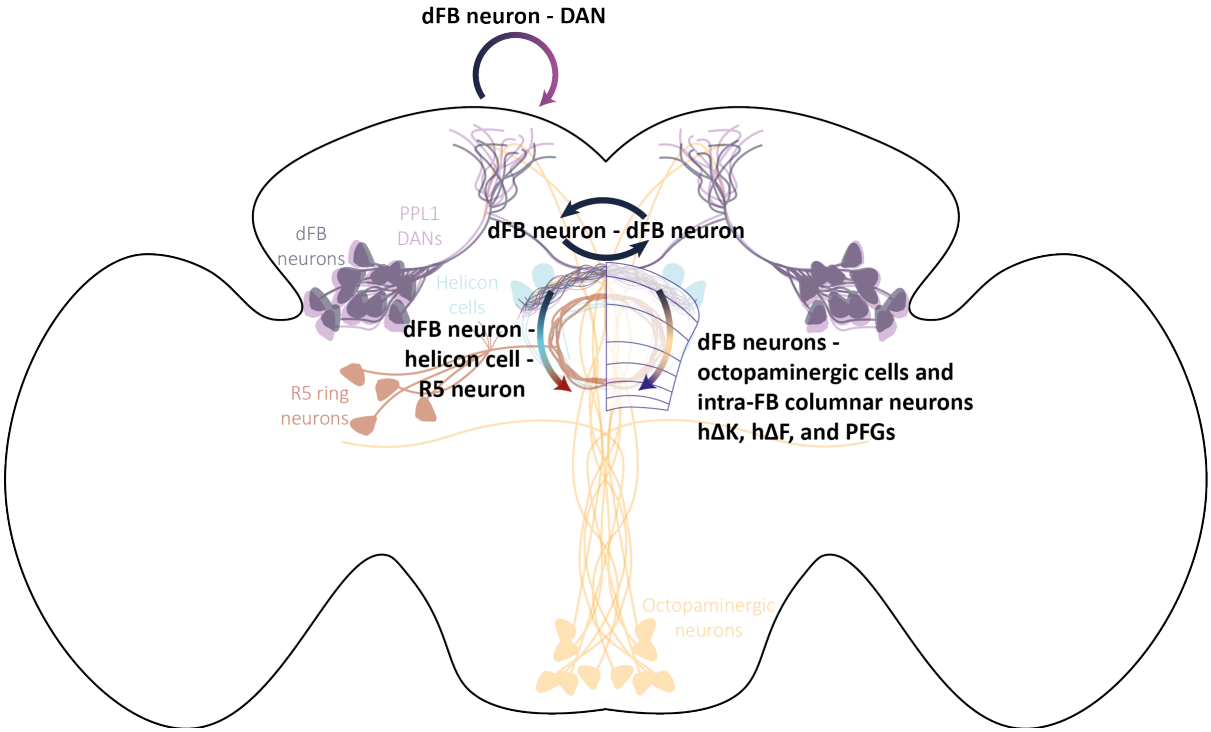

Figure 4.1 | Schematics of major circuits and cell types downstream of dFB neurons.
dFB neurons (Oxford blue) possess extensive reciprocal connections with DANs (purple), and intrinsic dFB neurons to dFB neurons synapses. dFB neurons inhibit helicon cells (turquoise), which relay their activity to ring neurons (red).
Additional circuits downstream of dFB neurons include octopaminergic cells (yellow), and intra-FB columnar hΔK, hΔF, and PFGs neurons (blue).

4.2 Results

To determine the identity of the major fast-acting neurotransmitter of dFB neurons, I examined the expression levels of the canonical fast-acting neurotransmitter markers in my single-cell transcriptome of dFB neurons: *VGlut* clearly stood out (**Figure 3.4b - e**), and dFB neurons distinctly clustered among glutamatergic neurons (**Figure 3.4f**). In the following experiments, I validated this finding with *in vivo* experiments.

4.2.1 VGlut repression and loss-of-function in dFB neurons abolishes sleep-control properties

The first strategy to probe the educated guess that glutamate is the major fast-acting neurotransmitter of dFB neurons relied on a combination of genetic repression and loss-of-function techniques.

The *Saccharomyces cerevisiae* GAL80 gene is a negative regulator of the yeast GAL4 transcriptional activator: binding of GAL80 to GAL4 blocks transcription from the UAS promoter[162,163].

I expressed the GAL80 repressor in all *VGlut*$^{+}$ cells of the fly, to evaluate whether this would abolish gene expression in dFB neurons labelled via the *R23E10-GAL4* driver. Indeed, in the presence of the *VGlut*-driven GAL80 repressor, fluorescent labelling of dFB neurons, generated by *R23E10-GAL4* driving the expression of GFP, was ablated (**Figure 4.2**).

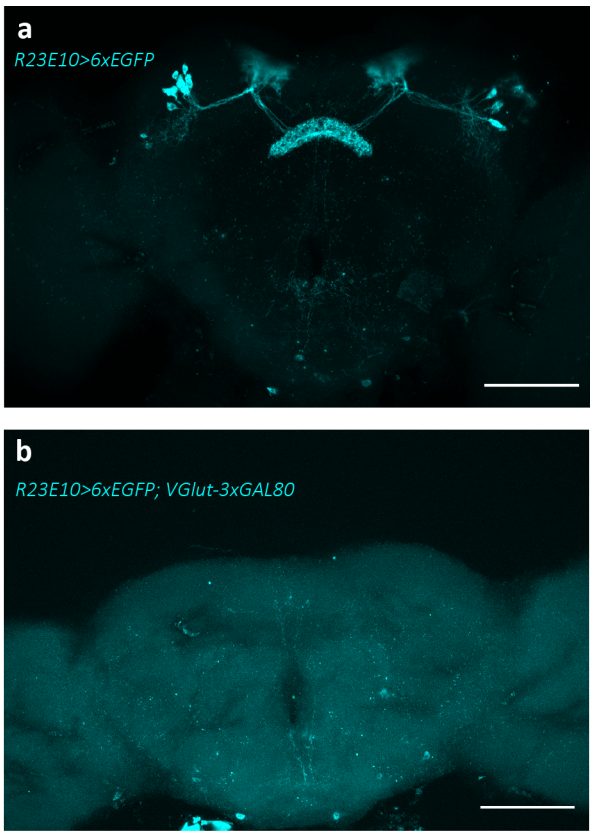

Figure 4.2 | *VGlut*-driven transcriptional repression abolishes gene expression in *R23E10-GAL4*-labelled dFB neurons.
Maximum intensity projections of confocal z-stacks of fly brains where *R23E10-GAL4* drives expression of hexameric GFP without (**a**) and with (**b**) co-expression of the transcriptional repressor GAL80 in glutamatergic cells. Scale bar = 100 µm.

Functionally, subtracting *VGlut*$^{+}$ cells from the expression domain of the *R23E10-GAL4* driver abolished the induction of sleep when these cells were activated by the heat-sensitive cation channel TrpA1 (**Figure 4.3**).

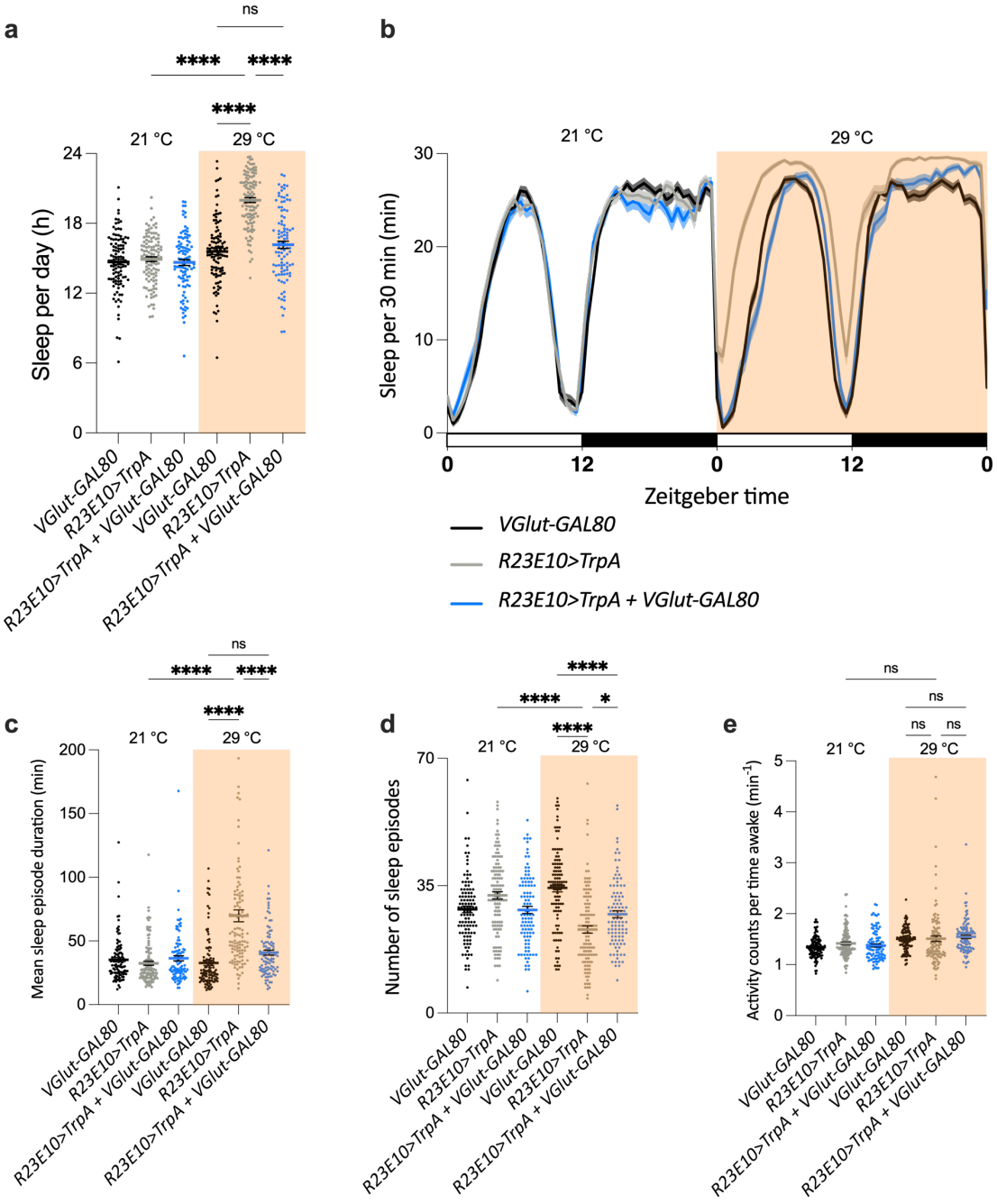

Figure 4.3 | *VGlut*-driven transcriptional repression abolishes the sleep-induction phenotype of dFB neurons.

a, Sleep per day and per 30 min bins (**b**) in flies expressing the transcriptional repressor GAL80 under the control of VGlut promoter, or *R23E10-GAL4* driving the thermogenetic actuator TrpA, or the three transgenes together, at 21 °C and when temperature was subsequently raised to 29 °C. While the increase in temperature induced sleep in *R23E10>TrpA* flies (P<0.0001 between 21 °C and 29 °C, one-way ANOVA with Šidák correction), the addition of VGlut-GAL80 dramatically decreased such effect (P<0.0001 between *R23E10>TrpA* and *R23E10>TrpA + VGlut-GAL80*, and no significant difference between *VGlut-GAL80* and *R23E10>TrpA + VGlut-GAL80* at 29 °C, one-way ANOVA with Šidák correction).

Mean sleep bout duration (**c**) and number of sleep episodes (**d**) of the same genotypes show a more consolidated sleep in *R23E10>TrpA* flies at higher temperature which was significantly abated by the addition of *VGlut-GAL80*. Activity counts per time spent awake (**e**) show no locomotor impairment underlies any of the observed differences.

Asterisks indicate significant differences between pairs. Individual values are plotted with mean ± SEM in **a**, **c**, **d** and **e**. Means (solid lines) ± SEM (shaded areas) are plotted in **b**.

To further strengthen my findings, I manipulated glutamatergic release of dFB neurons, by knocking-down the expression of *VGlut* in *R23E10-GAL4* cells: four independent RNAi lines revealed that blocking glutamate uptake into synaptic vesicles via *VGlut* decreased sleep (Figure 4.4).

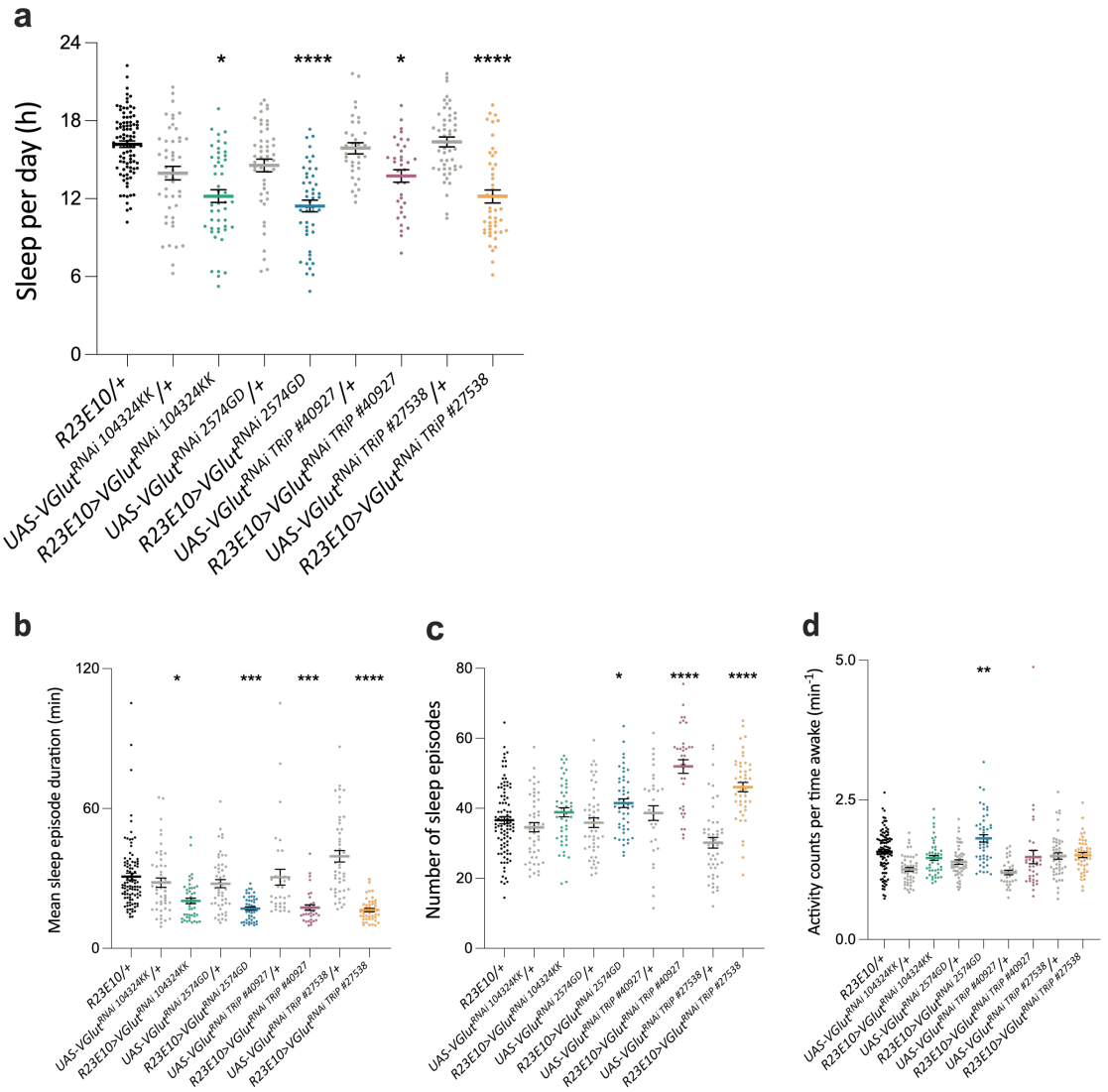

Figure 4.4 | Knockdown of *VGlut* in *R23E10-GAL4* neurons decreases sleep.

a, Total sleep per day in flies expressing four different *R23E10-GAL4*-driven *VGlut*^{RNAi} transgenes is decreased compared to parental controls. Mean sleep bout duration (**b**) and number of sleep episodes (**c**) of the same genotypes show sleep fragmentation in *R23E10-GAL4*-driven *VGlut*^{RNAi} flies. Activity counts per time spent awake (**d**) indicate locomotor activity is affected only in one experimental group.

Individual values are plotted with mean ± SEM. Asterisks indicate significant differences between each experimental group and both parental controls, with **** = p<0.0001, *** = p<0.001, ** = p<0.01, * = p<0.05, detected by one-way ANOVA on planned relevant pairwise post-hoc comparisons with Šidák correction.

4.2.2 *Genetic intersectional studies reveal dFB neurons are glutamatergic and sleep-controlling*

An alternative approach to evaluate the fast-acting neurotransmitter of dFB neurons is to take advantage of the split-GAL4 system[164,165], in particular by combining hemidrivers derived by various neurotransmitter markers' enhancers and the dFB-labelling *R23E10-GAL4* line, and then assessing the extent of the overlap of the marked neurons.

While no neuron was labelled in the midbrain by GFP driven by the combination of *R23E10-DBD* and *VAChT-AD*, only four non-dFB neurons in the subesophageal zone fluoresced when *Gad1-AD* and *R23E10-DBD* were present (**Figure 4.5**).

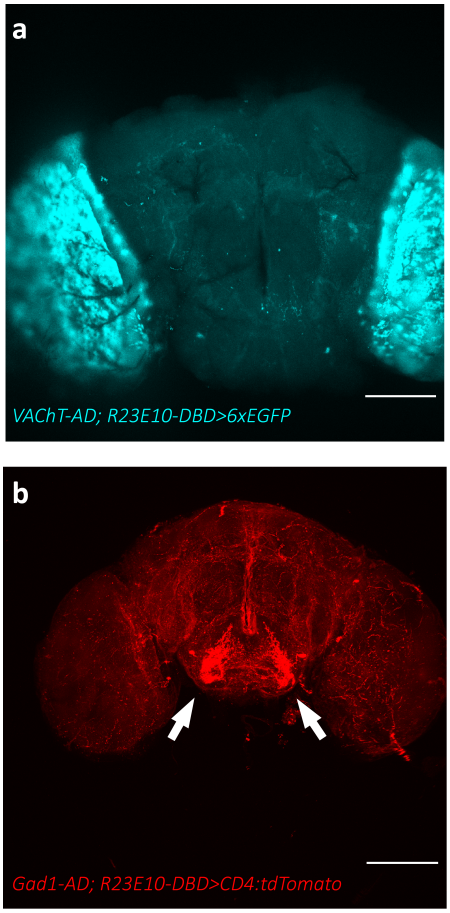

Figure 4.5 | Expression patterns of *VAChT-AD* and *Gad1-AD* combined with *R23E10-DBD*.
a, Maximum intensity projection of confocal z-stacks of *VAChT-AD; R23E10-DBD*-driven expression of hexameric EGFP. Native fluorescence (cyan) is present in the optic lobes, with no labelling in the midbrain.
b, Maximum intensity projection of confocal z-stacks of *Gad1-AD; R23E10-DBD*-driven expression of hexameric CD4:tdTomato. No native fluorescence (red) labels the midbrain, apart from 2 pairs of non-dFB neurons in the SEZ and their processes (arrows). Scale bars = 100 µm.

However, virtually all dFB neurons were labelled when *R23E10-DBD* was combined with *VGlut-AD* line for driving the expression of GFP (**Figure 4.6**).

In particular, detailed examination of this genetic combination showed that it marked around 12-13 pairs of dFB neurons in the brain, like the *R23E10-GAL4* line[66,79], and no neuron in the VNC (**Figure 4.6**).

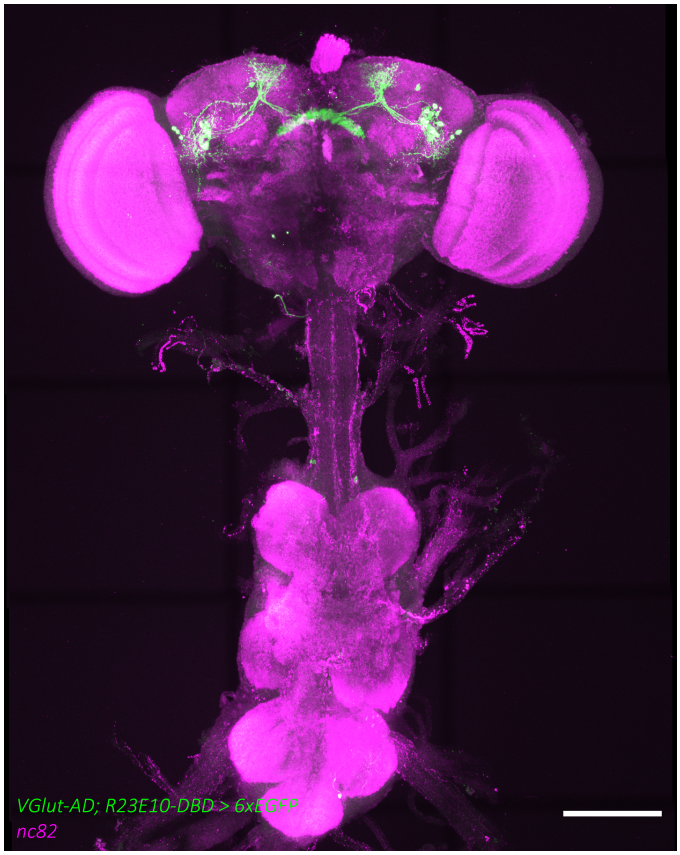

Figure 4.6 | Expression pattern of the *VGlut-AD; R23E10-DBD* line.
Maximum intensity projections of confocal z-stacks of *VGlut-AD; R23E10-DBD*-driven expression of hexameric EGFP, stained with anti-GFP (green), and neuropil stained with nc82 (magenta), in brain and VNC. This line only labels dFB neurons in the whole fly's CNS. Scale bar = 100 µm.

By comparing this pattern with the *R23E10-LexA* one (**Figure 4.7**) I noticed a total overlap in the dendritic and axonal regions, and while all *R23E10-LexA* somata were included in the pattern of the combined splits line, some *VGlut-AD; R23E10-DBD* cells were not co-labelled by *R23E10-LexA*, which is likely due to *R23E10-LexA* line labelling fewer cells than *R23E10-GAL4*[79].

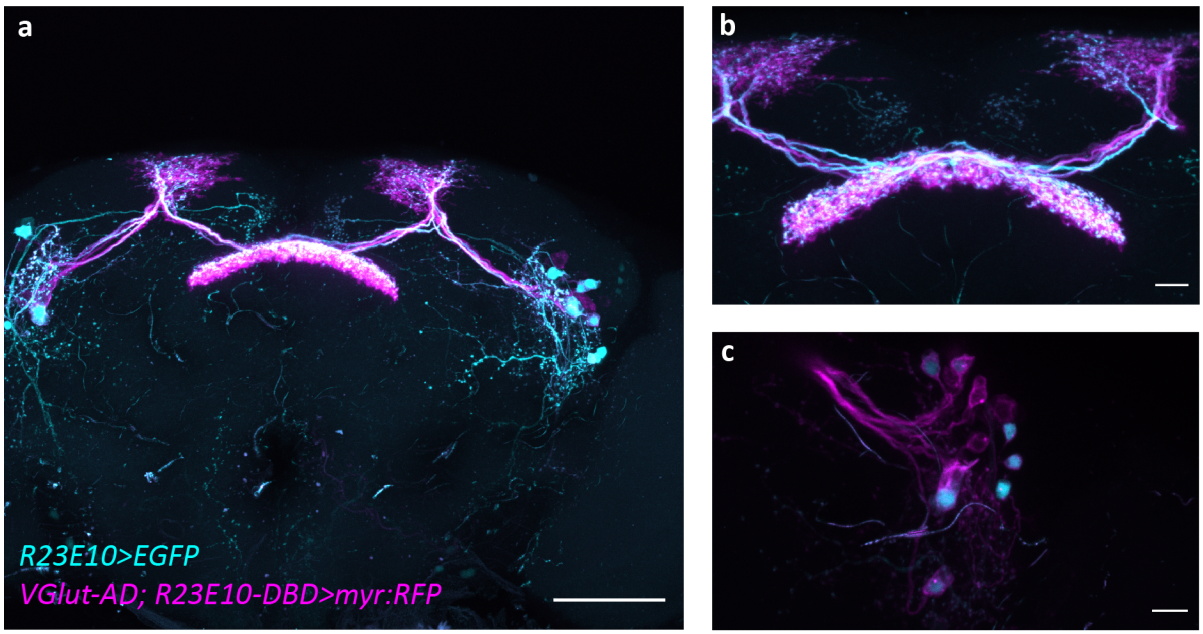

Figure 4.7 | Anatomical expression pattern overlap between VGlut-AD; R23E10-DBD and R23E10-LexA lines.
a, Maximum intensity projections of native fluorescence from confocal z-stacks for *VGlut-AD; R23E10-DBD*-driven expression of membrane-bound RFP shows complete overlap with the *R23E10-LexA* line. **b**, Detail of axonal layer and dendritic field. **c**, Detail of the somata. Scale bars = 50 µm (**a**), 10 µm (**b**, **c**).

Given the extensive dFB labelling provided by the *VGlut-AD; R23E10-DBD* line, I tried to manipulate the neuronal activity of the marked cells. Chronic inhibition of the *VGlut-AD; R23E10-DBD* neurons by expressing the inwardly rectifying potassium channel $K_{ir}2.1$ resulted in decreased sleep (**Figure 4.8**).

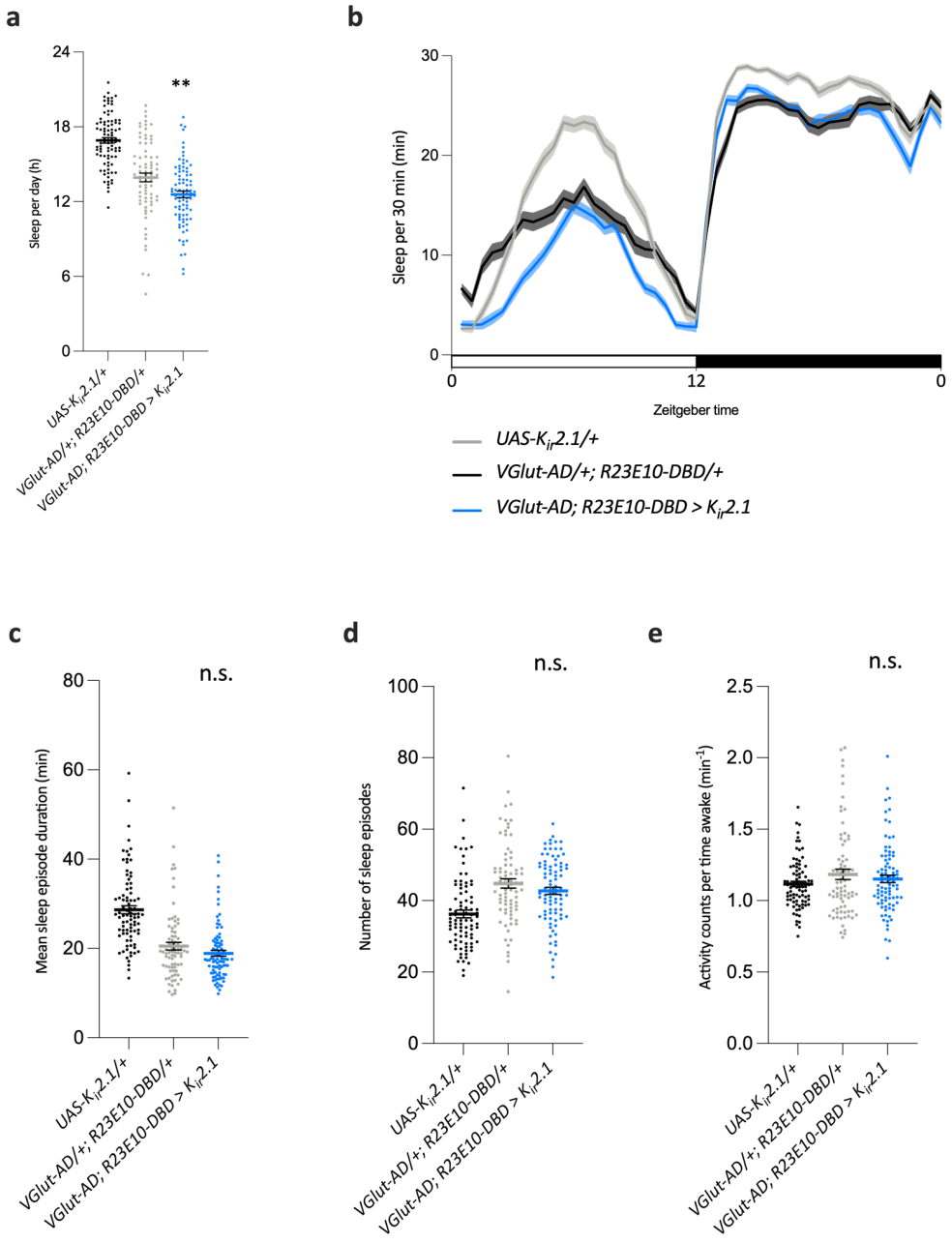

Figure 4.8 | Chronical inhibition of the glutamatergic subset of *R23E10-GAL4*-labelled dFB neurons decreases sleep.
a, Total sleep per day and (**b**) sleep profile in flies expressing the inwardly rectifying potassium channel $K_{ir}2.1$ is decreased compared to parental controls. Mean sleep bout duration (**c**), number of sleep episodes (**d**) and activity counts per time spent awake (**e**) of the same genotypes show no significant differences between experimental group and parental controls.
Individual values are plotted with mean ± SEM. Asterisks indicate significant differences between each experimental group and both parental controls, with **** = p<0.0001, *** = p<0.001, ** = p<0.01, * = p<0.05, detected by one-way ANOVA on planned relevant pairwise post-hoc comparisons with Šidák correction. Means (solid lines) ± SEM (shaded areas) are plotted in **b**.

Throttling synaptic release by expressing the light chain of tetanus toxin[166] (TNT_{Active}) reduced total sleep, while no significant effect was detected with an inactive version containing two point mutations ($TNT_{Inactive}$) (**Figure 4.9e**), which is consistent with a reduction in the chemical synaptic inhibition from dFB neurons to dopaminergic neurons, given the extensive connectivity between those two cells populations[33], resulting in enhanced arousal.

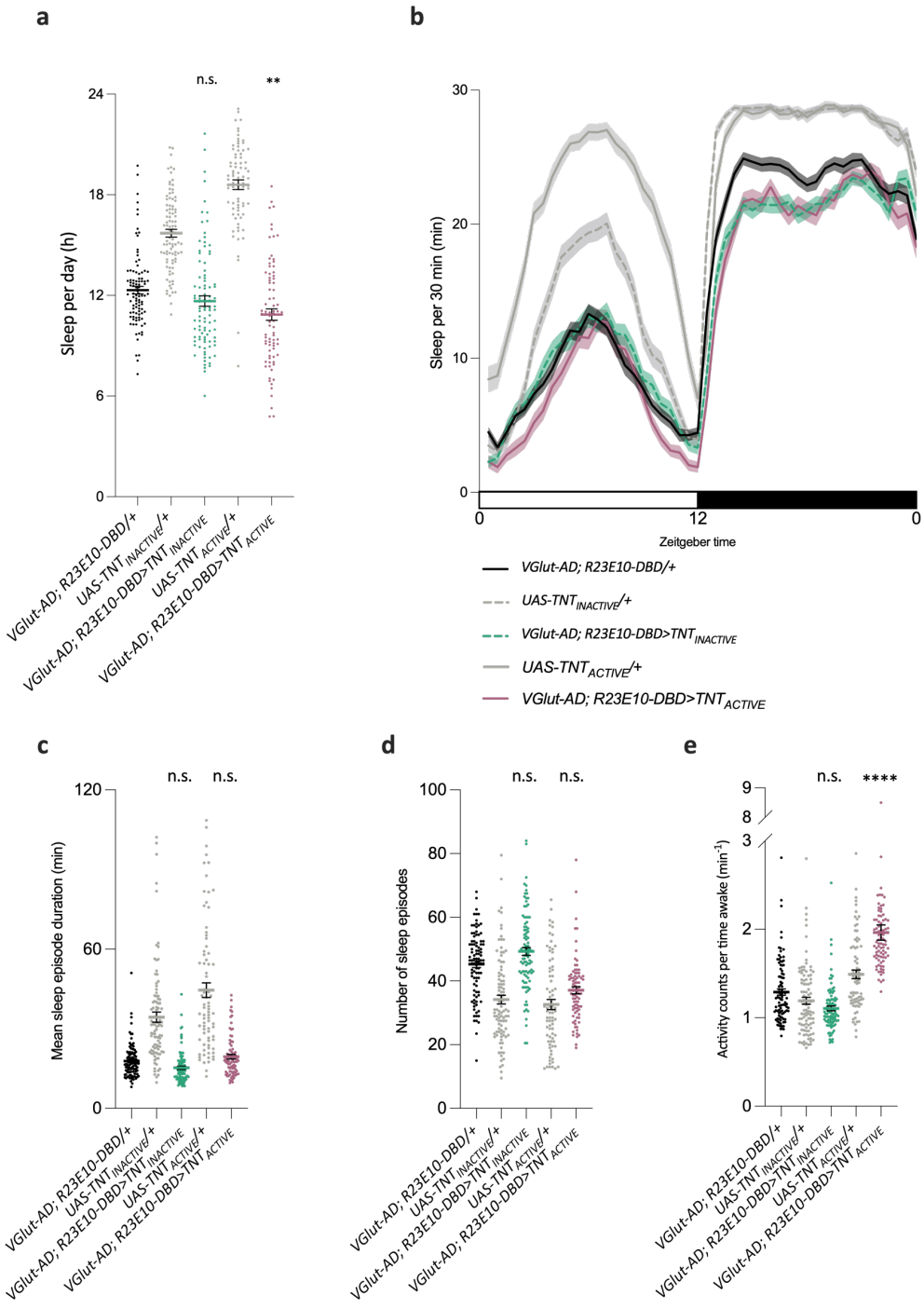

Figure 4.9 | Abolishing synaptic transmission from the glutamatergic subset of *R23E10-GAL4*-labelled dFB neurons decreases sleep. **a**, Total sleep per day and (**b**) sleep profile in flies expressing the light chain of tetanus toxin is decreased compared to parental controls, while no difference is detected for the expression of an inactivated version of the toxin. Mean sleep bout duration (**c**) and number of sleep episodes (**d**) show no significant differences between experimental group and parental controls. Activity counts per time spent awake (**e**) of the same genotypes shows only flies expressing the active toxin are significantly more active than controls. Individual values are plotted with mean ± SEM. Asterisks indicate significant differences between each experimental group and both parental controls, with **** = p<0.0001, *** = p<0.001, ** = p<0.01, * = p<0.05, detected by one-way ANOVA on planned relevant pairwise post-hoc comparisons with Šidák correction. Means (solid lines) ± SEM (shaded areas) are plotted in **b**.

For activating the *VGlut-AD; R23E10-DBD* line, I relied on optogenetic stimulation[167]: pre-print literature[56] and work in the laboratory[89] has revealed rhythmic calcium transients in dFB neurons, whose power peaks around 1 Hz both at night in cell bodies[56] and with high sleep pressure in axons[89]; bursts of action potentials underlie these oscillations[89].

Therefore, I reasoned that artificially replaying this rhythm, mimicking a physiological neuronal activity pattern of high sleep pressure, could be the optimal strategy to activate dFB cells and elicit sleep behaviour[168]. I activated cells bearing the optogenetic actuator CsChrimson::tdTomato with 1 Hz "bursts" made of 10 pulses of 3 ms each delivered at 20 Hz frequency; I first tested this pattern in *R23E10-GAL4* neurons driving *UAS-CsChrimson::tdTomato* and, during the 12 h stimulation, sleep increased in flies fed with the obligatory CsChrimson cofactor *all-trans* retinal, while no change was observed in vehicle-treated controls (**Figure 4.10**).

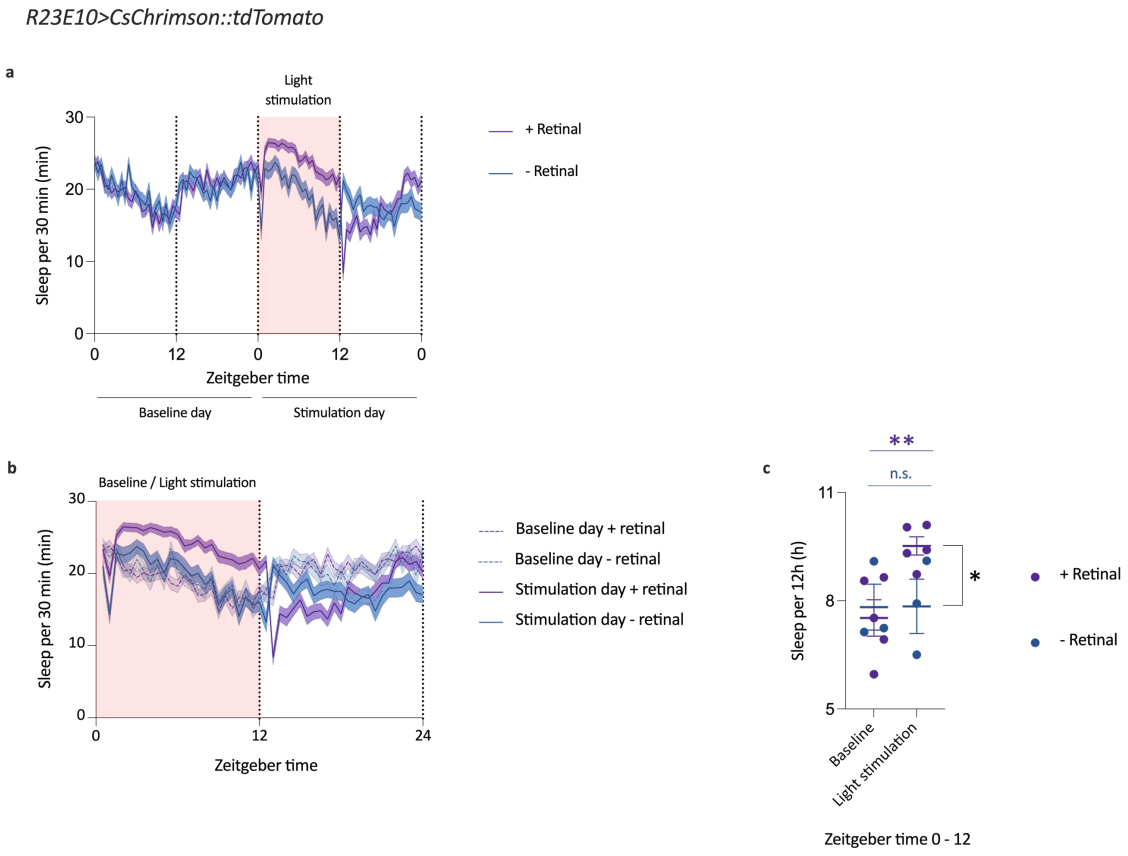

Figure 4.10 | Light activation of *R23E10-GAL4*-labelled neurons raises sleep.
a, Sleep profile obtained by movement video tracking of *R23E10>CsChrimson::tdTomato* flies fed with and without the cofactor *all-trans* retinal, over two days; at ZT 0-12 of the second day, flies were stimulated with red light. **b**, Sleep profile over the two days, overlaid. Means (solid lines) ± SEM (shaded areas) are plotted for **a** and **b**. **c**, Total sleep over ZT 0 – 12 on baseline and light stimulation day, shows a significant increase for flies fed with *all-trans* retinal, which slept significantly more than during baseline, and compared to vehicle-treated controls. Each dot represents total sleep per each replicate with mean ± SEM. Asterisks indicate significant differences between indicated groups, with ** = $p<0.01$ and * = $p<0.05$, detected by t-tests.

I then applied the same protocol to *VGlut-AD; R23E10-DBD* line and similarly observed increased sleep (although with smaller effect size) (**Figure 4.11**).

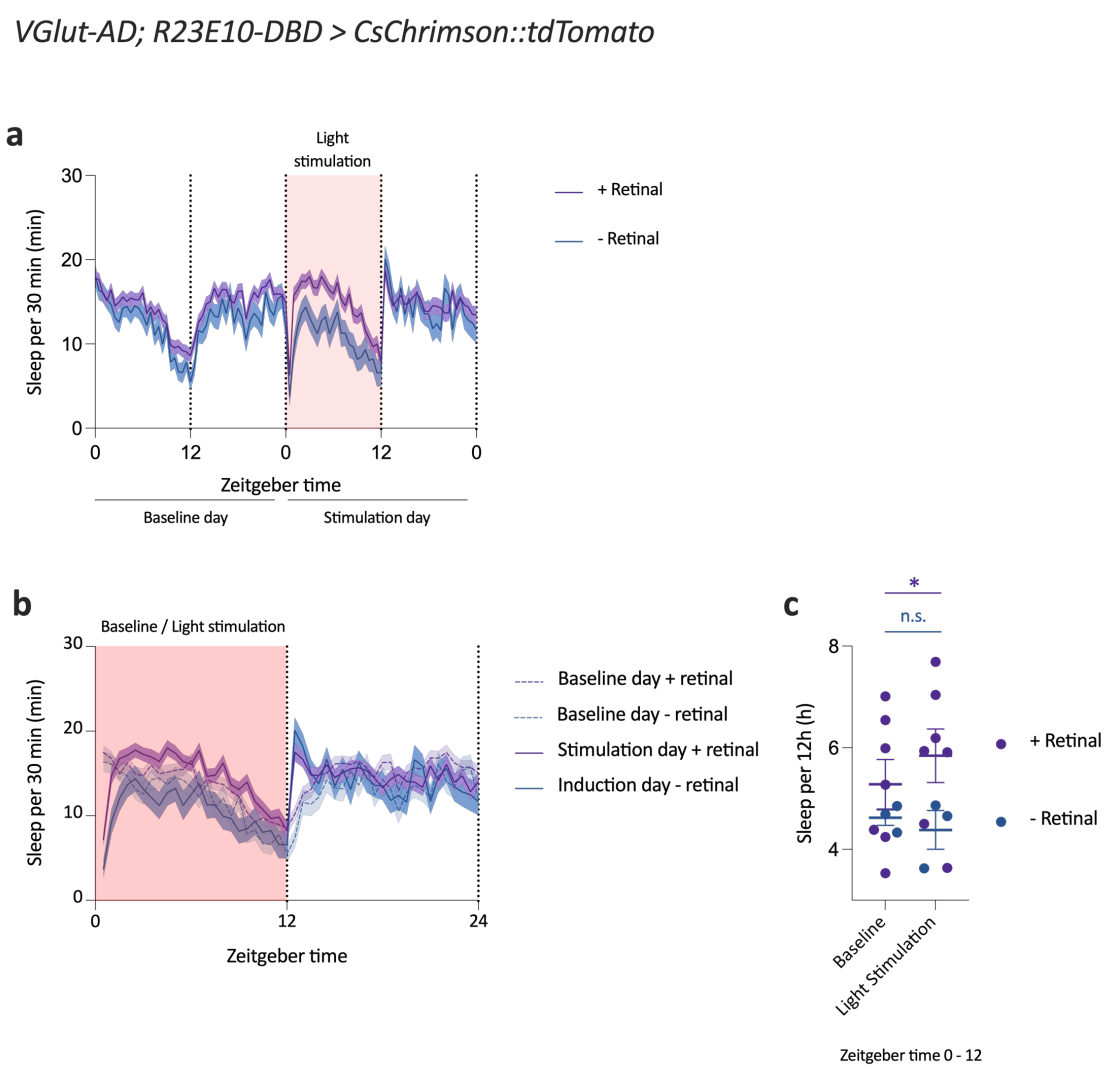

Figure 4.11 | Light activation of *VGlut-AD; R23E10-DBD*-labelled neurons raises sleep.
a, Sleep profile obtained by movement video tracking of *VGlut-AD; R23E10-DBD>CsChrimson::tdTomato* flies fed with and without the cofactor *all-trans* retinal, over two days; at ZT 0-12 of the second day, flies were stimulated with red light. **b**, Sleep profile over the two days, overlaid. Means (solid lines) ± SEM (shaded areas) are plotted for **a** and **b**. **c**, Total sleep over ZT 0 – 12 on baseline and light stimulation day, shows a significant increase for flies fed with *all-trans* retinal, which slept significantly more than during baseline, and compared to vehicle-treated controls. Each dot represents total sleep per each replicate with mean ± SEM. Asterisks indicate significant differences between indicated groups, with * = p<0.05, detected by paired t-tests.

4.2.3 *In vivo two-photon imaging of glutamate release in the dFB*

To observe *in vivo* the release of glutamate by dFB neurons, I measured the increase in fluorescence emission of the glutamate sensor iGluSnFR(A184V) expressed in *R23E10-GAL4* cells; in particular, I imaged the dFB neurons' axons via two-photon microscopy, while transiently activating dFB neurons via arousing stimuli or optogenetic activation.

Arousing stimuli have been observed to induce short-lived inhibition, likely due to the evoked transient dopamine inhibition[66,89], followed by strong excitation rebound in dFB neurons[89]. I aroused flies with an ethologically relevant stimulus by focusing an infrared beam onto the fly's abdomen and measured the change in fluorescence of iGluSnFR(A184V)[169–171], normalised over the TdTomato signal to correct for potential movement artefacts, especially during the laser stimulation, in flies where *R23E10-GAL4* was driving the expression of both fluorescent proteins. As the infrared beam stimulation started, the fly's sudden arousal resulted in a short decrease in the glutamate signal, followed by a strong rebound increase in fluorescence, mirroring the neuronal activity of dFB neurons (**Figure 4.12**).

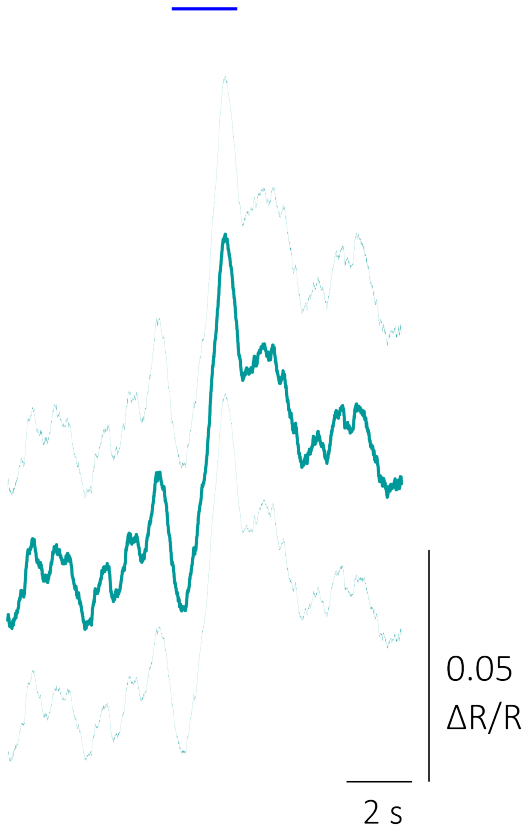

Figure 4.12 | Arousing stimulation of flies elicits glutamate release *in vivo* in the fan-shaped body.
Flies expressing the glutamate sensor iGluSnFR(A184V), and the red fluorescent protein TdTomato, both under *R23E10-GAL4* control were subjected to around 2 s-long infrared laser arousing stimulus (blue bar). Fluorescence was acquired via two-photon imaging of dorsal fan-shaped body of flies, and traces represent the differentiated ratio between green and red channels (mean ± SEM, 17 flies).

To ensure that the observed release of glutamate in the dorsal fan-shaped body region was specifically caused by *R23E10-GAL4* dFB-projecting neurons, I directly activated them via optogenetics. First, I ensured that the optical stimulation activates the cells by delivering repeatedly 500 ms light pulses to brains of live flies expressing the calcium indicator GCaMP6f and CsChrimson::TdTomato, and recording the calcium signals. The average response showed robust increases in the GCaMP6f signal upon light delivery (**Figure 4.13a**). To rule out potential spurious activation effects due to pure light responses not mediated by the optogenetic activation, I repeated the same experiment in flies raised in identical conditions but lacking the actuator CsChrimson::TdTomato, and no response was observed (**Figure 4.13a**). I then optically stimulated the dFB cells, with stimuli of various durations, and recorded the axonal glutamate sensor signal. I observed robust responses whose amplitude and duration were proportional to the stimulus length (**Figure 4.13b**).

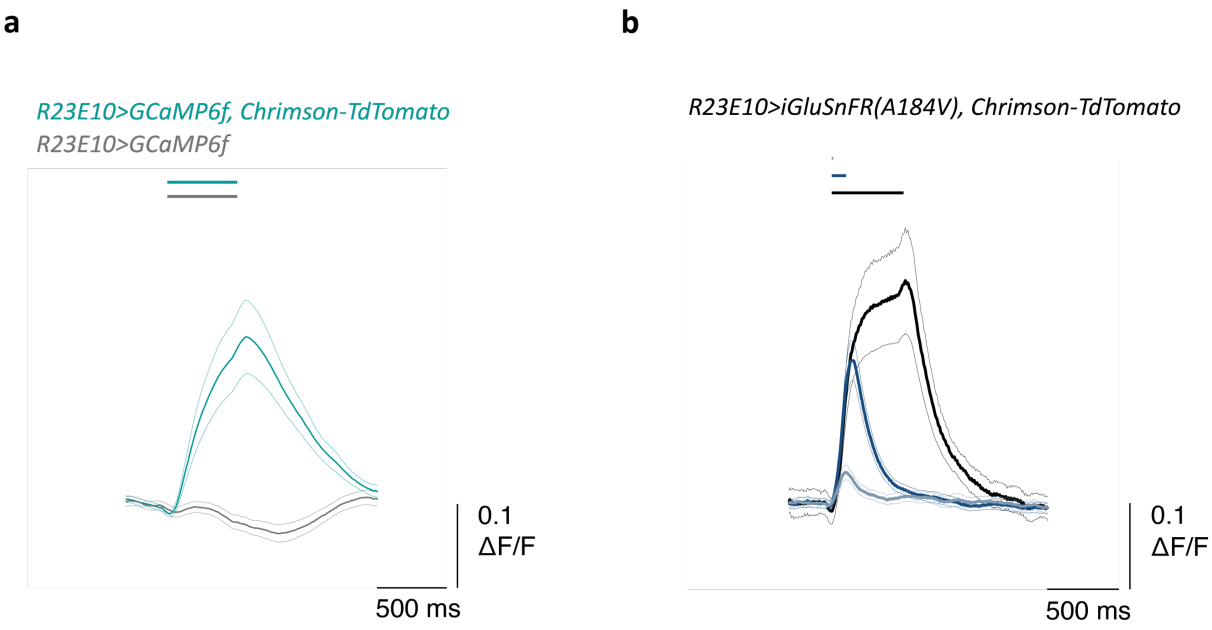

Figure 4.13 | Optogenetic stimulation of dFB neurons elicits glutamate release *in vivo* in the fan-shaped body.
Two-photon imaging of dorsal fan-shaped body of flies subjected to pulses of red light. **a**, Flies expressing the calcium indicator GCaMP6f with (green) and without (grey) the optogenetic actuator CsChrimson::TdTomato, both under the control of *R23E10-GAL4,* were subjected to 500 ms-long red light stimuli (mean ± SEM, 10 and 12 flies per group, respectively). **b**, Flies expressing the glutamate sensor iGluSnFR(A184V) and the optogenetic actuator CsChrimson::TdTomato, both under *R23E10-GAL4* control, were stimulated with 10 (light blue), 100 (dark blue), 500 (black) ms pulses of red light (mean ± SEM, 10 flies per group).

4.3 Discussion

In this chapter, I provide several lines of experimental evidence for identifying glutamate as the fast-acting neurotransmitter of dFB neurons, consistent with the significantly higher expression of the glutamatergic marker *VGlut* compared to other NT markers in my single-cell transcriptome (**Figure 3.4b**).

In addition to my own experimental evidence, I analysed in detail scRNA-seq data from a report published while this work was ongoing, which reported the full single-cell transcriptome of the fly brain across its lifespan and where via FACS sorting, a cluster of putative dFB neurons was identified within the brain[136], and this cluster also turned out to be VGlut$^+$.

Despite the predominance of *VGlut* transcripts, low expression levels of other NTs' markers could be still detected (**Figure 3.4b - e**). From my intersectional studies, it seems that other non-dFB *R23E10-GAL4*-labelled cells in the SEZ area are Gad1$^+$ (**Figure 4.5**), indicating they are GABAergic, and potentially responsible for the GABA markers detected in previous experiments of RNA purifications from *R23E10-GAL4* cells[53]. In fact, the GAL80 repression experiments show all dFB cells are glutamatergic (**Figure 4.2**), and that the glutamatergic cells labelled by *R23E10-GAL4* are necessary for inducing sleep (**Figure 4.3**). In addition, the split GAL4 line *VGlut-AD; R23E10-DBD* seems to label a number of cells equivalent to the full *R23E10-GAL4* line (**Figure 4.6**).

The split GAL4 line has proven to be useful not only for fluorescence labelling (**Figure 4.7**), but also for behavioural manipulations (**Figure 4.8, Figure 4.9, Figure 4.11**). In particular, both loss-of-function manipulations, with overexpression of an inwardly rectifying potassium channel (**Figure 4.8**) and of tetanus toxin (**Figure 4.9**), led to a decrease in sleep amount, although with different effect sizes and arousal states of the flies. These differences, present also in other work[172,173], might arise from different cellular mechanisms underlying the two inhibitory tools: the chronical hyperpolarisation of dFB neurons might plastically induce the circuitries (including the "flip-flop" DANs-dFB and the intra-dFB connections) to reset themselves to different firing levels resulting in lower baseline sleep need, while the tetanus toxin does not directly act on the membrane voltages and concurrent coincident detectors and plasticity actuators: occasional escape of a vesicle from the TNT-induced cleavage of its synaptobrevin would allow boluses of glutamate to be still released and therefore preventing a complete

plastic reset of the circuit. Alternatively, another explanation could be the differential effect of the manipulations on chemical and electrical dFB synapses[82], where the former might be dominant in the dFB-DAN interactions and the latter, which are unaffected by the toxin, in the dFB-dFB contacts.

Glutamatergic synapses are widespread throughout the whole brain, except for the mushroom body neuropils[174], and, within the fan-shaped body, its dorsal area is enriched in the glutamate transporter and classical marker VGlut[174].

Other authors have reported dFB neurons are GABAergic, via a single experiment of thermogenetic induction in the presence of RNAis targeting different neurotransmitters[84]. Although my work, which deploys several diverse methodologies and RNAi lines (**Figure 4.4**), shows that glutamate is the fast-acting neurotransmitter, this does not invalidate the current hypothesis that dFB neurons are inhibitory. Glutamate, in fact, like GABA, can exert inhibitory effects in the fly's CNS[47,71,175], via the glutamate-gated chloride channel GluClα[175,176], or the metabotropic mGluR receptor[177]. These two receptors thus represent prime targets for identifying and manipulating downstream partners of dFB neurons. Also, the effect of glutamate on sleep is dual, as it heavily depends on the circuit context in which it acts, and the receptors involved[42]: while a report on brain-wide manipulations has shown glutamate is wake-inducing[178], other studies focusing on NMDA[57,179,180] and AMPA[180] receptors demonstrated a sleep-promoting role. Therefore, targeted intervention in dedicated circuits, and probing results with *ad hoc* tools, could better reveal the specific role of glutamate transmission.

An example of such a specific probe is the glutamate sensor iGluSnFR: I established it reliably reports glutamate release in the dFB area (**Figure 4.12**, **Figure 4.13**), and could be then used to dissociate the activity of dFB cells from their actual transmission output. For example, combining this sensor with red calcium indicators, and measuring the iGluSnFR fluorescence output in correspondence of activity peaks reported by the calcium transients, in different states of sleep pressure, could reveal potential pre-synaptic plasticity. Such an experiment could complement functionally the transcriptomic and structural synaptic plasticity findings reported in Chapter 5.

Conversely, manipulations on inputs to dFB neurons, for example dopaminergic cells[33,66], could be probed in terms of glutamatergic output from dFB neurons. My experiment in which an

arousing stimulus was delivered to the fly and the glutamatergic release recorded, is an example: assuming, by educated guess, that the arousing stimulus acts mainly via dopamine, which could be experimentally verified, I observed immediate inhibition, followed by stronger excitation (**Figure 4.12**). While additional experiments might be needed to clarify the underlying dynamics of such responses, this experiment builds on the possibility of using a relevant NT sensor.

Finally, in terms of the three circuits proposed in the introduction (**Figure 4.1**), knowing the nature of the fast-acting NT means:

- For the potential DAN-dFB neuron "flip-flop" circuit, knowing that the dFB neurons' NT can be inhibitory leaves room for the postulated mutual inhibition between these two circuits. The dynamics of such interactions could be explored via simultaneous imaging recordings of the two cell populations using a combination of NT sensors and calcium indicators of different excitation/emission wavelengths, imaged in different cell compartments, and in different behavioural states. In addition, once the relevant DANs are identified, restricted manipulations of their glutamate receptors could potentially hamper such flip-flop resulting in altered oscillations of the circuit and sleep deficits.
- For the intrinsic dFB neuron to dFB neuron interactions, mutual inhibition of neurons could account for the observed oscillatory patterns and their variations over time and sleep pressure[56,89]. Disrupting the ability of dFB neurons to sense such mutual glutamate release could disrupt the physiological oscillation pattern and, in turn, sleep control. Conversely, applying glutamate exogenously by focal application or local uncaging, would reveal the acute response of dFB neurons to this NT.

  A main caveat to this sort of experiment is that dFB neurons seem to receive glutamatergic inputs[84], although of excitatory nature. It is then plausible that the receptors involved in the two processes are different, and therefore it would be possible to disentangle them. Additionally, simultaneous synaptic blockage of the glutamatergic inputs would also help dissecting the two transmission channels.
- For the additional downstream circuits of dFB neurons, it is possible that glutamate is the NT responsible for the reported inhibition of dFB neurons to octopaminergic VPM3 cells[33,84], and for the transmission to the anatomically connected, but yet not functionally studied, intra-FB columnar neurons hΔK, hΔF, and PFGs (protocerebral bridge – fan shaped body – gall neurons)[33].

Downstream synaptic partners could be identified among those labelled with my anterograde tracing experiments (Figure 9.1).

The connectivity of dFB neurons, combined with a potentially inhibitory fast-acting neurotransmission, allows me to hypothesise various levels of network activity control, in addition to the circuitry already known. Local inhibition among dFB cells could create and sustain coherent network oscillations[56,89,181], which could be entrained, modulated, and mutually inhibited by dopaminergic neurons, similar to the proposed flip-flop model of sleep control[23], with local inhibition, and akin to that from GABAergic VTA to dopaminergic VTA neurons[182]. Eventually, the resulting differences in total NT output from dFB neurons, or in their firing patterns, would be conveyed to downstream circuits eliciting the various manifestations of sleep behaviour.

5 Sleep history-regulated transcriptome of dFB neurons reveals presynaptic plasticity and bidirectional control of mitochondrial dynamics and sleep

5.1 Introduction

Sleep, and its loss, affect virtually every tissue of an animal, but is controlled by restricted neuronal populations in the brain. These neurons not only respond differently to sleep history, but are also causally responsible for the various manifestations of this behaviour[155].

Among these, a fundamental feature that defines sleep is its homeostatic control. Neurons that govern this aspect of sleep must have a privileged role as ultimate sensors and integrators of sleep need and first transducers of information towards behaviour-directed actuation circuits. Understanding these processes can provide important clues about the physiological variables linked to sleep, and in general regarding neural implementations of temporal accumulation and homeostats. In fact, sleep-control circuits react to lack of sleep by mobilising mechanisms that enable homeostatic compensation.

An experimental strategy to open a window on those mechanisms is to analyse the molecular fingerprint of dedicated brain regions, in individuals at high sleep pressure, and infer the underlying mechanisms. Many studies have investigated the whole brain or large brain areas of sleep deprived animals, shedding light on the consequences of sleep loss[183]; however, only few have comprehensively explored molecular changes in sleep-control centres[96], mostly due to their small size and limited genetic access.

This problem is tractable in *Drosophila*, where genetic access to the sleep-control neuronal population of dFB neurons is available.

In **Chapter 3,** I have illustrated the experimental design and validation of my scRNA-sequencing of the whole brain of *Drosophila*, enriched in identifiable dFB neurons. I obtained this transcriptome in conditions of high and low sleep pressure, in particular at the end of a night of sleep deprivation and *ad libitum* sleep. In this chapter, I will describe which genes are differentially expressed between these two conditions, generate hypotheses on the underlying molecular and cellular processes, and investigate them experimentally.

In my exploration, I will also try to provide insights towards two unknown matters regarding dFB neuron function:

First, what makes these neurons especially suitable to integrate and initiate the discharge of sleep pressure, and, second, how can mitochondrial ROS produced upon sleep loss affect components of the cell membrane? In particular, for the first open question, two hypotheses have been formulated[83]: either these cells lack sufficient defences against oxidative stress, or their metabolic state is mismatched with their firing rates; in particular, in awake and fed flies, the ATP/ADP ratio is high, but dFB neurons are less excitable[66,83], and since firing is one of the most energetically expensive tasks that a neuron performs[184,185], this condition favours superoxide and ROS generation by reverse electron transport[186,187].

As for the second point, ROS levels increase in dFB neurons upon sleep loss, and this is tracked by the conversion of Shaker's $K_V\beta$ subunit, Hyperkinetic, to the $NADP^+$-bound form[83]. The oxidation of the cofactor slows the A-type current inactivation and promotes higher action potential rates, inducing sleep[83]. However, it is unclear how ROS produced in the mitochondria reach the membrane and become substrates of the aldo-keto reductase Hyperkinetic. Lipid peroxidation products might be intermediates that locally serve as hydride acceptors for Hyperkinetic[83]. Still, how mitochondrial ROS peroxidise membrane lipids is unknown.

Among the molecular hallmarks of sleep deprived dFB neurons, I will try to detect patterns that can help elucidate how (this) sleep-control centre(s) can direct this behaviour.

5.2 Results

5.2.1 Sleep history-regulated transcriptome of dFB neurons

The sleep deprivation method used here effectively depleted experimental flies of sleep (**Figure 3.1a**), and mobilised genes that were differentially transcribed between the two states: for example, the established gene marker for sleep deprived fly brains *Cytochrome oxidase C, subunit I* (*mt:CoI)*[39] showed the same trend also in my whole brain dataset, while housekeeping genes used as normalisation controls in sleep studies were unchanged (*RpL32*[67,188,189], *Rap2l*[53], and *RpL13A*[190,191]) (**Figure 5.1a, b**).

Focusing on the dFB neurons population, I detected 237 cells coming from rested brains and 86 obtained from sleep deprived flies (**Figure 5.1c**); I compared the differentially expressed genes (DEGs), both in terms of percentage of cells expressing each gene, and expression levels themselves. The expression of 122 genes differed significantly between the two sleep pressure states (**Figure 5.1d**, full list of differentially expressed genes in **Table 9.2**). This set appeared not to be a random collection of genes. Rather, the identities of differentially expressed genes hinted towards two generic neuronal processes, cellular metabolism and synaptic neurotransmitter release, being engaged in sleep deprived dFB neurons: sleep loss led to the selective upregulation of genes encoding mitochondrial proteins and involved in OXPHOS and bioenergetic processes, while it selectively downregulated genes controlling pre-synaptic release (**Figure 5.1e**, **Appendix 9.9**). Two independent gene ontology analyses confirmed these findings and pinpointed to mitochondria and presynaptic active zones as main subcellular sites within dFB neurons where the cells experience changes driven by sleep pressure. (**Figure 5.1e**, **Appendix 9.8** and **9.7**).

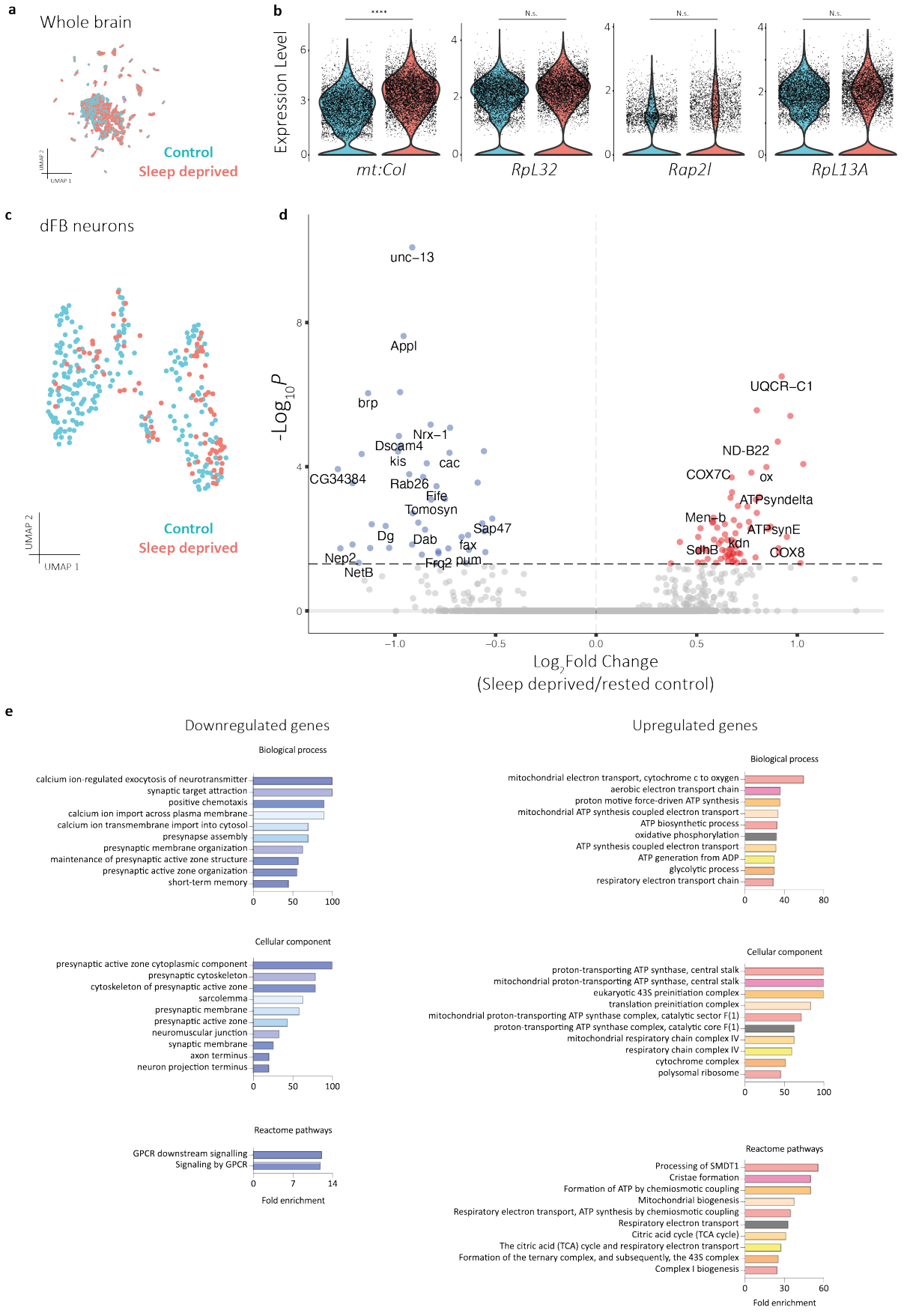

Figure 5.1 | Sleep history modulates transcriptome of dFB neurons for mitochondrial metabolism and synaptic genes.
a, Two-dimensional UMAP representation of the whole fly brain, grouped according to sleep history of the originating flies (as in **Figure 3.2a**). **b**, Gene expression distribution in the violin plots between rested (cyan) and sleep deprived **(continues on next page)**

(continues) (salmon) brain showed upregulation of the sleep deprivation marker *mt:CoI*, and no changes in the housekeeping genes *RpL32, Rap2l, RpL13A* (Wilcoxon Rank Sum test, with P-value adjusted using Bonferroni correction based on the total number of variable genes in the whole brain dataset, **** = P<0.0001). **c**, Two-dimensional UMAP representation of the dFB neurons, grouped according to sleep history of the originating flies. In **a-c**, each dot is an individual cell. **d**, Volcano plot of the differentially expressed genes within dFB neurons, between sleep deprived and rested control conditions, arranged according to the adjusted $-Log_{10}$P-value (genes with adjusted P-value<0.05 are coloured), and Log_2 of the fold change between sleep deprived and rested controls (genes significantly upregulated upon sleep deprivation are in red, while the significantly downregulated ones are in royal blue). To identify statistically significant genes, Wilcoxon Rank Sum test was used, with P-value adjusted using Bonferroni correction based on the total number of variable genes in the whole brain dataset. Some DEGs are labelled. **e**, Gene ontology terms (biological process, cellular component, and reactome pathways) enriched for the downregulated (left) and upregulated (right) dFB neurons' DEGs (the 10 most enriched terms are plotted, where possible; fold enrichments>100 were detected and plotted as 100).

Cell populations of similar size in my datasets, like Kenyon cells (KCs, 603 cells) and projection neurons of the antennal lobe (PNs, 317 cells), did not display analogous changes (**Figure 5.2**): while in the PNs only one gene, a translation regulator factor, was differentially expressed with sleep history (**Figure 5.2d**, **e**), the KCs' transcriptional response to sleep deprivation mobilised more genes (**Figure 5.2a**, **b**); their enrichment analysis pointed out several terms, and among those, only a few regarding the electron transport chain among the upregulated genes and synapse transmission among the downregulated ones (**Figure 5.2c**). However, these enrichments were not comparable to the ones observed in the dFB neurons, in terms of fold change and abundance of gene ontology terms.

The transcriptional signature of sleep deprivation in these different cell types thus suggests that the transcriptional changes induced by different sleep pressure states are cell-type specific, and the ones observed in dFB neurons are possibly specific to those cells.

Given these indications on the processes and subcellular compartments to investigate within dFB neurons, I deepened my study, starting by optically visualising the structures of interest, in different sleep pressure states.

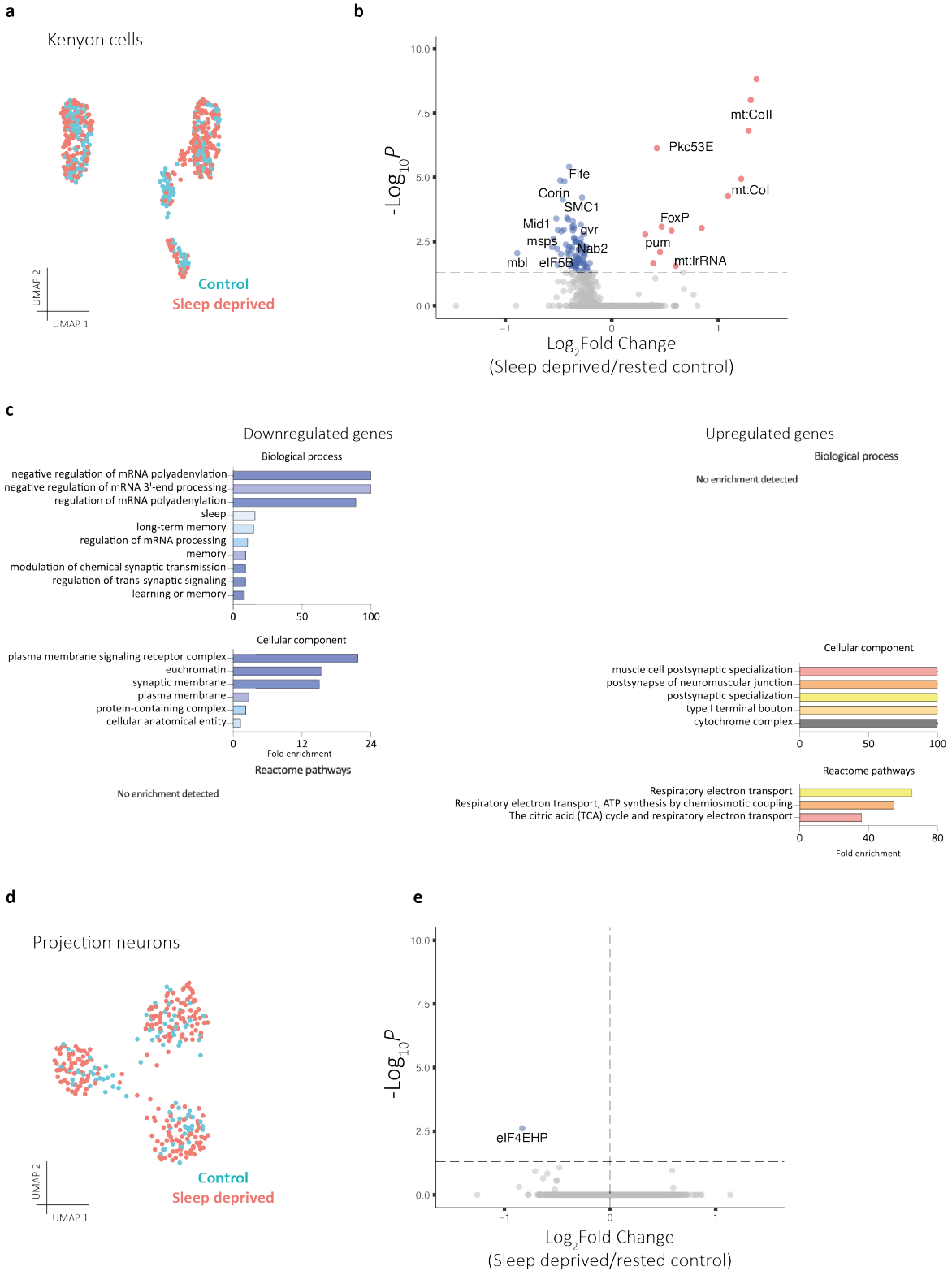

Figure 5.2 | Genes differentially expressed depending on sleep history, in Kenyon cells and projection neurons.
Two-dimensional UMAP representation of the Kenyon cells (**a**) and projection neurons (**d**), grouped according to sleep history of the originating flies. In both plots, each dot is an individual cell. Volcano plot of the differentially expressed genes within KCs (**b**) and PNs (**e**), between sleep deprived and rested control conditions, arranged according to the adjusted -Log_{10}P-value (genes with adjusted P-value<0.05 are coloured), and Log_2 of the fold change between sleep deprived and rested controls (genes significantly upregulated upon sleep deprivation are in red, while the significantly downregulated ones are in royal blue). To identify statistically significant genes, Wilcoxon Rank Sum test was used, with P-value adjusted using Bonferroni correction based on the total number of variable genes in the whole brain dataset. Some DEGs are labelled. **c**, Gene ontology terms (biological process, cellular component, and reactome pathways) enriched for the downregulated (left) and upregulated (right) KCs' DEGs (the 10 most enriched terms are plotted, where possible; fold enrichments >100 were detected and plotted as 100).

5.2.2 Sleep deprivation induces structural synaptic plasticity

I tagged the pre-synaptic sites of dFB neurons using the Synaptic Tagging with Recombination (STaR) method, which employs a transgenic version of the *Bruchpilot* gene (*brp*) fused to a peptide tag. *brp* is a major structural component of the cytoskeleton in the fly's pre-synaptic active zone, and its abundance is commonly used as a proxy for synaptic strength[192]. STaR allows the simultaneous expression of tagged *brp*, and a fluorophore used for normalising the expression intensity, in a genetically-identifiable cellular set[193] (**Figure 5.3a**).

I labelled synapses of dFB neurons, R5 neurons, and Kenyon cells, in animals either rested or sleep deprived for 12 hours (**Figure 5.3b, c**), at the same circadian timepoint (ZT 0).

Following sleep deprivation, axons showed decreased STaR labelling in dFB neurons relative to rested conditions, recapitulating the effects observed in the transcriptome, while the STaR signal was increased in R5 neurons, as previously reported[57], and no difference was observed in Kenyon cells (**Figure 5.3c**).

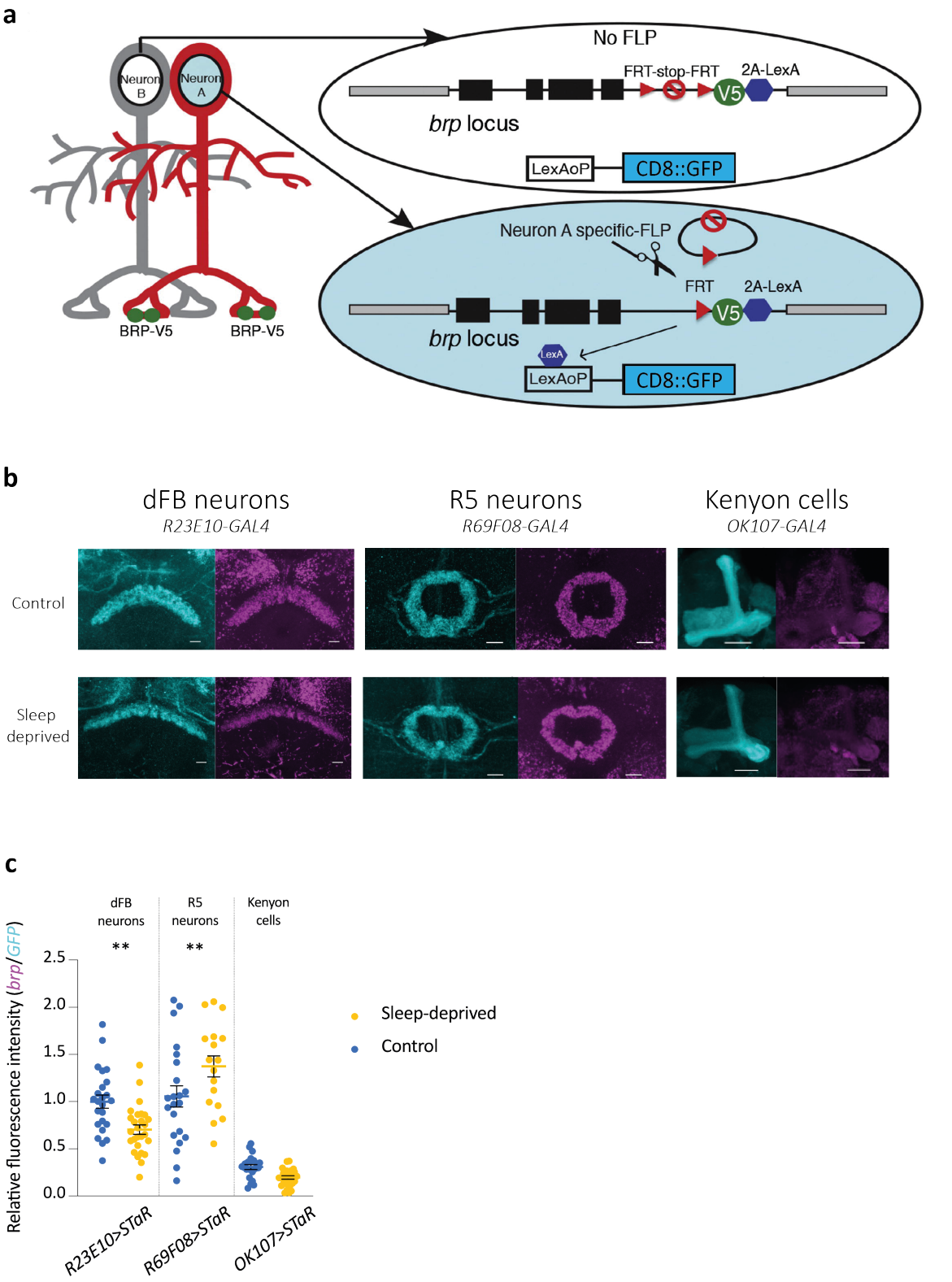

Figure 5.3 | Sleep deprivation affects synaptic plasticity in sleep-dedicated circuits.

a, Schematics of STaR methodology, adapted from[193], where neuron A is marked by a GAL4 line of interest and STaR labelled.

b, Maximum intensity projections of axons' z-stacks of *R23E10-GAL4*-labelled dFB neurons (left), *R69F08-GAL4*-labelled R5 neurons (middle) and *OK107-GAL4*-labelled Kenyon cells (right), from rested (top row) and sleep deprived (bottom row) flies. Representative images of CD8::GFP (cyan) and BRP::V5 (magenta) signals are shown. Scale bars = 10 µm.

c, Quantification of fluorescence ratio between BRP::V5 and CD8::GFP signal in dFB neurons, R5 neurons and Kenyon cells of rested (blue) and sleep deprived (yellow) flies. Two-way ANOVA detected a significant effect for sleep deprivation compared to rested control flies ($P<0.0001$, $F_{(2, 86)} = 19.88$), and was followed by one-way ANOVA on planned relevant pairwise post-hoc comparisons with Šidák correction, with ** = $p<0.01$. Values for individual anatomical structures are plotted with mean ± SEM.

5.2.3 Bidirectional control of sleep and mitochondrial dynamics

As described above, genes involved in mitochondrial OXPHOS and metabolism were selectively upregulated in sleep deprived dFB neurons (**Figure 5.1**). I therefore asked if these changes were also reflected in differences in mitochondrial number and morphology. To this end, I expressed a mitochondria-localised version of EGFP in dFB neurons (**Figure 5.4a**) and imaged mitochondria in dendrites of flies that had been sleep deprived overnight for 12 h, or time-matched control flies that had rested *ad libitum* during that time (**Figure 5.4b, left** and **centre**). In particular, I chose dendrites as they are a cellular compartment that showed ROS accumulation upon sleep deprivation[83]. On the mitochondria identified in these images, I performed a morphometric analysis which showed that the sleep deprived dFB neurons' mitochondria have smaller volume, surface area, and branch length compared to rested controls; they are also more spherical and show a trend towards increased numbers (**Figure 5.4c**).

If this observation was indeed due to a build-up of ROS, then shunting this accumulation ought to blunt the effect of sleep deprivation on mitochondrial morphology. The alternative oxidase (AOX) of *Ciona intestinalis* acts as a "pressure valve" in the electron transport chain, thus preventing the accumulation of ROS. When dFB neurons of sleep deprived flies expressed AOX, most of the above-mentioned phenotypes were reversed to control levels, in particular, because of the reduction in sphericity to levels of rested flies' mitochondria, and increased length of branches, indicative of less fragmented mitochondria (**Figure 5.4**). In addition, as AOX in sleep deprived brains increased the number of (less spherical) mitochondria, and improved (although not significantly) the mean surface area and volume of individual mitochondria, it resulted in an overall rescue of the total volume and surface area of the organelles.

Interestingly, sleep deprivation had no effect on mitochondrial morphology in dendrites of another neuronal population, the PNs of the antennal lobe (**Figure 5.4d top**, rested; **bottom**, sleep deprived) (**Figure 5.4e**). This finding is consistent with their weak or absent transcriptional response upon sleep deprivation (**Figure 5.2e**).

Thus far, I have described that the build-up of sleep pressure in dFB neurons resulted in an increase in the expression of genes involved in OXPHOS and mitochondrial metabolism and that this was associated with a fragmented mitochondrial morphology. Was this the mere

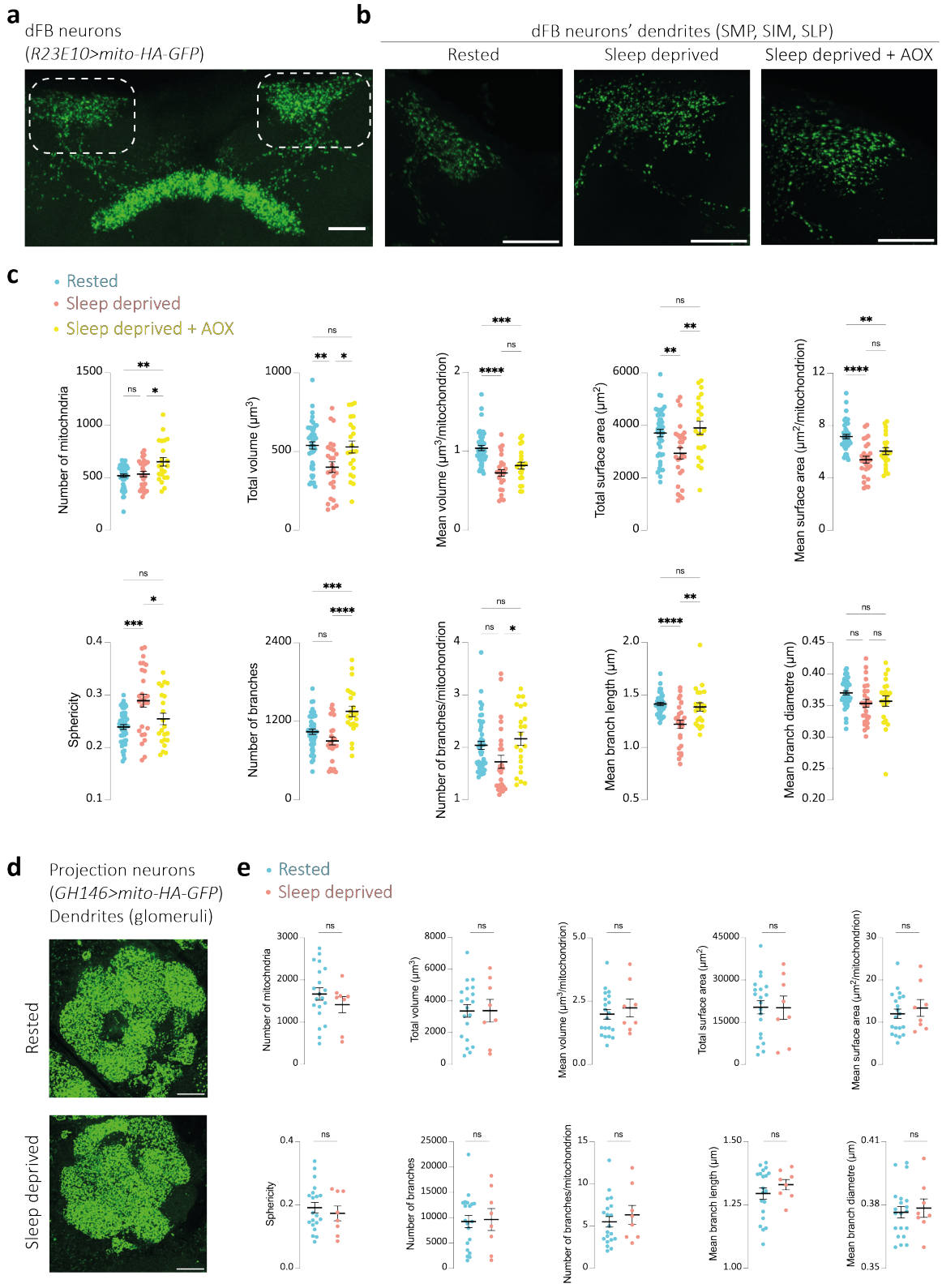

Figure 5.4 | Mitochondrial dynamics in dFB neurons is modulated by sleep pressure.
a, Expression pattern of GFP-labelled dFB neurons mitochondria (*R23E10>mito-HA-GFP*), with the dendritic SMP, SIP and SLP regions circled in dashed white line. **b**, Detail of dFB dendrites in flies rested, sleep deprived, and sleep deprived while expressing of AOX. **c**, Analysis of morphometric data, obtained from dendritic mitochondria. **d**, Maximum intensity projections of z-stacks of PNs glomeruli labelled with mitochondrial GFP (*GH146>mito-HA-GFP*), in rested (top) or sleep deprived (bottom) flies. **e**, Same metrics for PNs are plotted as in (**c**). Scale bars = 20 µm. Each dot represents the average value across all mitochondria per hemispheric anatomical structure of interest; mean and SEM are depicted. Asterisks indicate significant differences between each experimental group and both parental controls, with **** = p<0.0001, *** = p<0.001, ** = p<0.01, * = p<0.05, detected by one-way ANOVA in on planned relevant pairwise post-hoc comparisons with Šidák correction in (**c**), and t-tests in (**e**).

consequence of excess sleep debt, or are mitochondrial dynamics and metabolism *causally* involved in the control of sleep? To answer this question, one ought to gain experimental control over mitochondrial dynamics and directly test if their manipulation results in corresponding changes in sleep. I therefore manipulated master regulators of mitochondrial fission and fusion in dFB neurons and evaluated the effects of these interventions on sleep.

Dynamin-related protein 1 (*Drp1*) is a dynamin-like GTPase that plays a core role in the fission machinery. Promoting fission via the overexpression of this gene, using three different transgenic lines, decreased sleep (Figure 5.5).

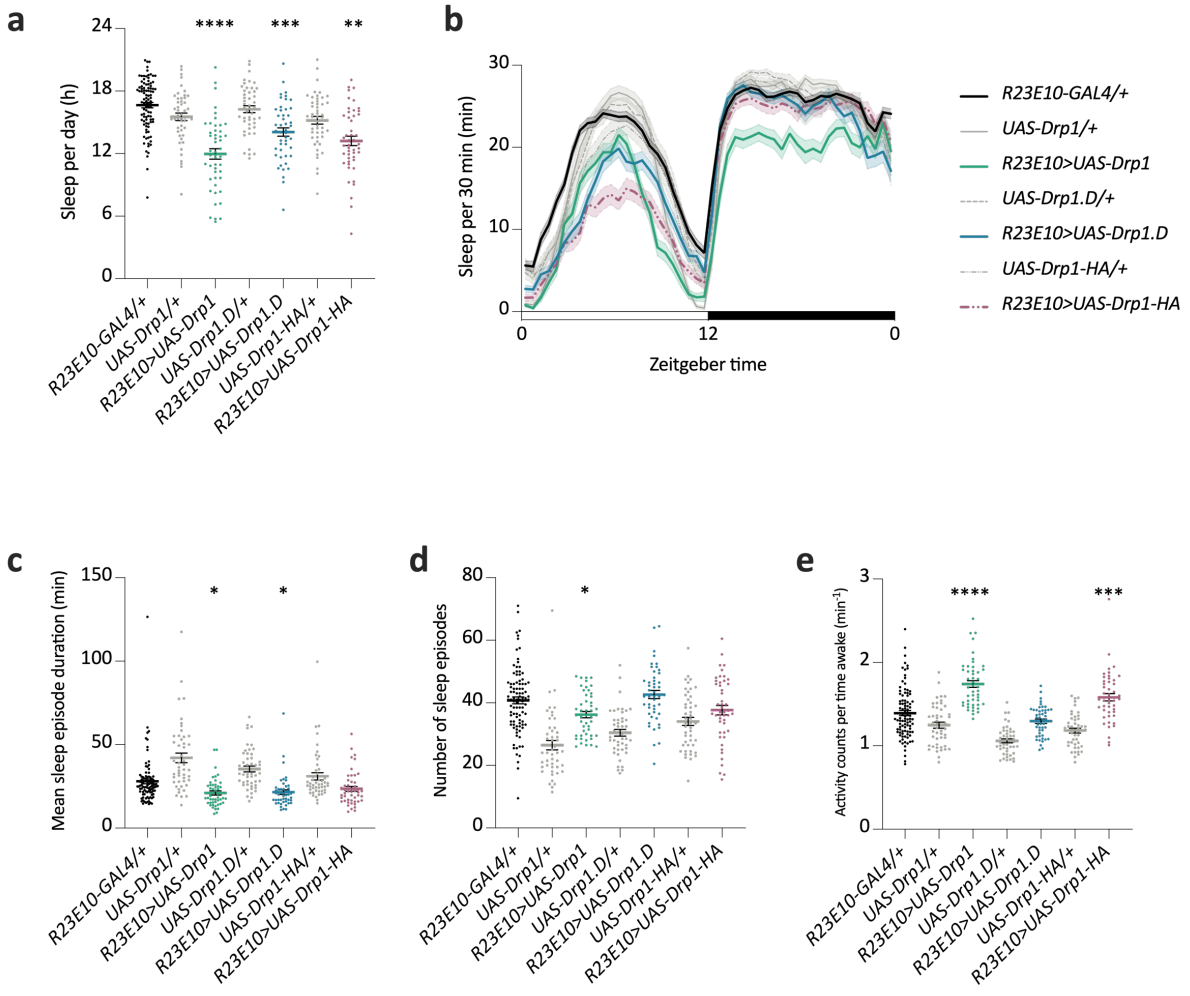

Figure 5.5 | Overexpression of the mitochondrial fission-promoting Dynamin-related protein 1 (*Drp1*) in dFB neurons reduces sleep.
a, Total sleep per day and (**b**) sleep profile in flies expressing three different *R23E10-GAL4*-driven *Drp1* overexpression transgenes is decreased compared to parental controls. Mean sleep bout duration (**c**) and number of sleep episodes (**d**) of the same genotypes show reduction of sleep episodes durations in two *R23E10-GAL4*-driven *Drp1* overexpressing flies. Activity counts per time spent awake (**e**) indicate locomotor activity is affected in two experimental groups.
Individual values are plotted with mean ± SEM. Asterisks indicate significant differences between each experimental group and both parental controls, with **** = p<0.0001, *** = p<0.001, ** = p<0.01, * = p<0.05, detected by one-way ANOVA on planned relevant pairwise post-hoc comparisons with Šidák correction. Means (solid lines) ± SEM (shaded areas) are plotted in **b**.

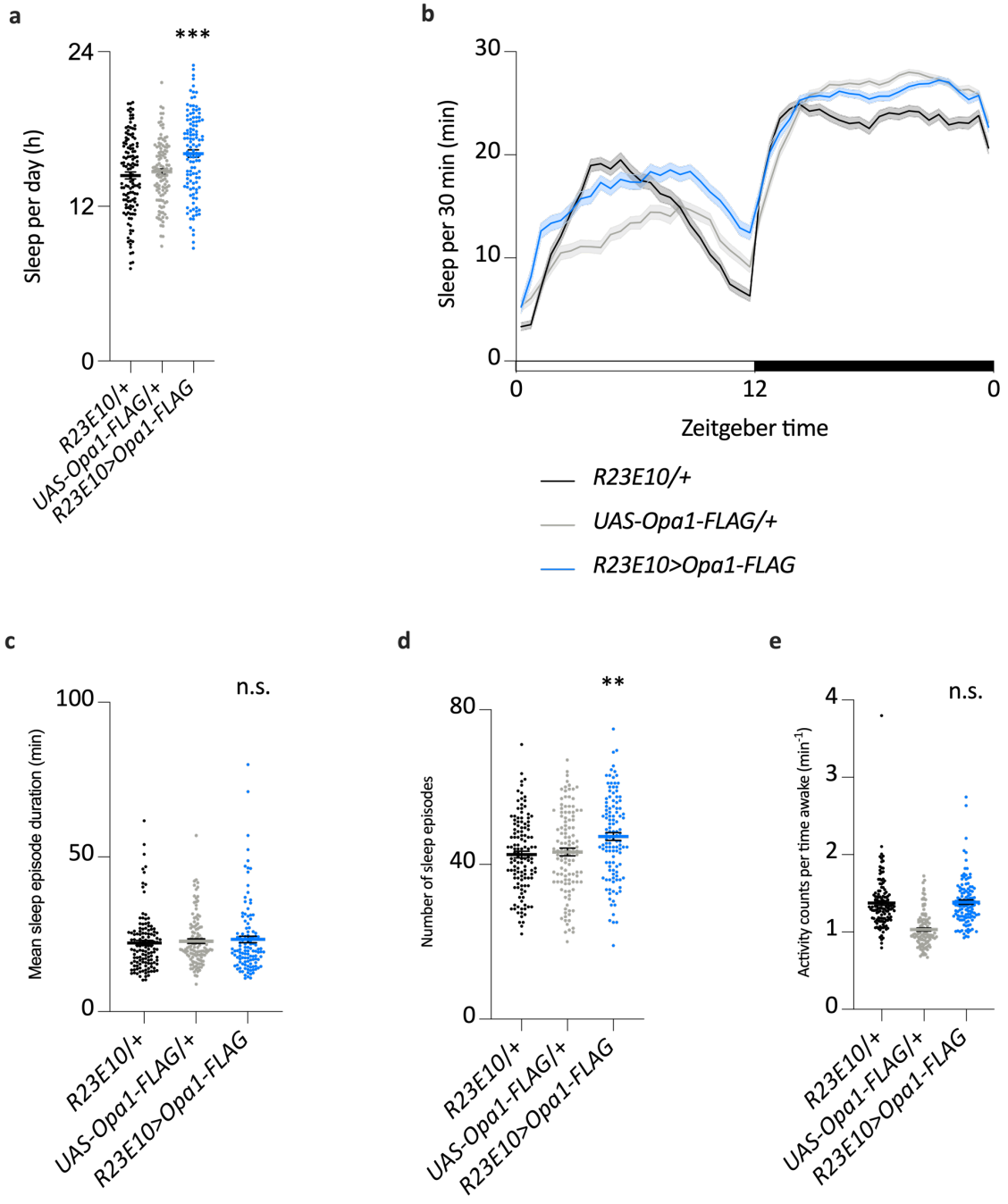

Figure 5.6 | Overexpression of the mitochondrial fusion-promoting Dynamin-like GTPase Opa1 in dFB neurons increases sleep.
a, Total sleep per day and (**b**) sleep profile in flies with *R23E10-GAL4*-driven *Opa1* overexpression is decreased compared to parental controls. Mean sleep bout duration (**c**) and number of sleep episodes (**d**) of the same genotypes show that this is underlied by an increase in number of sleep episodes. Activity counts per time spent awake (**e**) indicate locomotor activity is unaffected.
Individual values are plotted with mean ± SEM. Asterisks indicate significant differences between each experimental group and both parental controls, with *** = p<0.001, ** = p<0.01, detected by one-way ANOVA on planned relevant pairwise post-hoc comparisons with Šidák correction. Means (solid lines) ± SEM (shaded areas) are plotted in **b**.

Marf and *Opa1* are core proteins for fusion of the mitochondrial outer and inner membranes, respectively. I overexpressed both genes, using the three transgenic lines available: *Opa1* significantly increased sleep (**Figure 5.6**), as opposed to the sleep-decreasing effect of promoting fission via Drp1 (**Figure 5.5**), while no effect was detected when *Marf* was overexpressed (**Figure 5.7**).

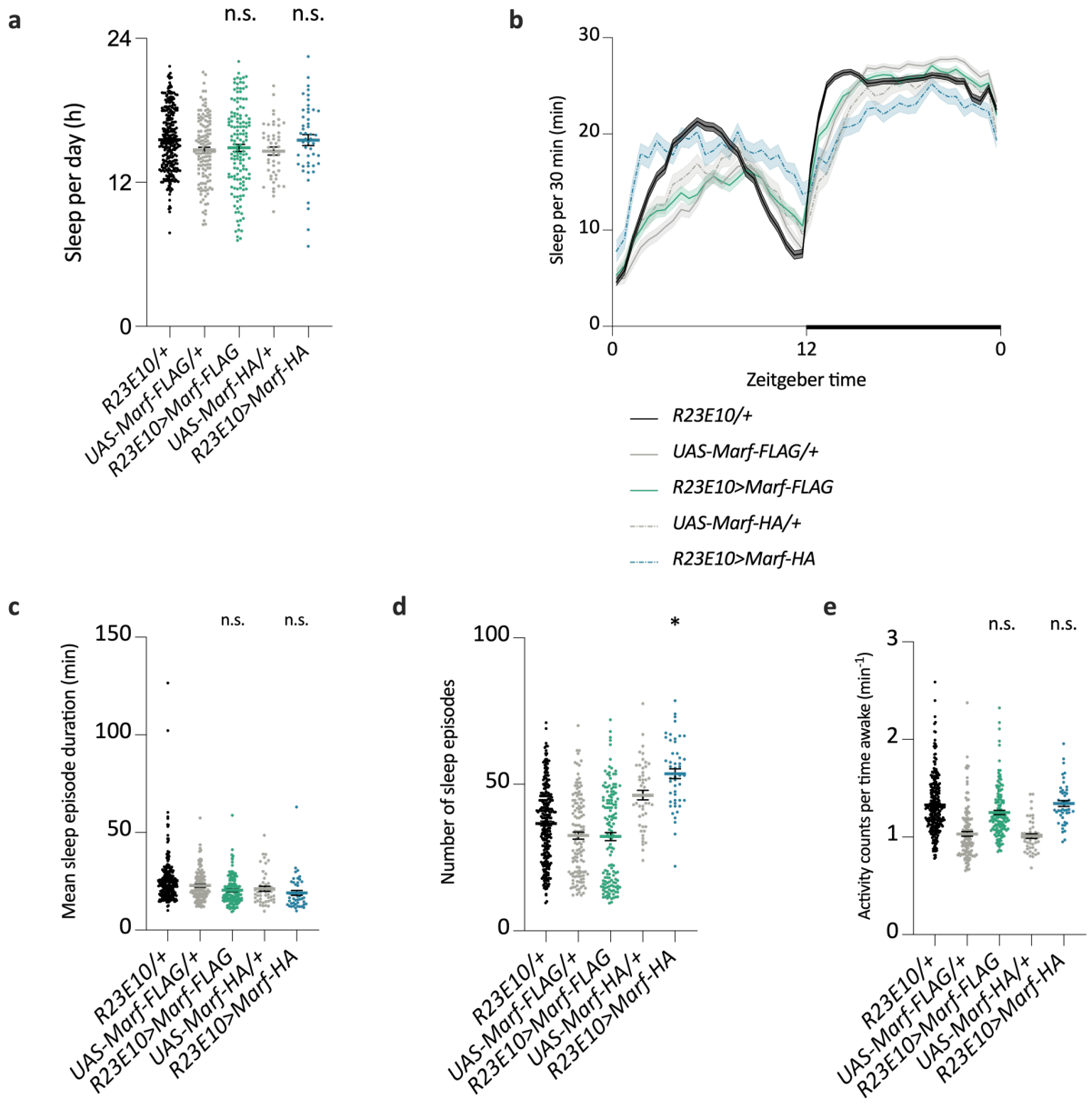

Figure 5.7 | Overexpression of the mitochondrial fusion-promoting Dynamin-family GTPase Marf in dFB neurons does not affect sleep.
a, Total sleep per day and (**b**) sleep profile in flies with two *R23E10-GAL4*-driven *Marf* overexpression constructs is not significantly different, compared to parental controls. Mean sleep bout duration (**c**) and number of sleep episodes (**d**) of the same genotypes show only an increase in number of sleep episodes for one experimental group, despite not sufficient to affect total sleep. Activity counts per time spent awake (**e**) indicate locomotor activity is unaffected.
Individual values are plotted with mean ± SEM. Asterisks indicate significant differences between each experimental group and both parental controls, with * = p<0.05, detected by one-way ANOVA on planned relevant pairwise post-hoc comparisons with Šidák correction. Means (solid lines) ± SEM (shaded areas) are plotted in **b**.

This suggests that, at least in dFB neurons, high levels of *Marf* might not be sufficient to promote the fusion process, while *Opa1* might suffice.

Such evidence is strengthened by my loss-of-function manipulations: I knocked down the expression of both *Marf* and *Opa1*, using a large set of transgenic lines (Figure 5.8). Out of 7 lines used to deplete *Opa1* transcripts, 4 showed a significant reduction in total sleep, and clear trends in the same direction were observed in the other 3 lines; however, only 1 line targeting *Marf*, out of 5, showed a similar effect (Figure 5.8).

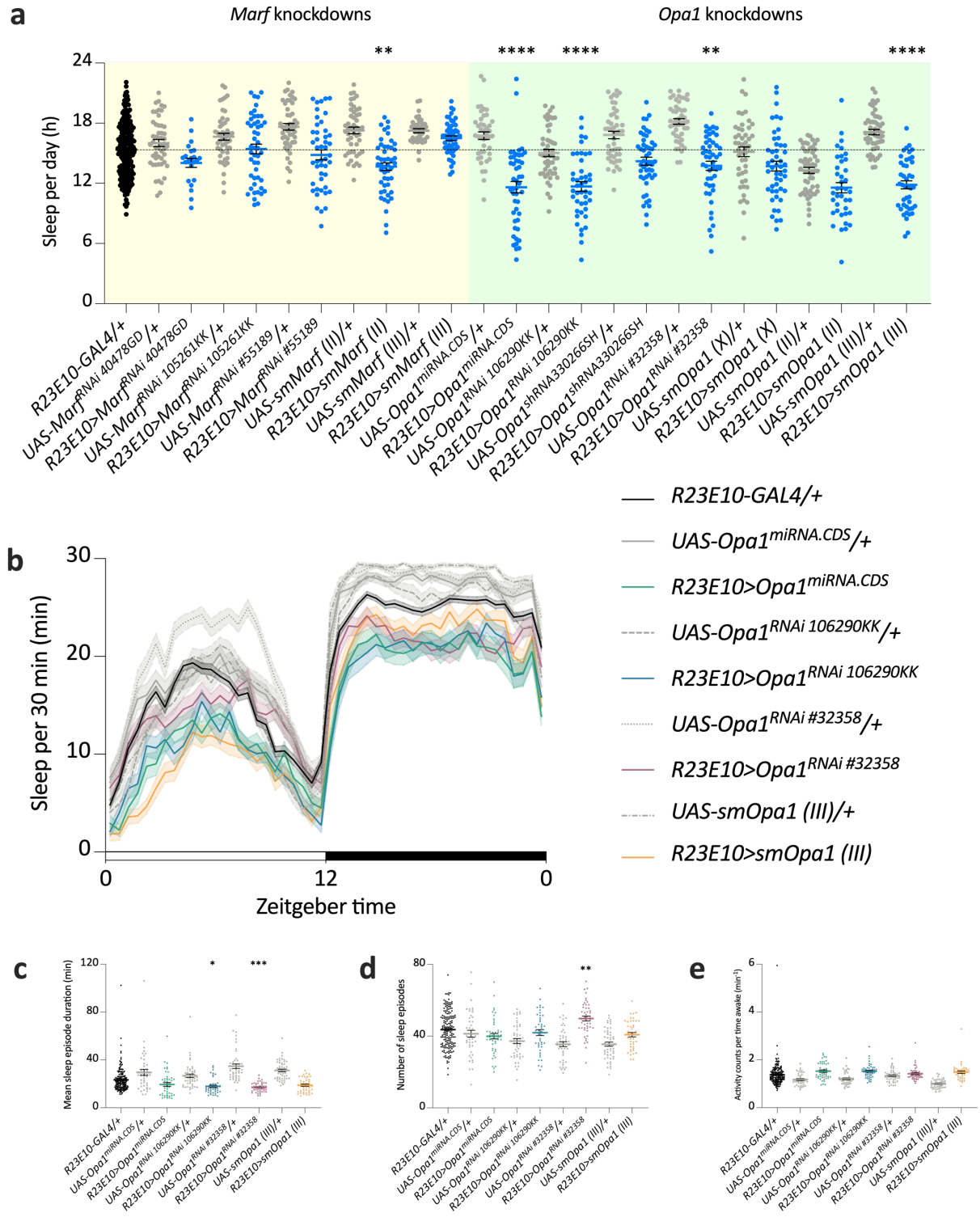

Figure 5.8 | Knockdown of mitochondrial fusion-promoting core genes in dFB neurons reduces sleep.
a, Total sleep per day in flies with several *R23E10-GAL4*-driven *Marf* (yellow background) and *Opa1* (green background) RNAi constructs decreases in several genotypes, mostly in *Opa1* knockdowns, compared to parental controls. Among the four constructs that significantly reduce sleep when *Opa1* is knocked-down, (**b**) shows their sleep profiles, while mean sleep bout duration (**c**) and number of sleep episodes (**d**) of the same genotypes show varying sleep architecture for some genotypes. Activity counts per time spent awake (**e**) indicate locomotor activity is unaffected.
Individual values are plotted with mean ± SEM. Asterisks indicate significant differences between each experimental group and both parental controls, with **** = p<0.0001, *** = p<0.001, ** = p<0.01, * = p<0.05, detected by one-way ANOVA on planned relevant pairwise post-hoc comparisons with Šidák correction. Means (solid lines) ± SEM (shaded areas) are plotted in **b**.

I asked if the observed disruption of sleep upon *Opa1* downregulation was due to impairment of the sleep homeostat. To this end, I selected the *Opa1*^{RNAi} line with the largest effect size whose parental controls had unaltered sleep levels, expressed it in dFB neurons, and measured sleep rebound following a night of 12 h of sleep deprivation: sleep rebound was significantly impaired (Figure 5.9), suggesting defective sleep homeostasis.

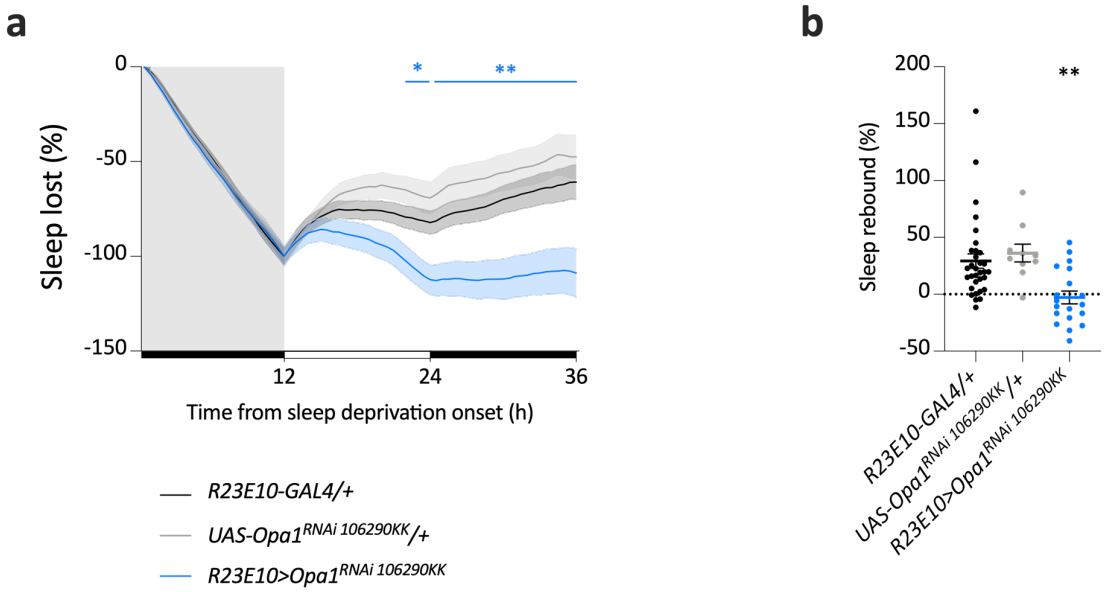

Figure 5.9 | Knockdown of the mitochondrial fusion-promoting dynamin-related GTPase *Opa1* in dFB neurons impairs sleep homeostasis.

a, The cumulative sleep lost plot shows that, after 12 h of sleep deprivation (grey area), the knockdown of *Opa1* in dFB neurons impairs sleep rebound. Two-way repeated-measures ANOVA of cumulative sleep percentage lost detected a significant genotype ($F_{(2, 58)}$ = 4.823, P=0.0115) and genotype x time ($F_{(142, 4118)}$ = 8.141, *P*<0.0001) interaction. Asterisks denote time points at which sleep percentage regained differs significantly between the experimental group and both parental controls in pairwise post hoc comparisons, with ** = *P*<0.01 and * = *P*<0.05. Means (lines) ± SEM (shaded areas) are plotted.

b., Sleep gained in the 24 h following the 12 h of sleep deprivation, as percentage of sleep in the baseline day, shows significant impairment in sleep regained when *Opa1* is knocked down in dFB neurons. Asterisks indicate significant differences between the experimental group and both parental controls, with ** = *P*<0.01, detected by one-way ANOVA on planned relevant pairwise post-hoc comparison with Šidák correction. Individual values are plotted with mean ± SEM.

5.2.3.1 Mitochondria-ER contact sites control sleep

These findings imply a bidirectional control of sleep and mitochondrial dynamics, which are not only necessary and sufficient to modulate sleep (**Figure 5.5, Figure 5.6, Figure 5.9**), but also physiologically occur in fly brains upon sleep loss (**Figure 5.4**).

I then asked how altered mitochondrial dynamics could impact sleep behaviour.

It is established that mitochondrial fission and fusion occur at contact sites between mitochondria and the endoplasmic reticulum (MERCs)[194,195]. This could provide the missing mechanistic link between the ROS produced in the mitochondria, and the effects at the plasma membrane: MERCs are known key hubs for lipid exchange between the two organelles[196–198]; therefore, ROS produced in mitochondria, or their peroxidised products, could be transferred from mitochondria to the ER, and from there be broadcasted to the whole cell membrane via the ER membrane system; such distributed waves of oxidised lipids would react locally producing longer-lived carbonyl substrates that would be reduced by Hyperkinetic, promoting its $NADP^+$-bound state, and therefore higher dFB neurons firing rates[83]. Alternatively, lipids damaged by ROS, fragmenting into short diffusible aldehydes reaching the cell membrane, would be replenished by novel lipids via lipid exchange at MERCs.

To test whether dFB neurons' MERCs are effectively involved in sleep control, I used two strategies: first, I knocked down the outer mitochondrial membrane protein Mitoguardin (Miga), which constitutes MERCs by interacting with ER protein partners[199], where it mediates lipid transport between the organelles[200,201]. Second, I optically detected MERCs via the use of a split green fluorescent protein-based contact site sensor (SPLICS)[202,203].

Knockdown of *Miga* reduced sleep, and the effect was reproduced with two independent RNAi lines (**Figure 5.10**), although the offspring of one line were hyperactive (**Figure 5.10e**).

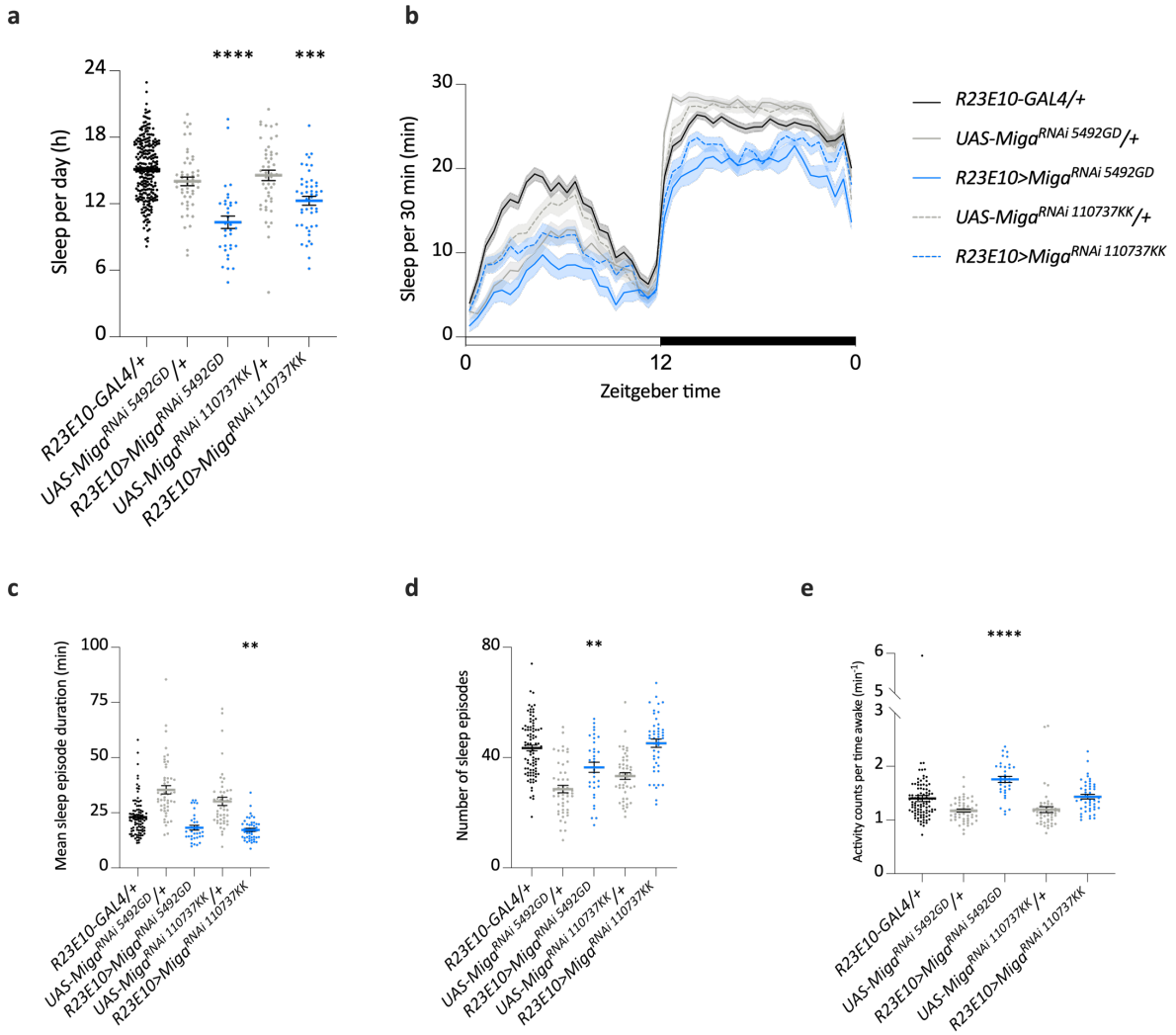

Figure 5.10 | Knockdown of MERCs-forming gene *Miga* decreases sleep.
a, Total sleep per day and (**b**) sleep profile in flies expressing two RNAis targeting *Miga,* is decreased compared to parental controls. Mean sleep bout duration (**c**), number of sleep episodes (**d**) and activity counts per time spent awake (**e**) of the same genotypes show that the sleep phenotypes are underlied by sleep fragmentation for the KK line and locomotor hyperactivity for the GD line.
Individual values are plotted with mean ± SEM. Asterisks indicate significant differences between each experimental group and both parental controls, with **** = p<0.0001, *** = p<0.001, ** = p<0.01, detected by one-way ANOVA on planned relevant pairwise post-hoc comparisons with Šidák correction. Means (lines) ± SEM (shaded areas) are plotted in **b**.

In order to visualise ER-mitochondria contact sites, I identified a SPLICS line that provided sufficient signal and validated its use in dFB neurons (**Figure 5.11**). Puncta were detected in the cell bodies, dendritic tufts, as well as in the fan-shaped body area, indicating ER-bearing pre-synaptic arborisations also populate that compartment, as previously shown[33] (**Figure 5.11**).
I will use this line in planned experiments to evaluate whether MERCs-labelling puncta abundance and their surface contact areas vary as a function of sleep history.

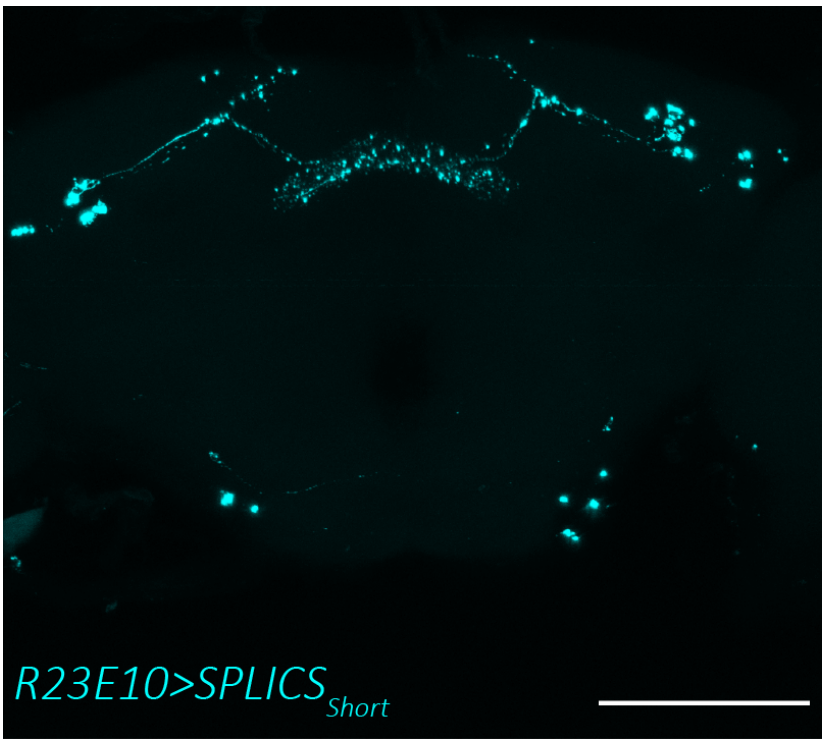

Figure 5.11 | Visualisation of MERCs in dFB neurons.
Maximum intensity projection of z-stacks of *R23E10-GAL4*-labelled dFB neurons expressing the split green fluorescent protein-based ER-mitochondria contact sites sensor (SPLICS). Puncta could be detected in cell bodies, along the processes, in the SMP and dFB regions. Scale bar = 100 µm.

5.2.3.2 Knockdown of mitochondrial phospholipases reduces sleep

I asked if other known pathways that control mitochondrial dynamics also affect sleep.

Mitochondrial phospholipases hydrolyse the phosphoric ester bonds of phospholipids, removing their head groups, to produce phosphatidic acid (PA), whose conical shape promotes membrane negative curvature and favours mitochondrial fusion[204–206].

In addition, among the genes downregulated in dFB neurons upon sleep deprivation (**Figure 5.1d**) is *CG34384*, a diacylglycerol kinase, which generates PA by phosphorylating diacylglycerol.

Finally, unpublished lipidomics work from the lab, where lipid composition was detected in rested and sleep deprived brains, has shown that PA is detectable only in rested fly brains.

These lines of evidence suggest that variations of lipid composition might be a pathway to control mitochondrial dynamics; the lipid composition itself is indeed partially modulated by the electron transport chain: in fact, cardiolipins are oxidised by a cardiolipin-specific peroxidase activity of cytochrome c[207].

The fusogenic lipid PA, or a high ratio of PA to cardiolipins could be a hallmark of "rested" brains, and its loss could trigger fission and its downstream effects.

In flies, two genes encoding mitochondrial phospholipases have been identified: zucchini (*zuc*, often called *MitoPld*) which hydrolyses cardiolipin releasing PA, and *Phospholipase D* (*Pld*), which converts phosphatidylcholine into PA. I manipulated both, starting with evaluating the effects of their loss-of-function, which resulted in sleep loss (**Figure 5.12a, b**); the knockdown of *zuc* produced the most robust sleep phenotypes, because of fragmented sleep architecture, and unaltered locomotor activity (**Figure 5.12c - e**). Planned overexpression experiments will complement these findings.

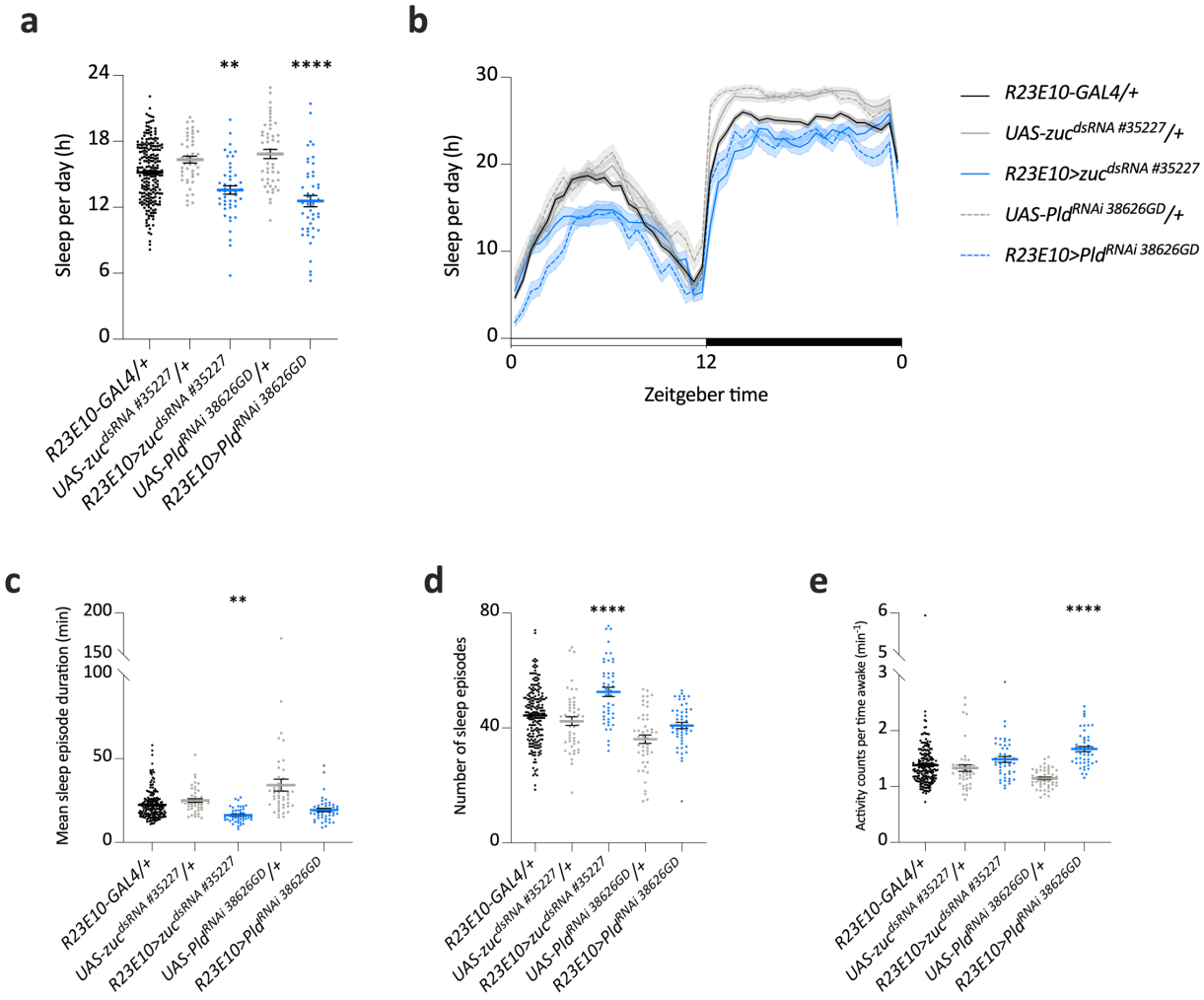

Figure 5.12 | Knockdown of mitochondrial phospholipases reduces sleep.

a, Total sleep per day and (**b**) sleep profile in flies expressing RNAis targeting mitochondrial phospholipases *zuc* and *Pld*, is decreased compared to parental controls. Mean sleep bout duration (**c**) and number of sleep episodes (**d**) show *zuc* knockdown fragments sleep, and activity counts per time spent awake (**e**) of the same genotypes show that loss of *Pld* makes flies hyperactive.
Individual values are plotted with mean ± SEM. Asterisks indicate significant differences between each experimental group and both parental controls, with **** = p<0.0001, ** = p<0.01, detected by one-way ANOVA on planned relevant pairwise post-hoc comparisons with Šidák correction. Means (lines) ± SEM (shaded areas) are plotted in **b**.

5.3 Discussion

The work presented in this chapter revealed unexpected findings regarding sleep-control neurons.

Standing apart from other cell types represented in my dataset in comparable numbers, dFB neurons showed a significant modulation of gene expression between different states of sleep pressure (**Figure 5.1**, **Figure 5.2**), which is coherent with their role of sensors and accumulators of sleep pressure and transducers of sleep homeostatic behaviours. Kenyon cells, which are intrinsic cells within memory centres of the fly brain, the mushroom bodies, downregulated genes involved in sleep, memory and learning, but mostly genes involved in mRNA processing, suggesting that the lack of sleep might affect the ability to learn via altered mRNA processing (**Figure 5.2b, c**). Interestingly, while these cells showed an upregulated *cytochrome oxidase subunit I* gene encoded by the mitochondrial genome (**Figure 5.2b**), like the whole brain (**Figure 5.1b**), as well as other mitochondrially encoded genes (**Figure 5.2b**), dFB neurons did not (**Table 9.2**). mtDNA, which only encodes OXPHOS-related genes, is known to reside in close proximity to the centre of oxidative metabolism and to be particularly exposed and vulnerable to ROS[208]; this suggests two possible phenomena: these cells might be highly prone to ROS production, or less competent towards their degradation, and such high oxidative stress could repress mtDNA differential regulation; alternatively, damaged mtDNA or its expression regulation machinery might affect the appropriate functioning of their encoded OXPHOS proteins, thus enhancing the vicious process of ROS increase[209]. The observation that dFB neurons express OXPHOS genes at higher levels compared to most cell types[136] could indeed suggest compensation to malfunctioning, or ROS-damaged, OXPHOS proteins.

Using my dataset to compare the effects of sleep history on gene expression in many different cell types is possible but beyond the scope of this work; instead, I compared only two well-studied cell types to dFB neurons. These comparisons inspired my subsequent investigations, which culminated in two new findings.

5.3.1 Sleep pressure and dFB plasticity

High sleep pressure seems to decrease synaptic strength in dFB neurons. My transcriptomics findings suggest that the machinery involved in pre-synaptic release (including *brp*) is

downregulated (**Figure 5.1e**), and brp protein levels, which underlie changes in synaptic structure, number and size of active zones, all proxies of synaptic strength[210], are lowered upon sleep deprivation (**Figure 5.3**); on the contrary, R5 neurons increase their synaptic strength upon sleep deprivation (**Figure 5.3c**), as previously reported (there named "R2 neurons")[57]. Interestingly, the same work found no effect on dFB neurons; however, in that study, brains were dissected after two hours from the end of sleep deprivation, which is a time usually largely dominated by rebound homeostatic sleep, and which might suffice to reshape plastic synaptic changes.

I propose various, not mutually exclusive, interpretations of the observed phenomenon.

- Pre-synaptic homeostatic plasticity serves to keep the total NT output from dFB neurons constant. As higher sleep pressure causes higher[81,83] and/or more structured[89] dFB neuron firing, it is likely that the pre-synaptic boutons would get potentiated over time. It is therefore plausible that what I observed is a cellular homeostatic response to excess release, akin to what happens in the fly's peripheral nervous system[211–213], where, interestingly, ROS mediate synaptic structural plasticity, in an activity-dependent fashion[212]. Such compensation could still carry the information for actuating sleep via a distinct temporal or population code[56,89], or altered output contribution of neuropeptides and fast-acting NT.
- The depotentiation serves as a plastic, LTD-like, rescaling of a recurrent circuit, either to keep coherent oscillations within the network[33,53,56,57,89] (may it be DAN-dFB neuron, dFB-dFB or dFB-helicon-R5), or to maintain its level of excitation/inhibition balance[214], or to decrease local dFB-dFB inhibition in order to produce stronger and more structured firing.
- It is generally thought, under the dominant SHY hypothesis, that sleep deprivation disrupts the main function of sleep, which is to renormalize and downscale net synaptic weights[13,215]. Under this hypothesis, sleep deprived synapses keep getting potentiated, resulting in a decreased signal-to-noise ratio in information transmission. If this applied also to dFB neurons, as it seems for most brain areas[16], the observed transcriptomic signature would show the neurons are priming their machinery for subsequent downscaling of their potentiated and sleep deprived synapses, similarly to what has been found in mouse frontal cortex, in response to sleep loss[216].

- On the contrary, if the transcriptome was reflecting a current state of synaptic depotentiation, as it seems from the STaR labelling, this would mean that dFB neurons' synaptic function is in countertrend to the rest of the sleep deprived brain (indeed, dopamine release hyperpolarises these cells). If homeostatic plasticity within dFB cells happens selectively during sleep as in primary visual cortex[217], lack of it should gate the plastic changes.
  This would could explain the distinct role for these neurons in sleep control.

In order to complement my findings, corroborate their physiological significance and test some of the abovementioned interpretations, one could examine dynamic responses of these neurons upon sleep deprivation either with paired electrophysiological recordings between dFB neurons and their downstream partners (including helicon cells[53], dopaminergic neurons[33,89], octopaminergic VPM3 neurons[33,84], intra-FB columnar neurons hΔK, hΔF, and PFGs cells[33], and potentially dFB neurons themselves[33,89]), where postsynaptic IPSP amplitudes, aligned to their originating pre-synaptic spikes, would be compared across conditions. An alternative (and technically more feasible) approach would be to record neurotransmitter release from dFB neurons directly in brains of sleep deprived and rested flies. More specifically, one would record fluorescence signals emitted by the genetically-encoded glutamate sensor iGluSnFR (*cf*. Chapter 4) and normalise them to the dFB neuron ensemble activity (e.g., by simultaneously recording ensemble dynamics via the red calcium sensor jRGECO1a). The activity-normalized iGluSnFR amplitude (and thus glutamate release) is predicted to be reduced upon sleep deprivation.

Synaptic plasticity could then represent one of the cellular and network mechanisms by which dFB neurons fine-tune sleep.

5.3.2 Mitochondria shaping (sleep) behaviour

Mitochondria are central hubs for cellular metabolism and homeostasis, and production sites of several metabolites, including ATP. Their functioning is coordinated with the cellular energetic state and needs; these organelles, in fact, undergo division (also called fission, or fragmentation) and fusion cycles[218] that produce diverse network morphologies, either within a physiological dynamic range, from transient "kiss-and-run" membrane exchange interactions[219], to stable filamentous nets[220], or irreversible pathological changes, because of cellular insults or stress, that result in fragmented giant or hyperfused morphologies[221,222]. These plastic changes are mostly independent from the global cell cycle.

Such plastic rearrangements regulate the homeostasis of mtDNA[223,224], a vestige of the mitochondria endosymbiotic origin[225] which mostly encodes rRNA and tRNA for mtDNA translation, and subunits of OXPHOS proteins whose complex partners are symbiotically encoded by nDNA; mitochondrial dynamics (fusion and fission) also result in exchanges and redistribution of mtDNA among the organelles[226].

Another interesting outcome of mitochondrial dynamics remodelling is the repercussion on their metabolism: both morphology is sensitive to metabolic alterations (mostly nutrients availability and metabolic demands[227,228]), and disturbed mitochondrial dynamics provoke metabolic changes[229]; also, mitochondrial morphology varies dramatically in different tissues and cell types[230]. While it is still not fully established whether fused mitochondria are more bioenergetically efficient than fragmented ones[231], increased fusion seems to positively correlate with higher ATP levels[232,233].

Given that spiking and maintenance of resting membrane potential account for a vast part of the total energy consumption in the brain[184,185], altered metabolic needs perturbing mitochondrial dynamics and consequently ATP production could result in altered neural activity, depending on the specificities of each circuit and neuronal basal firing rate[234].

This ability to sense metabolic states and transduce them into differential availability of cellular energy and, therefore, electrical activity, would be particularly advantageous for neural circuits that control behaviours directed towards those states themselves.

An example of such implementation is the hunger-promoting Agrp neuron population in the arcuate nucleus of the hypothalamus during metabolic switches[234]: food-deprived mice

showed fragmented mitochondria in Agrp cells, while in animals habituated to a high-fat diet, Agrp neurons showed increased mitochondrial fusion, which promotes storage of excess energy into fat; in these animals, and not in normally chow-fed ones, cell-specific genetically impaired fusion results in decreased firing rates, reversible upon intracellular administration of high concentration ATP, and animals were resistant to fat gain during high-fat diet[234]. Therefore, impairment of fusion decreases the firing rates, possibly due to lower ATP levels, and this controls the organismal response, causing lower fat accumulation. Despite the limitations of a study with mostly chronic manipulations, this represents an example of a behaviour linked to mitochondrial dynamics.

Sleep is another behaviour tightly linked to metabolism: animals are able to feed when awake, and not while asleep. It is then possible to hypothesise that mitochondrial dynamics play a role in tracking sleep (and need thereof). In the fly, dFB neurons are central to sleep control, and their mitochondria have been studied and manipulated mostly regarding the ROS generated therein and the coupled cellular electrical activity generating sleep[83].

The work presented here examines another angle of the intracellular mechanisms underlying the working of these neurons, and was prompted by my transcriptomics results (**Figure 5.1**). The upregulated genes indicated that mitochondria undergo plastic changes in a sleep history-dependent fashion. Similarly to studies in other contexts, from neural development[235,236] to Tibetan sheep[237], the upregulation of OXPHOS and metabolic genes corresponded to altered mitochondrial dynamics (**Figure 5.4**). In particular, in sleep deprived dFB neurons, I observed a reduction in mitochondrial surface and volume, decreased length of branches and more spherical mitochondria (**Figure 5.4c**); however, I was surprised by the unchanged number of mitochondria between conditions, also observed in other studies of mitochondrial dynamics[234]: it is possible that the reduced size of sleep deprived mitochondria renders (at least part of them) less detectable with my imaging approach, causing me to underestimate their number; however I tried different size thresholds in the analysis step, with no appreciable difference for any metrics (data not shown). Alternatively, the observed phenomena could be the first step to an increase in the number of mitochondria, or could represent the maximal endpoint within dFB's dynamic range limit. Mitophagy could, of course, be involved in these dynamics; to test this possibility, a convenient experimental strategy would be to use the

genetically encoded mitophagy reporter mitoQC[238], which is constituted by a membrane localised tandem mCherry-GFP: while GFP is quenched in the acidic microenvironment of the mitophagy lysosomes, mCherry is not, and therefore their fluorescence ratio is a proxy for mitophagy[238,239].

I established that the relationship between mitochondrial dynamics and sleep, in dFB neurons, is bidirectional: while manipulating sleep alters mitochondrial shape, modulating core proteins of the fission/fusion machineries modifies sleep amount and architecture (**Figure 5.5**, **Figure 5.6**, **Figure 5.8**, **Figure 5.9**). *Drp1* and *Opa1* seem to be the key molecular players, whereas, interestingly, overexpression and downregulation of *Marf* did not affect sleep (**Figure 5.7**); the efficacy of manipulations of *Marf* on mitochondrial dynamics is indeed variable between studies and is likely to be cell- and tissue-specific. To evaluate the physiological effects of any of these manipulations, one could record the electrical activity or image the calcium oscillations of these cells upon expression of the relevant transgenes, in addition to measuring their morphological repercussions. It would also be interesting to evaluate whether such manipulations exert effects on sleep when performed in different neurons other than dFB cells: however, my transcriptomics and morphological data, although limited to a few cell types, do not provide any indication of mitochondrial remodelling elsewhere upon sleep loss (**Figure 5.2**, **Figure 5.4**). I can therefore exclude that the effects seen in dFB neurons are a brain-wide phenomenon.

How do mitochondrial dynamics affect the electrical activity of sleep-inducing dFB neurons?
Two mechanisms are conceivable:
First, mitochondrial dynamics affect the production of ATP, which is necessary for cell spiking. This could be verified via imaging ATP levels, in different states, using the FRET sensor ATeam, for example[240], or via manipulating the ATP-generating mitochondrial proton gradient, for example by diminishing it with uncoupling proteins or by acutely increasing it with light-inducible mitochondrial proton pumps, or via a combination of those and ATP imaging[241].
The second putative mechanism entails ROS: while the causal relationship between their production and mitochondrial dynamics is still debated[231], in dFB neurons, curbing ROS production with AOX mitigates the mitochondrial fragmentation normally observed with sleep

deprivation (**Figure 5.4c**), and in general fusion seems to positively correlate with high ATP levels[232,233].

Therefore, how are mitochondrial dynamics, ATP, ROS, and sleep related in dFB neurons?

One possible working model is a result of cell-autonomous mechanisms and circuit properties (**Figure 5.13**).

During the day, awake feeding flies accumulate calories, which promote mitochondrial fusion and the generation of ATP; however, low firing activity of these cells[56] favours a high ATP:ADP ratio, and generates ROS[83], which integrated over time increases somnogenic drive and eventually imposes sleep. As animals sleep, calories diminish, and this is sensed by dFB neurons (akin to the glucose and lipid-sensing ventromedial and arcuate nucleus hypothalamic neurons[242–247]) whose mitochondria do fragment[248], ATP production decreases, together with ROS production, which, in combination with decreasing levels of ATP, decrease firing rates over time and in turn sleep pressure, up to the wake tipping point (**Figure 5.13**). This would also demystify how food deprivation lowers sleep pressure.

In this working model, metabolism dictates sleep via a physiological range of mitochondrial dynamics and ROS, where possibly excessive fragmentation or ROS amounts are homeostatically counteracted with small discharges of electrical activities, producing sleep bouts of varying lengths. The frequency and pattern of these electrical activities depend on the cells' membrane potential, which is modulated by dFB inputs, including circadian ones[84,86,249] and the recurrent circuits in which these neurons are embedded[33,53]; this could explain a circadian dependence of dFB neuron activity patterns[56].

However, when sleep is impeded by external agents, ATP levels cannot at all be discharged via firing, due to chronically decreased cellular excitability generated by releases of dopamine by the arousing stimuli[66], and ROS levels keep accumulating, pushing the system out of the physiological range (**Figure 5.13**). It is likely, then, that the ROS-dependent fission observed (**Figure 5.4c**) is a cellular compensation mechanism that homeostatically tends to diminish ATP production and further ROS generation. The transcriptomic signature of sleep deprived dFB neurons (**Figure 5.1**) could then reflect the need for replacement of the ROS-damaged organelles, or the need for components of the OXPHOS machinery necessary in each mitochondrion in a fragmented mitochondrial network. When the continuous sleep deprivation ceases, higher excitability translates into high spiking rates via Hyperkinetic bound to a vastly oxidised pool of cofactors. ATP can decrease in a low ATP-producing cellular

environment because of fragmented mitochondria, and sleep pressure can slowly lower over time, resetting the cells.

Some predictions of this model can be observed and manipulated with the tools aforementioned. Similarities to the proposed model are shared with a work linking Drp1 circadian oscillations to bioenergetics[233].

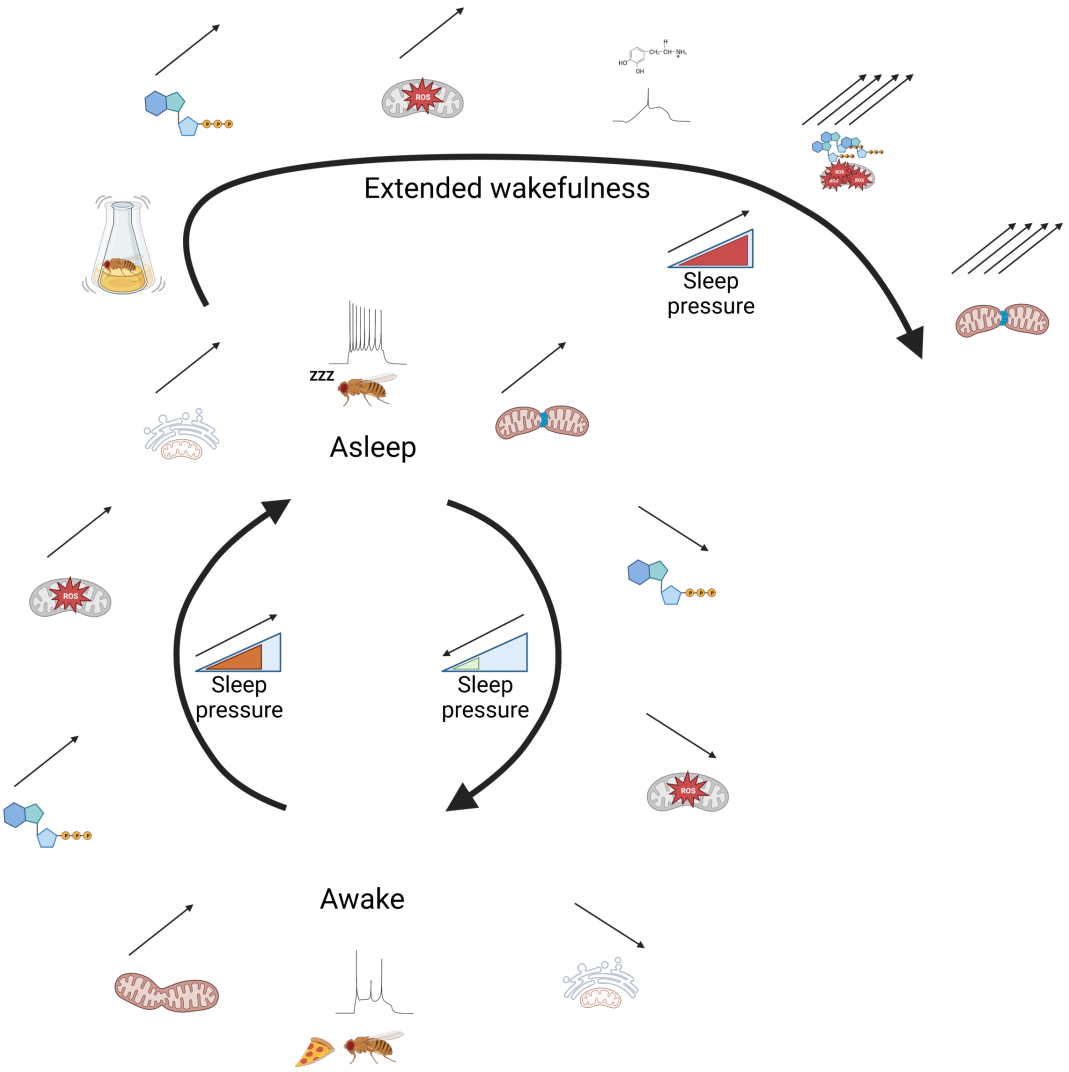

Figure 5.13 | Working model of the relationship between mitochondrial dynamics, bioenergetics, ROS, and sleep pressure.
In the proposed working model, mitochondria in the dFB neurons of awake and feeding flies respond to the increased caloric intake with fusion, higher ATP production and therefore higher ROS levels. Intracellular signaling (lipid transport and communication to the membrane system), transduces such altered biochemistry into higher dFB firing rates, which signal sleep pressure and eventually impose sleep on the animal. Sleeping animals decrease their sleep pressure, as well as caloric levels, their dFB mitochondria undergo fission and decrease their ATP/ATP ratio, as ATP is consumed by the high firing rates and lower levels are produced in fragmented mitochondria: this results in lower ROS levels which are translated into decreased firing rates back to basal levels. Instead, if flies are prevented from sleeping via continuous delivery of arousing stimuli, dFB neurons are unable to fire due to the release onto them of hyperpolarising dopamine, therefore ROS continue accumulating beyond physiological levels, and mitochondria fragment as homeostatic response.

The mitochondrial dynamics examined provide also a possible mechanistic explanation for how mitochondria-produced ROS induce oxidation of cofactors at the plasma membrane.

Fission and fusion occur at contact sites between mitochondria and the endoplasmic reticulum (MERCs)[194,195], which are also sites for lipid exchange. This permits two hypotheses: peroxidised lipids, in occasion of mitochondria reshaping at MERCs, could travel across the organelles' membranes, reach the ER and from there be broadcasted to the cell membrane. Alternatively, as ROS fragment lipids into short aldehydes diffusing to the cell membrane, novel lipids would replenish the damaged ones, via lipid exchange at MERCs.

My results after knockdown of *Miga* (Figure 5.10) suggest MERCs are involved, but of course gain-of-function experiments should complement these results[199].

To evaluate further whether dFB's MERCs are involved in sleep control, one strategy is to use the green fluorescent protein-based contact site sensor (SPLICS)[202,203] indicated in Figure 5.11; alternatively one could perform dual colour labelling of mitochondria and ER and analyse the colours contact surfaces[250]. Interestingly, a study in a Parkinson's disease model showed that the disrupted sleep pattern is caused by altered mitochondria-ER contact sites, resulting in abnormal lipid trafficking[250]. Also, peroxidised mitochondrial lipids could be measured *in vivo* using the ratiometric, fluorescent, mitochondria-targeted lipid peroxidation probe MitoPerOx[251].

Finally, other regulators of mitochondrial dynamics are phospholipases, like the fly's outer mitochondrial membrane-anchored zucchini (MitoPld)[206]. Its production of PA from cardiolipins is thought to permit curvatures of mitochondrial membrane that favour fusion[206]. PA is also known to inhibit Drp1[252]. In addition, zucchini, might also inhibit Drp1 via local clustering with this protein and locally produced Drp1-inhibiting PA[252]: this might add inhibition of mitochondrial division to the effect of stimulating mitochondrial fusion.

The findings of this chapter, and the proposed complementary experiments, could provide interesting implications for medical interventions; here, I will mention only a few: Drp1 and Opa1 are regulated by a plethora of post-translational modifications (PTMs)[231], which could be selectively targeted by PTMs-specific recombinant antibodies[253,254].

Also, as elaborated above, mtDNA is duplicated, exchanged and transported across mitochondria depending on their dynamics and MERCs[255,224,256,257]; heteroplasmy and

mutations in mtDNA correlate with stress[258] and major depressive disorder[259]. Therefore, a possible link via (chronical) disturbance of sleep and underlying mitochondrial dynamics could induce mtDNA-related conditions.

Also, mitochondrial shapes can affect their mobility: transport of mitochondria to synapses is known to be regulated by fission[260] and their location is key for sustaining the energetic demand of axons[185,261]. Combining the two main findings of this chapter, synaptic plasticity and mitochondrial dynamics, could help understanding the cell biology underlying sleep control.

6 Heterogeneity of octopamine receptors within dFB neurons

6.1 Introduction

Cerebral regions have been classically defined according to anatomical features, and therefore include assorted cell types, innervated by diverse inputs and projecting to different areas: this results in vast brain areas, associated with one or a few functions in simplified and quasi-phrenological views, encompassing highly complex underpinning cellular structures, connectivity and behavioural outputs.

In fact, the operating principles of the nervous system rely also on structural and functional heterogeneity. In some cases, physically close heterogeneous populations can integrate various inputs, efficiently modulate each other, vary the mutual excitation/inhibition balance, and flexibly produce outputs[262]. Finally, even the very same neuronal population can multiplex diverse variables, using various coding modes and anatomical organisation[263].

To elucidate this complexity, it is crucial to access the wiring diagram of a network, the cellular identity of each node, and record the various patterns of neuronal activity.

Single-cell transcriptomics provides a powerful method to identify different cell types within a particular population: given the vast amount of data generated for each cell, defining what determines a cell type becomes a challenging task, since annotating which genes are significant markers for a given population is not trivial, and any sensible definition needs to be based on functional corroboration.

The uncovering of functional heterogeneity has led to interesting findings in the field of sleep. For example, the discovery of NREM-inducing *Tac1*$^{+}$ or *Pdyn*$^{+}$ cells within the GABAergic cells of the mammalian pre-optic area, with a different function from previously identified GABAergic neurons in the same population, which induce both REM and NREM[133]. Another example is the identification of different functions for the glutamatergic/nitrergic and GABAergic neurons in the ventral tegmental area: while the first group was wake-inducing and

wake/REM-active, the latter were also wake/REM-active, but their activation produced NREM-like sleep, which led to the unveiling of local inhibition and novel sleep-control projections[182].

I sought to uncover potential heterogeneity within a key sleep-control population of the fly. Taking advantage of my single-cell RNA-sequencing dataset, I will show in this chapter that the octopamine β1 receptor is a major source of transcriptional heterogeneity within dFB neurons, and will proceed by investigating the related circuit and functional implications, and by producing tools that enable this refined analysis.

The fact that a receptor for octopamine stands out as source of heterogeneity within sleep-control cells is interesting because octopamine itself modulates sleep.

Octopamine (OA) is a tyramine-derived monoamine, structurally and functionally closely related to norepinephrine (NE, also called noradrenaline), for which dedicated receptors and circuits have been identified in invertebrates[264]. In flies, it modulates, among others, reward signalling[265], sex drive[266], is involved in microbiota-brain interactions[267,268], aggression[268], and, in fact, sleep[63,69,70].

Early studies showed that chronic activation of tyraminergic and octopaminergic cells labelled by *Tdc2-GAL4* induces wake, as does oral administration of OA, and, conversely, that mutants in the OA biosynthetic pathway exhibit increased sleep[69]. Among the around 100 OA^+ fly brain cells[269], it was shown that this wake-inducing effect is, at least partially, due to cells in the SMP, and signalled though cells in the pars intercerebralis via PKA and cAMP[69,70]. Despite limited genetic controls in those early reports, they highlighted a role for octopamine in sleep, similarly to the wake-promoting effects in fish[270], and to the noradrenergic cells of the locus coeruleus. These mammalian nuclei are electrically active in anticipation[271] and during the wake-active period, accompany spontaneous or sensory-evoked interruptions of sleep[272], and other behaviours, and their activity correlates with arousal levels during sleep[273]. In general, the effect of NE seems to be necessary for regulating arousal levels, rather than sleep states themselves, as mice lacking enzymes for NE biosynthesis did not present alterations in wake or rapid eye movement sleep, but were rather more difficult to wake up after sleep deprivation[274,275].

These pieces of evidence suggest that NE might be lowering the arousal level (rendering the transition to wake more likely) in several contexts, including during homeostatic rebound sleep, when the arousal level is higher.

A role for octopamine in sleep homeostasis has been, in fact, identified in flies[63]. The overnight activation of octopaminergic neurons not only decreased sleep during stimulation, but also decreased subsequent compensatory sleep, when the activation of neurons had stopped[63]. In addition, sleep deprivation combined with simultaneous activation of these neurons also resulted in reduced subsequent rebound sleep[63]. This suggested that octopaminergic cells impair the fly's sleep homeostat.

A key neuronal population that controls sleep homeostasis in flies are the dFB neurons: therefore, it was a natural step to investigate the role of octopamine and its receptors in defining functional heterogeneity within dFB neurons.

6.2 Results

6.2.1 Transcriptional heterogeneity within dFB neurons

To search my scRNA-seq dataset for major sources of heterogeneity within dFB neurons, I decided to start my investigation with an unsupervised clustering that would bisect my group of dFB cells, and evaluate the neurobiologically-relevant gene(s) that would contribute most to this dichotomy. To this end, I used a shared nearest neighbor (SNN) modularity optimization-based clustering algorithm, applied the highest resolution (0.3) that would result in two clusters (**Figure 6.1a**, n_{cells}Cluster 1 = 178, n_{cells}Cluster 2 = 145) and compared differentially expressed genes between them (**Appendix, Table 9.3**). The gene with the highest absolute value of fold-change was the octopamine receptor β1 (*Octβ1R*); which was also the 10th ranking gene among the DEGs listed by adjusted P-value, preceded by transcription factors, RNA-binding proteins, axon guidance and cadherin-related genes, a secreted phospholipase, and *DopEcR* (which is known not to have an effect on sleep if knocked-down in dFB neurons[66]). The expression levels of *Octβ1R* were substantially higher in sub-cluster 1 than in subcluster 2 (**Figure 6.1b**); interestingly, the expression patterns of *Octβ1R* and *DopEcR* seemed mutually exclusive (**Figure 6.1b**).

Given the prominent role of *Octβ1R* in generating transcriptional diversity among dFB neurons, and because of the known effect of this monoamine on sleep summarised in the **Introduction to this Chapter**, I decided to investigate the functional role of this heterogeneity, and in general (and as comparison) the diversity of octopamine (OA) receptors, and their function, in dFB neurons. Flies have six known octopamine receptors: *Octβ1R, Octβ2R*, *Octβ3R, Oamb, Oct-TyrR, Octα2R*[276]. I could detect expression of all OA receptors apart from the α2-adrenergic-like octopamine receptor (*Octα2R*); however, *Octβ2R*, *Oamb* and *Oct-TyrR* showed much lower expression levels than the other two receptors (**Figure 6.1c, d**). Additionally, *Octβ3R* was expressed more evenly across sub-clusters, while *Oct-TyrR* and *Octβ2R* were enriched in cluster 2 relative to cluster 1 (**Figure 6.1c, d**).

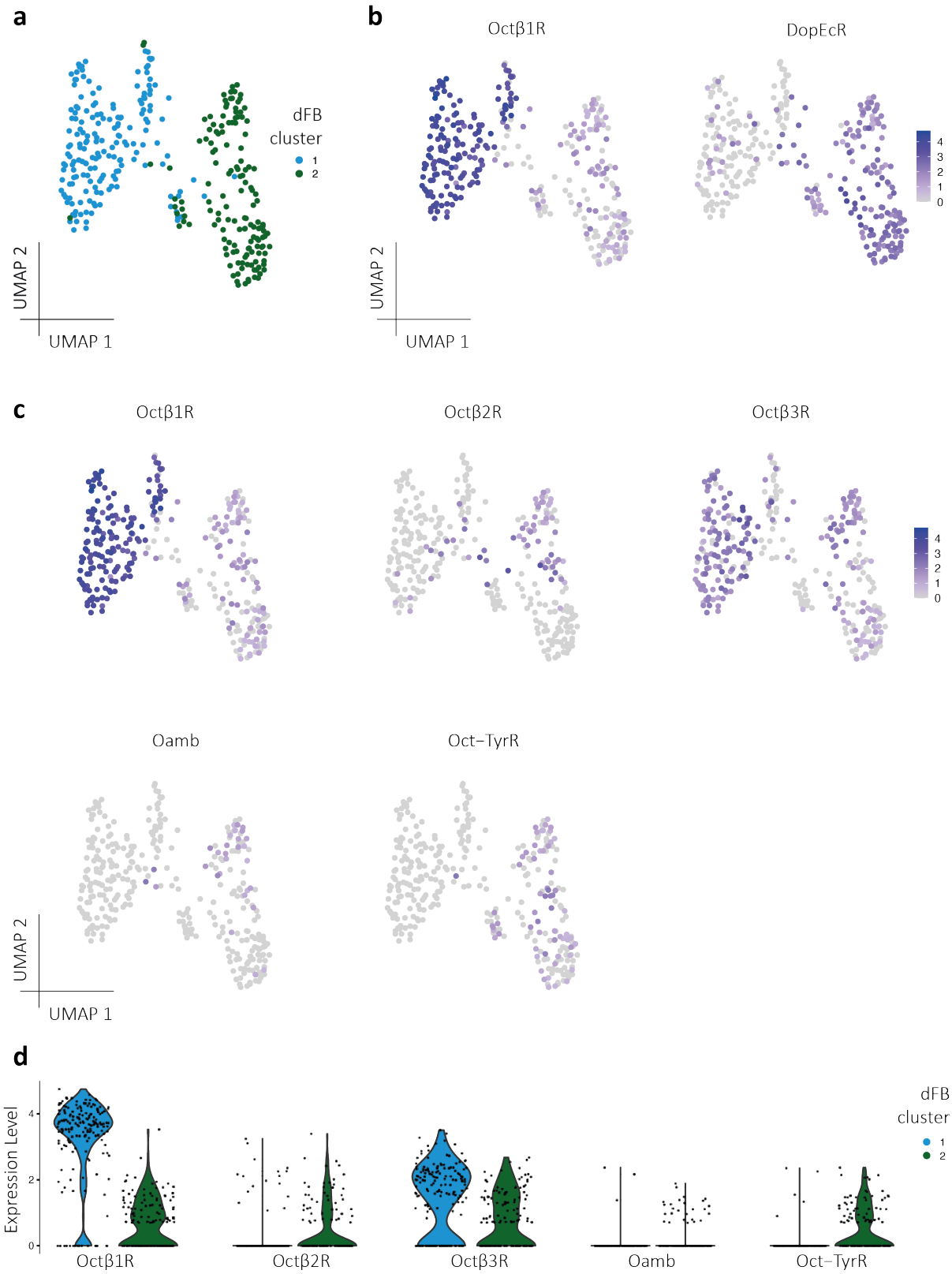

Figure 6.1 | Transcriptional heterogeneity for octopamine receptors within dFB neurons subpopulations.
a, Clustering of dFB neurons identified in the scRNA-seq analysis (resolution = 0.3) reveals two sub-clusters. **b**, *Octβ1R* and *DopEcR* are the top two genes involved in neuronal signaling differentially expressed between the two clusters, and seem to be expressed in mutually exclusive fashion. **c**, Expression pattern of OA receptors in clustered dFB neurons. In **b** and **c**, log-normalised expression levels are colour-coded according to the bars on the right. **d**, Expression level of OA receptors in both sub-clusters of dFB neurons. In all graphs, each dot is an individual cell.

6.2.2 Tools to target and manipulate octopamine receptors heterogeneity

Given this expression heterogeneity, I tried to obtain genetic access to the members of the two clusters. To this end, I deployed the split-GAL4 system, and combined different AD hemidrivers originating from OA receptors that showed expression in the dFB by visual inspection of their published expression patterns, with the *R23E10-DBD* hemidriver lines, targeting dFB neurons.

With these combinations, I drove the expression of hexameric GFP and visualised the resulting fluorescence pattern (**Figure 6.2**). Out of 8 lines tested, only 5 showed a fluorescence signal in the dFB. Of these, two lines originated from *Octβ1R*, two from *Octβ3R*, and one from *Oamb* (**Figure 6.2**). In particular, out of 12-13 pairs of dFB neurons labelled by *R23E10-GAL4*, 7-8 dFB pairs of cell bodies could be detected in the *Octβ1R-AD*$^{\#70104}$ line, 8-9 in the *Octβ1R-AD*$^{\#71441}$, 5 in the *Octβ3R-AD*$^{\#72058}$, 2-3 in *Octβ3R-AD*$^{\#71436}$, and 7-8 in *Oamb-AD*$^{\#71075}$ (**Figure 6.2**). Despite differences in the number of cells in the two *Octβ3R-AD* lines, and their not tight match with the corresponding number of cells labelled in the **Figure 6.1** clusters (especially for *Octβ3R-ADs and Oamb-AD*), these lines provided access to a restricted subset of dFB neurons, enriched in the expression of the relevant OA receptor.

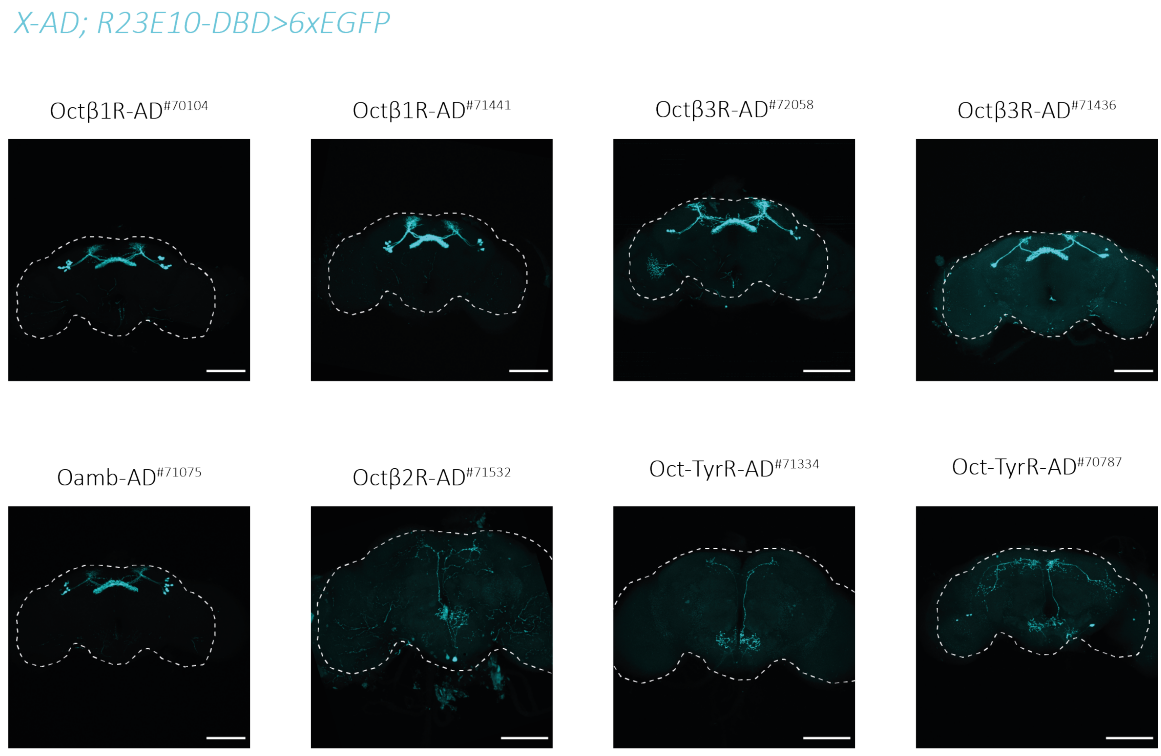

Figure 6.2 | Expression patterns of OA receptors-derived AD lines, combined with *R23E10-DBD*.
Maximum intensity projection of confocal images of fly brains expressing various OA receptors-derived AD lines, combined with *R23E10-DBD* line and driving the expression of hexameric EGFP. Scale bars = 100 µm. Brain profile is highlighted by dashed lines.

I then sought to manipulate the expression levels of those OA receptors, starting with loss-of-function. To this end, I used both genetic knockdowns and knockouts.

As for the genetic knockdowns, I expressed RNAis against OA receptors in the whole dFB population (Figure 6.3).

While the expression of single RNAis against any of the receptors did not show any significant effect (apart from 1 line against *Octβ2R*) (Figure 6.3a), to increase the knockdown efficiency, I expressed two RNAis against the same receptors (Figure 6.3b). The effect was a decrease in total sleep and fragmentation of sleep for the knockdown of both genes (Figure 6.3b - e).

The other method used was a cell-specific knockout: to this end, I generated transgenic flies bearing single guide RNAs (sgRNAs) directed against OA receptors, under the control of a UAS promoter (Figure 6.4a). The designed sgRNAs targeted different exons of the genes and were successfully cloned in tandem as groups of four, three and two (Figure 6.4b, c). For the following analyses, I used only lines that expressed four sgRNAs against *Octβ*1R and *Octβ*3R. I confirmed the lines were effective by crossing them with the ubiquitous driver *tub-GAL4*, in parallel to *R23E10-GAL4* (both in combination with a Cas9 transgene): while I obtained 77 to 122 flies per each experimental genotype when crossed with *R23E10-GAL4*, only 2 to 14 experimental flies were produced when the driver was *tub-GAL4* (data not shown). Since the number of flies in the parental driver and reporter line controls in the *tub-GAL4* experiments were similar to what I obtained for *R23E10-GAL4* (data not shown), this suggests a highly detrimental effect of the expression of these sgRNAs in the whole organism.

The sleep behaviour of flies expressing sgRNAs under the control of *R23E10-GAL4* was unchanged, in terms of total sleep amount and architecture, while two lines showed hyperactivity (Figure 6.4d - g).

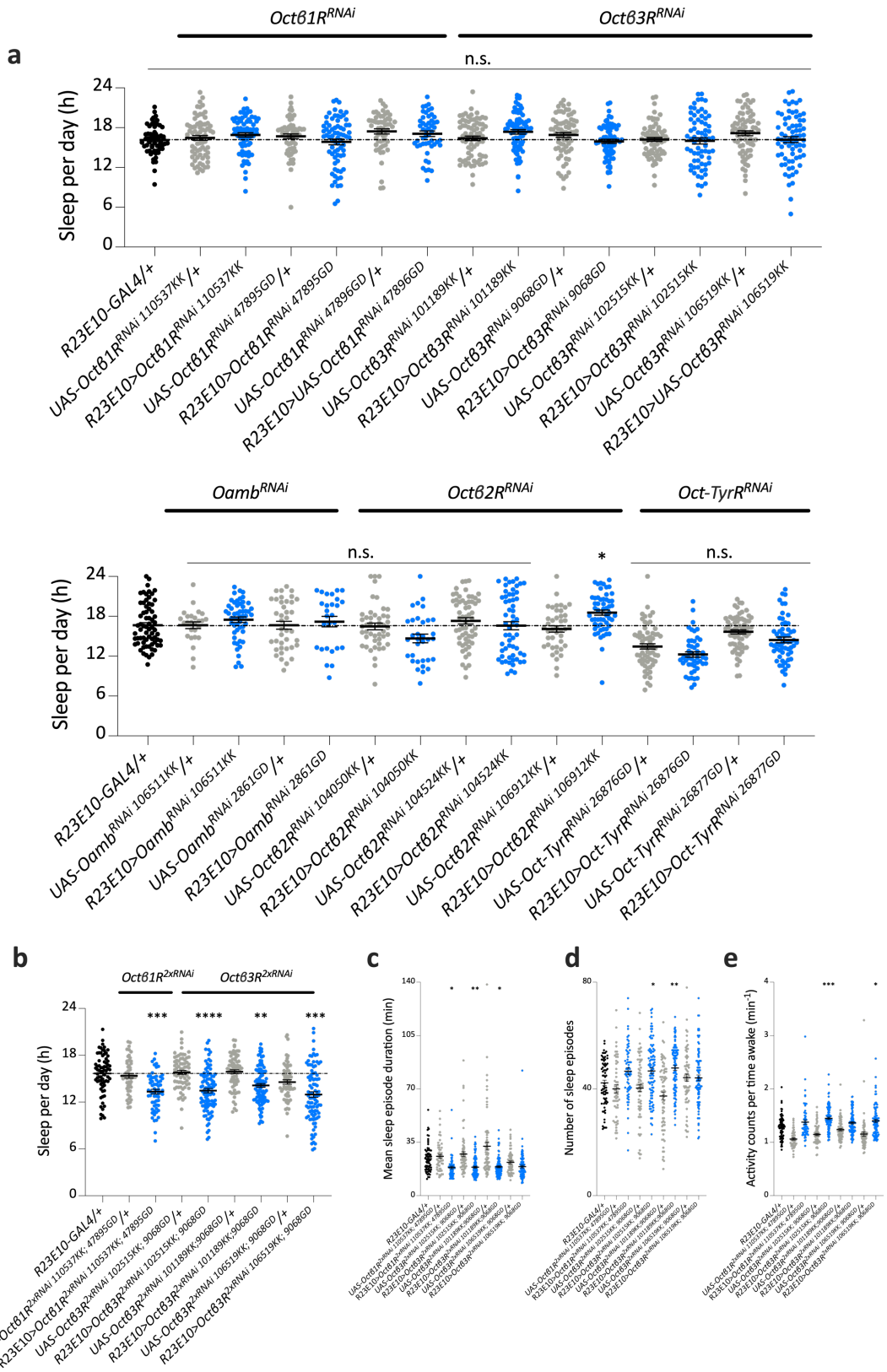

Figure 6.3 | Knockdown of *Octβ1R* and *Octβ3R* receptors with double, but not with single, RNAis decreases sleep.
a, Total sleep per day in flies expressing different *R23E10-GAL4*-driven RNAi transgenes against OA receptors is unchanged compared to parental controls, apart from one line. **b**, Total sleep per day in flies expressing different *R23E10-GAL4*-driven 2xRNAi transgenes against *Octβ1R* and *Octβ3R* decreases sleep, mostly due to sleep fragmentation, evident from differences in mean sleep bout duration (**c**) and number of sleep episodes (**d**) of the same genotypes. Activity counts per time spent awake (**d**) indicate locomotor activity is augmented in two experimental groups. Individual values are plotted with mean ± SEM. Asterisks indicate significant differences between each experimental group and both parental controls, with **** = p<0.0001, *** = p<0.001, ** = p<0.01, * = p<0.05, detected by one-way ANOVA on planned relevant pairwise post-hoc comparisons with Šidák correction.

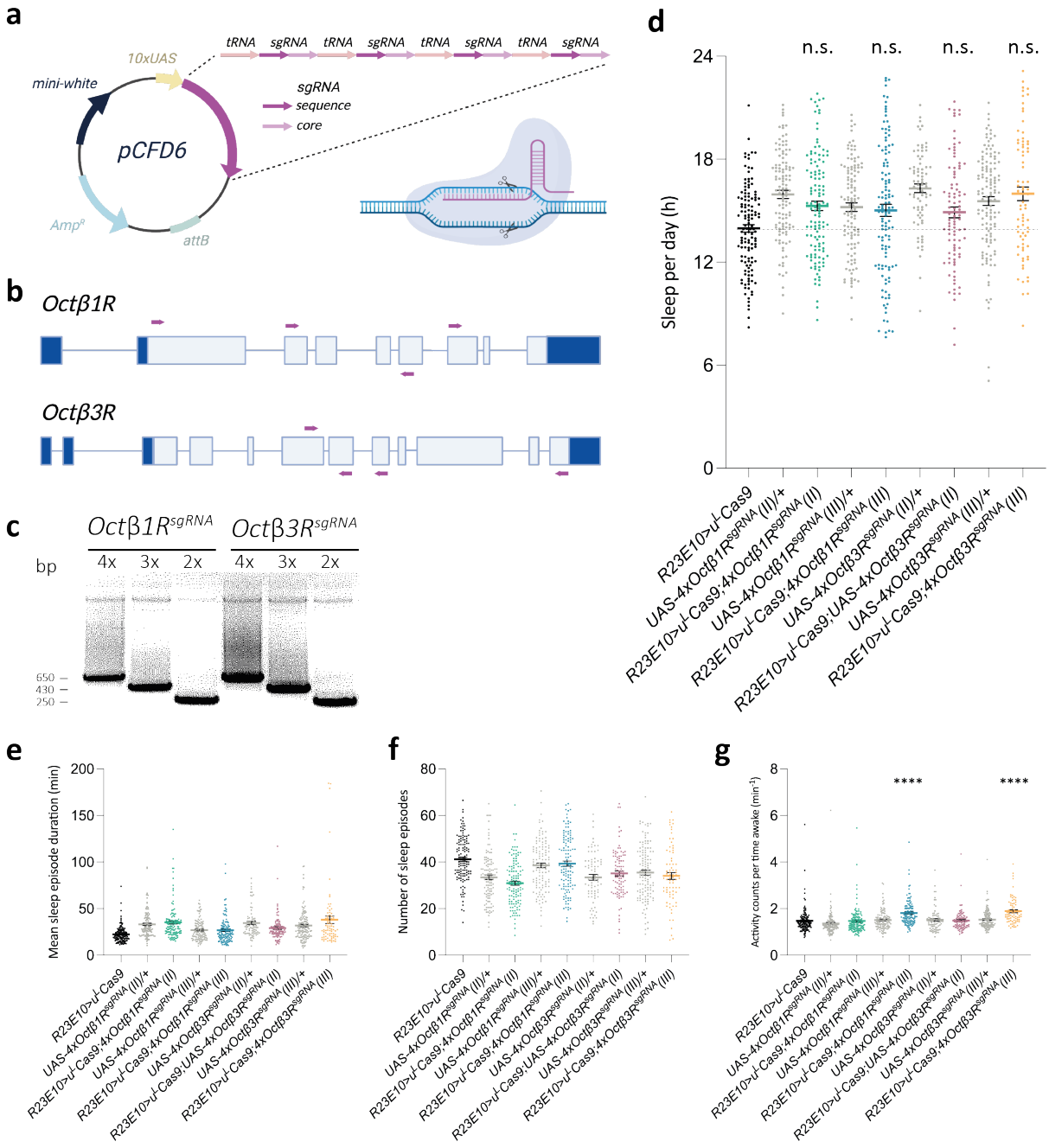

Figure 6.4 | Cell-specific CRISPR knockout of octopamine receptors does not affect total sleep.
a, Scheme of the recombinant plasmid used to generate transgenic cell-specific CRISPR knockouts. In PCFD6, I cloned sgRNAs in tandem, spaced by core sgRNA and tRNA regions. **b**, The sgRNAs (magenta arrows) targeted different exons (white rectangles) on different strands. **c**, Gel electrophoresis of the amplified insertions in PCFD6, in constructs bearing four, three and two sgRNAs against *Octβ1R* or *Octβ3R*. **d**, Total sleep per day in flies expressing different *R23E10-GAL4*-driven 4xsgRNAs and a Cas9 transgenes against OA receptors, is unchanged compared to parental controls. No differences were detected in mean sleep bout duration (**e**) and number of sleep episodes (**f**) of the same genotypes. Activity counts per time spent awake (**g**) indicate locomotor activity is augmented in two experimental groups. Individual values are plotted with mean ± SEM. Asterisks indicate significant differences between each experimental group and both parental controls, with **** = p<0.0001, detected by one-way ANOVA on planned relevant pairwise post-hoc comparisons with Šidák correction.

6.2.3 Octopaminergic inputs to dFB neurons

Finally, I asked whether octopaminergic neurons making pre-synaptic contacts onto dFB neurons had been identified in connectomics studies, and if so, which ones. A recent analysis of the fly hemibrain connectome has identified a pair of VPM3 neurons as recurrently connected to *R23E10-GAL4*-labelled dFB cells[33]. This neuron is therefore the most likely candidate for delivering OA inputs to dFB neurons. My analysis showed this neuron has elaborate arborisations in the FB, SMP, SIP, and SLP region, which correspond to regions where dFB neurons' axons and dendrites are located (**Figure 6.5a**). Most pre- and post-synaptic connections of VPM3 are located in these four areas (**Figure 6.5b**), and VPM3 forms direct pre- and post-synaptic connection with the main classes of *R23E10-GAL4*-labelled dFB neurons (FB6A and FB6C_b, which constitute roughly a third of all *R23E10-GAL4*-labelled dFB cells[33]) (**Figure 6.5c**).

While no driver line is currently available to obtain genetic access exclusively to the VPM3 pair of neurons, one could use the two driver lines available that target both VPM3 and VPM4 (an octopaminergic pair of cells with arborisations in very different regions than VPM3) neurons, and evaluate the effects by subtracting the contribution of VPM4 neurons, which instead have dedicated drivers lines (**Figure 6.5d**). I artificially activated via thermogenetics two of these lines (**Figure 6.5e**) and, while activation of VPM3 and VPM4 neurons decreased sleep, activating only VPM4 neurons did not produce either effect, therefore suggesting a wake-inducing ability of VPM3 neurons (**Figure 6.5e**).

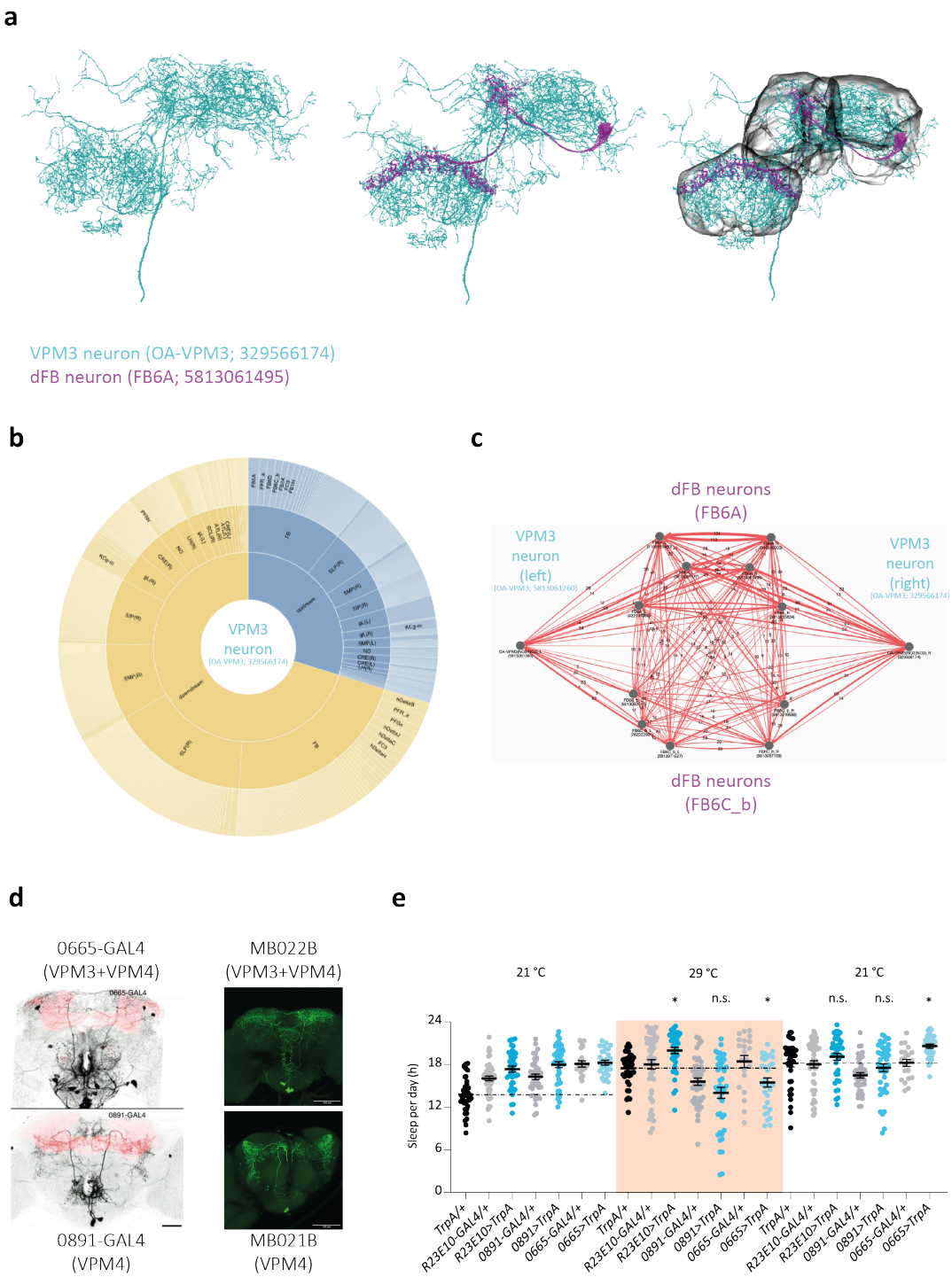

Figure 6.5 | VPM3 neurons are synaptically connected to *R23E10-GAL4*-labelled dFB neurons and affect sleep.
a, Structural reconstruction of a VPM3 neuron (right hemisphere), show vast arborizations in the FB, SMP, SIP and SLP areas (in grey, right), which are also sites where processes of dFB neurons (in magenta, one FB6A neuron) are located. **b**, Upstream and downstream connections of VPM3 neuron are located mostly in the FB, SMP, SIP and SLP areas. **c**, VPM3 neurons form a vast and recurrent network of connections with main classes of *R23E10-GAL4*-labelled dFB neurons (FB6A and FB6C_b). **d**, Driver lines available to target VPM3 and VPM4 neurons (top) and only VPM4 neurons (bottom); images on the left are adapted from[265] and scale bar is 50 µm; scale bars for images on the right are 100 µm. **e**, Sleep per day in flies expressing thermogenetic actuator TrpA, under the control of *R23E10-* (dFB neurons), *0891-* (VPM4), or *0665-* (VPM3 + VPM4) GAL4, showed increase in sleep in the positive control *R23E10>TrpA* when the temperature was raised from 21° to 29°, and sleep decrease for the activated *0665-GAL4* line, followed by compensatory sleep rebound when the temperature was lowered back. Asterisks indicate significant differences between each experimental group and both parental controls, and the same group on the day before, with * = p<0.05, detected by one-way ANOVA on planned relevant pairwise post-hoc comparisons with Šidák correction. Individual values are plotted with mean ± SEM.

6.3 Discussion

In this chapter, I have presented data that show that a major gene that determines a dichotomous transcriptional heterogeneity within dFB neurons is the octopamine β1 receptor (**Figure 6.1**). I continued my investigation focused on this group of receptors, but the data generated in this work can be the base for following studies, using DEGs between these two clusters (**Table 9.3**), including the apparently mutually exclusive expression of *Octβ1R* and *DopEcR*, or by increasing the clustering resolution and identifying even more clusters.
While *Octβ1R* was expressed only in half of dFB neurons, the other half expressed *Octβ2R* and *Oct-TyrR*, although at lower levels, whereas *Octβ3R* was instead more evenly distributed.

To understand whether this segregation has any functional relevance, I generated and tested tools to manipulate these receptors.
The results obtained with different tools, though, are different.
Cell-specific CRISPR knockout is a novel technology that combines the ease of generating knockout with CRISPR, with the refined genetic access provided by *Drosophila* genetics. Our constructs made in-house, though, did not show any behavioural sleep phenotype, although they did affect viability when expressed in the whole body, suggesting they do work (**Figure 6.4**). Instead, the effect of knockdown was different: while it is conceivable that using two RNAis instead of one increases the knockdown efficiency (**Figure 6.3**), the behavioural effect of 2xRNAi knockdown (sleep decreased) was different from the effect of CRISPR-knockout (no effect). The explanation might be that compensatory effects intervene in the knockout context, and mask any behavioural phenotype, or that, conversely, RNAis, especially if double, produce off-target effects that provoke the sleep phenotypes observed. Another possibility is that the actual effect of OA is evident mostly when sleep pressure is elevated.
Also, it is possible that the expression of these tools in the whole dFB population might mask sub-population effects: to verify this hypothesis, one could either KD or KO octopamine receptors specifically in dFB subsets enriched in the relevant receptor, using the split-GAL4 lines produced (**Figure 6.2**). In addition, one could verify the efficacy of the CRISPR KOs by sequencing the targeted gene in flies where the sgRNAs are expressed in the whole organism. Also, the CRISPR lines produced could be used by the fly community for other studies.

Finally, the observed effects with loss-of-function (sleep reduction) are opposite to the reported wake-inducing effects of OA. This could either due to off-target effects or to a special role of OA in the sleep homeostat cells.

Independent studies of the fly connectome have revealed vast recurrent connections between an octopaminergic pair of cells (VPM3 neurons) and dFB neurons, which I have verified (**Figure 6.5**). Interestingly, activating VPM3 led to increased wake, which is the opposite of what would have been expected by the KD results (**Figure 6.3b**). There are several hypotheses to explain this discrepancy: the GAL4 lines used for this experiment do label also other cells, in the antennal lobe, and, in addition, the effect I observed is a "subtraction" of the effect of two lines, which complicates the study; lines with more restricted expression pattern (like MB021B and MB022B) might better complement this experiment. Potentially, the effects of *Tdc2-GAL4* or VPM3 activation might be pleiotropic and while inducing wake overall, they also activate sleep-promoting dFB neurons. Also, it is possible that the effect of chronically depleting dFB neurons of OA receptors is mismatched with the physiological relevance of OA, which seems to acutely intervene in the NREM-wake transitions: to test this, one could acutely activate VPM3 neurons (with optogenetics or thermogenetics) in flies where dFB neurons (or their subsets) are depleted of OA receptors and evaluate the differential effect. Such an experiment would also functionally prove the VPM3-dFB connection; this could be additionally anatomically tested with GFP reconstitution methods, and with anterograde tracing.

In parallel to these behavioural investigations, it would be crucial to assess the physiological effects of octopamine inputs to dFB neurons. To validate the VPM3-dFB connection, one could activate VPM3 cells optogenetically and visualise the resulting increase in octopamine signal in different compartments (is it prevalent in the dFB or in the protocerebrum?) by using novel sensors (like the available, but yet unpublished $GRAB_{OA}$[277]). In addition, release of OA via injection or activation of OA neurons, and electrophysiological or calcium imaging recording of dFB neurons, will clarify the effect on dFB activity. In addition, the CRISPR and 2xRNAi lines produced could help identifying the responsible receptors, and the split-GAL4 lines, instead, could be useful to restrict the recordings to the relevant dFB neurons (as VPM3 seems to connect mostly to one third of dFB neurons[33]). Another way to abolish the functional interaction would be to use OA receptor antagonists mianserin[69,265], or the more specific compound epinastine[278].

It would be interesting to assess the effect of OA on dFB neurons; Octβ1R activates the inhibitory G protein $G\alpha_o$ limiting cAMP production, but its physiological effects in dFB cells are unknown[279]. Given its role in inhibiting the sleep homeostat[63], and the effects of the analogous NE, it is possible that acute releases of OA boluses onto dFB neurons would either inhibit them or disrupt their oscillation patterns, shattering their network activity and allowing the animal to suddenly wake up.

Finally, what would be the functional result of octopamine inputs only on a subset of dFB neurons?

Given that VPM3 mostly connects to dFB projecting to layer 6, it is possible that inhibition mediated by OA would locally gate the information processing, leaving unaltered the neuronal computations in other layers, such as layer 7, which is also innervated by *R23E10-GAL4*-labelled dFB neurons.

Alternatively, it is plausible that the action of OA would selectively gate certain aspects of sleep controlled by dFB neurons and not others: if one compares the expression pattern of *Octβ1R* in **Figure 6.1** and the expression of dFB markers in **Figure 3.5e**, and knowing the selective VPM3-dFB connectivity, it is possible that OA effects would leave the secretion of AstA (and its related downstream effects) unaltered, allowing a sudden awakening but still permitting the flowing of sleep pressure to downstream circuits.

7 Conclusions

The content of this thesis mostly revolves around a neuronal population controlling sleep in flies: the dorsal fan-shaped body-projecting neurons. My analysis touched on several aspects of their molecular, (sub)cellular and circuit properties. I will summarise here the main findings.

In **Chapter 3**, I generated the first single-cell transcriptome of a(ny) brain and its sleep-control centres in conditions of high and low sleep pressure. While the abundance of data contained in this dataset can be a valuable resource for several lines of investigation, I focused on my neurons of interest, and identified them in my dataset. Access to their transcriptome has generated hypotheses and inspired the work contained in the following chapters.

In **Chapter 4**, I experimentally verified that dFB neurons are glutamatergic, with several complementary techniques. Knowing the nature of the fast-acting NT of these cells allows me to make educated guesses on the nature of receptors and inputs on post-synaptic partners of these neurons, and their role in the circuits in which they are embedded.

In **Chapter 5**, I evaluated the transcriptional changes occurring in the dFB between sleep pressure states, investigated their physiological correlates, and assessed their specificity. I discovered that plastic synaptic changes occur in dFB neurons depending on sleep pressure, and that there is a bidirectional and causal relationship between mitochondrial dynamics and sleep. The latter finding sheds light on a potential mechanism that bridges the molecular signatures of sleep deprivation identified in these cells, to their electrical properties, via adaptive cellular bioenergetics and subcellular organisation.

In **Chapter 6**, I addressed the question of heterogeneity within this neuronal population, and identified an octopamine receptor as a principal marker of diversity. I explored the functional implications of these findings, the origin of OA inputs, and generated tools and hypotheses that will be useful in future investigations.

7.1 Methodological considerations and limitations

Limitations of this study have been described in each chapter, but I will report here the main and general ones.

The single-cell transcriptomics technique adopted generated hypotheses and data that led to all the presented work. However, this methodology inevitably brings with it a loss of spatial information, which would have been extremely precious, for example in the investigation of heterogeneity, cell markers, NT expression, and their combinations. The recently established spatial transcriptomics techniques could provide additional insights.

My transcriptomics dataset included the optic lobes, as they were dissected together with the midbrain, and included in the sequenced samples. While this could provide a useful resource, the optic lobes are usually thought not to be directly involved in the sleep-control process that was the object of this study, and their inclusion might have unnecessarily enlarged the dataset. Even though many optic lobe clusters could be identified *in silico* and removed *a posteriori*, one cannot rule out that unidentified optic lobe cells are present in the large unannotated clusters of my and most transcriptomic datasets.

Regarding scRNA-seq processing, even though samples from sleep deprived and rested flies were processed in parallel, this could still lead to some discrepancies, given the numerous experimental steps from dissection to sequencing (and, in fact, the number of cells recovered from control and sleep deprived brains is not exactly the same). Even if such discrepancies can be regressed out, if one could process the two conditions together and de-multiplex them *a posteriori*, the technical noise might have decreased. Recently, pooled designs of transcriptional profiling experiments have been developed in *Drosophila*, taking advantage of lines bearing unique single-nucleotide polymorphisms, which would be captured in mRNA sequences, and traced back to the original groups[280].

The identification of glutamate as the fast-acting NT of dFB neurons still does not clarify whether this provides inhibitory or excitatory inputs to downstream circuits. While glutamate has mostly an inhibitory role in the fly's CNS, this cannot be concluded for the dFB from this work, and further studies will be necessary (mostly looking at physiological responses in

downstream partners of dFB neurons – dopaminergic cells, columnar cells, or synaptically connected dFB themselves – upon their activation). That said, in the one electrophysiological study that has been performed, the direct activation of dFB neurons powerfully hyperpolarised helicon cells.

The analysis of the specificity of transcriptional and mitochondrial changes observed in dFB neurons in Chapter 5 has mostly relied on the comparison with two cell types, Kenyon cells and olfactory projection neurons. Although this approach can rule out that changes observed in dFB neurons are brain-wide phenomena, it would be interesting to have a more comprehensive assessment of their extent. To this end, one could determine the expression levels of all differentially expressed genes that are up- or downregulated in dFB neurons, across all cell clusters.

In my study of the NT identity of dFB neurons I did not formally test the effects of loss-of-function of other neurotransmitters, even though split-GAL4 lines using hemidrivers specific for of NTs other than glutamate did not label any dFB neurons. For the sake of completeness, one could nonetheless have used tools like RNAis or GAL80 directed towards other NTs; in addition, using fluorescence sensors for other neurotransmitters could have been instrumental in revealing if any (or confirming that no) release of those occur *in vivo* from dFB neurons.

Another inherent problem of my loss- and gain-of-function manipulations is that they are mostly chronic, and one must consider that they could impact and impair the correct cellular development. A way to circumvent this would be to implement inducible gene expression systems, and switch on the desired manipulations only at the appropriate developmental stage (i.e., the adult); also, one could use acute manipulations were possible, like a light-driven mitochondrial proton pump. In addition, a coarse method to detect major developmental defects is to inspect whether the overall morphology of cells is altered after the genetic manipulation.

A linked limitation is that the efficacy of RNAi lines on 1) targeting and depleting the endogenous transcript, and 2) reducing the corresponding protein levels is often unclear. While some of the constructs used in this work have been developed and functionally tested

in other studies, this is not systematically the case. In addition, verifying the changes in endogenous protein levels upon RNAi manipulation is difficult in *Drosophila*, as significantly fewer antibodies targeting fly proteins are available, compared to mammalian proteins. An alternative is to either use *ad hoc* fluorescence *in situ* hybridisation probes, or to express those lines brain- or body-wide and evaluate the reduction in RNA levels via canonical qRT-PCR. However, the best solution is to validate the functional readouts of those manipulations. I plan, for example, to test whether the KD and overexpression lines for mitochondrial fission and fusion factors produce the expected morphological phenotypes in dFB mitochondria.

Similar considerations can be made for the cell-specific CRISPR KO lines made in-house: they could be validated in systems where the effect of eliminating octopamine receptors is known[265,281], or genetically validated by body-wide expression and sequencing.

Another limitation is that I mostly used loss-of-function interventions: this is because there are vast publicly available repositories of fly lines bearing knockdown constructs. However, I am planning on using gain-of-function constructs, such as overexpression transgenes or synthetic tethers between mitochondria and ER, in order to artificially inflate the number of MERCs.

Imaging mitochondria with confocal microscopy has intrinsic limitations, due to the Nyquist resolution limit, faced by all studies that have used the same method to quantify and analyse mitochondria. Methods to improve image acquisition and analysis include super-resolution microscopy techniques, or expansion microscopy, at least on a subset of samples. Indeed, the low throughput of time-consuming acquisition and deconvolution of images, even by confocal microscopy, represent a logistic limitation.

Finally, in my analysis of mitochondrial dynamics, I did not factor in two other processes that contribute to the organelles' dynamics: mitophagy and transport. To assess whether the former is involved, I will use fluorescent mitophagy reporters, and as for the latter, I will measure mitochondrial abundance in other cell compartments, to evaluate whether their numbers vary. However, tracking of mitochondria *in vivo* in intact fly brains is currently technologically challenging, and might remain an unaddressed point.

7.2 Future work

Despite the outlined limitations, my work has delineated novel players and additional complexity in the operating modes of dFB neurons: not only do these neurons (or a subset of them) secrete AstA, their fast-acting NT is also functional in regulating sleep; and not only do their mitochondria produce high ROS levels upon sleep loss, but they also undergo dynamic changes; their transcriptional profile is not homogeneous and they do not all receive the same inputs but some are likely specific to a subset of cells.

I see future research based on the findings of this work evolving into two directions: one could further explore the circuitry of these cells, and extrapolate network principles of coding; in another direction, the metabolic coupling of electrical activity, bioenergetics and behavioural control could be explored in other circuits and comparatively in other animals.

- It would be highly informative to understand the nature of the reciprocal connectivity between dFB and dopaminergic neurons: if they comprise mutual inhibition, on which timescales they occur and what the implications are in terms of circuit synchronisation and behaviour-directed coding. Second, it would be interesting to dissect the circuits downstream of dFB neurons, to understand how sleep is conveyed through the layers of the FB, and how this is multiplexed with the navigation cues also computed in this structure[33]. As for the inputs to these cells, further efforts are needed to elucidate the role of OA on these cells, and in particular how its role differs from DA inputs: if DANs innervate most dFB neurons, and OA neurons project to fewer, what is the role of the dFB cells not targeted by OA neurons? Do they differ in the aspects of sleep control conveyed downstream? Or are they instead indirectly affected by OA inputs via dFB-dFB connectivity? If so, what is the functional meaning of having two monoamines acting on this circuit?
- If mitochondrial dynamics couple bioenergetics to a subcellular mechanism that enables different electrical activity patterns (may those subcellular mechanisms be MERCs, contact sites with other organelles, mechanical coupling, transport or others), it is possible that other behaviours where animal metabolism is engaged exploit similar

mechanisms to track and either reinforce or homeostatically temper the behaviours, as other work has shown for feeding and nutrition-sensing behaviours. Possible behaviours to investigate might be parental caring or sex drive (where the "fitness drive" would suppress even metabolic needs), or in contexts where feeding itself cannot happen, like during animal long-range migration.

Whether time-keeping mechanisms based on mitochondrial dynamics exist in neurons controlling these behaviours is a hypothesis that needs future exploration.

Finally, one could test to what extent these findings have value in more naturalistic environments, using novel high resolution techniques that can better capture the full complexity of a given behaviour and the intricate related neural activity patterns[282].

In conclusion, with the investigation reported here, inputs, inner molecular working, and outputs of dFB neurons have been revealed to have diverse physiological manifolds, which suit the regulation of multifaceted behaviours, like sleep, and can inspire future work.

7.3 Concluding remarks

The findings reported in this work, in addition to uncovering new features of an exemplar implementation of sleep control, bring more evidence to the suggested analogy between this system and hypothalamic nuclei[83,91]. In fact, akin to VLPO^{Gal} or POA$^{Tac1/Pdyn96,133}$ neuropeptide-secreting cells in sleep-control regions, which are inhibitory, the VGlut^{+} fly dFB$^{(AstA)}$ neurons are also likely to be inhibitory (**Chapter 4**). In addition, the metabolic reshaping of mitochondria in dFB neurons resembles phenomena observed in the arcuate nucleus of the hypothalamus, like the anorexigenic pro-opiomelanocortin (POMC) neurons and the orexigenic neuropeptide Y (NPY)/agouti-related peptide (AgRP) neurons[234,242], or in the ventromedial hypothalamus[244,283] (**Chapter 5**). Finally, like locus coeruleus-NE neurons projecting to certain nuclei of the hypothalamus[284] and thereby controlling behaviours (or suddenly suppressing them)[285], octopaminergic cells project to certain dFB neurons and might tune their control of arousal thresholds (**Chapter 6**). While these analogies have to be conclusively proven, they could foster further investigations and underscore the value of comparative neuroscience[282]. Conversely, the highly detailed findings in fly's dFB neurons related to sleep could generate hypotheses to be tested in other animal systems, in hypothesis-driven approaches. Given that sleep is a basic behaviour, and fulfils a yet undefined need universally felt by animals, principles regarding the tracking and accumulation of sleep need, and its discharge, could represent general rules conserved across the evolutionary tree.

The strategy adopted in the line of investigation that led to the discovery and characterisation of the fly's sleep control via dFB neurons[53,66,80,81,83] represents a successful example of an approach to mechanistically understand the operating principles underlying a behaviour; decomposing a cognitive process into its circuits and cellular substrates, carefully scrutinising its molecular components, and reconstituting their interplay, providing comprehensive insights at the computational, algorithmic and implementational levels of information processing.

There is grandeur in this view of neuroscience: from so simple molecular interactions, endless behaviours most beautiful and most wonderful, emerge and unfold.

8 Acknowledgments

For inspiring, supporting, and motivating the achievement of the work included in this thesis, I want to express my gratitude to several people.

To Gero Miesenböck, *elegantiae arbiter*. Working in his lab and under his supervision has been and is an enormous privilege: his inspirational style, teachings and intellectual influence have deeply shaped the way I reason of science, research and experiments. His wit, support, motivation and mentoring have made my time in Oxford truly intellectually stimulating, and a crucial step in my personal growth.

To Vladyslav Vyazovskiy for his continuous support, welcoming mentoring, and for teaching me a great deal about sleep.

To Peter Hasenhuetl, for his genuine interest in teaching me methods and theories, for thorough scientific exchanges and fruitful collaborations, personal friendship and support, via mentoring and lemon juices.

To Anissa Kempf and Diogo Pimentel, for having introduced me to the CNCB (lab) life, having looked after my first steps in the lab and helping me maturing as a student.

To Eleftheria Vrontou for the scientific collaborations and cultural interactions, motivational and personal support.

To all the other Miesenböck lab members, Katerina Christodolou, Olof Rorsman, Timothy Wong, Alina Krebbers, Laura Garmendia-Sanchez, Clifford Talbot, Jan Kropf, Laura Chan Wah Hak, Bohan Zhao, Lukas Groshner, Susanne Szydlowski, Giacomo Bertuzzi, Celina Hartmann, Haram Park, Yeonsoo Choi, Patrick Liu, John-Paul Moszynski, Lea Ballenberger, Zelie Britton, Emma Charlett-Green. It would be impossible to list all the exchanges, support and wonderful interactions of the past 4+ years. Indeed, each of them, in different ways, has taught me something, thus this work is somehow also a product of theirs, and I am extremely thankful for

that. With them I have shared friendships, camaraderie, ups and downs of experiments and life, and plenty of fond memories.

To Rice Yiu Ching Siu, Nicholas Monaco, and Marissa Mueller, whom I had the fortune to supervise during these years and whose work contributed to some of the projects discussed in this thesis.

To Ruth Brain and Fiona Woods, for their dedicated high professionality.

To the whole CNCB, and especially to Homero Barrocas Soares Esmeraldo, Paola Vargas Gutierrez, Charlie Treiber, Eleonora Meschi, Lucille Duquenoy, Zeynep Okray, Ashwin Miriyala, Ammerins de Haan, Chaitanya Chintaluri for making the centre such a vibrant and sparkling community. I had been dreaming of joining the CNCB for a long time, and still after more than four years, I cannot get used to the brilliance intensity concentrated in this place.

To the unique Oxford environment, Cortex Club members and friends, my wonderful first lab rotation supervisors, my generous doctoral programme and its considerate organisers, my college's warm community and academic fabric.

To Scuola Normale Superiore, for having given me the chance to stand out, live in an unparalleled brilliant environment, and make me land in unexpected and unthinkable ports, including Oxford.

To my friends, from Oxford, Italy and around the world, for being wonderful anchors of veracity, happiness and lightheartedness.

To my family, for paving the way with values, support, and love.

To Francesca, for her courageous choices, and for radiating me with her love, passion and joy.

9 Appendices

9.1 Criteria and markers used to label cell clusters

- Kenyon cells: clustered in three close-by groups *ey*$^{+}$, *Dop1R2*$^{+}$
  - αβ: cluster *sNPF*$^{+}$, *Fas2*$^{+}$, *trio*$^{-}$
  - α'β': cluster *sNPF*$^{-}$, *Fas2*$^{-}$, *trio*$^{+}$
  - γ: cluster *sNPF*$^{+}$, *Fas2*$^{+}$, *trio*$^{+}$
- Monoaminergic cells: clusters *Vmat*$^{+}$
  - Dopaminergic*:* cluster *Ddc*$^{+}$, *ple, DAT*
  - Serotonergic*:* cluster *Ddc*$^{+}$, *SerT*$^{+}$, *Trh*$^{+}$
  - Octopaminergic/Tyraminergic*:* cluster *Tdc2*$^{+}$
- Projection neurons: clusters *ct*$^{+}$, *acj6*$^{+}$
  - ventral Projection neurons: cluster *Lim1*$^{+}$
- Fat body: cluster *SPARC*$^{+}$, *MtnA*$^{+}$, *Indy*$^{+}$, *pdgy*$^{+}$
- Glia: clusters *nrv2*$^{+}$
  - Astrocytes: cluster *alrm*$^{+}$
- ***Bona fide*** dFB neurons: *elav>0*, *nSyb>0*, *AstA-R>0*, *EGFP*>2
- ***dFB neurons*:** clusters within the glutamatergic stringent dataset, populated by *bona fide* dFB neurons

Relaxed criteria for determining glutamatergic, cholinergic, and GABAergic neurons were, respectively: *VGlut*>0, *VAChT*>0, *Gad1*>0.

Stringent criteria for determining glutamatergic, cholinergic, and GABAergic neurons were, respectively: *VGlut*>2, *VAChT*>2, *Gad1*>2.

The values of "2" for *EGFP*, *VGlut*, *VAChT* and *Gad1* were chosen to bisect the roughly bimodal distributions of their expression levels.

9.2 Transcriptomic reads alignment and annotation script

Requires DropSeqtools and STARAligner. Full instructions on Drop-seq Core Computational Protocol[110].

```
######
# 1. #
######
cd /Path/Working_directory
######

mkdir file_name_summaries

######
# 2. #
######
java -jar /Path/Drop-seq_tools-2.1.0/3rdParty/picard/picard.jar FastqToSam \
F1=/Path/936810_TY90_S42_L004_R1_001.fastq.gz \
F2=/Path/936810_TY90_S42_L004_R2_001.fastq.gz \
O=./01_file_name_unmapped.bam \
SM=file_name \
        &&
#########

/Path/Drop-seq_tools-2.1.0/TagBamWithReadSequenceExtended \
        SUMMARY=./file_name_summaries/01to02_unaligned_tagged_Cellular.bam_summary.txt \
        BASE_RANGE=1-16 \
        BASE_QUALITY=10 \
        BARCODED_READ=1 \
        DISCARD_READ=false \
        TAG_NAME=XC \
        NUM_BASES_BELOW_QUALITY=1 \
        INPUT=./01_file_name_unmapped.bam \
        OUTPUT=./02_file_name_unaligned_tagged_Cell.bam \
        &&

rm 01_file_name_unmapped.bam &&

/Path/Drop-seq_tools-2.1.0/TagBamWithReadSequenceExtended \
        SUMMARY=./file_name_summaries/02to03_unaligned_tagged_Molecular.bam_summary.txt \
        BASE_RANGE=17-28 \
        BASE_QUALITY=10 \
        BARCODED_READ=1 \
        DISCARD_READ=true \
        TAG_NAME=XM \
        NUM_BASES_BELOW_QUALITY=1 \
        INPUT=./02_file_name_unaligned_tagged_Cell.bam \
        OUTPUT=03_file_name_unaligned_tagged_CellMolecular.bam \
        &&

rm 02_file_name_unaligned_tagged_Cell.bam &&

/Path/Drop-seq_tools-2.1.0/FilterBam \
        TAG_REJECT=XQ \
        INPUT=03_file_name_unaligned_tagged_CellMolecular.bam \
        OUTPUT=05_file_name_unaligned_tagged_trimmed_smart.bam \
        &&

rm 03_file_name_unaligned_tagged_CellMolecular.bam &&

/Path/Drop-seq_tools-2.1.0/PolyATrimmer \
        OUTPUT=06_file_name_unaligned_mc_tagged_polyA_filtered.bam \
        OUTPUT_SUMMARY=file_name_summaries/05to06_polyA_trimming_report.txt \
        MISMATCHES=0 \
        NUM_BASES=6 \
        INPUT=05_file_name_unaligned_tagged_trimmed_smart.bam \
        &&

rm 05_file_name_unaligned_tagged_trimmed_smart.bam &&

java -jar /Path/Drop-seq_tools-2.1.0/3rdParty/picard/picard.jar SamToFastq \
        INPUT=06_file_name_unaligned_mc_tagged_polyA_filtered.bam \
```

```
		FASTQ=07_file_name_unaligned_mc_tagged_polyA_filtered.fastq \
		&&

######
# 4. STAR #
######
 /Path/STAR-master/bin/MacOSX_x86_64/STAR --genomeDir //Path/Genome_index \
		--runThreadN 9 \
		--outFileNamePrefix 08_file_name_dmel613_star_ \
		--readFilesIn ./07_file_name_unaligned_mc_tagged_polyA_filtered.fastq \
		&&
######
mv 08_file_name_dmel613_star_Log* ./file_name_summaries/ \
		&&
rm 07_file_name_unaligned_mc_tagged_polyA_filtered.fastq &&
######
java -jar /Path/Drop-seq_tools-2.1.0/3rdParty/picard/picard.jar SortSam \
		INPUT=08_file_name_dmel613_star_Aligned.out.sam \
		OUTPUT=09_file_name_dmel613_aligned_sorted.bam \
		SORT_ORDER=queryname \
		TMP_DIR=./ \
		&&

rm 08_file_name_dmel613_star_Aligned.out.sam &&

######
# 5. #
######
java -jar /Path/Drop-seq_tools-2.1.0/3rdParty/picard/picard.jar MergeBamAlignment \
		ALIGNED=09_file_name_dmel613_aligned_sorted.bam \
		UNMAPPED=06_file_name_unaligned_mc_tagged_polyA_filtered.bam \
		O=10_file_name_dmel613_merged.bam \
		R=/Path/drosophila_genome_simplified/dmtot_EGFP-p10_SplitGAL4_GAL4.fa \
		INCLUDE_SECONDARY_ALIGNMENTS=false \
		PAIRED_RUN=false \
		&&
######

rm 06_file_name_unaligned_mc_tagged_polyA_filtered.bam &&

rm 09_file_name_dmel613_aligned_sorted.bam &&

######
# 6. #
######
java -jar /Path/Drop-seq_tools-2.1.0/TagReadWithGeneFunction \
		O=11_file_name_dmel613_merged_gene_exon_tagged.bam \
		ANNOTATIONS_FILE=/Path/dmtot_EGFP-p10_SplitGAL4_GAL4.refFlat \
		TMP_DIR= /Path/Working_directory \
		INPUT=10_file_name_dmel613_merged.bam \
		&&
######

rm 10_file_name_dmel613_merged.bam &&

#####
# BAMTagHistogram #
#####

/Path/Drop-seq_tools-2.1.0/BamTagHistogram
\		INPUT=/Path/Working_directory/11_file_name_dmel613_merged_gene_exon_tagged.bam		\		O=
/Path/Working_directory/11_file_name_dmel613_out_cell_readcounts.txt.gz \
TAG=XC

### Create .bai file
/Path/samtools-1.9/samtools \
index /Path/Working_directory/11_file_name_dmel613_merged_gene_exon_tagged.bam \

#####
# DGE #
#####
/Path/Drop-seq_tools-2.1.0/DigitalExpression \
		I=11_file_name_dmel613_merged_gene_exon_tagged.bam \
		O=12_file_name_dmel613_merged_gene_exon_tagged_top2500cells.dge.txt.gz \
		SUMMARY=./file_name_summaries/12_out_gene_exon_tagged_top2500cells_dge_summary.txt \
		NUM_CORE_BARCODES=2500
```

9.3 Genes differentially expressed in dFB neurons, compared to the rest of fly brain

	p_val	avg_log2FC	pct.1	pct.2	p_val_adj
CG33958	0	1.14894487	0.279	0.002	0
EGFP-p10	0	4.17504718	0.641	0.072	0
Kr	0	1.65922176	0.288	0.007	0
bsh	0	1.85596114	0.384	0.018	0
y	0	1.61747286	0.235	0.004	0
CG5541	0	0.73938508	0.207	0.001	0
hec	9.83E-295	1.43350522	0.331	0.016	9.94E-291
SmydA-1	2.36E-288	0.75159113	0.161	0.002	2.38E-284
CG14516	2.09E-270	0.73619189	0.186	0.004	2.11E-266
Osi4	7.22E-266	0.49891938	0.108	0	7.30E-262
dac	6.73E-261	2.03619906	0.672	0.09	6.80E-257
AstA-R1	2.05E-235	1.76829543	0.755	0.129	2.07E-231
dve	5.57E-234	1.96550963	0.39	0.032	5.64E-230
CG43689	2.95E-195	1.98407496	0.421	0.044	2.98E-191
Jhl-21	1.46E-183	1.01842777	0.269	0.018	1.48E-179
Ac78C	5.54E-181	1.97928886	0.424	0.052	5.60E-177
VGlut	1.41E-174	1.92335638	1	0.309	1.42E-170
Nep2	5.85E-173	1.11696893	0.204	0.011	5.92E-169
rgr	2.65E-170	0.98238381	0.257	0.018	2.68E-166
bi	4.29E-168	1.87359984	0.867	0.248	4.34E-164
Gyc89Da	2.48E-160	0.52974374	0.149	0.005	2.51E-156
CG32532	5.45E-157	1.24205624	0.347	0.037	5.51E-153
CG42663	2.74E-155	1.37495521	0.514	0.083	2.77E-151
a	6.28E-154	1.40270367	0.365	0.043	6.35E-150
Dscam4	2.17E-153	2.1743457	0.898	0.334	2.19E-149
Imp	8.37E-148	1.92757344	0.619	0.126	8.46E-144
CR41501	1.32E-140	0.15741394	0.05	0	1.34E-136
GAL4	6.64E-125	0.32559066	0.139	0.007	6.72E-121
orb	1.57E-123	1.86020936	0.517	0.108	1.59E-119
vn	3.24E-120	0.87773909	0.217	0.018	3.28E-116
Lmpt	1.04E-119	1.8889616	0.412	0.072	1.06E-115
CG14431	7.48E-119	1.4031421	0.545	0.116	7.57E-115
CR44981	3.66E-113	0.63045274	0.17	0.012	3.70E-109
CG45782	2.76E-109	0.95602708	0.368	0.058	2.79E-105
CG31323	1.12E-108	1.18861121	0.523	0.115	1.14E-104
svp	7.16E-106	1.12789478	0.375	0.061	7.24E-102
lov	2.68E-104	0.82059412	0.344	0.052	2.71E-100
bru3	1.86E-103	1.5606159	0.988	0.628	1.88E-99
Octbeta1R	1.32E-97	2.70037108	0.746	0.276	1.33E-93
RYa	3.04E-97	0.16437172	0.034	0	3.07E-93
Grd	1.97E-96	0.77430315	0.214	0.022	1.99E-92
CG1578	2.81E-95	1.64697817	0.777	0.301	2.84E-91
CG43373	1.19E-92	1.39941513	0.415	0.088	1.21E-88
jim	1.22E-92	-1.5923806	0.916	0.981	1.24E-88
CG42521	4.14E-92	0.25099667	0.053	0.001	4.19E-88
fbp	3.74E-91	0.35110299	0.099	0.005	3.78E-87
Hsp70Bb	6.27E-88	2.18345386	0.563	0.172	6.34E-84
Dop1R1	1.88E-87	1.94976604	0.737	0.272	1.90E-83
Sytbeta	2.49E-86	1.44280924	0.632	0.204	2.52E-82
CG6959	1.76E-84	0.89689912	0.471	0.11	1.78E-80

Table 9.1 | Genes differentially expressed in dFB neurons compared to the rest of the brain.

First 50 genes differentially regulated (enriched or depleted) in dFB neurons, as identified in Figure 3.5, compared to the transcriptome of the rest of the brain. Genes are ordered by adjusted P-value, scored by Wilcoxon Rank Sum test, with P-value adjusted using Bonferroni correction based on the total number of variable genes within the whole brain. The table also shows the Log_2 of the fold change of gene expression between dFB neurons and the rest of the brain (positive values indicate enrichment in dFB neurons) and the percentage of cells in each group in which the gene is detected.

9.4 Two-photon imaging analysis script of response to arousing stimulus

```
% Version 2022-01-06: analysis script imaging dFB glutamate sensor arousing stimulus;
Peter S. Hasenhuetl and Raffaele Sarnataro

%% First, get recordings to analyse
punishment_flies = get_recorded_punishment_flies;

%% Then, calls the custom analysis function
punish_summary = get_all(punishment_flies);

%% Then, plots the results
close all
get_fig_panel_punishment_aligned(punish_summary)


%% Below are the custom functions called above

function punishment_flies = get_recorded_punishment_flies
function punish_summary = get_all(punishment_flies)

fields_flies = fieldnames(punishment_flies);
aligned_signal = [];

% Loops through individual flies
for fly_idx = 1:length(fields_flies)
        fly_name = fields_flies{fly_idx};
        input_fly = punishment_flies.(string(fly_name));
        fields_sessions = fieldnames(input_fly.img);

        % Loops through imaging sessions of individual flies
         for session_idx = 1:1
                session_name = fields_sessions{session_idx};
                input_img = input_fly.img.(string(session_name));
                output_img = get_img_measures(input_img);

%For now, I just consider the first punishment/imaging-session
        if session_idx == 1
                aligned_signal = [aligned_signal, output_img.aligned_ratio];
                end
        end

end

punish_summary.aligned_signal = aligned_signal;
punish_summary.t_v_aligned = output_img.t_v_align;
punish_summary.fr=output_img.fr;
punish_summary.pre_window=output_img.pre_window;
punish_summary.post_window=output_img.post_window;

end

function output_img = get_img_measures(input_img)

fr = 208.56; % frame-rate in Hz

raw_green = input_img.green_signal;
background_green = input_img.green_background;
img_green = raw_green - mean(background_green);

raw_red = input_img.red_signal;
background_red = input_img.red_background;
```

```
img_red = raw_red - mean(background_red);

channel3 = input_img.channel3;

t_v = (0:length(raw_green))/fr;

%% First, tests for ROI to be included

if mean(img_green) < 10
 excl_cond = 1;
 img_green(:,1) = NaN(length(img_green(:,1)),1);
 img_red(:,1) = NaN(length(img_red(:,1)),1);
else
 excl_cond = 0;
end

%% Then, computes dF/F and dR/R

g = img_green;
output_img.raw_green = img_green;
dFg = (g - mean(g))./abs(mean(g));
output_img.dFg = dFg;

r = img_red;
output_img.raw_red = img_red;
dFr = (r - mean(r))./abs(mean(r));
output_img.dFr = dFr;

ratio=img_green./img_red;
output_img.raw_ratio = ratio;
dR=(ratio-mean(ratio)./abs(mean(ratio)));
output_img.dR = dR;

ch3 = channel3+10000;
ch3 = (ch3-min(ch3))/max(ch3-min(ch3));
output_img.ch3 = ch3;

%% Aligns the imaging traces to the onset of punishment

pre_window = round(5*fr);
post_window = round(7*fr);

output_img.punish_idx = (find(ch3 > 0.1,1,'first'))+round(3*fr); % Finds the index when the punishment starts

% Computes aligned signal for green channel
aligned_green = g(output_img.punish_idx-pre_window:output_img.punish_idx+post_window,1);
output_img.aligned_green = (aligned_green -
mean(aligned_green(1:pre_window,1)))./abs(mean(aligned_green(1:pre_window,1)));

% Computes aligned signal for red channel
aligned_red = r(output_img.punish_idx-pre_window:output_img.punish_idx+post_window,1);
output_img.aligned_red = (aligned_red - mean(aligned_red(1:pre_window,1)))./abs(mean(aligned_red(1:pre_window,1)));

% Computes aligned signal for ratio between green and red channels
aligned_ratio = aligned_green./aligned_red;
output_img.aligned_ratio = (aligned_ratio -
mean(aligned_ratio(1:pre_window,1)))./abs(mean(aligned_ratio(1:pre_window,1)));

% Computes the aligned time
output_img.t_v_align = (1:length(output_img.aligned_green))/fr;
output_img.t_v_align = (output_img.t_v_align-((pre_window)/fr));

output_img.fr=fr;
```

```
output_img.pre_window=pre_window;
output_img.post_window=post_window;

end

function get_fig_panel_punishment_aligned(punish_summary)

figure('Name','punishment figure','Color','white',...
 'Units','centimeters','Position',[10 12 18.3 18],'Resize','off')

% Defining some variables beforehand
f_s = 12; % Font size
x_cord = 2; % x-coordinates of panel in cm
y_cord = 2; % y-coordinates of panel in cm
s_z = 6; % x-dimension of panel in cm
h_t = 9; % y-dimension of panel in cm
ylm_img = [-0.05, 0.12]; % limits in y-dimension
xlm_img = [-6,10];
bw_hist = 0.0125; % bin-width of histogram
pt1=movmean(mean(punish_summary.aligned_signal,2),100); %moving mean
pt2=movmean(std(punish_summary.aligned_signal,0,2),100)./sqrt(size(punish_summary.aligned_signal,2)); %std

pnl1 = axes('Units','Centimeters','Position',[x_cord, y_cord, s_z, h_t]);
hold on
plot(pnl1,punish_summary.t_v_aligned,pt1,'Color','r','LineWidth',2)
plot(pnl1,punish_summary.t_v_aligned,pt1+pt2,'Color','r','LineWidth',0.1)
plot(pnl1,punish_summary.t_v_aligned,pt1-pt2,'Color','r','LineWidth',0.1)
plot(pnl1,[0, 2],[ylm_img(2),ylm_img(2)],'k','LineWidth',2,'Color','b')
plot(pnl1,[3,5],[ylm_img(1),ylm_img(1)],'k','LineWidth',1)
xlim(xlm_img)
ylim(ylm_img)
pnl1.Box = 'off';
pnl1.FontSize = f_s;
ylabel('dR/R')
xlabel({'time from onset'; 'of stimulus (s)'})
pnl1.XAxis.Color='none';
pnl1.YAxis.Color='none';
pnl1 = axes('Units','Centimeters','Position',[x_cord+s_z+0.1, y_cord, 0.2, h_t]);
plot(pnl1,[1,1],[ylm_img(1),ylm_img(1)+0.05],'k','Linewidth',1)
pnl1.Color='none';
pnl1.XAxis.Color='none';
pnl1.YAxis.Color='none';
xlim(xlm_img)
ylim(ylm_img)

annotation('textbox', 'Units','centimeters','Position',[x_cord, y_cord+h_t+1.2, 10, 0.5], 'string', ...
 {'R23E10>iGluSnFR(A184V);TdTomato';'dFB response to punishment';'208.16 Hz';'n=17'}, 'EdgeColor','none',...
 'FontSize',7,'FontWeight','bold','Color','k')

annotation('textbox', 'Units','centimeters','Position',[x_cord+s_z-0.5, y_cord-0.5, 10, 0.5], 'string', ...
 '2s', 'EdgeColor','none',...
 'FontSize',12,'FontWeight','normal','Color','k')

annotation('textbox', 'Units','centimeters','Position',[x_cord+s_z+0.1, y_cord+0.2, 10, 0.5], 'string', ...
 {'0.05';' dF / F'}, 'EdgeColor','none',...
 'FontSize',12,'FontWeight','normal','Color','k')

saveas(gcf,'Figure1','svg')

end
```

9.5 Two photon imaging analysis script of response to optogenetic stimuli

```
Analysis script imaging dFB glutamate sensor upon optogenetic stimulation
Version 2022-05-25
Peter S. Hasenhuetl and Raffaele Sarnataro

%% First, get recordings to analyse
optogenetics_flies = get_recorded(summary_optoGluSnFR);

%% Then, calls the custom analysis function
optogenetics_summary = get_all(optogenetics_flies);

%% Then, plots the results
close all
get_fig_panel_optogenetics_aligned(optogenetics_summary)

%% Below are the custom functions called above

function optogenetics_flies = get_recorded(summary_optoGluSnFR)
optogenetics_flies = summary_optoGluSnFR;

end

function optogenetics_summary = get_all(optogenetics_flies)

fields_flies = fieldnames(optogenetics_flies);
aligned_signal = [];
aligned_signal.Chrimson_iGluSnFR_500ms = [];
aligned_signal.Chrimson_iGluSnFR_100ms = [];
aligned_signal.Chrimson_iGluSnFR_10ms = [];
aligned_signal.Chrimson_GCaMP_500ms= [];
aligned_signal.opto_GCaMP_500ms= [];

% Loops through individual flies
for fly_number = 1:size(optogenetics_flies,1)
% fly_name = optogenetics_flies.fly_idx{fly_number};
 input_fly = optogenetics_flies.data{fly_number};
 fields_sessions = fieldnames(input_fly.img);

 % Loops through imaging sessions of individual flies
 for session_idx = 1:length(fields_sessions)
 session_name=fields_sessions{session_idx};
 input_img = input_fly.img.(session_name);
 output_img = get_img_measures(input_img);

 % Segment the experiments
 if session_idx == 1
 if optogenetics_flies.experiment{fly_number} == "Chrimson_iGluSnFR"
  aligned_signal.Chrimson_iGluSnFR_500ms = [aligned_signal.Chrimson_iGluSnFR_500ms,mean(output_img.aligned_green(:,:),2)];
 % end
 % if optogenetics_flies.experiment{fly_number} == "Chrimson_GCaMP"
 %  aligned_signal.Chrimson_GCaMP_500ms = [aligned_signal.Chrimson_GCaMP_500ms,mean(output_img.aligned_green(:,:),2)];
 % end
 % if optogenetics_flies.experiment{fly_number} == "opto_GCaMP"
 %  aligned_signal.opto_GCaMP_500ms = [aligned_signal.opto_GCaMP_500ms,mean(output_img.aligned_green(:,:),2)];
  end
 end
 if session_idx == 2
  if optogenetics_flies.experiment{fly_number} == "Chrimson_iGluSnFR"
  aligned_signal.Chrimson_iGluSnFR_100ms = [aligned_signal.Chrimson_iGluSnFR_100ms,mean(output_img.aligned_green(:,:),2)];
  end
 end
 if session_idx == 3
  if optogenetics_flies.experiment{fly_number} == "Chrimson_iGluSnFR"
  aligned_signal.Chrimson_iGluSnFR_10ms = [aligned_signal.Chrimson_iGluSnFR_10ms,mean(output_img.aligned_green(:,:),2)];
```

```
 end
 end
 end
end

optogenetics_summary.aligned_signal = aligned_signal;
optogenetics_summary.t_v_aligned = output_img.t_v_align;
optogenetics_summary.fr=output_img.fr;
optogenetics_summary.pre_window=output_img.pre_window;
optogenetics_summary.post_window=output_img.post_window;

end

function output_img = get_img_measures(input_img)

f_r = 208.56; % frame-rate in Hz

raw_green = input_img.green_signal;
background_green = input_img.green_background;
img_green = raw_green - mean(background_green);

channel3 = input_img.channel3;

t_v = (0:length(raw_green))/f_r; %%Time in seconds

%% Then, computes dF/F

g_signal = img_green;
output_img.raw_green = img_green;
dFg = (g_signal - mean(g_signal))./abs(mean(g_signal));
output_img.dFg = dFg;

ch3 = channel3+10000;
ch3 = (ch3-min(ch3))/max(ch3-min(ch3));
output_img.ch3 = ch3;

%% Aligns the imaging traces to the onset of light stimulation

pre_window = round(0.3*f_r);
post_window = round(1.5*f_r);

output_img.stimulus_idx = find(diff(ch3)>0.5);

 for n_stimulus = 1:(length(output_img.stimulus_idx))

% Computes aligned signal for green channel
aligned_green(:,n_stimulus) = g_signal(output_img.stimulus_idx(n_stimulus,1)-...
 pre_window:output_img.stimulus_idx(n_stimulus,1)+post_window,:);
output_img.aligned_green(:,n_stimulus) = (aligned_green(:,n_stimulus) - ...
 mean(aligned_green(1:pre_window,n_stimulus)))./abs(mean(aligned_green(1:pre_window,n_stimulus)));

 end

% Computes the aligned time
output_img.t_v_align = (1:length(output_img.aligned_green))/f_r;
output_img.t_v_align = (output_img.t_v_align-((pre_window)/f_r));

output_img.fr=f_r;
output_img.pre_window=pre_window;
output_img.post_window=post_window;
end

function get_fig_panel_optogenetics_aligned(optogenetics_summary)

figure('Name','Optogenetics + GluSnFR figure','Color','white',...
 'Units','centimeters','Position',[10 17 18.3 18],'Resize','off')
```

```
% Defining some variables beforehand
f_s = 5; % Font size
x_cord = 2; % x-coordinates of panel in cm
y_cord = 2; % y-coordinates of panel in cm
s_z = 12.5; % x-dimension of panel in cm
h_t = 12.5; % y-dimension of panel in cm
ylm_img = [-0.1, 0.4]; % limits in y-dimension
xlm_img = [-1,2];
bw_hist = 0.0125; % bin-width of histogram
pnl1 = axes('Units','Centimeters','Position',[x_cord, y_cord, s_z, h_t]); %axis
color=get_color;
plotting_colors=[[0 0 0];color.dark_blue;color.grey_blue;color.greenish;color.gray];

 for curr_exp=fieldnames(optogenetics_summary.aligned_signal)
 for numb_curr_exp=[1:length(fieldnames(optogenetics_summary.aligned_signal))]
pt1=movmean(mean(optogenetics_summary.aligned_signal.(curr_exp{numb_curr_exp}),2),20); %moving mean
pt2=movmean(std(optogenetics_summary.aligned_signal.(curr_exp{numb_curr_exp}),0,2),20)...
 ./sqrt(size(optogenetics_summary.aligned_signal.(curr_exp{numb_curr_exp}),2)); %std

hold on

%Plot curves
plot(pnl1,optogenetics_summary.t_v_aligned,pt1+pt2,'Color',plotting_colors(numb_curr_exp,:),'LineWidth',0.25)
plot(pnl1,optogenetics_summary.t_v_aligned,pt1-pt2,'Color',plotting_colors(numb_curr_exp,:),'LineWidth',0.25)
plot(pnl1,optogenetics_summary.t_v_aligned,pt1,'Color',plotting_colors(numb_curr_exp,:),'LineWidth',1)

%Plot lines on top
plot(pnl1,[0, 0.5],[ylm_img(2)-0.04,ylm_img(2)-0.04],'LineWidth',1,'Color',plotting_colors(4,:))
plot(pnl1,[0, 0.5],[ylm_img(2)-0.02,ylm_img(2)-0.02],'LineWidth',1,'Color',plotting_colors(5,:))
hold on
 end
 end

plot(pnl1,[1.5,2],[ylm_img(1),ylm_img(1)],'k','LineWidth',1) %x axis
%plot(pnl1,[xlm_img(2),xlm_img(2)],[ylm_img(1),ylm_img(1)+0.05],'k','LineWidth',1)
xlim(xlm_img)
ylim(ylm_img)
pnl1.Box = 'off';
pnl1.FontSize = f_s;
ylabel('dF/F')
xlabel({'time from onset'; 'of stimulus (s)'})
pnl1.XAxis.Color='none';
pnl1.YAxis.Color='none';
pnl1 = axes('Units','Centimeters','Position',[x_cord+s_z+0.1, y_cord, 0.2, h_t]);
plot(pnl1,[1,1],[ylm_img(1),ylm_img(1)+0.1],'k','Linewidth',1) %y axis
pnl1.Color='none';
pnl1.XAxis.Color='none';
pnl1.YAxis.Color='none';
xlim(xlm_img)
ylim(ylm_img)

annotation('textbox', 'Units','centimeters','Position',[x_cord+s_z-0.5, y_cord-0.5, 10, 0.5], 'string', ...
 '500ms', 'EdgeColor','none',...
 'FontSize',f_s,'FontWeight','normal','Color','k')

annotation('textbox', 'Units','centimeters','Position',[x_cord+s_z+0.25, y_cord, 10, 0.5], 'string', ...
 {'0.1';'dF/F'}, 'EdgeColor','none',...
 'FontSize',f_s,'FontWeight','normal','Color','k')

saveas(gcf,'Figure1','svg')

end
```

9.6 Anterograde trans-synaptic tracing of dFB neurons

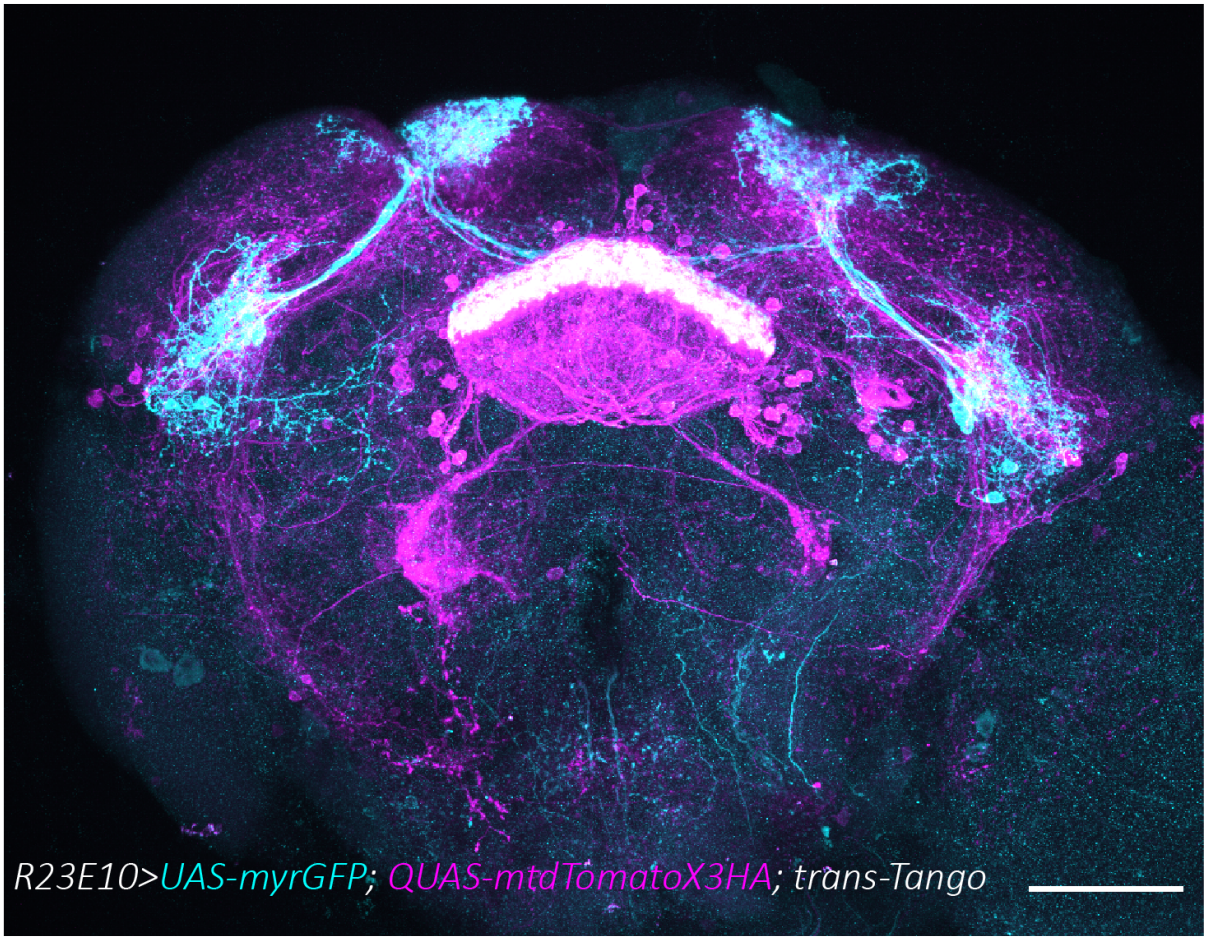

Figure 9.1 | Anterograde trans-synaptic mapping of dFB neurons.
Maximum intensity projection of z-stacks of fly brains where anterograde trans-synaptic tracing of dFB neuron was obtained via trans-Tango technique. Scale bar = 50 µm. dFB neurons are labelled with GFP (cyan), and their post-synaptic mapped partners with mtdTomato (magenta). Genetic crosses and flies used for trans-synaptic tracing were cultured and kept at 18 °C, and flies dissected for imaging were at least 28 days old.

9.7 Genes differentially expressed in dFB neurons, upon sleep deprivation

	p_val	avg_log$_2$FC (SD/rested)	pct.1 (SD)	pct.2 (rested)	p_val_adj
unc-13	8.10E-15	-0.9142607	0.988	0.983	8.20E-11
Appl	2.34E-12	-0.9572576	0.919	0.962	2.36E-08
UQCR-C1	3.08E-11	0.92245601	0.837	0.473	3.11E-07
IA-2	7.99E-11	-1.3433666	1	0.996	8.08E-07
CG42450	8.42E-11	-0.9744782	0.953	0.97	8.52E-07
brp	9.00E-11	-1.1337422	0.953	0.954	9.10E-07
CG41378	2.68E-10	0.79882496	0.488	0.152	2.71E-06
Neb-cGP	3.86E-10	0.96553176	0.779	0.506	3.90E-06
Nrx-1	6.70E-10	-0.8227218	0.849	0.907	6.77E-06
Ank2	8.18E-10	-0.7262325	0.919	0.928	8.27E-06
Dscam4	1.39E-09	-0.9805825	0.849	0.916	1.41E-05
tinc	1.90E-09	-1.4438579	0.349	0.633	1.92E-05
CG3009	1.98E-09	0.90313587	0.686	0.338	2.01E-05
CG42613	2.71E-09	-0.9782798	0.907	0.928	2.74E-05
spen	3.66E-09	-0.5577133	1	0.97	3.70E-05
kis	3.73E-09	-0.9848247	0.698	0.857	3.78E-05
cac	4.06E-09	-0.7290469	0.907	0.937	4.10E-05
CG4467	4.38E-09	-1.1658158	0.872	0.928	4.43E-05
orb	6.66E-09	-1.4591952	0.256	0.612	6.74E-05
CG30116	7.78E-09	-1.7250068	0.558	0.747	7.87E-05
mub	7.94E-09	-0.8422289	0.907	0.941	8.03E-05
CG33199	8.33E-09	1.02986169	0.698	0.435	8.42E-05
ox	1.01E-08	0.84678435	0.721	0.397	0.00010204
CG34384	1.15E-08	-1.2838255	0.349	0.671	0.00011647
miple1	1.44E-08	0.77184773	0.93	0.865	0.00014528
Rab26	1.60E-08	-0.9292164	0.744	0.873	0.00016175
Corin	1.91E-08	-0.8597865	0.744	0.865	0.00019288
CG13404	1.95E-08	0.67393603	0.442	0.156	0.00019718
Mmp2	2.30E-08	-1.4900577	0.674	0.806	0.00023295
bru3	2.73E-08	-0.5893209	0.988	0.987	0.00027617
CG11000	2.83E-08	-1.2108201	0.895	0.907	0.00028634
Fife	3.44E-08	-0.7938049	0.86	0.903	0.00034762
RpS21	5.08E-08	0.67587172	0.849	0.578	0.00051329
ATPsyndelta	6.83E-08	0.81118419	0.674	0.384	0.00069057
RpS29	7.16E-08	0.6683178	0.942	0.806	0.00072386
elav	7.72E-08	-0.7509591	0.953	0.949	0.0007809
Hsp60A	8.02E-08	0.79350997	0.733	0.456	0.00081123
Tomosyn	8.14E-08	-0.8201174	0.872	0.895	0.00082275
ND-B22	1.21E-07	0.70529004	0.744	0.451	0.00121966
Tim10	1.26E-07	0.7520926	0.628	0.367	0.00127775
levy	1.89E-07	0.79891417	0.767	0.557	0.00191364

CG17816	1.92E-07	-0.9120932	0.93	0.92	0.00194541
CG7946	2.56E-07	0.58308993	0.442	0.173	0.00258769
Sap47	2.72E-07	-0.5163225	0.977	1	0.00274894
Argk	2.99E-07	0.68443119	0.919	0.772	0.0030212
mRpL13	3.32E-07	0.58215961	0.384	0.131	0.00335628
Gapdh1	3.35E-07	0.75984828	0.64	0.38	0.00338888
CG42795	3.51E-07	-0.8843137	0.453	0.696	0.0035506
Rpn10	3.51E-07	0.57853322	0.488	0.219	0.00355129
para	3.68E-07	-0.5660539	0.977	0.958	0.00372089
Men-b	3.84E-07	0.63982505	0.709	0.397	0.0038858
kek3	3.91E-07	-1.1157453	0.186	0.498	0.0039536
ND-30	4.25E-07	0.71253745	0.64	0.359	0.00429777
Dg	4.36E-07	-1.0465479	0.5	0.722	0.00440622
Ald	4.56E-07	0.86820955	0.895	0.806	0.00461223
Octbeta1R	4.71E-07	-1.389658	0.628	0.789	0.00476245
Vha13	4.84E-07	0.6021122	0.907	0.789	0.00489407
Ac78C	5.01E-07	-1.3168815	0.209	0.502	0.00506987
Prosbeta3	5.06E-07	0.51875146	0.43	0.165	0.00512121
Eno	5.17E-07	0.76762575	0.802	0.734	0.00522919
cype	5.31E-07	0.8548444	0.802	0.616	0.00536679
Dab	5.51E-07	-0.8507135	0.407	0.671	0.00557485
pan	6.10E-07	-0.5559644	0.93	0.949	0.00616693
sesB	6.95E-07	0.69260548	0.919	0.827	0.00702776
ATPsynE	7.47E-07	0.64074237	0.744	0.46	0.00755123
fax	7.82E-07	-0.6365613	0.849	0.945	0.00791105
CG14232	8.74E-07	0.94865527	0.558	0.312	0.00884174
Bacc	8.77E-07	0.50745069	0.965	0.903	0.00886501
Gug	8.79E-07	-0.6688996	0.744	0.844	0.00888462
Tctp	1.04E-06	0.58585876	0.779	0.544	0.01049576
RpL37a	1.05E-06	0.67234092	0.872	0.726	0.01061721
TM4SF	1.07E-06	0.65264935	0.86	0.679	0.01079164
ytr	1.10E-06	0.6229703	0.616	0.338	0.01108588
sun	1.18E-06	0.68619949	0.709	0.477	0.01198091
nAChRalpha2	1.21E-06	0.41624644	0.43	0.16	0.01224376
CG12025	1.34E-06	0.61045713	0.709	0.43	0.01358408
Eip93F	1.42E-06	-1.2112594	0.802	0.852	0.01438716
CG1578	1.43E-06	-0.9149588	0.698	0.806	0.01444662
ND-SGDH	1.64E-06	0.69459306	0.698	0.447	0.01658289
dpr3	1.77E-06	-1.0289308	0.256	0.527	0.01785514
Pde8	1.79E-06	-1.1234526	0.337	0.578	0.01806495
klg	1.80E-06	0.90646	0.733	0.46	0.01822805
Nep2	1.83E-06	-1.2715801	0.023	0.27	0.01850678
tou	1.83E-06	-0.7347642	0.756	0.89	0.01851662
CG11137	1.85E-06	0.67090065	0.5	0.236	0.01875048
kdn	1.88E-06	0.66426358	0.709	0.477	0.01901253

eIF1A	1.88E-06	0.53150358	0.837	0.624	0.01904022
pum	2.00E-06	-0.6332886	0.988	0.983	0.02019006
RpL34b	2.01E-06	0.62722206	0.779	0.574	0.0203156
CG17734	2.10E-06	0.51244705	0.64	0.367	0.02121431
CG3887	2.16E-06	0.55274402	0.488	0.232	0.02181539
CG30172	2.19E-06	0.64276936	0.814	0.667	0.0221685
Ten-m	2.20E-06	-0.7847923	0.593	0.776	0.02228404
mRpS26	2.21E-06	0.50937177	0.395	0.156	0.02233077
mmd	2.32E-06	-0.5507678	0.953	0.928	0.02345335
COX8	2.38E-06	0.90938516	0.698	0.502	0.02405425
Adk1	2.46E-06	0.7069874	0.5	0.245	0.02491687
COX5A	2.50E-06	0.68375701	0.756	0.553	0.02525294
Frq2	2.50E-06	-0.7835618	0.709	0.857	0.02527946
UQCR-14	2.58E-06	0.67942251	0.698	0.451	0.02609863
Gbeta5	2.58E-06	0.71719251	0.698	0.477	0.02611146
noe	2.69E-06	0.66315259	1	1	0.02721173
hec	2.72E-06	-0.8663532	0.116	0.409	0.02749182
Fer2LCH	2.87E-06	0.65695412	0.895	0.827	0.02907447
Jafrac1	3.16E-06	0.64258414	0.605	0.35	0.0319609
CG11306	3.23E-06	0.67142388	0.395	0.169	0.03261453
Gapdh2	3.24E-06	0.79238257	0.756	0.578	0.03281601
SdhB	3.56E-06	0.6203194	0.663	0.397	0.03601517
EMRE	3.56E-06	0.55466733	0.616	0.376	0.03603248
ND-MWFE	3.92E-06	0.68723276	0.663	0.405	0.0396605
ND-20	4.14E-06	0.65666254	0.628	0.38	0.04182676
CR45312	4.25E-06	0.73459752	0.628	0.329	0.04295254
CG2852	4.36E-06	0.67814038	0.733	0.523	0.04406785
eIF3h	4.45E-06	0.50523134	0.581	0.325	0.04501931
RpS27	4.54E-06	0.52849269	0.895	0.793	0.04589336
COX7C	4.57E-06	0.70135815	0.698	0.464	0.04621853
NetB	4.58E-06	-1.1799052	0.267	0.519	0.04636198
DnaJ-H	4.58E-06	0.59618962	0.628	0.359	0.04636309
Nmdar2	4.69E-06	-0.6475392	0.279	0.561	0.04737947
CG6044	4.69E-06	1.01606773	0.605	0.384	0.04740314
Calx	4.76E-06	-0.7943045	0.686	0.823	0.04809744
wls	4.76E-06	0.37159281	0.291	0.089	0.0481256

Table 9.2 | Genes differentially expressed in dFB neurons upon sleep deprivation.
Significantly DEGs in dFB neurons between sleep deprived and rested control conditions, ordered by adjusted P-value, scored by Wilcoxon Rank Sum test, with P-value adjusted using Bonferroni correction based on the total number of variable genes within dFB neurons. The table also shows the Log_2 of the fold change between sleep deprived and rested flies (positive values indicate enrichment in sleep deprived flies) and the percentage of cells in each group in which the gene is detected.

9.8 Heatmaps of Gene Ontology for differentially expressed genes in dFB neurons

In addition to PANTHER, I used a combination of ViSEAGO and topGO to analyse the gene ontology of the differentially expressed genes, and produced the following heatmaps, where genes upregulated or downregulated upon sleep deprivation were used as inputs.



Figure 9.2 | Gene ontology of differentially expressed genes upon sleep deprivation in dFB neurons.
Gene ontology terms significantly enriched in dFB neurons for the genes upregulated and downregulated upon sleep deprivation: the annotation datasets refer to biological processes (right, Oxford blue), and cellular component (left, green). Colours' intensities indicate the statistical significance of the terms.

9.9 Gene ontology on DEGs in dFB neurons (PANTHER full tables)

9.9.1 Genes upregulated upon sleep deprivation, "biological process"

This and the following tables in chapter 9.9 are the full gene ontology enrichment tables generated in PANTHER with the upregulated and downregulated genes, according to the GO terms "biological process", "cellular component" and "reactome".

Analysis Type:	**PANTHER Overrepresentation Test (Released 20220712)**						
Annotation Version and Release Date:	GO Ontology database DOI: 10.5281/zenodo.6799722 Released 2022-07-01						
Analyzed List:	upload_1 (Drosophila melanogaster)						
Reference List:	Drosophila melanogaster (all genes in database)						
Test Type:	FISHER						
Correction:	FDR						
GO biological process complete	Drosophila melanogaster - REFLIST (13821)	upload_1 (55)	upload_1 (expected)	upload_1 (over/ under)	upload_1 (fold Enrichment)	upload_1 (raw P-value)	upload_1 (FDR)
mitochondrial electron transport, cytochrome c to oxygen (GO:0006123)	21	5	0.08	+	59.83	5.01E-08	2.60E-05
aerobic electron transport chain (GO:0019646)	62	9	0.25	+	36.48	7.50E-12	9.74E-09
proton motive force-driven ATP synthesis (GO:0015986)	21	3	0.08	+	35.9	1.12E-04	1.86E-02
mitochondrial ATP synthesis coupled electron transport (GO:0042775)	67	9	0.27	+	33.76	1.41E-11	1.57E-08
ATP biosynthetic process (GO:0006754)	23	3	0.09	+	32.78	1.44E-04	2.28E-02
oxidative phosphorylation (GO:0006119)	78	10	0.31	+	32.22	1.44E-12	2.25E-09
ATP synthesis coupled electron transport (GO:0042773)	71	9	0.28	+	31.85	2.27E-11	2.21E-08
ATP generation from ADP (GO:0006757)	25	3	0.1	+	30.15	1.80E-04	2.80E-02
glycolytic process (GO:0006096)	25	3	0.1	+	30.15	1.80E-04	2.75E-02
respiratory electron transport chain (GO:0022904)	78	9	0.31	+	29	4.93E-11	4.26E-08
ADP metabolic process (GO:0046031)	27	3	0.11	+	27.92	2.22E-04	3.26E-02
purine ribonucleoside triphosphate biosynthetic process (GO:0009206)	27	3	0.11	+	27.92	2.22E-04	3.20E-02
purine ribonucleoside diphosphate metabolic process (GO:0009179)	27	3	0.11	+	27.92	2.22E-04	3.14E-02
purine nucleoside triphosphate biosynthetic process (GO:0009145)	27	3	0.11	+	27.92	2.22E-04	3.09E-02
purine nucleoside diphosphate metabolic process (GO:0009135)	27	3	0.11	+	27.92	2.22E-04	3.03E-02
ATP metabolic process (GO:0046034)	55	6	0.22	+	27.41	1.38E-07	5.36E-05
aerobic respiration (GO:0009060)	110	12	0.44	+	27.41	3.92E-14	1.53E-10
electron transport chain (GO:0022900)	85	9	0.34	+	26.61	1.00E-10	7.79E-08
ribonucleoside diphosphate metabolic process (GO:0009185)	29	3	0.12	+	26	2.69E-04	3.56E-02
pyruvate metabolic process (GO:0006090)	39	4	0.16	+	25.77	2.43E-05	4.98E-03
purine ribonucleoside triphosphate metabolic process (GO:0009205)	59	6	0.23	+	25.56	2.02E-07	7.50E-05
ribonucleoside triphosphate biosynthetic process (GO:0009201)	30	3	0.12	+	25.13	2.96E-04	3.71E-02
purine nucleoside triphosphate metabolic process (GO:0009144)	60	6	0.24	+	25.13	2.22E-07	7.85E-05
nucleoside diphosphate phosphorylation (GO:0006165)	30	3	0.12	+	25.13	2.96E-04	3.65E-02
glucose metabolic process (GO:0006006)	30	3	0.12	+	25.13	2.96E-04	3.60E-02
cellular respiration (GO:0045333)	121	12	0.48	+	24.92	1.12E-13	2.92E-10
ribonucleoside triphosphate metabolic process (GO:0009199)	62	6	0.25	+	24.32	2.65E-07	8.99E-05
nucleotide phosphorylation (GO:0046939)	31	3	0.12	+	24.32	3.23E-04	3.87E-02
nucleoside triphosphate biosynthetic process (GO:0009142)	33	3	0.13	+	22.84	3.84E-04	4.46E-02
nucleoside triphosphate metabolic process (GO:0009141)	67	6	0.27	+	22.5	4.07E-07	1.32E-04
energy derivation by oxidation of organic compounds (GO:0015980)	145	12	0.58	+	20.8	8.31E-13	1.62E-09
generation of precursor metabolites and energy (GO:0006091)	193	15	0.77	+	19.53	1.83E-15	1.43E-11
proton transmembrane transport (GO:1902600)	57	4	0.23	+	17.63	9.75E-05	1.69E-02
mitochondrial transport (GO:0006839)	77	4	0.31	+	13.05	2.93E-04	3.74E-02
cytoplasmic translation (GO:0002181)	118	6	0.47	+	12.78	9.14E-06	2.23E-03
purine ribonucleotide metabolic process (GO:0009150)	172	7	0.68	+	10.23	6.36E-06	1.77E-03
determination of adult lifespan (GO:0008340)	172	7	0.68	+	10.23	6.36E-06	1.71E-03
purine nucleotide metabolic process (GO:0006163)	178	7	0.71	+	9.88	7.90E-06	2.05E-03

ribonucleotide metabolic process (GO:0009259)	181	7	0.72	+	9.72	8.78E-06	2.21E-03
response to oxidative stress (GO:0006979)	132	5	0.53	+	9.52	2.04E-04	3.06E-02
ribose phosphate metabolic process (GO:0019693)	185	7	0.74	+	9.51	1.01E-05	2.38E-03
translation (GO:0006412)	304	11	1.21	+	9.09	3.41E-08	2.04E-05
peptide biosynthetic process (GO:0043043)	310	11	1.23	+	8.92	4.13E-08	2.30E-05
purine-containing compound metabolic process (GO:0072521)	203	7	0.81	+	8.67	1.80E-05	3.90E-03
nucleotide metabolic process (GO:0009117)	221	7	0.88	+	7.96	3.06E-05	6.11E-03
amide biosynthetic process (GO:0043604)	350	11	1.39	+	7.9	1.36E-07	5.58E-05
nucleoside phosphate metabolic process (GO:0006753)	226	7	0.9	+	7.78	3.52E-05	6.85E-03
mitochondrion organization (GO:0007005)	239	7	0.95	+	7.36	4.97E-05	9.00E-03
cation transmembrane transport (GO:0098655)	245	7	0.97	+	7.18	5.78E-05	1.02E-02
inorganic cation transmembrane transport (GO:0098662)	223	6	0.89	+	6.76	2.79E-04	3.63E-02
peptide metabolic process (GO:0006518)	410	11	1.63	+	6.74	6.33E-07	1.97E-04
nucleobase-containing small molecule metabolic process (GO:0055086)	278	7	1.11	+	6.33	1.25E-04	2.03E-02
ion transmembrane transport (GO:0034220)	322	8	1.28	+	6.24	4.32E-05	8.21E-03
cellular amide metabolic process (GO:0043603)	494	11	1.97	+	5.6	3.73E-06	1.12E-03
cellular macromolecule biosynthetic process (GO:0034645)	505	11	2.01	+	5.47	4.58E-06	1.32E-03
cation transport (GO:0006812)	328	7	1.31	+	5.36	3.37E-04	3.97E-02
cellular nitrogen compound biosynthetic process (GO:0044271)	714	15	2.84	+	5.28	9.24E-08	4.00E-05
organonitrogen compound biosynthetic process (GO:1901566)	811	16	3.23	+	4.96	7.26E-08	3.33E-05
organophosphate metabolic process (GO:0019637)	411	8	1.64	+	4.89	2.27E-04	3.05E-02
macromolecule biosynthetic process (GO:0009059)	707	11	2.81	+	3.91	9.78E-05	1.66E-02
organic substance biosynthetic process (GO:1901576)	1218	16	4.85	+	3.3	1.46E-05	3.26E-03
biosynthetic process (GO:0009058)	1244	16	4.95	+	3.23	1.90E-05	4.01E-03
cellular biosynthetic process (GO:0044249)	1194	15	4.75	+	3.16	4.90E-05	9.09E-03
gene expression (GO:0010467)	1129	13	4.49	+	2.89	4.10E-04	4.70E-02
cellular nitrogen compound metabolic process (GO:0034641)	1835	20	7.3	+	2.74	1.41E-05	3.23E-03
cellular metabolic process (GO:0044237)	3578	37	14.24	+	2.6	1.67E-10	1.18E-07
metabolic process (GO:0008152)	4578	38	18.22	+	2.09	6.36E-08	3.10E-05
cellular process (GO:0009987)	7238	50	28.8	+	1.74	1.62E-09	1.05E-06

9.9.2 Genes upregulated upon sleep deprivation, "cellular component"

Analysis Type:	PANTHER Overrepresentation Test (Released 20220712)						
Annotation Version and Release Date:	GO Ontology database DOI: 10.5281/zenodo.6799722 Released 2022-07-01						
Analyzed List:	upload_1 (Drosophila melanogaster)						
Reference List:	Drosophila melanogaster (all genes in database)						
Test Type:	FISHER						
Correction:	FDR						
GO cellular component complete	Drosophila melanogaster - REFLIST (13821)	upload_1 (55)	upload_1 (expected)	upload_1 (over/under)	upload_1 (fold Enrichment)	upload_1 (raw P-value)	upload_1 (FDR)
proton-transporting ATP synthase, central stalk (GO:0045269)	4	2	0.02	+	> 100	2.29E-04	6.92E-03
mitochondrial proton-transporting ATP synthase, central stalk (GO:0005756)	4	2	0.02	+	> 100	2.29E-04	6.77E-03
eukaryotic 43S preinitiation complex (GO:0016282)	5	2	0.02	+	> 100	3.20E-04	9.05E-03
translation preinitiation complex (GO:0070993)	6	2	0.02	+	83.76	4.25E-04	1.18E-02
mitochondrial proton-transporting ATP synthase complex, catalytic sector F(1) (GO:0000275)	7	2	0.03	+	71.8	5.46E-04	1.48E-02
proton-transporting ATP synthase complex, catalytic core F(1) (GO:0045261)	8	2	0.03	+	62.82	6.80E-04	1.81E-02
mitochondrial respiratory chain complex IV (GO:0005751)	20	5	0.08	+	62.82	4.06E-08	2.16E-06
respiratory chain complex IV (GO:0045277)	21	5	0.08	+	59.83	5.01E-08	2.57E-06
cytochrome complex (GO:0070069)	34	7	0.14	+	51.74	2.10E-10	1.55E-08
polysomal ribosome (GO:0042788)	11	2	0.04	+	45.69	1.17E-03	2.94E-02
proton-transporting ATP synthase complex (GO:0045259)	24	4	0.1	+	41.88	4.21E-06	1.51E-04
mitochondrial proton-transporting ATP synthase complex (GO:0005753)	24	4	0.1	+	41.88	4.21E-06	1.47E-04
respiratory chain complex III (GO:0045275)	13	2	0.05	+	38.66	1.57E-03	3.86E-02
mitochondrial respiratory chain complex III (GO:0005750)	13	2	0.05	+	38.66	1.57E-03	3.79E-02
mitochondrial respirasome (GO:0005746)	88	13	0.35	+	37.12	8.18E-17	1.21E-14
respiratory chain complex (GO:0098803)	89	13	0.35	+	36.71	9.35E-17	1.13E-14
respirasome (GO:0070469)	89	13	0.35	+	36.71	9.35E-17	1.04E-14
inner mitochondrial membrane protein complex (GO:0098800)	155	18	0.62	+	29.18	2.08E-21	6.92E-19
respiratory chain complex I (GO:0045271)	49	5	0.19	+	25.64	2.22E-06	9.21E-05
NADH dehydrogenase complex (GO:0030964)	49	5	0.19	+	25.64	2.22E-06	8.93E-05
mitochondrial respiratory chain complex I (GO:0005747)	49	5	0.19	+	25.64	2.22E-06	8.67E-05
oxidoreductase complex (GO:1990204)	91	8	0.36	+	22.09	4.65E-09	2.69E-07
mitochondrial inner membrane (GO:0005743)	245	21	0.97	+	21.54	1.83E-22	2.44E-19
proton-transporting two-sector ATPase complex (GO:0016469)	59	5	0.23	+	21.3	5.19E-06	1.77E-04
organelle inner membrane (GO:0019866)	258	21	1.03	+	20.45	5.03E-22	3.35E-19
mitochondrial protein-containing complex (GO:0098798)	269	21	1.07	+	19.62	1.14E-21	5.04E-19
cytosolic small ribosomal subunit (GO:0022627)	43	3	0.17	+	17.53	7.93E-04	2.07E-02
mitochondrial membrane (GO:0031966)	313	21	1.25	+	16.86	2.20E-20	5.85E-18
transporter complex (GO:1990351)	163	10	0.65	+	15.42	1.26E-09	7.62E-08
cytosolic ribosome (GO:0022626)	98	6	0.39	+	15.39	3.30E-06	1.22E-04
mitochondrial envelope (GO:0005740)	343	21	1.36	+	15.39	1.31E-19	2.91E-17
transmembrane transporter complex (GO:1902495)	152	9	0.6	+	14.88	1.23E-08	6.80E-07
small ribosomal subunit (GO:0015935)	73	4	0.29	+	13.77	2.41E-04	6.97E-03
cytosolic large ribosomal subunit (GO:0022625)	56	3	0.22	+	13.46	1.64E-03	3.89E-02
ribosome (GO:0005840)	186	9	0.74	+	12.16	6.47E-08	3.19E-06
ribosomal subunit (GO:0044391)	175	8	0.7	+	11.49	5.63E-07	2.50E-05
envelope (GO:0031975)	474	21	1.89	+	11.13	7.14E-17	1.36E-14
organelle envelope (GO:0031967)	474	21	1.89	+	11.13	7.14E-17	1.19E-14
membrane protein complex (GO:0098796)	542	21	2.16	+	9.74	9.53E-16	9.05E-14

large ribosomal subunit (GO:0015934)	105	4	0.42	+	9.57	9.03E-04	2.31E-02
mitochondrion (GO:0005739)	894	26	3.56	+	7.31	9.09E-17	1.21E-14
organelle membrane (GO:0031090)	889	23	3.54	+	6.5	1.21E-13	1.01E-11
ribonucleoprotein complex (GO:1990904)	567	11	2.26	+	4.88	1.34E-05	4.15E-04
cytosol (GO:0005829)	972	17	3.87	+	4.4	1.42E-07	6.49E-06
catalytic complex (GO:1902494)	1119	17	4.45	+	3.82	1.01E-06	4.34E-05
protein-containing complex (GO:0032991)	2772	37	11.03	+	3.35	5.18E-14	4.59E-12
cytoplasm (GO:0005737)	4552	48	18.11	+	2.65	1.09E-16	1.11E-14
membrane (GO:0016020)	2997	30	11.93	+	2.52	1.15E-07	5.44E-06
intracellular organelle (GO:0043229)	5583	45	22.22	+	2.03	6.62E-10	4.40E-08
organelle (GO:0043226)	5687	45	22.63	+	1.99	9.54E-10	6.04E-08
intracellular anatomical structure (GO:0005622)	6639	51	26.42	+	1.93	1.92E-12	1.50E-10
intracellular membrane-bounded organelle (GO:0043231)	4949	37	19.69	+	1.88	3.06E-06	1.16E-04
membrane-bounded organelle (GO:0043227)	5152	37	20.5	+	1.8	8.48E-06	2.82E-04
cellular anatomical entity (GO:0110165)	9284	55	36.95	+	1.49	5.62E-10	3.93E-08
cellular_component (GO:0005575)	11115	55	44.23	+	1.24	9.34E-06	2.96E-04
Unclassified (UNCLASSIFIED)	2706	0	10.77	-	< 0.01	9.34E-06	3.03E-04

9.9.3 Genes upregulated upon sleep deprivation, "reactome"

Analysis Type:	PANTHER Overrepresentation Test (Released 20220712)						
Annotation Version and Release Date:	Reactome version 65 Released 2021-10-01						
Analyzed List:	upload_1 (Drosophila melanogaster)						
Reference List:	Drosophila melanogaster (all genes in database)						
Test Type:	FISHER						
Correction:	FDR						
Reactome pathways	Drosophila melanogaster - REFLIST (13821)	upload_1 (55)	upload_1 (expected)	upload_1 (over/under)	upload_1 (fold Enrichment)	upload_1 (raw P-value)	upload_1 (FDR)
Processing of SMDT1 (R-DME-8949664)	9	2	0.04	+	55.84	8.29E-04	3.96E-02
Cristae formation (R-DME-8949613)	15	3	0.06	+	50.26	4.61E-05	3.15E-03
Formation of ATP by chemiosmotic coupling (R-DME-163210)	15	3	0.06	+	50.26	4.61E-05	3.00E-03
Mitochondrial biogenesis (R-DME-1592230)	20	3	0.08	+	37.69	9.87E-05	6.15E-03
Respiratory electron transport, ATP synthesis by chemiosmotic coupling, and heat production by uncoupling proteins. (R-DME-163200)	108	15	0.43	+	34.9	6.02E-19	4.31E-16
Respiratory electron transport (R-DME-611105)	91	12	0.36	+	33.14	4.88E-15	2.33E-12
Citric acid cycle (TCA cycle) (R-DME-71403)	24	3	0.1	+	31.41	1.61E-04	9.62E-03
The citric acid (TCA) cycle and respiratory electron transport (R-DME-1428517)	164	18	0.65	+	27.58	5.31E-21	7.61E-18
Formation of the ternary complex, and subsequently, the 43S complex (R-DME-72695)	49	5	0.19	+	25.64	2.22E-06	3.53E-04
Complex I biogenesis (R-DME-6799198)	51	5	0.2	+	24.64	2.66E-06	3.81E-04
Ribosomal scanning and start codon recognition (R-DME-72702)	55	5	0.22	+	22.84	3.76E-06	4.49E-04
Translation initiation complex formation (R-DME-72649)	56	5	0.22	+	22.44	4.08E-06	4.18E-04
TP53 Regulates Metabolic Genes (R-DME-5628897)	56	5	0.22	+	22.44	4.08E-06	3.90E-04
Activation of the mRNA upon binding of the cap-binding complex and eIFs, and subsequent binding to 43S (R-DME-72662)	57	5	0.23	+	22.04	4.43E-06	3.97E-04
Formation of a pool of free 40S subunits (R-DME-72689)	91	6	0.36	+	16.57	2.20E-06	3.93E-04
Cellular response to chemical stress (R-DME-9711123)	114	7	0.45	+	15.43	4.62E-07	1.10E-04
Cytoprotection by HMOX1 (R-DME-9707564)	100	6	0.4	+	15.08	3.69E-06	4.80E-04
L13a-mediated translational silencing of Ceruloplasmin expression (R-DME-156827)	101	6	0.4	+	14.93	3.89E-06	4.29E-04
Cap-dependent Translation Initiation (R-DME-72737)	109	6	0.43	+	13.83	5.92E-06	4.99E-04
Eukaryotic Translation Initiation (R-DME-72613)	109	6	0.43	+	13.83	5.92E-06	4.71E-04
GTP hydrolysis and joining of the 60S ribosomal subunit (R-DME-72706)	78	4	0.31	+	12.89	3.07E-04	1.76E-02
SRP-dependent cotranslational protein targeting to membrane (R-DME-1799339)	83	4	0.33	+	12.11	3.85E-04	2.12E-02
Nonsense Mediated Decay (NMD) independent of the Exon Junction Complex (EJC) (R-DME-975956)	86	4	0.34	+	11.69	4.38E-04	2.33E-02
Nonsense-Mediated Decay (NMD) (R-DME-927802)	99	4	0.39	+	10.15	7.30E-04	3.74E-02
Nonsense Mediated Decay (NMD) enhanced by the Exon Junction Complex (EJC) (R-DME-975957)	99	4	0.39	+	10.15	7.30E-04	3.61E-02
Translation (R-DME-72766)	211	8	0.84	+	9.53	2.18E-06	4.46E-04
Cellular responses to stimuli (R-DME-8953897)	349	9	1.39	+	6.48	1.02E-05	7.70E-04
Cellular responses to stress (R-DME-2262752)	349	9	1.39	+	6.48	1.02E-05	7.32E-04
Metabolism (R-DME-1430728)	1173	22	4.67	+	4.71	2.52E-10	9.02E-08
Unclassified (UNCLASSIFIED)	9472	16	37.69	-	0.42	3.22E-09	9.24E-07

9.9.4 Genes downregulated upon sleep deprivation, "biological process"

Analysis Type:	PANTHER Overrepresentation Test (Released 20220712)						
Annotation Version and Release Date:	GO Ontology database DOI: 10.5281/zenodo.6799722 Released 2022-07-01						
Analyzed List:	upload_1 (Drosophila melanogaster)						
Reference List:	Drosophila melanogaster (all genes in database)						
Test Type:	FISHER						
Correction:	FDR						
GO biological process complete	Drosophila melanogaster - REFLIST (13821)	upload_1 (44)	upload_1 (expected)	upload_1 (over/under)	upload_1 (fold Enrichment)	upload_1 (raw P-value)	upload_1 (FDR)
calcium ion-regulated exocytosis of neurotransmitter (GO:0048791)	4	2	0.01	+	> 100	1.46E-04	1.23E-02
synaptic target attraction (GO:0016200)	5	2	0.02	+	> 100	2.05E-04	1.61E-02
positive chemotaxis (GO:0050918)	7	2	0.02	+	89.75	3.49E-04	2.45E-02
calcium ion import across plasma membrane (GO:0098703)	7	2	0.02	+	89.75	3.49E-04	2.43E-02
calcium ion transmembrane import into cytosol (GO:0097553)	9	2	0.03	+	69.8	5.32E-04	3.45E-02
presynapse assembly (GO:0099054)	9	2	0.03	+	69.8	5.32E-04	3.42E-02
presynaptic membrane organization (GO:0097090)	10	2	0.03	+	62.82	6.37E-04	3.97E-02
maintenance of presynaptic active zone structure (GO:0048790)	11	2	0.04	+	57.11	7.51E-04	4.61E-02
presynaptic active zone organization (GO:1990709)	17	3	0.05	+	55.43	3.27E-05	3.31E-03
short-term memory (GO:0007614)	28	4	0.09	+	44.87	2.97E-06	4.29E-04
regulation of neurotransmitter secretion (GO:0046928)	28	3	0.09	+	33.66	1.26E-04	1.10E-02
regulation of neurotransmitter transport (GO:0051588)	28	3	0.09	+	33.66	1.26E-04	1.09E-02
regulation of neuromuscular synaptic transmission (GO:1900073)	30	3	0.1	+	31.41	1.52E-04	1.25E-02
segment specification (GO:0007379)	35	3	0.11	+	26.92	2.33E-04	1.81E-02
regulation of synaptic plasticity (GO:0048167)	37	3	0.12	+	25.47	2.71E-04	2.05E-02
modulation of chemical synaptic transmission (GO:0050804)	145	10	0.46	+	21.66	4.08E-11	5.29E-08
regulation of trans-synaptic signaling (GO:0099177)	145	10	0.46	+	21.66	4.08E-11	4.54E-08
neurotransmitter secretion (GO:0007269)	77	5	0.25	+	20.4	5.80E-06	8.06E-04
signal release from synapse (GO:0099643)	77	5	0.25	+	20.4	5.80E-06	7.92E-04
neuromuscular junction development (GO:0007528)	85	5	0.27	+	18.48	9.16E-06	1.17E-03
memory (GO:0007613)	120	7	0.38	+	18.32	1.32E-07	2.72E-05
signal release (GO:0023061)	87	5	0.28	+	18.05	1.02E-05	1.26E-03
regulation of secretion (GO:0051046)	106	6	0.34	+	17.78	1.33E-06	2.12E-04
learning or memory (GO:0007611)	161	9	0.51	+	17.56	2.48E-09	1.38E-06
cognition (GO:0050890)	162	9	0.52	+	17.45	2.62E-09	1.36E-06
long-term memory (GO:0007616)	74	4	0.24	+	16.98	1.06E-04	9.72E-03
motor neuron axon guidance (GO:0008045)	75	4	0.24	+	16.75	1.11E-04	1.01E-02
negative regulation of translation (GO:0017148)	77	4	0.25	+	16.32	1.23E-04	1.09E-02
negative regulation of cellular macromolecule biosynthetic process (GO:2000113)	79	4	0.25	+	15.9	1.35E-04	1.14E-02
regulation of secretion by cell (GO:1903530)	101	5	0.32	+	15.55	2.04E-05	2.30E-03
synapse organization (GO:0050808)	182	9	0.58	+	15.53	6.92E-09	2.07E-06
neurotransmitter transport (GO:0006836)	106	5	0.34	+	14.82	2.54E-05	2.75E-03
negative regulation of cellular amide metabolic process (GO:0034249)	86	4	0.27	+	14.61	1.85E-04	1.48E-02
regulation of neurotransmitter levels (GO:0001505)	108	5	0.34	+	14.54	2.77E-05	2.92E-03
regulation of synaptic assembly at neuromuscular junction (GO:0008582)	113	5	0.36	+	13.9	3.42E-05	3.41E-03

regulation of synapse organization (GO:0050807)	160	7	0.51	+	13.74	8.54E-07	1.48E-04
exocytosis (GO:0006887)	92	4	0.29	+	13.66	2.37E-04	1.83E-02
chemical synaptic transmission (GO:0007268)	213	9	0.68	+	13.27	2.56E-08	6.66E-06
anterograde trans-synaptic signaling (GO:0098916)	213	9	0.68	+	13.27	2.56E-08	6.44E-06
trans-synaptic signaling (GO:0099537)	214	9	0.68	+	13.21	2.67E-08	6.49E-06
regulation of neuromuscular junction development (GO:1904396)	119	5	0.38	+	13.2	4.33E-05	4.27E-03
regulation of synapse structure or activity (GO:0050803)	191	8	0.61	+	13.16	1.78E-07	3.56E-05
regulation of synapse assembly (GO:0051963)	120	5	0.38	+	13.09	4.50E-05	4.39E-03
synaptic vesicle cycle (GO:0099504)	97	4	0.31	+	12.95	2.88E-04	2.12E-02
vesicle-mediated transport in synapse (GO:0099003)	97	4	0.31	+	12.95	2.88E-04	2.10E-02
synaptic signaling (GO:0099536)	223	9	0.71	+	12.68	3.75E-08	8.86E-06
regulation of cell junction assembly (GO:1901888)	125	5	0.4	+	12.56	5.43E-05	5.16E-03
cell junction organization (GO:0034330)	250	10	0.8	+	12.56	6.41E-09	2.00E-06
cell-cell signaling (GO:0007267)	296	11	0.94	+	11.67	2.10E-09	1.36E-06
axonogenesis (GO:0007409)	300	11	0.96	+	11.52	2.40E-09	1.44E-06
secretion by cell (GO:0032940)	169	6	0.54	+	11.15	1.76E-05	2.02E-03
axon development (GO:0061564)	311	11	0.99	+	11.11	3.46E-09	1.35E-06
neuron recognition (GO:0008038)	115	4	0.37	+	10.93	5.37E-04	3.43E-02
export from cell (GO:0140352)	178	6	0.57	+	10.59	2.34E-05	2.56E-03
cell recognition (GO:0008037)	119	4	0.38	+	10.56	6.09E-04	3.82E-02
secretion (GO:0046903)	181	6	0.58	+	10.41	2.56E-05	2.73E-03
regulation of locomotion (GO:0040012)	124	4	0.39	+	10.13	7.07E-04	4.37E-02
axon guidance (GO:0007411)	250	8	0.8	+	10.05	1.28E-06	2.08E-04
neuron projection guidance (GO:0097485)	258	8	0.82	+	9.74	1.61E-06	2.51E-04
cell morphogenesis involved in neuron differentiation (GO:0048667)	392	12	1.25	+	9.62	2.89E-09	1.41E-06
segmentation (GO:0035282)	230	7	0.73	+	9.56	8.72E-06	1.15E-03
neuron projection morphogenesis (GO:0048812)	395	12	1.26	+	9.54	3.14E-09	1.44E-06
cell projection morphogenesis (GO:0048858)	397	12	1.26	+	9.49	3.32E-09	1.44E-06
plasma membrane bounded cell projection morphogenesis (GO:0120039)	397	12	1.26	+	9.49	3.32E-09	1.36E-06
chemotaxis (GO:0006935)	268	8	0.85	+	9.38	2.12E-06	3.12E-04
cell part morphogenesis (GO:0032990)	405	12	1.29	+	9.31	4.13E-09	1.40E-06
embryonic pattern specification (GO:0009880)	204	6	0.65	+	9.24	4.91E-05	4.72E-03
neuron projection development (GO:0031175)	421	12	1.34	+	8.95	6.30E-09	2.05E-06
growth (GO:0040007)	179	5	0.57	+	8.77	2.78E-04	2.08E-02
developmental growth (GO:0048589)	179	5	0.57	+	8.77	2.78E-04	2.06E-02
cell morphogenesis involved in differentiation (GO:0000904)	435	12	1.38	+	8.67	9.00E-09	2.50E-06
behavior (GO:0007610)	526	14	1.67	+	8.36	6.12E-10	5.30E-07
developmental maturation (GO:0021700)	189	5	0.6	+	8.31	3.55E-04	2.45E-02
blastoderm segmentation (GO:0007350)	189	5	0.6	+	8.31	3.55E-04	2.43E-02
cell morphogenesis (GO:0000902)	501	13	1.59	+	8.15	3.89E-09	1.38E-06
locomotion (GO:0040011)	364	9	1.16	+	7.77	2.07E-06	3.10E-04
nervous system process (GO:0050877)	568	14	1.81	+	7.74	1.62E-09	1.15E-06
taxis (GO:0042330)	328	8	1.04	+	7.66	9.06E-06	1.18E-03
neuron development (GO:0048666)	560	13	1.78	+	7.29	1.43E-08	3.84E-06
cellular component morphogenesis (GO:0032989)	530	12	1.69	+	7.11	7.58E-08	1.74E-05
system process (GO:0003008)	640	14	2.04	+	6.87	7.25E-09	2.09E-06
regulation of transport (GO:0051049)	323	7	1.03	+	6.81	7.29E-05	6.85E-03

regulation of cellular component biogenesis (GO:0044087)	298	6	0.95	+	6.32	3.70E-04	2.51E-02
plasma membrane bounded cell projection organization (GO:0120036)	635	12	2.02	+	5.94	5.14E-07	9.30E-05
cell projection organization (GO:0030030)	647	12	2.06	+	5.83	6.25E-07	1.11E-04
neuron differentiation (GO:0030182)	702	13	2.23	+	5.82	1.92E-07	3.75E-05
signaling (GO:0023052)	1198	22	3.81	+	5.77	1.59E-12	1.24E-08
regulation of localization (GO:0032879)	443	8	1.41	+	5.67	7.45E-05	6.91E-03
negative regulation of macromolecule biosynthetic process (GO:0010558)	395	7	1.26	+	5.57	2.48E-04	1.89E-02
embryo development (GO:0009790)	510	9	1.62	+	5.54	2.96E-05	3.03E-03
cell communication (GO:0007154)	1268	22	4.04	+	5.45	4.87E-12	9.49E-09
nervous system development (GO:0007399)	982	17	3.13	+	5.44	3.55E-09	1.32E-06
generation of neurons (GO:0048699)	755	13	2.4	+	5.41	4.38E-07	8.32E-05
negative regulation of cellular biosynthetic process (GO:0031327)	411	7	1.31	+	5.35	3.14E-04	2.25E-02
regionalization (GO:0003002)	475	8	1.51	+	5.29	1.20E-04	1.08E-02
negative regulation of biosynthetic process (GO:0009890)	416	7	1.32	+	5.29	3.38E-04	2.39E-02
vesicle-mediated transport (GO:0016192)	493	8	1.57	+	5.1	1.55E-04	1.25E-02
neurogenesis (GO:0022008)	807	13	2.57	+	5.06	9.22E-07	1.56E-04
regulation of cell communication (GO:0010646)	940	15	2.99	+	5.01	1.16E-07	2.50E-05
regulation of signaling (GO:0023051)	940	15	2.99	+	5.01	1.16E-07	2.43E-05
pattern specification process (GO:0007389)	512	8	1.63	+	4.91	2.00E-04	1.59E-02
system development (GO:0048731)	1339	20	4.26	+	4.69	1.03E-09	8.00E-07
morphogenesis of an epithelium (GO:0002009)	578	8	1.84	+	4.35	4.47E-04	2.95E-02
tissue morphogenesis (GO:0048729)	596	8	1.9	+	4.22	5.47E-04	3.46E-02
signal transduction (GO:0007165)	1000	13	3.18	+	4.08	9.61E-06	1.21E-03
regulation of cellular component organization (GO:0051128)	697	9	2.22	+	4.06	3.11E-04	2.24E-02
animal organ morphogenesis (GO:0009887)	721	9	2.3	+	3.92	3.98E-04	2.65E-02
response to external stimulus (GO:0009605)	933	11	2.97	+	3.7	1.31E-04	1.12E-02
cell development (GO:0048468)	1303	15	4.15	+	3.62	6.97E-06	9.36E-04
regulation of biological quality (GO:0065008)	1248	14	3.97	+	3.52	2.10E-05	2.34E-03
anatomical structure morphogenesis (GO:0009653)	1466	15	4.67	+	3.21	2.85E-05	2.96E-03
cell differentiation (GO:0030154)	1567	16	4.99	+	3.21	1.41E-05	1.67E-03
cellular developmental process (GO:0048869)	1577	16	5.02	+	3.19	1.53E-05	1.78E-03
response to chemical (GO:0042221)	1093	11	3.48	+	3.16	5.13E-04	3.36E-02
multicellular organism development (GO:0007275)	2125	21	6.77	+	3.1	4.73E-07	8.78E-05
negative regulation of cellular process (GO:0048523)	1244	12	3.96	+	3.03	3.94E-04	2.65E-02
response to stimulus (GO:0050896)	2530	24	8.05	+	2.98	8.02E-08	1.78E-05
cellular response to stimulus (GO:0051716)	1496	14	4.76	+	2.94	1.52E-04	1.26E-02
multicellular organismal process (GO:0032501)	3331	31	10.6	+	2.92	1.25E-10	1.22E-07
regulation of cellular process (GO:0050794)	3690	34	11.75	+	2.89	4.31E-12	1.12E-08
anatomical structure development (GO:0048856)	2531	22	8.06	+	2.73	1.97E-06	3.01E-04
regulation of biological process (GO:0050789)	4030	35	12.83	+	2.73	7.16E-12	1.12E-08
developmental process (GO:0032502)	2665	23	8.48	+	2.71	1.07E-06	1.78E-04
cellular component organization (GO:0016043)	2644	22	8.42	+	2.61	4.18E-06	5.92E-04
biological regulation (GO:0065007)	4471	37	14.23	+	2.6	2.18E-12	8.48E-09
positive regulation of biological process (GO:0048518)	1751	14	5.57	+	2.51	7.74E-04	4.71E-02
cellular component organization or biogenesis (GO:0071840)	2810	22	8.95	+	2.46	1.17E-05	1.42E-03
cellular process (GO:0009987)	7238	37	23.04	+	1.61	1.39E-05	1.66E-03

9.9.5 Genes downregulated upon sleep deprivation, "cellular component"

Analysis Type:	PANTHER Overrepresentation Test (Released 20220712)						
Annotation Version and Release Date:	GO Ontology database DOI: 10.5281/zenodo.6799722 Released 2022-07-01						
Analyzed List:	upload_1 (Drosophila melanogaster)						
Reference List:	Drosophila melanogaster (all genes in database)						
Test Type:	FISHER						
Correction:	FDR						
GO cellular component complete	Drosophila melanogaster - REFLIST (13821)	upload_1 (44)	upload_1 (expected)	upload_1 (over/under)	upload_1 (fold Enrichment)	upload_1 (raw P-value)	upload_1 (FDR)
presynaptic active zone cytoplasmic component (GO:0098831)	9	3	0.03	+	> 100	6.43E-06	4.50E-04
presynaptic cytoskeleton (GO:0099569)	8	2	0.03	+	78.53	4.36E-04	2.15E-02
cytoskeleton of presynaptic active zone (GO:0048788)	8	2	0.03	+	78.53	4.36E-04	2.07E-02
sarcolemma (GO:0042383)	10	2	0.03	+	62.82	6.37E-04	2.92E-02
presynaptic membrane (GO:0042734)	27	5	0.09	+	58.17	4.81E-08	8.00E-06
presynaptic active zone (GO:0048786)	29	4	0.09	+	43.33	3.38E-06	2.64E-04
neuromuscular junction (GO:0031594)	86	9	0.27	+	32.87	1.32E-11	5.83E-09
synaptic membrane (GO:0097060)	74	6	0.24	+	25.47	1.81E-07	2.40E-05
axon terminus (GO:0043679)	79	5	0.25	+	19.88	6.53E-06	4.34E-04
neuron projection terminus (GO:0044306)	80	5	0.25	+	19.63	6.92E-06	4.38E-04
terminal bouton (GO:0043195)	70	4	0.22	+	17.95	8.63E-05	4.59E-03
distal axon (GO:0150034)	108	6	0.34	+	17.45	1.48E-06	1.31E-04
postsynapse (GO:0098794)	77	4	0.25	+	16.32	1.23E-04	6.28E-03
synapse (GO:0045202)	315	16	1	+	15.95	1.77E-15	2.35E-12
presynapse (GO:0098793)	174	8	0.55	+	14.44	8.95E-08	1.32E-05
axon (GO:0030424)	253	10	0.81	+	12.42	7.15E-09	1.36E-06
cell junction (GO:0030054)	466	16	1.48	+	10.79	6.04E-13	4.02E-10
neuron projection (GO:0043005)	482	13	1.53	+	8.47	2.47E-09	5.47E-07
plasma membrane region (GO:0098590)	353	9	1.12	+	8.01	1.61E-06	1.34E-04
intrinsic component of plasma membrane (GO:0031226)	538	11	1.71	+	6.42	7.93E-07	7.53E-05
integral component of plasma membrane (GO:0005887)	521	10	1.66	+	6.03	4.78E-06	3.53E-04
plasma membrane bounded cell projection (GO:0120025)	729	13	2.32	+	5.6	2.95E-07	3.57E-05
cell projection (GO:0042995)	736	13	2.34	+	5.55	3.29E-07	3.64E-05
plasma membrane (GO:0005886)	1510	23	4.81	+	4.78	1.73E-11	5.74E-09
cell periphery (GO:0071944)	1896	25	6.04	+	4.14	2.93E-11	7.79E-09
intrinsic component of membrane (GO:0031224)	1551	16	4.94	+	3.24	1.24E-05	7.50E-04
integral component of membrane (GO:0016021)	1521	15	4.84	+	3.1	4.39E-05	2.54E-03
membrane (GO:0016020)	2997	25	9.54	+	2.62	4.52E-07	4.62E-05
cellular anatomical entity (GO:0110165)	9284	41	29.56	+	1.39	7.12E-05	3.94E-03

9.9.6 Genes downregulated upon sleep deprivation, "reactome"

Analysis Type:	**PANTHER Overrepresentation Test (Released 20220712)**						
Annotation Version and Release Date:	Reactome version 65 Released 2021-10-01						
Analyzed List:	upload_1 (Drosophila melanogaster)						
Reference List:	Drosophila melanogaster (all genes in database)						
Test Type:	FISHER						
Correction:	FDR						
Reactome pathways	Drosophila melanogaster - REFLIST (13821)	upload_1 (44)	upload_1 (expected)	upload_1 (over/under)	upload_1 (fold Enrichment)	upload_1 (raw P-value)	upload_1 (FDR)
GPCR downstream signalling (R-DME-388396)	156	6	0.5	+	12.08	1.13E-05	1.62E-02
Signaling by GPCR (R-DME-372790)	159	6	0.51	+	11.85	1.26E-05	9.02E-03

9.10 Genes differentially expressed between two dFB neurons sub-clusters

	p_val	avg_log2FC	pct.1	pct.2	p_val_adj
Rbp6	1.75E-47	-3.3051823	0.41	0.993	1.77E-43
SoxN	7.24E-45	-3.4480973	0.022	0.814	7.33E-41
CG3009	1.93E-43	-1.993181	0.073	0.869	1.95E-39
CG30116	1.88E-42	3.49247192	0.927	0.414	1.90E-38
esn	2.85E-42	-2.0503896	0	0.738	2.88E-38
mbl	1.16E-40	-3.4083557	0.146	0.89	1.17E-36
CG43689	5.73E-40	-2.3438466	0.067	0.855	5.79E-36
beat-Ic	2.96E-39	-2.2315598	0.073	0.848	3.00E-35
DopEcR	6.11E-39	-1.9749336	0.219	0.972	6.18E-35
Octbeta1R	7.39E-39	3.85396041	0.904	0.552	7.47E-35
msi	1.06E-38	-2.110502	0.309	0.945	1.07E-34
levy	3.14E-38	-1.9690928	0.343	0.945	3.18E-34
Con	5.75E-38	3.11640924	0.871	0.234	5.82E-34
Ald	2.46E-37	-2.0476537	0.713	0.972	2.49E-33
CG43737	3.14E-37	-1.8997479	0.258	0.945	3.18E-33
sesB	5.34E-37	-1.8388003	0.736	0.993	5.40E-33
COX4	5.66E-37	-1.7828537	0.545	0.979	5.72E-33
br	7.02E-37	-1.7981721	0.079	0.828	7.10E-33
pum	7.41E-37	1.56272156	0.978	0.993	7.50E-33
Hasp	7.59E-37	-1.849952	0.635	0.979	7.67E-33
shakB	1.30E-36	-1.6365141	0.118	0.91	1.31E-32
Ac78C	1.58E-36	2.81882672	0.747	0.028	1.60E-32
brp	2.66E-36	1.95998294	0.955	0.952	2.69E-32
nmo	6.01E-36	-2.0941817	0.781	0.986	6.08E-32
Cyt-c1	7.41E-36	-1.7673858	0.315	0.924	7.49E-32
svp	9.17E-36	-1.9236988	0.056	0.766	9.27E-32
CG17816	1.23E-35	1.90955716	0.944	0.897	1.25E-31
rad	1.43E-35	2.74400036	0.91	0.497	1.44E-31
Eip93F	2.11E-35	3.04113558	0.91	0.752	2.13E-31
CG7215	1.64E-34	-1.8339826	0.41	0.931	1.65E-30
Pde1c	1.68E-34	2.72415301	0.82	0.248	1.70E-30
CG4467	2.05E-34	2.35297769	0.933	0.89	2.07E-30
shep	2.24E-34	1.17060309	1	1	2.27E-30
ATPsynF	3.34E-34	-1.8615928	0.427	0.945	3.38E-30
Hsp60A	3.73E-34	-1.7055626	0.247	0.876	3.77E-30
Lim3	4.41E-34	-1.7391062	0.034	0.71	4.46E-30
nrv3	5.58E-34	-1.1246084	0.978	1	5.65E-30
ND-39	7.89E-34	-1.7033412	0.202	0.869	7.98E-30
dve	1.13E-33	2.81953607	0.697	0.014	1.14E-29
IA-2	1.28E-33	2.23555583	0.994	1	1.30E-29
Sox102F	1.95E-33	-1.8821899	0.034	0.697	1.97E-29
TM4SF	1.95E-33	-1.6782473	0.539	0.959	1.97E-29
Tsp66E	2.70E-33	-1.6168348	0.169	0.841	2.73E-29
CG32698	2.83E-33	2.46200701	0.798	0.11	2.86E-29
alphaSnap	5.46E-33	-1.4887241	0.545	0.966	5.52E-29
beat-Ib	5.49E-33	-1.7777223	0.18	0.841	5.55E-29
Lmpt	5.55E-33	2.63995552	0.719	0.034	5.61E-29
Sema2b	5.84E-33	-2.4692188	0.051	0.69	5.91E-29
COX8	1.19E-32	-2.1533052	0.292	0.876	1.20E-28
Ggamma30A	1.45E-32	-2.3640755	0.663	0.993	1.46E-28

Table 9.3 | Genes differentially expressed between the two dFB neurons sub-clusters reported in Figure 6.1.
First 50 DEGs between dFB neurons' cluster 1 and cluster 2 of **Figure 6.1**, ordered by adjusted P-value, scored by Wilcoxon Rank Sum test, with P-value adjusted using Bonferroni correction based on the total number of variable genes within dFB neurons. The table also shows the Log_2 of the fold change between group 1 and group 2 (positive values indicate enrichment in group 1) and the percentage of cells in each group in which the gene is detected.

10 Bibliography

1. Nath, R. D. *et al.* The Jellyfish Cassiopea Exhibits a Sleep-like State. *Current Biology* **27**, 2984-2990.e3 (2017).
2. Campbell, S. S. & Tobler, I. Animal sleep: A review of sleep duration across phylogeny. *Neuroscience and Biobehavioral Reviews* **8**, 269–300 (1984).
3. Borbely, A. A. A two process model of sleep regulation. *Human Neurobiology* **1**, 195–204 (1982).
4. Konopka, R. J. & Benzer, S. Clock mutants of Drosophila melanogaster. *Proceedings of the National Academy of Sciences of the United States of America* **68**, 2112–2116 (1971).
5. Borbely, A. & Tononi, G. The quest for the essence of sleep. *Daedalus* **127**, 167–196 (1998).
6. Borbély, A. A., Daan, S., Wirz-Justice, A. & Deboer, T. The two-process model of sleep regulation: A reappraisal. *Journal of Sleep Research* **25**, 131–143 (2016).
7. Borbély, A. The two-process model of sleep regulation: Beginnings and outlook †. *Journal of Sleep Research* **31**, (2022).
8. Thomas, C. W., Guillaumin, M. C., McKillop, L. E., Achermann, P. & Vyazovskiy, V. V. Global sleep homeostasis reflects temporally and spatially integrated local cortical neuronal activity. *eLife* **9**, e54148 (2020).
9. Noya, S. B. *et al.* The forebrain synaptic transcriptome is organized by clocks but its proteome is driven by sleep. *Science* **366**, eaav2642 (2019).
10. Tononi, G. & Cirelli, C. Sleep and synaptic homeostasis: A hypothesis. *Brain Research Bulletin* **62**, 143–150 (2003).

11. Vyazovskiy, V. V., Cirelli, C., Pfister-Genskow, M., Faraguna, U. & Tononi, G. Molecular and electrophysiological evidence for net synaptic potentiation in wake and depression in sleep. *Nature Neuroscience* **11**, 200–208 (2008).

12. De Vivo, L. *et al.* Ultrastructural evidence for synaptic scaling across the wake/sleep cycle. *Science* **355**, 507–510 (2017).

13. Tononi, G. & Cirelli, C. Sleep and the Price of Plasticity: From Synaptic and Cellular Homeostasis to Memory Consolidation and Integration. *Neuron* **81**, 12–34 (2014).

14. Gilestro, G. F., Tononi, G. & Cirelli, C. Widespread changes in synaptic markers as a function of sleep and wakefulness in drosophila. *Science* (2009) doi:10.1126/science.1166673.

15. Spano, G. M. *et al.* Sleep Deprivation by Exposure to Novel Objects Increases Synapse Density and Axon-Spine Interface in the Hippocampal CA1 Region of Adolescent Mice. *The Journal of neuroscience : the official journal of the Society for Neuroscience* **39**, 6613–6625 (2019).

16. Tononi, G. & Cirelli, C. Sleep and synaptic down-selection. *Eur J Neurosci* **51**, 413–421 (2020).

17. Brinkman, J. E., Reddy, V. & Sharma, S. Physiology of Sleep. in *StatPearls* (StatPearls Publishing, 2022).

18. Bentivoglio, M. & Grassi-Zucconi, G. The pioneering experimental studies on sleep deprivation. *Sleep* **20**, 570–576 (1997).

19. Moruzzi, G. The Functional Significance of Sleep with Particular Regard to the Brain Mechanisms Underlying Consciousness. in *Brain and Conscious Experience* (ed. Eccles, J. C.) 345–388 (Springer Berlin Heidelberg, 1965). doi:10.1007/978-3-642-49168-9_15.

20. von ECONOMO, C. SOME NEW METHODS OF STUDING THE BRAINS OF EXCEPTIONAL PERSONS (ENCEPHALOMETRY AND BRAIN CASTS): *The Journal of Nervous and Mental Disease* **71**, 300–302 (1930).

21. Moruzzi, G. & Magoun, H. W. Brain stem reticular formation and activation of the EEG. *Electroencephalogr Clin Neurophysiol* **1**, 455–473 (1949).

22. Saper, C. B., Chou, T. C. & Scammell, T. E. The sleep switch: hypothalamic control of sleep and wakefulness. *Trends in Neurosciences* **24**, 726–731 (2001).

23. Saper, C. B., Fuller, P. M., Pedersen, N. P., Lu, J. & Scammell, T. E. Sleep State Switching. *Neuron* **68**, 1023–1042 (2010).

24. Sherin, J. E., Elmquist, J. K., Torrealba, F. & Saper, C. B. Innervation of histaminergic tuberomammillary neurons by GABAergic and galaninergic neurons in the ventrolateral preoptic nucleus of the rat. *Journal of Neuroscience* **18**, 4705–4721 (1998).

25. Vyazovskiy, V. V. *et al.* Local sleep in awake rats. *Nature* **472**, 443–447 (2011).

26. Krone, L. B. *et al.* A role for the cortex in sleep–wake regulation. *Nat Neurosci* **24**, 1210–1215 (2021).

27. M. Krueger, J. & P. Wisor, J. Editorial [Hot Topic: Local Use-Dependent Sleep (Guest Editors: J.M. Krueger & J.P. Wisor)]. *CTMC* **11**, 2390–2391 (2011).

28. Alfonsa, H. *et al. Intraneuronal chloride levels encode tiredness in cortex*. http://biorxiv.org/lookup/doi/10.1101/2021.05.14.444189 (2021) doi:10.1101/2021.05.14.444189.

29. Kubota, K. Kuniomi Ishimori and the first discovery of sleep-inducing substances in the brain. *Neuroscience Research* **6**, 497–518 (1989).

30. Porkka-Heiskanen, T. *et al.* Adenosine: A mediator of the sleep-inducing effects of prolonged wakefulness. *Science* **276**, 1265–1267 (1997).

31. Davis, G. W. HOMEOSTATIC CONTROL OF NEURAL ACTIVITY: From Phenomenology to Molecular Design. *Annu. Rev. Neurosci.* **29**, 307–323 (2006).

32. Scheffer, L. K. *et al.* A connectome and analysis of the adult Drosophila central brain. *eLife* **9**, e57443 (2020).

33. Hulse, B. K. *et al.* A connectome of the Drosophila central complex reveals network motifs suitable for flexible navigation and context-dependent action selection. *eLife* **10**, e66039 (2021).

34. Croset, V., Treiber, C. D. & Waddell, S. Cellular diversity in the Drosophila midbrain revealed by single-cell transcriptomics. *eLife* **7**, (2018).

35. Konstantinides, N. *et al.* Phenotypic Convergence: Distinct Transcription Factors Regulate Common Terminal Features. *Cell* **174**, 622-635.e13 (2018).

36. Allen, A. M. *et al.* A single-cell transcriptomic atlas of the adult Drosophila ventral nerve cord. *eLife* **9**, e54074 (2020).

37. Li, H. *et al.* Fly Cell Atlas: A single-nucleus transcriptomic atlas of the adult fruit fly. *Science* **375**, eabk2432 (2022).

38. Panda, S., Hogenesch, J. B. & Kay, S. A. Circadian rhythms from flies to human. *Nature* **417**, 329–335 (2002).

39. Shaw, Paul J., Cirelli Chiara, Greenspan J. Ralph, T. G. & Tononi, G. Correlates of Sleep and Waking in Drosophila melanogaster. *Science* **287**, 1834–1837 (2000).

40. Hendricks, J. C. *et al.* Rest in Drosophila is a sleep-like state. *Neuron* **25**, 129–138 (2000).

41. Dissel, S., Melnattur, K. & Shaw, P. J. Sleep, Performance, and Memory in Flies. *Curr Sleep Medicine Rep* **1**, 47–54 (2015).

42. Ly, S., Pack, A. I. & Naidoo, N. The neurobiological basis of sleep: Insights from Drosophila. *Neuroscience & Biobehavioral Reviews* **87**, 67–86 (2018).

43. Cirelli, C., LaVaute, T. M. & Tononi, G. Sleep and wakefulness modulate gene expression in Drosophila. *Journal of Neurochemistry* (2005) doi:10.1111/j.1471-4159.2005.03291.x.

44. van Alphen, B., Yap, M. H. W., Kirszenblat, L., Kottler, B. & van Swinderen, B. A Dynamic Deep Sleep Stage in Drosophila. *Journal of Neuroscience* **33**, 6917–6927 (2013).

45. Yap, M. H. W. *et al.* Oscillatory brain activity in spontaneous and induced sleep stages in flies. *Nature Communications* **8**, (2017).

46. van Alphen, B., Semenza, E. R., Yap, M., van Swinderen, B. & Allada, R. A deep sleep stage in *Drosophila* with a functional role in waste clearance. *Sci. Adv.* **7**, eabc2999 (2021).

47. Raccuglia, D. *et al.* Network-Specific Synchronization of Electrical Slow-Wave Oscillations Regulates Sleep Drive in Drosophila. *Current Biology* **29**, 3611-3621.e3 (2019).

48. Huber, R. *et al.* Sleep Homeostasis in Drosophila Melanogaster. *Sleep* **27**, 628–639 (2004).

49. Donelson, N. *et al.* High-Resolution Positional Tracking for Long-Term Analysis of Drosophila Sleep and Locomotion Using the "Tracker" Program. *PLoS ONE* **7**, e37250 (2012).

50. Xu, X. *et al.* Quantitative investigation reveals distinct phases in Drosophila sleep. *Commun Biol* **4**, 364 (2021).

51. Dissel, S. *et al.* Sleep Restores Behavioral Plasticity to Drosophila Mutants. *Current Biology* **25**, 1270–1281 (2015).

52. Dissel, S. *et al.* Enhanced sleep reverses memory deficits and underlying pathology in drosophila models of Alzheimer's disease. *Neurobiology of Sleep and Circadian Rhythms* **2**, 15–26 (2017).

53. Donlea, J. M. *et al.* Recurrent Circuitry for Balancing Sleep Need and Sleep. *Neuron* **97**, 378-389.e4 (2018).

54. Aleman, A. *et al. Opposing subclasses of* Drosophila *ellipsoid body neurons promote and suppress sleep*. http://biorxiv.org/lookup/doi/10.1101/2021.10.19.464469 (2021) doi:10.1101/2021.10.19.464469.

55. Tainton-Heap, L. A. L. *et al.* A Paradoxical Kind of Sleep in Drosophila melanogaster. *Current Biology* **31**, 578-590.e6 (2021).

56. Raccuglia, D., Suárez-Grimalt, R., Brodersen, C. B., Geiger, J. R. & Owald, D. *Coherent network oscillations regulate quiescence and behavioral responsiveness in* Drosophila. http://biorxiv.org/lookup/doi/10.1101/2022.03.11.483976 (2022) doi:10.1101/2022.03.11.483976.

57. Liu, S., Liu, Q., Tabuchi, M. & Wu, M. N. Sleep drive is encoded by neural plastic changes in a dedicated circuit. *Cell* **165**, 1347–1360 (2016).

58. Blum, I. D. *et al.* Astroglial Calcium Signaling Encodes Sleep Need in Drosophila. *Current Biology* **31**, 150-162.e7 (2021).

59. Ingiosi, A. M. *et al.* A Role for Astroglial Calcium in Mammalian Sleep and Sleep Regulation. *Current Biology* **30**, 4373-4383.e7 (2020).

60. Brancaccio, M. *et al.* Cell-autonomous clock of astrocytes drives circadian behavior in mammals. *Science* **363**, 187–192 (2019).

61. Andretic, R., van Swinderen, B. & Greenspan, R. J. Dopaminergic Modulation of Arousal in Drosophila. *Current Biology* **15**, 1165–1175 (2005).

62. Van Swinderen, B. & Andretic, R. Dopamine in *Drosophila* : setting arousal thresholds in a miniature brain. *Proc. R. Soc. B.* **278**, 906–913 (2011).

63. Seidner, G. *et al.* Identification of Neurons with a Privileged Role in Sleep Homeostasis in Drosophila melanogaster. *Current Biology* **25**, 2928–2938 (2015).

64. Liu, Q., Liu, S., Kodama, L., Driscoll, M. R. & Wu, M. N. Two Dopaminergic Neurons Signal to the Dorsal Fan-Shaped Body to Promote Wakefulness in Drosophila. *Current Biology* **22**, 2114–2123 (2012).

65. Ueno, T. *et al.* Identification of a dopamine pathway that regulates sleep and arousal in Drosophila. *Nature Neuroscience* (2012) doi:10.1038/nn.3238.

66. Pimentel, D. *et al.* Operation of a homeostatic sleep switch. *Nature* **536**, 333–337 (2016).

67. Liu, C. *et al.* A Serotonin-Modulated Circuit Controls Sleep Architecture to Regulate Cognitive Function Independent of Total Sleep in Drosophila. *Current Biology* **29**, 3635-3646.e5 (2019).

68. Qian, Y. *et al.* Sleep homeostasis regulated by 5HT2b receptor in a small subset of neurons in the dorsal fan-shaped body of drosophila. *eLife* **6**, (2017).

69. Crocker, A. & Sehgal, A. Octopamine Regulates Sleep in Drosophila through Protein Kinase A-Dependent Mechanisms. *Journal of Neuroscience* **28**, 9377–9385 (2008).

70. Crocker, A., Shahidullah, M., Levitan, I. B. & Sehgal, A. Identification of a Neural Circuit that Underlies the Effects of Octopamine on Sleep:Wake Behavior. *Neuron* **65**, 670–681 (2010).

71. Guo, F. *et al.* Circadian neuron feedback controls the Drosophila sleep–activity profile. *Nature* **536**, 292–297 (2016).

72. Pitman, J. L., McGill, J. J., Keegan, K. P. & Allada, R. A dynamic role for the mushroom bodies in promoting sleep in Drosophila. *Nature* **441**, 753–756 (2006).

73. Sitaraman, D. *et al.* Propagation of Homeostatic Sleep Signals by Segregated Synaptic Microcircuits of the Drosophila Mushroom Body. *Current Biology* **25**, 2915–2927 (2015).

74. Sitaraman, D., Aso, Y., Rubin, G. M. & Nitabach, M. N. Control of Sleep by Dopaminergic Inputs to the Drosophila Mushroom Body. *Front. Neural Circuits* **9**, (2015).

75. Weiss, J. T. & Donlea, J. M. Sleep deprivation results in diverse patterns of synaptic scaling across the Drosophila mushroom bodies. *Current Biology* **31**, 3248-3261.e3 (2021).

76. Park, S., Sonn, J. Y., Oh, Y., Lim, C. & Choe, J. SIFamide and SIFamide receptor define a novel neuropeptide signaling to promote sleep in Drosophila. *Molecules and Cells* **37**, 295–301 (2014).

77. Tomita, J., Ban, G., Kato, Y. S. & Kume, K. Protocerebral Bridge Neurons That Regulate Sleep in Drosophila melanogaster. *Front. Neurosci.* **15**, 647117 (2021).

78. Satterfield, L. K., De, J., Wu, M., Qiu, T. & Joiner, W. J. Inputs to the Sleep Homeostat Originate Outside the Brain. *J. Neurosci.* **42**, 5695–5704 (2022).

79. Jones, J. D. *et al. A Split-GAL4 screen identifies novel sleep-promoting neurons in the Ventral Nerve Cord of* Drosophila. http://biorxiv.org/lookup/doi/10.1101/2022.02.02.478882 (2022) doi:10.1101/2022.02.02.478882.

80. Donlea, J. M., Thimgan, M. S., Suzuki, Y., Gottschalk, L. & Shaw, P. J. Inducing sleep by remote control facilitates memory consolidation in Drosophila. *Science* **332**, 1571–1576 (2011).

81. Donlea, J. M., Pimentel, D. & Miesenböck, G. Neuronal machinery of sleep homeostasis in Drosophila. *Neuron* **81**, 860–872 (2014).

82. Troup, M. *et al.* Acute control of the sleep switch in drosophila reveals a role for gap junctions in regulating behavioral responsiveness. *eLife* **7**, (2018).

83. Kempf, A., Song, S. M., Talbot, C. B. & Miesenböck, G. A potassium channel β-subunit couples mitochondrial electron transport to sleep. *Nature* **568**, 230–234 (2019).

84. Ni, J. D. *et al.* Differential regulation of the drosophila sleep homeostat by circadian and arousal inputs. *eLife* **8**, (2019).

85. Toda, H., Williams, J. A., Gulledge, M. & Sehgal, A. A sleep-inducing gene, *nemuri* , links sleep and immune function in *Drosophila*. *Science* **363**, 509–515 (2019).

86. Schwarz, J. E., King, A. N., Hsu, C. T., Barber, A. F. & Sehgal, A. *Hugin* $^{+}$ neurons provide a link between sleep homeostat and circadian clock neurons. *Proc. Natl. Acad. Sci. U.S.A.* **118**, e2111183118 (2021).

87. Chung, B. Y. *et al.* Drosophila Neuropeptide F Signaling Independently Regulates Feeding and Sleep-Wake Behavior. *Cell Reports* **19**, 2441–2450 (2017).

88. Dissel, S., Klose, M. K., van Swinderen, B., Cao, L. & Shaw, P. J. *Sleep promoting neurons remodel their response properties to calibrate sleep drive with environmental demands.* http://biorxiv.org/lookup/doi/10.1101/2021.11.05.467459 (2021) doi:10.1101/2021.11.05.467459.

89. Hasenhuetl, P. S. Personal communication, Miesenböck lab, University of Oxford.

90. Kaitin, K. I. Preoptic area unit activity during sleep and wakefulness in the cat. *Experimental Neurology* **83**, 347–357 (1984).

91. Sherin, J. E., Shiromani, P. J., McCarley, R. W. & Saper, C. B. Activation of ventrolateral preoptic neurons during sleep. *Science* **271**, 216–219 (1996).

92. Kottler, B. *et al.* A Sleep/Wake Circuit Controls Isoflurane Sensitivity in Drosophila. *Current Biology* **23**, 594–598 (2013).

93. Kroeger, D. *et al.* Galanin neurons in the ventrolateral preoptic area promote sleep and heat loss in mice. *Nat Commun* **9**, 4129 (2018).

94. Reichert, S., Pavón Arocas, O. & Rihel, J. The Neuropeptide Galanin Is Required for Homeostatic Rebound Sleep following Increased Neuronal Activity. *Neuron* **104**, 370-384.e5 (2019).

95. Ma, Y. *et al.* Galanin Neurons Unite Sleep Homeostasis and α2-Adrenergic Sedation. *Current Biology* **29**, 3315-3322.e3 (2019).

96. Guo, X. *et al.* RNA-seq analysis of galaninergic neurons from ventrolateral preoptic nucleus identifies expression changes between sleep and wake. *BMC Genomics* **21**, 633 (2020).

97. Shearin, H. K., MacDonald, I. S., Spector, L. P. & Steven Stowers, R. Hexameric GFP and mCherry reporters for the Drosophila GAL4, Q, and LexA transcription systems. *Genetics* **196**, 951–960 (2014).

98. Klapoetke, N. C. *et al.* Independent optical excitation of distinct neural populations. *Nat Methods* **11**, 338–346 (2014).

99. Singh, P. & Donlea, J. M. Bidirectional Regulation of Sleep and Synapse Pruning after Neural Injury. *Current Biology* **30**, 1063-1076.e3 (2020).

100. Fernandez-Ayala, D. J. M. *et al.* Expression of the Ciona intestinalis Alternative Oxidase (AOX) in Drosophila Complements Defects in Mitochondrial Oxidative Phosphorylation. *Cell Metabolism* **9**, 449–460 (2009).

101. DuBoff, B., Götz, J. & Feany, M. B. Tau Promotes Neurodegeneration via DRP1 Mislocalization In Vivo. *Neuron* **75**, 618–632 (2012).

102. Park, J., Lee, G. & Chung, J. The PINK1–Parkin pathway is involved in the regulation of mitochondrial remodeling process. *Biochemical and Biophysical Research Communications* **378**, 518–523 (2009).

103. Deng, H., Dodson, M. W., Huang, H. & Guo, M. The Parkinson's disease genes *pink1* and *parkin* promote mitochondrial fission and/or inhibit fusion in *Drosophila*. *Proc. Natl. Acad. Sci. U.S.A.* **105**, 14503–14508 (2008).

104. Port, F. *et al.* A large-scale resource for tissue-specific CRISPR mutagenesis in Drosophila. *eLife* **9**, e53865 (2020).

105. French, A. S., Geissmann, Q., Beckwith, E. J. & Gilestro, G. F. Sensory processing during sleep in Drosophila melanogaster. *Nature* **598**, 479–482 (2021).

106. Shaw, P. J., Tononi, G., Greenspan, R. J. & Robinson, D. F. Stress response genes protect against lethal effects of sleep deprivation in Drosophila. *Nature* **417**, 287–291 (2002).

107. Melnattur, K., Morgan, E., Duong, V., Kalra, A. & Shaw, P. J. The Sleep Nullifying Apparatus: A Highly Efficient Method of Sleep Depriving Drosophila. *JoVE* 62105 (2020) doi:10.3791/62105.

108. Macosko, E. Z. *et al.* Highly parallel genome-wide expression profiling of individual cells using nanoliter droplets. *Cell* **161**, 1202–1214 (2015).

109. Satija, R., Farrell, J. A., Gennert, D., Schier, A. F. & Regev, A. Spatial reconstruction of single-cell gene expression data. *Nature Biotechnology* **33**, 495–502 (2015).

110. Nemesh, J. *Drop-seq Core Computational Protocol V2.0.0*. 1–23 (2018).

111. Arzalluz-Luque, Á., Devailly, G., Mantsoki, A. & Joshi, A. Delineating biological and technical variance in single cell expression data. *The International Journal of Biochemistry & Cell Biology* **90**, 161–166 (2017).

112. Harrell, E. R., Pimentel, D. & Miesenböck, G. Changes in Presynaptic Gene Expression during Homeostatic Compensation at a Central Synapse. *J. Neurosci.* **41**, 3054–3067 (2021).

113. Chaudhry, A., Shi, R. & Luciani, D. S. A pipeline for multidimensional confocal analysis of mitochondrial morphology, function, and dynamics in pancreatic β-cells. *American Journal of Physiology-Endocrinology and Metabolism* **318**, E87–E101 (2020).

114. Kirshner, H., Aguet, F., Sage, D. & Unser, M. 3-D PSF fitting for fluorescence microscopy: implementation and localization application: 3-D PSF FITTING FOR FLUORESCENCE MICROSCOPY. *Journal of Microscopy* **249**, 13–25 (2013).

115. Dey, N. *et al.* Richardson–Lucy algorithm with total variation regularization for 3D confocal microscope deconvolution. *Microsc. Res. Tech.* **69**, 260–266 (2006).

116. Sage, D. *et al.* DeconvolutionLab2: An open-source software for deconvolution microscopy. *Methods* **115**, 28–41 (2017).

117. Port, F. & Bullock, S. L. Augmenting CRISPR applications in Drosophila with tRNA-flanked sgRNAs. *Nat Methods* **13**, 852–854 (2016).

118. Port, F. *pCFD6 cloning protocol (CRISPR Fly Design)*. http://www.crisprflydesign.org/wp-content/uploads/2017/01/pCFD6cloningprotocol.pdf.

119. Labun, K. *et al.* CHOPCHOP v3: expanding the CRISPR web toolbox beyond genome editing. *Nucleic Acids Research* **47**, W171–W174 (2019).

120. Schindelin, J. *et al.* Fiji: an open-source platform for biological-image analysis. *Nat Methods* **9**, 676–682 (2012).

121. Hao, Y. *et al.* Integrated analysis of multimodal single-cell data. *Cell* **184**, 3573-3587.e29 (2021).

122. Ashburner, M. *et al.* Gene Ontology: tool for the unification of biology. *Nat Genet* **25**, 25–29 (2000).

123. The Gene Ontology Consortium *et al.* The Gene Ontology resource: enriching a GOld mine. *Nucleic Acids Research* **49**, D325–D334 (2021).

124. Mi, H. *et al.* PANTHER version 16: a revised family classification, tree-based classification tool, enhancer regions and extensive API. *Nucleic Acids Research* **49**, D394–D403 (2021).

125. Brionne, A., Juanchich, A. & Hennequet-Antier, C. ViSEAGO: a Bioconductor package for clustering biological functions using Gene Ontology and semantic similarity. *BioData Mining* **12**, 16 (2019).

126. Alexa, A. & Rahnenfuhrer, J. topGO: Enrichment Analysis for Gene Ontology. R package version 2.48.0. (2022).

127. Clements, J. *et al.* neu *Print: Analysis Tools for EM Connectomics*. http://biorxiv.org/lookup/doi/10.1101/2020.01.16.909465 (2020) doi:10.1101/2020.01.16.909465.

128. Ghazalpour, A. *et al.* Comparative Analysis of Proteome and Transcriptome Variation in Mouse. *PLoS Genet* **7**, e1001393 (2011).

129. Vogel, C. & Marcotte, E. M. Insights into the regulation of protein abundance from proteomic and transcriptomic analyses. *Nat Rev Genet* **13**, 227–232 (2012).

130. Khan, Z. *et al.* Primate Transcript and Protein Expression Levels Evolve Under Compensatory Selection Pressures. *Science* **342**, 1100–1104 (2013).

131. Brown, M. P. S. *et al.* Knowledge-based analysis of microarray gene expression data by using support vector machines. *Proc. Natl. Acad. Sci. U.S.A.* **97**, 262–267 (2000).

132. Sanguinetti, G., Lawrence, N. D. & Rattray, M. Probabilistic inference of transcription factor concentrations and gene-specific regulatory activities. *Bioinformatics* **22**, 2775–2781 (2006).

133. Chung, S. *et al.* Identification of preoptic sleep neurons using retrograde labelling and gene profiling. *Nature* **545**, 477–481 (2017).

134. Henry, F. E., Sugino, K., Tozer, A., Branco, T. & Sternson, S. M. Cell type-specific transcriptomics of hypothalamic energy-sensing neuron responses to weight-loss. *eLife* **4**, e09800 (2015).

135. Tang, F. *et al.* mRNA-Seq whole-transcriptome analysis of a single cell. *Nat Methods* **6**, 377–382 (2009).

136. Davie, K. *et al.* A Single-Cell Transcriptome Atlas of the Aging Drosophila Brain. *Cell* **174**, 982-998.e20 (2018).

137. Norimoto, H. *et al.* A claustrum in reptiles and its role in slow-wave sleep. *Nature* **578**, 413–418 (2020).

138. Campbell, J. N. *et al.* A molecular census of arcuate hypothalamus and median eminence cell types. *Nat Neurosci* **20**, 484–496 (2017).

139. Osterhout, J. A. *et al.* A preoptic neuronal population controls fever and appetite during sickness. *Nature* **606**, 937–944 (2022).

140. Moffitt, J. R. *et al.* Molecular, spatial, and functional single-cell profiling of the hypothalamic preoptic region. *Science* **362**, eaau5324 (2018).

141. Cirelli, C., Gutierrez, C. M. & Tononi, G. Extensive and Divergent Effects of Sleep and Wakefulness on Brain Gene Expression. *Neuron* **41**, 35–43 (2004).

142. Anafi, R. C. *et al.* Sleep is not just for the brain: transcriptional responses to sleep in peripheral tissues. *BMC Genomics* **14**, 362 (2013).

143. Haberkern, H. & Jayaraman, V. Studying small brains to understand the building blocks of cognition. *Current Opinion in Neurobiology* **37**, 59–65 (2016).

144. Hong, R. *et al.* Comprehensive generation, visualization, and reporting of quality control metrics for single-cell RNA sequencing data. *Nat Commun* **13**, 1688 (2022).

145. Xie, X. *et al.* Semaphorin 2b Regulates Sleep-Circuit Formation in the Drosophila Central Brain. *Neuron* **104**, 322-337.e14 (2019).

146. Jenett, A. *et al.* A GAL4-Driver Line Resource for Drosophila Neurobiology. *Cell Reports* **2**, 991–1001 (2012).

147. Ma, D. *et al.* A transcriptomic taxonomy of Drosophila circadian neurons around the clock. *eLife* **10**, e63056 (2021).

148. Barnstedt, O. *et al.* Memory-Relevant Mushroom Body Output Synapses Are Cholinergic. *Neuron* **89**, 1237–1247 (2016).

149. Rout, R., Basu, S. & Mishra, M. Reactive Oxygen Species Detection of Drosophila Cells by Flow Cytometry. in *Fundamental Approaches to Screen Abnormalities in Drosophila* (ed. Mishra, M.) 97–109 (Springer US, 2020). doi:10.1007/978-1-4939-9756-5_9.

150. Yousefi, O. S. *et al.* Optogenetic control shows that kinetic proofreading regulates the activity of the T cell receptor. *eLife* **8**, e42475 (2019).

151. Zheng, Z. *et al.* A Complete Electron Microscopy Volume of the Brain of Adult Drosophila melanogaster. *Cell* **174**, 730-743.e22 (2018).

152. Scheffer, L. K. & Meinertzhagen, I. A. A connectome is not enough – what is still needed to understand the brain of *Drosophila* ? *Journal of Experimental Biology* **224**, jeb242740 (2021).

153. Greengard, P. The Neurobiology of Slow Synaptic Transmission. *Science* **294**, 1024–1030 (2001).

154. Richter, C., Woods, I. G. & Schier, A. F. Neuropeptidergic Control of Sleep and Wakefulness. *Annu. Rev. Neurosci.* **37**, 503–531 (2014).

155. Eban-Rothschild, A., Appelbaum, L. & de Lecea, L. Neuronal Mechanisms for Sleep/Wake Regulation and Modulatory Drive. *Neuropsychopharmacol.* **43**, 937–952 (2018).

156. Cong, X. *et al.* Regulation of Sleep by Insulin-like Peptide System in Drosophila melanogaster. *Sleep* **38**, 1075–1083 (2015).

157. King, A. N. *et al.* A Peptidergic Circuit Links the Circadian Clock to Locomotor Activity. *Current Biology* **27**, 1915-1927.e5 (2017).

158. Melnattur, K., Zhang, B. & Shaw, P. J. Disrupting flight increases sleep and identifies a novel sleep-promoting pathway in *Drosophila*. *Sci. Adv.* **6**, eaaz2166 (2020).

159. Oh, Y. *et al.* A Homeostatic Sleep-Stabilizing Pathway in Drosophila Composed of the Sex Peptide Receptor and Its Ligand, the Myoinhibitory Peptide. *PLoS Biology* **12**, (2014).

160. Ma, S., Hangya, B., Leonard, C. S., Wisden, W. & Gundlach, A. L. Dual-transmitter systems regulating arousal, attention, learning and memory. *Neuroscience & Biobehavioral Reviews* **85**, 21–33 (2018).

161. Kim, J. hyung *et al.* The voltage-gated potassium channel Shaker promotes sleep via thermosensitive GABA transmission. *Communications Biology* (2020) doi:10.1038/s42003-020-0902-8.

162. Nogi, Y. & Fukasawa, T. Nucleotide sequence of the yeast regulatory gene *GAL80*. *Nucl Acids Res* **12**, 9287–9298 (1984).

163. Nogi, Y., Shimada, H., Matsuzaki, Y., Hashimoto, H. & Fukasawa, T. Regulation of expression of the galactose gene cluster in Saccharomyces cerevisiae: II. The isolation and dosage effect of the regulatory gene GAL80. *Mol Gen Genet* **195**, 29–34 (1984).

164. Luan, H., Peabody, N. C., Vinson, C. R. R. & White, B. H. Refined Spatial Manipulation of Neuronal Function by Combinatorial Restriction of Transgene Expression. *Neuron* **52**, 425–436 (2006).

165. Pfeiffer, B. D. *et al.* Refinement of tools for targeted gene expression in Drosophila. *Genetics* **186**, 735–755 (2010).

166. Schiavo, G. G. *et al.* Tetanus and botulinum-B neurotoxins block neurotransmitter release by proteolytic cleavage of synaptobrevin. *Nature* **359**, 832–835 (1992).

167. Zemelman, B. V., Lee, G. A., Ng, M. & Miesenböck, G. Selective photostimulation of genetically chARGed neurons. *Neuron* **33**, 15–22 (2002).

168. Miesenböck, G. The optogenetic catechism. *Science* **326**, 395–399 (2009).

169. Marvin, J. S. *et al.* An optimized fluorescent probe for visualizing glutamate neurotransmission. *Nat Methods* **10**, 162–170 (2013).

170. Richter, F. G., Fendl, S., Haag, J., Drews, M. S. & Borst, A. Glutamate Signaling in the Fly Visual System. *iScience* **7**, 85–95 (2018).

171. Marvin, J. S. *et al.* Stability, affinity, and chromatic variants of the glutamate sensor iGluSnFR. *Nat Methods* **15**, 936–939 (2018).

172. Thum, A. S. *et al.* Differential potencies of effector genes in adultDrosophila. *J. Comp. Neurol.* **498**, 194–203 (2006).

173. Bajar, B. T. *et al.* A discrete neuronal population coordinates brain-wide developmental activity. *Nature* **602**, 639–646 (2022).

174. Daniels, R. W., Gelfand, M. V., Collins, C. A. & DiAntonio, A. Visualizing glutamatergic cell bodies and synapses inDrosophila larval and adult CNS. *J. Comp. Neurol.* **508**, 131–152 (2008).

175. Liu, W. W. & Wilson, R. I. Glutamate is an inhibitory neurotransmitter in the *Drosophila* olfactory system. *Proc. Natl. Acad. Sci. U.S.A.* **110**, 10294–10299 (2013).

176. McCarthy, E. v. *et al.* Synchronized Bilateral Synaptic Inputs to Drosophila melanogaster Neuropeptidergic Rest/Arousal Neurons. *Journal of Neuroscience* **31**, 8181–8193 (2011).

177. Hamasaka, Y. *et al.* Glutamate and its metabotropic receptor in *Drosophila* clock neuron circuits. *J. Comp. Neurol.* **505**, 32–45 (2007).

178. Zimmerman, J. E. *et al.* Glutamate Is a Wake-Active Neurotransmitter in Drosophila melanogaster. *Sleep* **40**, (2017).

179. Tomita, J., Ueno, T., Mitsuyoshi, M., Kume, S. & Kume, K. The NMDA Receptor Promotes Sleep in the Fruit Fly, Drosophila melanogaster. *PLoS ONE* **10**, e0128101 (2015).

180. Robinson, J. E., Paluch, J., Dickman, D. K. & Joiner, W. J. ADAR-mediated RNA editing suppresses sleep by acting as a brake on glutamatergic synaptic plasticity. *Nature Communications* **7**, (2016).

181. Li, W.-C., Merrison-Hort, R., Zhang, H.-Y. & Borisyuk, R. The Generation of Antiphase Oscillations and Synchrony by a Rebound-Based Vertebrate Central Pattern Generator. *Journal of Neuroscience* **34**, 6065–6077 (2014).

182. Yu, X. *et al.* GABA and glutamate neurons in the VTA regulate sleep and wakefulness. *Nat Neurosci* **22**, 106–119 (2019).

183. Jha, P. K., Valekunja, U. K., Ray, S., Nollet, M. & Reddy, A. B. Single-cell transcriptomics and cell-specific proteomics reveals molecular signatures of sleep. *Commun Biol* **5**, 846 (2022).

184. Laughlin, S. Energy as a constraint on the coding and processing of sensory information. *Current Opinion in Neurobiology* **11**, 475–480 (2001).

185. Attwell, D. & Laughlin, S. B. An Energy Budget for Signaling in the Grey Matter of the Brain. *J Cereb Blood Flow Metab* **21**, 1133–1145 (2001).

186. Murphy, M. P. How mitochondria produce reactive oxygen species. *Biochemical Journal* **417**, 1–13 (2009).

187. Robb, E. L. *et al.* Control of mitochondrial superoxide production by reverse electron transport at complex I. *Journal of Biological Chemistry* **293**, 9869–9879 (2018).

188. Kunst, M. *et al.* Calcitonin Gene-Related Peptide Neurons Mediate Sleep-Specific Circadian Output in Drosophila. *Current Biology* **24**, 2652–2664 (2014).

189. Soshnev, A. A. *et al.* A Conserved Long Noncoding RNA Affects Sleep Behavior in *Drosophila*. *Genetics* **189**, 455–468 (2011).

190. Jaggard, J. B. *et al.* Hypocretin underlies the evolution of sleep loss in the Mexican cavefish. *eLife* **7**, e32637 (2018).

191. Lee, D. A. *et al.* Genetic and neuronal regulation of sleep by neuropeptide VF. *eLife* **6**, e25727 (2017).

192. Kittel, R. J. *et al.* Bruchpilot Promotes Active Zone Assembly, Ca^{2+} Channel Clustering, and Vesicle Release. *Science* **312**, 1051–1054 (2006).

193. Chen, Y. *et al.* Cell-type-Specific Labeling of Synapses In Vivo through Synaptic Tagging with Recombination. *Neuron* **81**, 280–293 (2014).

194. Abrisch, R. G., Gumbin, S. C., Wisniewski, B. T., Lackner, L. L. & Voeltz, G. K. Fission and fusion machineries converge at ER contact sites to regulate mitochondrial morphology. *Journal of Cell Biology* **219**, e201911122 (2020).

195. Friedman, J. R. *et al.* ER Tubules Mark Sites of Mitochondrial Division. *Science* **334**, 358–362 (2011).

196. Kornmann, B. *et al.* An ER-Mitochondria Tethering Complex Revealed by a Synthetic Biology Screen. *Science* **325**, 477–481 (2009).

197. Tatsuta, T., Scharwey, M. & Langer, T. Mitochondrial lipid trafficking. *Trends in Cell Biology* **24**, 44–52 (2014).

198. Lahiri, S. *et al.* A Conserved Endoplasmic Reticulum Membrane Protein Complex (EMC) Facilitates Phospholipid Transfer from the ER to Mitochondria. *PLoS Biol* **12**, e1001969 (2014).

199. Xu, L. *et al.* Miga-mediated endoplasmic reticulum–mitochondria contact sites regulate neuronal homeostasis. *eLife* **9**, e56584 (2020).

200. Kim, H., Lee, S., Jun, Y. & Lee, C. Structural basis for mitoguardin-2 mediated lipid transport at ER-mitochondrial membrane contact sites. *Nat Commun* **13**, 3702 (2022).

201. Freyre, C. A. C., Rauher, P. C., Ejsing, C. S. & Klemm, R. W. MIGA2 Links Mitochondria, the ER, and Lipid Droplets and Promotes De Novo Lipogenesis in Adipocytes. *Molecular Cell* **76**, 811-825.e14 (2019).

202. Cieri, D. *et al.* SPLICS: a split green fluorescent protein-based contact site sensor for narrow and wide heterotypic organelle juxtaposition. *Cell Death Differ* **25**, 1131–1145 (2018).

203. Hewitt, V. L. *et al.* Decreasing pdzd8-mediated mito–ER contacts improves organismal fitness and mitigates $A\beta_{42}$ toxicity. *Life Sci. Alliance* **5**, e202201531 (2022).

204. Frohman, M. A. Role of mitochondrial lipids in guiding fission and fusion. *J Mol Med* **93**, 263–269 (2015).

205. Ha, E. E.-J. & Frohman, M. A. Regulation of mitochondrial morphology by lipids: Lipid Signal Regulation of Mitochondrial Morphology. *BioFactors* **40**, 419–424 (2014).

206. Kameoka, S., Adachi, Y., Okamoto, K., Iijima, M. & Sesaki, H. Phosphatidic Acid and Cardiolipin Coordinate Mitochondrial Dynamics. *Trends in Cell Biology* **28**, 67–76 (2018).

207. Kagan, V. E. *et al.* Cytochrome c acts as a cardiolipin oxygenase required for release of proapoptotic factors. *Nat Chem Biol* **1**, 223–232 (2005).

208. Nissanka, N. & Moraes, C. T. Mitochondrial DNA damage and reactive oxygen species in neurodegenerative disease. *FEBS Lett* **592**, 728–742 (2018).

209. Shokolenko, I., Venediktova, N., Bochkareva, A., Wilson, G. L. & Alexeyev, M. F. Oxidative stress induces degradation of mitochondrial DNA. *Nucleic Acids Research* **37**, 2539–2548 (2009).

210. Weyhersmuller, A., Hallermann, S., Wagner, N. & Eilers, J. Rapid Active Zone Remodeling during Synaptic Plasticity. *Journal of Neuroscience* **31**, 6041–6052 (2011).

211. Daniels, R. W. Increased Expression of the Drosophila Vesicular Glutamate Transporter Leads to Excess Glutamate Release and a Compensatory Decrease in Quantal Content. *Journal of Neuroscience* **24**, 10466–10474 (2004).

212. Oswald, M. C. W. *et al.* Reactive oxygen species regulate activity- dependent neuronal plasticity in Drosophila. *eLife* (2018) doi:10.7554/eLife.39393.

213. Karunanithi, S. *et al.* Activity-Dependent Global Downscaling of Evoked Neurotransmitter Release across Glutamatergic Inputs in *Drosophila*. *J. Neurosci.* **40**, 8025–8041 (2020).

214. Bridi, M. C. D. *et al.* Daily Oscillation of the Excitation-Inhibition Balance in Visual Cortical Circuits. *Neuron* **105**, 621-629.e4 (2020).

215. Vyazovskiy, V. V. & Faraguna, U. Sleep and synaptic homeostasis. *Current Topics in Behavioral Neurosciences* **25**, 91–121 (2015).

216. Bjorness, T. E. *et al.* An essential role for MEF2C in the cortical response to loss of sleep in mice. *eLife* **9**, e58331 (2020).

217. Torrado Pacheco, A., Bottorff, J., Gao, Y. & Turrigiano, G. G. Sleep Promotes Downward Firing Rate Homeostasis. *Neuron* **109**, 530-544.e6 (2021).

218. Westermann, B. Mitochondrial fusion and fission in cell life and death. *Nat Rev Mol Cell Biol* **11**, 872–884 (2010).

219. Liu, X., Weaver, D., Shirihai, O. & Hajnóczky, G. Mitochondrial 'kiss-and-run': interplay between mitochondrial motility and fusion–fission dynamics. *EMBO J* **28**, 3074–3089 (2009).

220. Popov, V., Medvedev, N. I., Davies, H. A. & Stewart, M. G. Mitochondria form a filamentous reticular network in hippocampal dendrites but are present as discrete bodies in axons: A three-dimensional ultrastructural study. *J. Comp. Neurol.* **492**, 50–65 (2005).

221. Yoon, Y.-S. *et al.* Formation of elongated giant mitochondria in DFO-induced cellular senescence: Involvement of enhanced fusion process through modulation of Fis1. *J. Cell. Physiol.* **209**, 468–480 (2006).

222. Bossy-Wetzel, E., Barsoum, M. J., Godzik, A., Schwarzenbacher, R. & Lipton, S. A. Mitochondrial fission in apoptosis, neurodegeneration and aging. *Current Opinion in Cell Biology* **15**, 706–716 (2003).

223. Busch, K. B., Kowald, A. & Spelbrink, J. N. Quality matters: how does mitochondrial network dynamics and quality control impact on mtDNA integrity? *Phil. Trans. R. Soc. B* **369**, 20130442 (2014).

224. Silva Ramos, E. *et al.* Mitochondrial fusion is required for regulation of mitochondrial DNA replication. *PLoS Genet* **15**, e1008085 (2019).

225. Sagan, L. On the origin of mitosing cells. *Journal of Theoretical Biology* **14**, 225-IN6 (1967).

226. Legros, F., Malka, F., Frachon, P., Lombès, A. & Rojo, M. Organization and dynamics of human mitochondrial DNA. *Journal of Cell Science* **117**, 2653–2662 (2004).

227. Rambold, A. S., Kostelecky, B., Elia, N. & Lippincott-Schwartz, J. Tubular network formation protects mitochondria from autophagosomal degradation during nutrient starvation. *Proc. Natl. Acad. Sci. U.S.A.* **108**, 10190–10195 (2011).

228. Gomes, L. C., Di Benedetto, G. & Scorrano, L. Essential amino acids and glutamine regulate induction of mitochondrial elongation during autophagy. *Cell Cycle* **10**, 2635–2639 (2011).

229. Wai, T. & Langer, T. Mitochondrial Dynamics and Metabolic Regulation. *Trends in Endocrinology & Metabolism* **27**, 105–117 (2016).

230. Yamaguchi, J. *et al.* Comprehensive application of an mtDsRed2-Tg mouse strain for mitochondrial imaging. *Transgenic Res* **21**, 439–447 (2012).

231. Willems, P. H. G. M., Rossignol, R., Dieteren, C. E. J., Murphy, M. P. & Koopman, W. J. H. Redox Homeostasis and Mitochondrial Dynamics. *Cell Metabolism* **22**, 207–218 (2015).

232. Liesa, M. & Shirihai, O. S. Mitochondrial Dynamics in the Regulation of Nutrient Utilization and Energy Expenditure. *Cell Metabolism* **17**, 491–506 (2013).

233. Schmitt, K. *et al.* Circadian Control of DRP1 Activity Regulates Mitochondrial Dynamics and Bioenergetics. *Cell Metabolism* **27**, 657-666.e5 (2018).

234. Dietrich, M. O., Liu, Z.-W. & Horvath, T. L. Mitochondrial Dynamics Controlled by Mitofusins Regulate Agrp Neuronal Activity and Diet-Induced Obesity. *Cell* **155**, 188–199 (2013).

235. Khacho, M. *et al.* Mitochondrial Dynamics Impacts Stem Cell Identity and Fate Decisions by Regulating a Nuclear Transcriptional Program. *Cell Stem Cell* **19**, 232–247 (2016).

236. Khacho, M. & Slack, R. S. Mitochondrial dynamics in the regulation of neurogenesis: From development to the adult brain: Mitochondrial Dynamics and Brain Neurogenesis. *Dev. Dyn.* **247**, 47–53 (2018).

237. Wen, Y. *et al.* Changes in the Mitochondrial Dynamics and Functions Together with the mRNA/miRNA Network in the Heart Tissue Contribute to Hypoxia Adaptation in Tibetan Sheep. *Animals* **12**, 583 (2022).

238. McWilliams, T. G. *et al.* mito-QC illuminates mitophagy and mitochondrial architecture in vivo. *Journal of Cell Biology* **214**, 333–345 (2016).

239. Lee, J. J. *et al.* Basal mitophagy is widespread in Drosophila but minimally affected by loss of Pink1 or parkin. *Journal of Cell Biology* **217**, 1613–1622 (2018).

240. Imamura, H. *et al.* Visualization of ATP levels inside single living cells with fluorescence resonance energy transfer-based genetically encoded indicators. *Proc. Natl. Acad. Sci. U.S.A.* **106**, 15651–15656 (2009).

241. Imai, Y. *et al.* Light-driven activation of mitochondrial proton-motive force improves motor behaviors in a Drosophila model of Parkinson's disease. *Commun Biol* **2**, 424 (2019).

242. Dietrich, M. O. & Horvath, T. L. Hypothalamic control of energy balance: insights into the role of synaptic plasticity. *Trends in Neurosciences* **36**, 65–73 (2013).

243. Carneiro, L. *et al.* Importance of Mitochondrial Dynamin-Related Protein 1 in Hypothalamic Glucose Sensitivity in Rats. *Antioxidants & Redox Signaling* **17**, 433–444 (2012).

244. Toda, C. *et al.* UCP2 Regulates Mitochondrial Fission and Ventromedial Nucleus Control of Glucose Responsiveness. *Cell* **164**, 872–883 (2016).

245. Desmoulins, L. *et al.* Mitochondrial Dynamin-Related Protein 1 (DRP1) translocation in response to cerebral glucose is impaired in a rat model of early alteration in hypothalamic glucose sensing. *Molecular Metabolism* **20**, 166–177 (2019).

246. Lam, T. K. T., Schwartz, G. J. & Rossetti, L. Hypothalamic sensing of fatty acids. *Nat Neurosci* **8**, 579–584 (2005).

247. Lee, K., Li, B., Xi, X., Suh, Y. & Martin, R. J. Role of Neuronal Energy Status in the Regulation of Adenosine 5′-Monophosphate-Activated Protein Kinase, Orexigenic Neuropeptides Expression, and Feeding Behavior. *Endocrinology* **146**, 3–10 (2005).

248. Alan, L. & Scorrano, L. Shaping fuel utilization by mitochondria. *Current Biology* **32**, R618–R623 (2022).

249. Reinhard, N. *et al.* The Neuronal Circuit of the Dorsal Circadian Clock Neurons in Drosophila melanogaster. *Front. Physiol.* **13**, 886432 (2022).

250. Valadas, J. S. *et al.* ER Lipid Defects in Neuropeptidergic Neurons Impair Sleep Patterns in Parkinson's Disease. *Neuron* **98**, 1155-1169.e6 (2018).

251. Prime, T. A. *et al.* A ratiometric fluorescent probe for assessing mitochondrial phospholipid peroxidation within living cells. *Free Radical Biology and Medicine* **53**, 544–553 (2012).

252. Adachi, Y. *et al.* Coincident Phosphatidic Acid Interaction Restrains Drp1 in Mitochondrial Division. *Molecular Cell* **63**, 1034–1043 (2016).

253. Chirichella, M. *et al.* Post-translational selective intracellular silencing of acetylated proteins with de novo selected intrabodies. *Nature Methods* **14**, 279–282 (2017).

254. Cattaneo, A. & Chirichella, M. Targeting the Post-translational Proteome with Intrabodies. *Trends in Biotechnology* **37**, 578–591 (2019).

255. Malka, F., Lombès, A. & Rojo, M. Organization, dynamics and transmission of mitochondrial DNA: Focus on vertebrate nucleoids. *Biochimica et Biophysica Acta (BBA) - Molecular Cell Research* **1763**, 463–472 (2006).

256. Qin, J. *et al.* ER-mitochondria contacts promote mtDNA nucleoids active transportation via mitochondrial dynamic tubulation. *Nat Commun* **11**, 4471 (2020).

257. Chen, Z. *et al.* Mitochondrial DNA segregation and replication restrict the transmission of detrimental mutation. *Journal of Cell Biology* **219**, e201905160 (2020).

258. Cai, N. *et al.* Molecular Signatures of Major Depression. *Current Biology* **25**, 1146–1156 (2015).

259. Cai, N. *et al.* Genetic Control over mtDNA and Its Relationship to Major Depressive Disorder. *Current Biology* **25**, 3170–3177 (2015).

260. Verstreken, P. *et al.* Synaptic Mitochondria Are Critical for Mobilization of Reserve Pool Vesicles at Drosophila Neuromuscular Junctions. *Neuron* **47**, 365–378 (2005).

261. Li, Z., Okamoto, K.-I., Hayashi, Y. & Sheng, M. The Importance of Dendritic Mitochondria in the Morphogenesis and Plasticity of Spines and Synapses. *Cell* **119**, 873–887 (2004).

262. Morton, D. W. & Chiel, H. J. Neural architectures for adaptive behavior. *Trends in Neurosciences* **17**, 413–420 (1994).

263. Engelhard, B. *et al.* Specialized coding of sensory, motor and cognitive variables in VTA dopamine neurons. *Nature* **570**, 509–513 (2019).

264. Pauls, D., Blechschmidt, C., Frantzmann, F., el Jundi, B. & Selcho, M. A comprehensive anatomical map of the peripheral octopaminergic/tyraminergic system of Drosophila melanogaster. *Sci Rep* **8**, 15314 (2018).

265. Burke, C. J. *et al.* Layered reward signalling through octopamine and dopamine in Drosophila. *Nature* **492**, 433–437 (2012).

266. Machado, D. R. *et al.* Identification of octopaminergic neurons that modulate sleep suppression by male sex drive. *eLife* **6**, e23130 (2017).

267. O'Donnell, M. P., Fox, B. W., Chao, P.-H., Schroeder, F. C. & Sengupta, P. A neurotransmitter produced by gut bacteria modulates host sensory behaviour. *Nature* **583**, 415–420 (2020).

268. Jia, Y. *et al.* Gut microbiome modulates Drosophila aggression through octopamine signaling. *Nat Commun* **12**, 2698 (2021).

269. Sinakevitch, I. & Strausfeld, N. J. Comparison of octopamine-like immunoreactivity in the brains of the fruit fly and blow fly. *J. Comp. Neurol.* **494**, 460–475 (2006).

270. Singh, C., Oikonomou, G. & Prober, D. A. Norepinephrine is required to promote wakefulness and for hypocretin-induced arousal in zebrafish. *eLife* **4**, e07000 (2015).

271. Aston-Jones, G. & Bloom, F. Activity of norepinephrine-containing locus coeruleus neurons in behaving rats anticipates fluctuations in the sleep-waking cycle. *J. Neurosci.* **1**, 876–886 (1981).

272. Hayat, H. *et al.* Locus coeruleus norepinephrine activity mediates sensory-evoked awakenings from sleep. *Sci. Adv.* **6**, eaaz4232 (2020).

273. Carter, M. E. *et al.* Tuning arousal with optogenetic modulation of locus coeruleus neurons. *Nat Neurosci* **13**, 1526–1533 (2010).

274. Hunsley, M. S. & Palmiter, R. D. Norepinephrine-deficient mice exhibit normal sleep-wake states but have shorter sleep latency after mild stress and low doses of amphetamine. *Sleep* **26**, 521–526 (2003).

275. Hunsley, M. S. & Palmiter, R. D. Altered sleep latency and arousal regulation in mice lacking norepinephrine. *Pharmacology Biochemistry and Behavior* **78**, 765–773 (2004).

276. Qi, Y. *et al.* A new Drosophila octopamine receptor responds to serotonin. *Insect Biochemistry and Molecular Biology* **90**, 61–70 (2017).

277. Zeng, J., Sun, F., Wan, J., Feng, J. & Li, Y. New optical methods for detecting monoamine neuromodulators. *Current Opinion in Biomedical Engineering* **12**, 68–74 (2019).

278. Roeder, T., Degen, J. & Gewecke, M. Epinastine, a highly specific antagonist of insect neuronal octopamine receptors. *European Journal of Pharmacology* **349**, 171–177 (1998).

279. Koon, A. C. & Budnik, V. Inhibitory Control of Synaptic and Behavioral Plasticity by Octopaminergic Signaling. *Journal of Neuroscience* **32**, 6312–6322 (2012).

280. Kurmangaliyev, Y. Z., Yoo, J., Valdes-Aleman, J., Sanfilippo, P. & Zipursky, S. L. Transcriptional Programs of Circuit Assembly in the Drosophila Visual System. *Neuron* **108**, 1045-1057.e6 (2020).

281. Sabandal, J. M., Sabandal, P. R., Kim, Y.-C. & Han, K.-A. Concerted Actions of Octopamine and Dopamine Receptors Drive Olfactory Learning. *J. Neurosci.* **40**, 4240–4250 (2020).

282. Branco, T. & Murthy, M. Editorial overview: Neurobiology of behavior. *Current Opinion in Neurobiology* **73**, 102559 (2022).

283. Jin, S. & Diano, S. Mitochondrial Dynamics and Hypothalamic Regulation of Metabolism. *Endocrinology* **159**, 3596–3604 (2018).

284. Palkovits, M. *et al.* Noradrenergic innervation of the rat hypothalamus: Experimental biochemical and electron microscopic studies. *Brain Research* **191**, 161–171 (1980).

285. Sciolino, N. R. *et al.* Natural locus coeruleus dynamics during feeding. *Sci. Adv.* **8**, eabn9134 (2022).